SPATIOTEMPORAL CHANGES IN CARBON AND ANTHROPOGENIC CONTRIBUTIONS IN AN AGRICULTURAL-FOREST WATERSHED

By

Gabriela Shirkey

A DISSERTATION

Submitted to
Michigan State University
in partial fulfillment of the requirements
for the degree of

Geography – Doctor of Philosophy
Environmental Science and Public Policy – Dual Major

2023

ABSTRACT

In this dissertation, I explore the socioeconomic contributions of landscape ecosystem C production in context of conventional biophysical regulations, resulting in spatiotemporal changes of global warming potential (GWP). To accurately model landscape-scale C production and estimate GWP at ecosystem and landscape levels, both socioeconomic and biophysical processes must be considered. Using an interdisciplinary approach, this work identifies factors that drive landscape C production and evaluates the sensitivity of terrestrial C sinks and sources. Chapter 2 uses fine spatiotemporal resolution remote sensing imagery to estimate terrestrial carbon production in heterogeneous agroecosystems. In Chapter 3, a structural equation model (SEM) assesses the relationships between historical agricultural intensification, land tenure, abiotic climate factors, and land cover land use change (LCLUC) on landscape terrestrial carbon production. Chapter 4 discusses the potential use of these estimates in a spatiotemporal life cycle assessment (LCA) for calculating carbon offset for carbon neutral goals. This work provides an innovative protocol that integrates geospatial and engineering methods to measure, validate, and summarize terrestrial and anthropogenic C emissions in life cycle assessment for calculating CO_2-equivalent ($CO_{2\text{-eq}}$)—GWP. Key contributions and lessons from this research will advance policy- and decision-making at landscape scales, where social and ecological processes must be considered for sustainable climate mitigation.

This dissertation is dedicated to the memory of Dr. Shengpan Lin.

ACKNOWLEDGMENTS

I would like to express my deepest gratitude and appreciation to all those who have supported me throughout my journey in completing this dissertation. Without their unwavering assistance, guidance, and encouragement, this accomplishment would not have been possible.

First and foremost, I would like to extend my heartfelt gratitude to my supervisor, Dr. Jiquan Chen. His expertise, constant guidance, and invaluable feedback have been instrumental in shaping and refining my research. His patience, availability, and dedication to my academic development have truly been remarkable. I am also immensely grateful to the members of my dissertation committee, Drs. Annick Anctil, Ilke Celik, Kyla Dahlin, and Ashton Shortridge, for their valuable insights, constructive criticism, and thoughtful suggestions. Their collective expertise and diverse perspectives have greatly enriched my research, pushing me to explore new horizons and refine my arguments.

I am indebted to my colleagues and peers from the Department of Geography, Center for Global Change and Earth Observations, Supporting Women in Geography, MSU Writing Center, and the FLUXNET Early Career Network for their support and intellectual discussions. Drs. Cheyenne Lei and Pietro Sciusco shared this graduate journey alongside me and shared every high and low. Drs. Ranjeet John, Housen Chu, Hogeun Park, Vincenzo Giannico, David Reed, Shengpan Lin, Maowei Liang, and Jing Yuan offered sincere compassion and guidance as mentors. Their camaraderie and willingness to engage in scholarly debates have contributed significantly to the development of my ideas and helped me overcome various challenges along the way.

I would like to express my deep appreciation to the staff and administration at the

Department of Geography and the Center for Global Change and Earth Observations. The access to extensive research materials, databases, and facilities has been crucial in conducting this study. The friendly and knowledgeable assistance provided by Jean Lepard, Kathleen Mills, Cameron Williams, Joni Burns, and Sharron Ruggles was greatly appreciated.

I owe a tremendous debt of gratitude to my friends and family members who have been a constant source of encouragement and support. Their belief in my abilities and their understanding during the demanding periods of this dissertation are truly invaluable. My parents, Bruce and Elvia (Letty) Shirkey never doubted my strength, my sister and brother-in-law Sarah and Bryan Stanley lifted my spirits when I needed it most, and my partner Uziel Mendez gave me boundless encouragement and support. Their unwavering love, encouragement, and understanding have been the pillars of strength that sustained me throughout this academic journey.

Lastly, I want to acknowledge the anonymous reviewers and Centennial Farmer participants who generously gave their time and shared their experiences for the purpose of this research. Their contributions have been instrumental in shaping the findings of this study, and I am deeply grateful for their willingness to participate.

I am humbled and grateful for the countless individuals who have contributed to the completion of this dissertation. Each person mentioned above and countless more played a unique and indispensable role in my academic journey, and I am sincerely thankful for their support, guidance, and belief in my abilities. This achievement would not have been possible without them, and for that, I am forever grateful.

TABLE OF CONTENTS

LIST OF ABBREVIATIONS

AGR	Agriculturally Cultivated lands
AVE	Average Variance Extracted
BAR	Bare land cover
C	Carbon
C flux	Carbon flux, referring to the amount of carbon exchanged between any two components of a biosphere over a specified time
C sequestration	Carbon sequestration, referring to a process within a terrestrial system to capture and store carbon
C stock	Carbon stock, referring to the amount of carbon stored in a specific component of an ecosystem
CH_4	Methane
CIg	Green Chlorophyll Index (unitless)
CIr	Red-edge chlorophyll index (unitless)
CLD	Average Clay in Soil (5-15 cm km^{-2})
CLS	Average Clay in Soil (0-5 cm km^{-2})
CO_2	Carbon-Dioxide
$CO_{2\text{-eq}}$	Carbon-Dioxide equivalent
CONUS	Conterminous United States
CRO	Cropland land cover
CRP	Conservation Reserve Program
CST	Conservation till (%)
CVT	Conventional till (%)
DOY	Day of Year
DEM	Digital Elevation Model
EC	Eddy Covariance

EGLE	Environment, Great Lakes, and Energy
EPA	Environmental Protection Agency
EVI/2	Enhanced Vegetation Index/2 (unitless)
FD	Count of farms (km^{-2})
FINC	Net farm income (km^{-2})
FINO	Income per farm operation (km^{-2})
FLD	Farmland (km^{-2})
FN	Farmland nitrogen (kg km^{-2})
FOR	Forest land cover
FOW	Farmland owned by farmer (km^{-2})
FP	Farmland phosphorus (kg km^{-2})
FRF	Farmland rented from (km^{-2})
FRT	Farmland rented (km^{-2})
*f*PAR	Fraction of the Photosynthetically Active Radiation
GEE	Google Earth Engine
GHG	Greenhouse Gas
GLBRC	Great Lakes Bioenergy Research Center
GPP	Gross Primary Production (g CO_2 m^{-2} d^{-1})
GPP_{Tower}	GPP estimate from an eddy covariance tower
GPP_{MODIS}	MOD17A2H V6 GPP
GPP_{CONUS}	Landsat CONUS GPP
$GPP_{VPM-MODIS}$	Vegetation Photosynthesis Model with MODIS data (500 m)
$GPP_{VPM-LS8}$	Vegetation Photosynthesis Model with Landsat 8 data (30 m)
GPP_{VPM-S2}	Vegetation Photosynthesis Model with Sentinel-2 data (20 m)
GRA	Grassland land cover

GSL	Growing season length (days)
GWP	Global Warming Potential (g $CO_{2\text{-}eq}$)
HTMT	Heterotrait-Monotrait Ratio
IRR	Irrigated (%)
INC	Income per capita (km^{-2})
IPCC	Intergovernmental Panel on Climate Change
KBS	W. K. Kellogg Biological Station
LAI	Leaf Area Index (unitless)
LCA	Life Cycle Assessment
LCC	Land Cover Change
LCLUC	Land Cover and Land Use Change
LCM	Land Change Model
LTER	Long-Term Ecological Research
LUE	Light use efficiency
LSWI	Land surface water index
MAUP	Modifiable Areal Unit Problem
MLP	Multi-Layer Perception Neural Network Model
MOD17A2H V6	Terra MODIS Gross Primary Productivity Version 6 (500 m)
MODIS	Moderate Resolution Imaging Spectroradiometer
MTCI	MERIS terrestrial red-edge chlorophyll index (unitless)
N_2O	Nitrous Oxide
NASS	National Agricultural Statistic Service
NbCS	Nature-based Climate Solutions
NDVI	Normalized Difference Vegetation Index (unitless)
NDRE1	Normalized difference red-edge index 1 (unitless)

NDRE2	Normalized difference red-edge index 2 (unitless)
NEE	Net Ecosystem Exchange (g CO_2 m^{-2} d^{-1})
NFN	Non-farmland Nitrogen (kg km^{-2})
NFP	Non-farmland Phosphorus (kg km^{-2})
NIR	Near-Infrared (nm)
NLCD	National Land Cover Database
NPP	Net Primary Production (g CO_2 m^{-2} d^{-1})
NT	No Till (%)
NWL	Natural Working Lands
OMD	Organic Matter (5-15 cm km^{-2})
OMS	Organic Matter (0-5 cm km^{-2})
PAR	Photosynthetically Active Radiation (μmol m^{-2} d^{-1})
PEM	Production Efficiency Model
PCA	Principal Component Analysis
PDI	Self-Calibrated Palmer Drought Severity Index
PHD	Average soil PH (5-15 cm km^{-2})
PHS	Average soil PH (0-5 cm km^{-2})
PLS-SEM	Partial Least Squares Structural Equation Model
POPD	Population Density (km^{-2})
PPFD	Photosynthetic Photon Flux Density
PPT	Precipitation (mm)
PRISM	Parameter-Elevation Regression of Independent Slopes Model Group
PTY	Total annal precipitation (mm)
R^2	R-Squared Score
RHD	Rural housing unit density (km^{-2})

RMSE	Root Mean Square Error
S1/2	Sentinel-1/2
SAD	Sand (5-15 cm km^{-2})
SAS	Sand (0-5 cm km^{-2})
SEM	Structural Equation Model
SES	Socio-Ecological System
SDG	United Nations Sustainable Development Goal
SID	Sild (5-15 cm km^{-2})
SIS	Silt (0-5 cm km^{-2})
SPEI	Standardized Precipitation Evapotranspiration Index
SWIR	Shortwave Infrared (nm)
T_{air}	Air Temperature (°C or K)
TPM	Maximum air temperature standard deviation (°C)
UHD	Urban Housing Unit Density (km^{-2})
UN	United Nations
UNFCCC	United Nations Framework Convention on Climate Change
URB	Urban Land Cover
US	United States
USGS	United States Geological Survey
VI	Vegetation Index
VPD	Vapor Pressure Deficit (kPa)
VPM	Vegetation Photosynthesis Model
$VPM_{S2\text{-}Clg}$	Vegetation Photosynthesis Model with Sentinel-2 (20 m) CIg
$VPM_{S2\text{-}Clr}$	Vegetation Photosynthesis Model with Sentinel-2 (20 m) CIr
$VPM_{S2\text{-}NDRE1}$	Vegetation Photosynthesis Model with Sentinel-2 (20 m) NDRE1

$VPM_{S2-NDRE2}$	Vegetation Photosynthesis Model with Sentinel-2 (20 m) NDRE2
$VPM_{S2-MTCI}$	Vegetation Photosynthesis Model with Sentinel-2 (20 m) MERIS MTCI
WAT	Water Body Land Cover
WET	Wetland Land Cover

CHAPTER 1. INTRODUCTION

General introduction

Increasing demands for food, biofuel, and other commodities worldwide are driving cropland cover and productivity increases, which directly and indirectly affect ecosystems at all scales (Godfray et al., 2010; Potapov et al., 2022; Tilman et al., 2011). Understanding the consequences of land management and use intensity at different scales is crucial to developing sustainable solutions, particularly in agroecosystems where the demands of ecosystem services should minimize environmental impact. Agricultural intensification raises greenhouse gas (GHG) emissions, threatens ecosystem health by fragmenting and losing habitats, and impacts biodiversity (Houghton et al., 2012; USGCRP, 2018; Zabel et al., 2019). As such, the United Nations Sustainable Development Goals (SDGs) have called on economies to become carbon neutral by 2030 and prioritize food security and ecological resource protection (United Nations, 2015). To achieve this ambitious goal, accurate carbon estimates are necessary to aid our understanding of how ecosystem functions respond to the changing climate, particularly where cropland is dominant.

According to the Intergovernmental Panel on Climate Change (IPCC), human activity significantly influences carbon (C) flux and storage, beyond biophysical feedback caused by climate change alone (Pachauri et al., 2014). Humans also play a critical role in land use/cover change, affecting potential C production and storage and global warming potential (GWP) at different spatiotemporal scales (Allred et al., 2015), where disturbances at the individual level amount to thousands of uncoordinated land use decisions (Lind-Riehl et al., 2015). Uncertainties in the global carbon cycle include land cover land use change statistics (LCLUC) (Houghton et al., 2012), sequestration under varying temperature and rainfall (Cox et al., 2013), and complex processes (e.g., management, CO_2

fertilization effect). Understanding the relationships and drivers of anthropogenic activities with terrestrial ecosystem production is crucial since humans contribute significantly to GWP.

Ecosystem C production is estimated in three stages throughout the carbon cycle. Gross primary production (GPP) is the amount of carbon dioxide "fixed" as organic material through photosynthesis. It is an important indicator of ecosystem productivity and carbon cycling. Accurate estimates of GPP are crucial for understanding the global carbon cycle, predicting future climate change, and managing ecosystems sustainably. Additionally, GPP is a key input for estimating net primary production (NPP), which is the amount of carbon that remains in the ecosystem after accounting for respiration by plants and other organisms. NPP is an important indicator of ecosystem health and can be used to estimate carbon sequestration rates. Therefore, accurate estimates of GPP are essential for understanding and managing ecosystems sustainably and mitigating climate change. Lastly, net ecosystem exchange (NEE) is the net flux of C between the land and atmosphere after a plant takes up carbon dioxide for photosynthesis, releases it during respiration and other ecosystem processes. When policy and decision-makers discuss emissions, NEE is the best measure for ecosystem contributions to total C emissions as other measures NPP and GPP include stored C within plant biomass. However, NEE is difficult to estimate and scale beyond ground-observations (i.e., *in situ*) to regional and global estimates due to several factors. One challenge is that NEE is highly variable in time and space due to land use change, climate variability, and disturbance. Second, heterogeneity in the landscape includes fragments of managed and unmanaged land, slope, and biodiversity that can contribute to the diversity of ecosystem processes and therein the NEE. Therefore, researchers may adopt GPP or NPP as a proxy to NEE in estimating carbon emissions from vegetation, but the accuracy may be affected by numerous factors including ecosystem type, structure, disturbance history, and environmental conditions (Law et al., 2001).

In tandem with monitoring ecosystem C production, efforts to regulate anthropogenic C emissions continue globally. Particularly, renewed efforts have risen to understand the potential terrestrial stock to offset emissions through ecosystem production known as nature-based climate solutions (NbCS) (Hemes et al., 2021; Novick et al., 2022; Robertson et al., 2022; Wiesner et al., 2022). To achieve this sustainably, it is crucial to consider how anthropogenic activities and abiotic factors interact with terrestrial C production. However, specific land management practices significantly affect terrestrial C stock and vary across a landscape due to economic motivations, land use, cultural ecosystem services, and ownership. These socioeconomic processes consume resources not included in ecological C models, resulting in biased estimates of global warming potential (GWP) and uncertainty in regional-global estimates. Agricultural development further complicates observations and resolutions, as land use and management vary across systems. As such, understanding the relationships and shifts in socioecological systems are essential for contextualizing anthropogenic emissions. Understanding the relationships between land use, ecosystem processes, abiotic drivers, and their spatial representation can inform decision makers on where to allocate resources for climate mitigation approaches. In turn, understanding human impacts on the C budget improves predictions of human-nature interactions and carbon cycle dynamics by quantifying C production, sinks, and terrestrial biosphere sensitivity (Fernández-Martínez et al., 2019).

To advance our understanding of C budgets, we need increased spatiotemporal resolution on landscape scale processes, including inferred fluxes from satellite CO_2 estimates and socioeconomic inputs not included in traditional ecosystem models. This dissertation integrates socioeconomic processes with ecosystem modeling to answer the research question: What are the contributions of socioeconomic processes to changes in landscape terrestrial carbon and GWP, and can estimate these relationships spatially? This research provides valuable knowledge on long-term anthropogenic impacts on C production at the landscape scale including how terrestrial C production estimates are influenced by land management, how human-nature interactions drive C production, and a unique framework to link historical land management records with innovative earth observations.

Research context and background

Scientists have modeled GWP and C flux in managed landscapes and heavily relied on biophysical inputs and responses alone. However, this approach fails to consider the energy, materials and fuels introduced by socioeconomic processes that occur within the same extent. Classic ecosystem/landscape C production is estimated by a combination of remote sensing, ecosystem models, and *in situ* measurements, but a net carbon offset must also consider the anthropogenic activities from land management/use (Fig. 1.1). Conversely, environmental engineering approaches to reduce anthropogenic carbon emissions, such as carbon capture or offset, overlook ecosystem processes within the system and are limited to case studies within a fixed extent. Connecting the anthropogenic activities with ecosystem processes is further complicated by spatiotemporal resolution. The advances in spatiotemporal resolution for ecological, climate, and land cover data have outpaced programs and resources monitoring land management and land use.

Generalizations, assumptions, and aggregation are the foremost challenges to connecting socioecological processes. A framework is urgently needed to connect existing records of land management and land use data to high spatiotemporal resolution environmental data, allowing for the evaluation of patterns and processes of socioecological systems across scales.

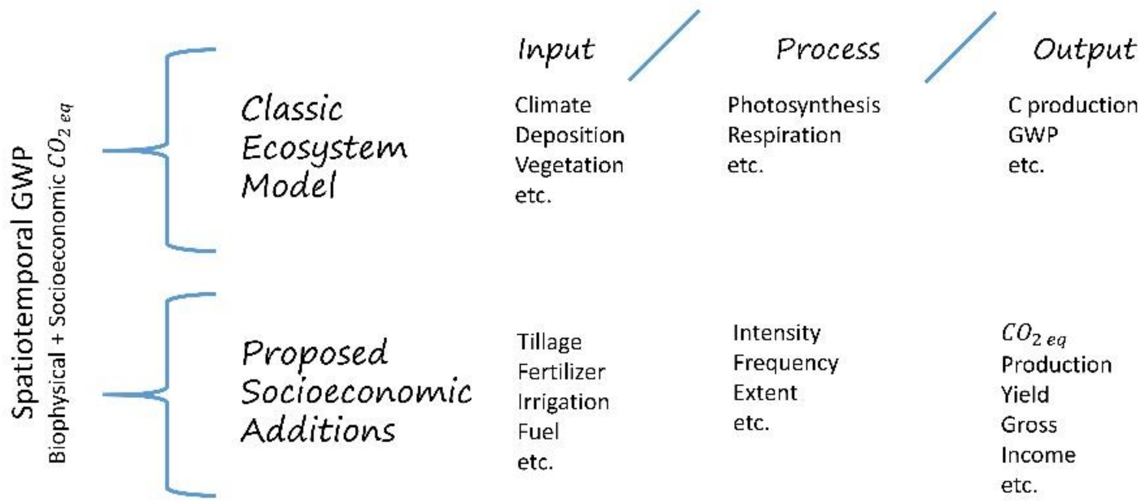

Figure 1.1. Classic ecosystem C production models do not reflect socioeconomic processes albeit their direct/indirect contributions to the actual values. This research incorporates spatiotemporal measures (e.g., extent, intensity, frequency) of these processes to quantify the explicit contributions of both physical and social C production to ecosystem-landscape GWP.

My approach is rooted in landscape ecology, which explains spatial patterns and ecological processes across scales and processes (Wu, 2006). Landscape ecology is suited for exploring the interacting heterogeneity of a landscape and complex human processes, integrating geophysical, ecological, and social science. Landscape characteristics across a landscape may couple with ecological and socioeconomic systems and introduce functional changes due to synchronized dynamics of physical, ecological, and social processes (Lausch et al., 2015; Sciusco et al., 2020; Tian & Chen, 2022; Turner, 1989). Synchronized dynamics of the physical, ecological, and social processes can be approached with socio-ecological system (SES) modeling (Chen et al., 2020; Elsawah et al., 2020), advancing a framework where human decision-making and actions have agency, context, and feedback within an ecosystem. This research builds on traditional biophysical and geographic research to develop this framework, moving beyond a flat, dimension-less, and moment in time contribution to GWP.

Aggregation and spatiotemporal resolution of socioecological processes

Carbon productivity in heterogeneous landscapes is difficult to estimate due to the variability in land management practices, and coarse remote sensing models may mischaracterize landscape processes (Gelybó et al., 2013; Shirkey et al., 2022). Field-scale measurements of carbon, water, and energy cycles provide detailed knowledge on cropland contributions to greenhouse gas exchanges and carbon budgets. However, scaling these measurements to regional or global extents using data-driven models may inflate or underestimate GPP in heterogeneous agricultural lands. Agricultural development can fragment the landscape into smaller patches than conventional remote sensing products can provide spatial resolution. Consequently, coarse remote sensing models may aggregate nearby land cover patches within the same estimate of land cover carbon productivity, introducing a mischaracterization of landscape processes (Reeves et al., 2005; Shirkey et al., 2022). The choice of model and spatial resolution may either inflate or underestimate GPP in heterogeneous agricultural lands, which may have significant consequences when scaled to regional or global extents. Eddy covariance (EC) field-scale measures of carbon, water and energy cycles have provided detailed knowledge on cropland and grassland contributions to greenhouse gas exchanges, carbon budgets and opportunities for natural climate solutions (Abraha et al., 2019; Hemes et al., 2021; Shao et al., 2017). At regional or to global scales, many studies have scaled EC tower observations regionally or globally using data-driven (or statistical) models (Beer et al., 2010; Jung et al., 2009). The choice of model and spatial resolution may either inflate or underestimate GPP in heterogeneous agricultural lands, which may have significant consequences when scaled to regional or global extents.

Conversely, land management and land use information are not conventionally recorded using remote sensing or *in situ* instrumentation, but rather with surveys of landowners. Efforts to utilize remote sensing data may estimate vegetation greenness and stress, which can be used to indicate irrigation and nutrient applications; but these have not yet produced annual land management data products. In the USA, cropland management is monitored nationally through the United States Department of Agriculture's National Agricultural Statistics Service (NASS). The NASS provides estimates of cropland acreage, yield, production, and management practices, such as tillage, irrigation, fertilizer use and much more through regular surveys. The NASS conducts a variety of surveys to gather information from farmers, including the Census of Agriculture, which is conducted every five years and provides detailed information on the characteristics of farm operators and their farming practices, as well as annual surveys on crop acreage and production. However, the finer the spatiotemporal scale of the survey data, the less dependable it becomes due to limitations such as stakeholder privacy, response rates, and administrative costs.

When integrating social and ecological datasets, caution is advised regarding the spatiotemporal resolution selected for resampling due to the Modifiable Areal Unit Problem (MAUP). This problem is described as (1) the “scale problem”, when areal data is aggregated into several sets of larger units; and (2) the “zoning problem”, when a given set of areal units are recombined into zones that are of the same size but located differently. Both problems result in variation in data values and subsequently different conclusions (Jelinski & Wu, 1996). Therefore, when cross examining carbon production and socioeconomic activities, caution is advised as to how these MAUPs may influence our understanding of land management and land use in the global carbon budget.

Land management, land use and land cover change intensification

Historical changes in biophysical landscape carbon relate to anthropogenic emissions of CO_2 and should be monitored spatially to disentangle the relationships between the two. For example, increased C production in urbanizing Michigan landscapes suggests that low-density development may enhance regional CO_2 uptake in the atmosphere compared to the pre-existing agricultural land (Zhao et al., 2007). As landowners make thousands of uncoordinated land use decisions that collectively and critically impact the landscape (Euskirchen et al., 2002; Lind-Riehl et al., 2015), it is imperative to include these in transformative models for accurate estimates landscape C. These contributions to the regional ecosystem functions (e.g., C budget) are unknown and may reveal key insights to spatial variation in anthropogenic drivers of global warming potential.

Understanding landscape composition must be considered for accurate net carbon exchange. While the terrestrial system has absorbed 15-30% of all anthropogenic emissions in recent decades (Le Quéré et al., 2018), it is unknown at the landscape scale what the dynamics are of these sinks by land cover type. Various ecosystems within a single landscape mosaic each carry their own respective C production cycle (Chen et al., 2004) and may have unique feedback to net C exchange, particularly in agricultural-forest lands. Cropland and managed grasslands are the dominant land cover types of many industrial, newly industrializing as well as developing countries (Bondeau et al., 2007; Foley et al., 2005), totaling 38% of the global land surface (Ramankutty et al., 2008) and ~30% of global net primary production appropriated by humans (Haberl et al., 2007). By investigating landscape composition and their spatiotemporal variability, as well as the contributions between physical and social carbon, a more accurate understanding of how human management and disturbance influences the role of terrestrial ecosystems within the global carbon budget (Kugler et al., 2019).

Dissertation focus and organization

In this dissertation, I apply an approach that integrates socio-ecological data within social science, ecological and environmental engineering models to tease apart the interrelationships between anthropogenic and terrestrial carbon emissions, using Southwest Michigan as a testbed. The contribution of this work advances the field of carbon cycle research, carbon offset and climate change mitigation, and addresses a key question facing our transition to a carbon-neutral economy, "What contributions do socioeconomic processes make to the magnitude and spatiotemporal changes of landscape C production?" To evaluate these processes, I utilize the Kalamazoo River Watershed (Michigan, USA) as a case study and apply landscape ecology to evaluate the causal and reciprocal interconnections between biological communities and their environment within a section of a landscape. To expound on human-nature interactions, I build upon traditional incorporate socioeconomic inputs with ecological processes for a socioecological study: where human decision making and actions have agency, context, and feedback within an ecosystem rather than a flat, dimension-less and moment in time contribution to GWP.

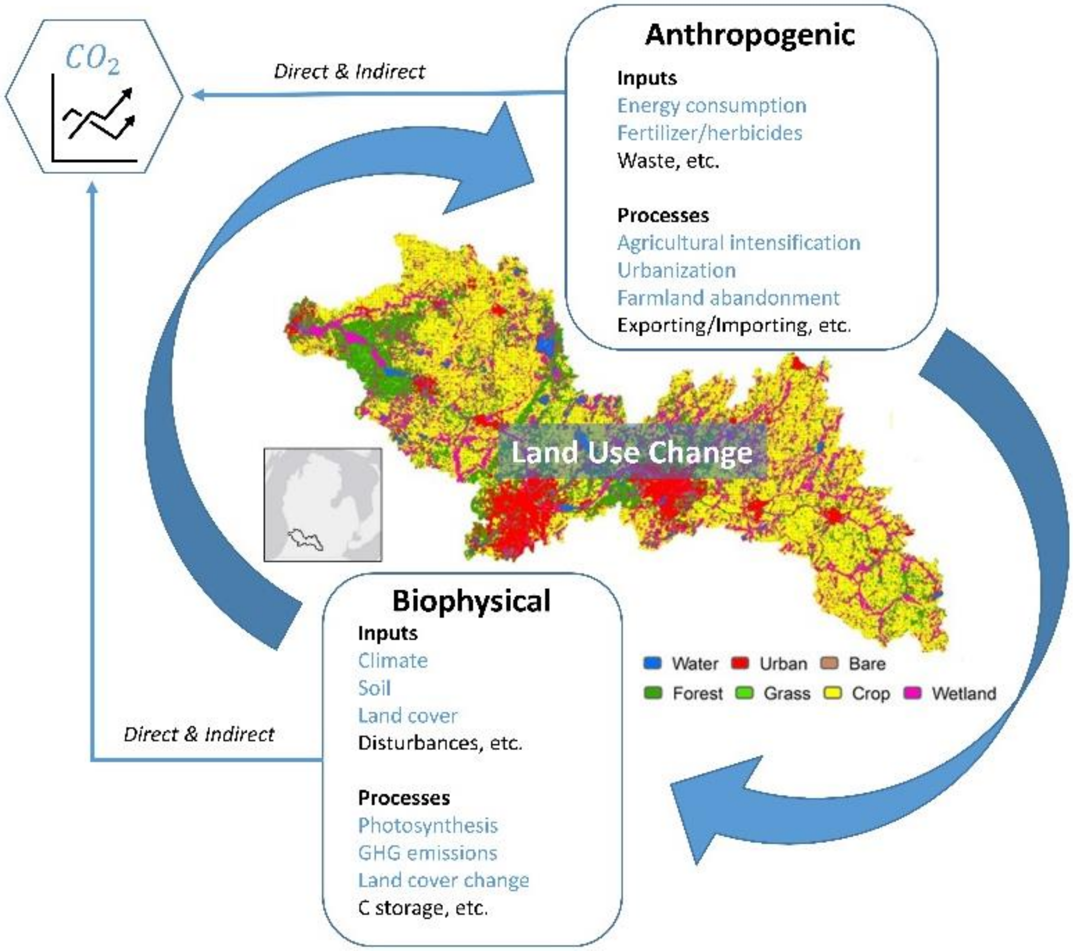

Figure 1.2. Conceptual illustration of the research scope. Human-nature relationships within the Kalamazoo River Watershed, MI include anthropogenic and biophysical inputs, processes and resulting $CO_{2\text{-eq}}$ that over time drive land use change. These complex interactions include multiple components, but for this study I consider the blue text only.

The site location is the Kalamazoo River Watershed (HUC8; 5261 km^2), which falls within southwest Michigan, USA (Fig. 1.2). The study boundary represents a common extent for land management, where the hydrological unit HUC8 is often state or locally managed by stakeholder participation and municipalities that seek state and federal support. The Kalamazoo River is listed as a Great Lakes "Area of Concern" in the 1987 Great Lakes Water Quality Agreement due to serious water quality concerns that have since attracted public attention from residents and governments in the region, such as the Kalamazoo River Watershed Council, to address existing pollution, wetland loss, deteriorating dams, and to establish long-term plans to restore and protect natural resources. The Kalamazoo Watershed is approximately 150 km wide and includes portions of ten counties in southwest Michigan: Allegan, Barry, Eaton, Van Buren, Kalamazoo, Calhoun, Jackson, Hillsdale, Kent, and Ottawa. The approximate center of the watershed is also its urban center, Battle Creek, MI, USA at latitude 42.32 and longitude -85.18. The primary river, the Kalamazoo River, flows westward into Saugatuck and Lake Michigan. The Kalamazoo Watershed is in a humid continental temperate climate with a mean annual air temperature of 9.9 °C and a cumulative average annual precipitation of 1027 mm (Abraha et al., 2019). Soils are Typic Hapludalfs, well-drained sandy loams (Bhardwaj et al., 2011; Thoen, 1990). From May through September, representing the growing season, mean air temperature and total precipitation are 19.7°C and 523 mm, respectively, with the highest temperatures in July (Abraha et al., 2018).

My overarching hypothesis is that socioeconomic practices may be more responsible than the biophysical processes in total landscape GWP, intensifying C fluxes and emissions during and post land conversion (i.e., legacy effects) and throughout dynamic practices. My objective is to integrate socioeconomic processes into conventional ecosystem modeling. In this dissertation, I estimate net carbon production across spatiotemporal landscapes using multiple methods to collect and analyze various data sources (Fig. 1.2), including climate (e.g., temperature, precipitation, drought), landscape composition via land cover classification, ecosystem carbon production (e.g., gross primary production and net primary production estimates), energy consumed (e.g., fossil fuels, natural gas), and carbon emissions (i.e., GWP). The outcome of this dissertation provides a novel approach to a spatiotemporal analysis of carbon production in agricultural-forest landscapes to enhance our ability to project future projections of the coupled carbon cycle and climate system in a spatiotemporal context at the landscape scale. This work is presented across five chapters.

In Chapter 2, I estimate carbon production in managed agricultural landscapes and validate remote sensing products with *in situ* eddy covariance estimates. The work identifies potential for red-edge spectroscopy and demonstrates improved remotely sensed terrestrial carbon estimates within heterogeneous agricultural-forest landscapes for landscape C assessment. In Chapter 3, I identify the interrelations of anthropogenic and abiotic activities, including land cover change, land management, and climate, and their collective impact on terrestrial carbon production within a structural equation model. This chapter determines if landscape composition is critical in estimating overall carbon production directly or indirectly. Within Chapter 4, I apply a life cycle assessment (LCA) to estimate the net contributions of anthropogenic activities and terrestrial carbon production to global warming potential and relate this to sustainable development goals, including a net-zero carbon economy. I evaluate landscape C stock as comprised of both terrestrial and social C contributions (Fig. 1.1) and determine whether the latter contributes the most to landscape C and how climate mitigation efforts may consider this approach. Lastly, Chapter 5 reviews key findings from this dissertation, addressing how socioecological processes influence and contribute to landscape ecosystem C production. Here, I summarize areas for research applications and future investigations into landscape-scale socioecological system research.

CHAPTER 2. FINE RESOLUTION REMOTE SENSING SPECTRA IMPROVES ESTIMATES OF GROSS PRIMARY PRODUCTION OF CROPLANDS

This chapter was previously published by *Agricultural and Forest Meteorology*: Shirkey, G., John, R., Chen, J., Dahlin, K., Abraha, M., Sciusco, P., ... & Reed, D. E. (2022). Fine resolution remote sensing spectra improves estimates of gross primary production of croplands. *Agricultural and Forest Meteorology*, 326, 109175.

Abstract

Gross primary production (GPP) is a fundamental measure of the terrestrial carbon cycle critical to our understanding of ecosystem function under the changing climate and land use. Remote sensing enables access to continuous spatial coverage but remains challenged in heterogeneous croplands. Coarse resolution products, like MODIS (500 m), may aggregate fragmented land cover types commonly found in heavily managed landscapes and misrepresent their respective contribution to carbon production. Consequently, this study demonstrates the capability of fine-resolution imagery (20-30 m) and available red-edge vegetation indices to characterize GPP across seven Midwest cropping systems. Four sites were established on a 22-year-old USDA Conservation Reserve Program (CRP); and the other three on land conventionally farmed with corn-soybean-wheat rotation (AGR). I compare *in situ* GPP estimates from eddy-covariance towers with ten satellite models: eight variants of the vegetation photosynthesis model (VPM), of which five include a red-edge vegetation index, as well as conventional products Landsat CONUS GPP (30 m) and MOD17A2H V6 (500 m). Daily and cumulative fine-resolution imagery integrated within VPM agreed with tower-based GPP in heterogeneous landscapes more than those from MODIS 500 m VPM or conventional GPP products from MOD17A2H V6 or Landsat 8 CONUS. Replacing EVI2 with red-edge indices NDRE2, NDRE1, and MTCI in Sentinel 2 VPMs notably improved explanation of variance and estimation of cumulative GPP. While existing methods using MODIS- and Landsat-derived GPP are important baselines for regional and global studies, future research may benefit from the higher spatial, temporal, and radiometric resolution.

Introduction

Rising demands for food, biofuel, and other commodities across the globe are driving increases in cropland cover and productivity (Godfray et al., 2010; Potapov et al., 2022; Tilman et al., 2011). This intensity increases greenhouse gas (GHG) emissions and threatens ecosystem health through fragmentation and loss of habitat (Houghton et al., 2012; USGCRP, 2018; Zabel et al., 2019). Cropland and managed grasslands are the dominant land cover types of many industrial, newly industrializing as well as developing countries (Bondeau et al., 2007; Foley et al., 2005), totaling 38% of the global land surface (Ramankutty et al., 2008) and ~30% of global net primary production appropriated by humans (Haberl et al., 2007). Given the association between cropland intensification, rising GHG emissions, and threat to biodiversity and ecosystem functions, the United Nations Sustainable Development Goals (SDGs) call for economies to become carbon (C) neutral by 2030 as well as to prioritize food security and ecological resource protection (United Nations, 2015). To aid our understanding of how ecosystem functions respond to changing climate, particularly where cropland is dominant, accurate C estimations are essential.

Terrestrial GPP is the major driver of land C sequestration and vital to the global C balance but is highly variable in croplands due to land management practices (e.g., crop rotation, irrigation, abandonment, and others). As intensification continues, croplands will also experience an increase in terrestrial gross primary production (GPP), the amount of carbon dioxide 'fixed' as organic material through photosynthesis. In addition to physical influences and disturbances (i.e., climate, geo-morphology, land cover change, wildfires, floods), the magnitude and dynamics of GPP are also driven by anthropogenic activities that alter land use and land cover dynamics, as well as biogeochemical cycles (Abraha et al., 2018a; Anav et al., 2015; Hibbard et al., 2017; Lei et al., 2021; Piao et al., 2009; Sciusco et al., 2020). Therefore, it is challenging to generate specific C balance estimates within croplands (Gelybó et al., 2013). While GPP cannot be directly measured, it can be modeled using the eddy-covariance (EC) method, which partitions net ecosystem exchange (NEE) into GPP and ecosystem respiration (Aubinet et al., 2012; Baldocchi et al., 2012; Lasslop et al., 2010; Papale et al., 2006; Reichstein et al., 2005). Eddy covariance field-scale measures of C, water and energy cycles have provided detailed knowledge on cropland and grass-land contributions to GHG exchanges, C budgets and opportunities for natural climate solutions (Abraha et al., 2019; Chen et al., 2018; Hemes et al., 2021; Shao et al., 2017). At regional to global scales, many studies have scaled EC tower observations using data-driven, process-based models (Beer et al., 2010; Jung et al., 2009) and found meteorological data have minor impact on upscaled GPP with high-quality satellite data (Joiner & Yoshida, 2020). Measures are scaled by evaluating the relationships between tower-based GPP estimates and satellite-based, gridded and reanalysis data of climate, meteorological, and surface-reflectance estimates to constrain and calibrate models that monitor vegetation health and yield (Cai et al., 2021; Kumar & Mutanga, 2017; Lin et al., 2019; Wolanin et al., 2019; Xiao et al., 2011). Scaling and extrapolation to regional or global representativeness should be exercised with caution as it can increase uncertainty (Beer et al., 2010; Chu et al., 2017). This can be understood as the Modifiable Areal Unit Problem (MAUP) that includes (1) the “scale problem”, when areal data is aggregated into several sets of larger units; and (2) the “zoning problem”, when a given set of areal units are recombined into zones that are of the same size but located differently. Both problems result in variation in data values and subsequently different conclusions (Jelinski & Wu, 1996).

Similarly, the choice of model and spatial resolution may either inflate or underestimate GPP in heterogeneous croplands. Model comparison is necessary, as it identifies variations that could help identify shortcomings and areas for future improvement (Morales et al., 2005). Comparison is also a prerequisite for analyzing spatiotemporal biosphere-atmosphere fluxes as it reveals effects from different model structures (i.e., structural uncertainty) (Wang et al., 2011; Zhao et al., 2012), parameter values, meteorological input data, and vegetation and soil C pools (Anav et al., 2015). Therefore, examination of various GPP models and their spatial and temporal variations in croplands is necessary to advance our understanding of land management and land use effects on the global C budget.

Integration of EC and remote sensing methods have advanced our ability to estimate GPP. However, due to the intense fragmentation, there can be a mismatch between small patches and conventional remote sensing spatial resolution (Ustin & Middleton, 2021). For example, global products, like the highly utilized 8-day Moderate-Resolution Imaging Spectroradiometer (MODIS) MOD17A2/A3 and MYD17A2/A3 GPP products (1 km–500 m), can be challenging if used in the context of land cover areas with complex vegetation or mixed pixels (Running & Zhao, 2015). In fact, coarse remote sensing models may aggregate nearby land cover patches within the same estimate of land cover GPP productivity, introducing a mischaracterization of landscape processes (Reeves et al., 2005; Zhang et al., 2012). To estimate GPP within fragmented landscapes under various management practices, remote sensing offers several approaches to estimate GPP using measurements of optical parameters related to vegetation activity (Damm et al., 2015; Myneni & Ross, 2012). Advancements in optical sensors, such as those carried aboard Landsat-8 (2013–

now) and -9 (2021–now), offer 30 m spatial resolution whereas Sentinel-2 A and B (2015/2017–now) offer 10-20 m spatial resolution and narrow red-edge bands—enabling phenology studies and parametrization at a much higher resolution than previously possible (Li & Roy, 2017).

Of the primary remote-sensing based models, the most common are light use efficiency (LUE) based estimates that are built on function convergence theory (Field et al., 1995; Monteith, 1972, 1977), which states that plant canopies will harvest the most light to fix C given the constraints from the environment (Goetz et al., 2000). Following this framework are the production efficiency models (PEMs), where GPP is estimated as a product of the fraction of the photosynthetically active radiation (*f*PAR) absorbed by the canopy (e.g., Goetz et al., 1999; Ruimy et al., 1999; Running et al., 2004). For example, the Landsat conterminous United States (CONUS) GPP product captures fine spatial scale (30 m) variability in GPP production with biome-specific inputs and pro-vides ready-to-use product covering croplands, forests, grasslands and shrublands (Robinson et al., 2018). The vegetation photosynthesis model (VPM) similarly estimates GPP in various ecosystems, and its performance aligns well with EC GPP (John et al., 2013; Li et al., 2007; Wagle et al., 2015; Xiao et al., 2004a; Xiao et al., 2004b; Zhang et al., 2016).

Further, many remote sensing based GPP models, such as VPM, rely on vegetation indices (VI) as input variables that serve as a proxy of *f*PAR and associated nutrient and absorption characteristics. Red-edge bands offered from the Sentinel-2A and B satellites offer additional VIs capable of estimating GPP, as vegetation red-edge (680-780 nm) captures the absorption of chlorophyll at 680 nm and higher absorption at 780 nm, detecting both moderate-to-high values (Gates et al., 1965; Gitelson & Merzlyak, 1996;

Horler et al., 1983). This is significant as chlorophyll has demonstrated a high sensitivity to seasonal changes and a strong relationship to GPP in croplands (Clevers & Gitelson, 2013; Lin et al., 2019; Wu et al., 2008). In addition, fine spatial resolution of the Sentinel-2 data provides temporally detailed information for characterizing spatially heterogeneous GPP best in croplands and grasslands compared to forest sites (Lin et al., 2019). Across grassland sites in southeast Australia, Sentinel-2 red-edge data estimates of GPP agreed well with EC GPP (R^2 =0.77 and RMSE =0.81 g C m^2 day^{-1}) (Lin et al., 2019). Sentinel-2 and Landsat 8 data have also been used to estimate a neural network GPP model on five crop fields (four in the USA and one in Germany) (R^2 =0.92 and RMSE =1.38 g C m^2 day^{-1}) (Wolanin et al., 2019). EVI2-derived GPP from MODIS (500m, 250m) and Sentinel-2 (10m) and EC-derived were evaluated in eight sites in the Nordic region (R^2 0.69-0.91 and RMSE 0.49-2.19 g C m^2 day^{-1}) (Cai et al., 2021). Few studies, however, cross-compare product resolutions in VPM to investigate changes across scales within the same cover type; or have evaluated red-edge VIs. More commonly, VPM is cross-evaluated with other GPP products, such as MOD17A2H, a temperature and greenness model, a greenness and radiation model, and the EC-LUE model (Li et al., 2013; Wu et al., 2011). Therefore, red-edge VIs from Sentinel-2 integrated into the VPM may enhance our ability to estimate GPP in heterogeneous croplands (Chen et al., 2011; Turner et al., 2003).

In this study, we evaluate whether GPP estimates derived using higher spatial resolution of satellite data are advantageous to conventional remote sensing products in managed croplands. We ask the following questions: (1) Can fine resolution GPP products built with red- edge VIs effectively capture significant differences at field-scale? (2) Are they significantly different from the conventionally used models—MOD17A2H V6 (500m) and Landsat-8 CONUS (30m)? and (3) How consistent are GPP anomalies across models within each site? While coarse resolution GPP products are reasonable for studies of large spatial extents, like global and regional (Running & Zhao, 2015), local-scale estimates of GPP are needed for local-scale management, estimates of C sequestration, and for C accounting. We generate site-specific LUE coefficients and model GPP, utilizing the VPM across MODIS (500 m), Landsat-8 (30 m), and Sentinel-2 (20 m) resolutions. By comparing multiple approaches to estimating GPP, we show which products are the most accurate in our managed cropping systems.

Methods

Study sites

Our study sites are located within the northeast portion of the US Midwest Corn Belt in southwest Michigan, USA, at the Great Lakes Bioenergy Research Center (GLBRC) of the W. K. Kellogg Biological Station (KBS) Long-Term Ecological Research (LTER) sites (42 ∘ 24′N, 85 ∘ 24′W, 288m a.s.l.; Fig. 2.1, Table A1). The sites are in a humid continental temperate climate with mean annual air temperature 9.9 ∘ C and mean total annual precipitation 1027 mm (Michigan State Climatologist's Office, 2013). Soils are Typic Hapludalfs, well-drained sandy loams (Bhardwaj et al., 2011; Thoen, 1990). From May through September, representing the growing season, mean air temperature and total precipitation are 19.7 ∘ C and 523 mm, respectively, with highest temperatures in July (Abraha et al., 2018b). Our study period spans March through November (DOY 60–334), including the growing season as well as its onset and offset, for years 2018 and 2019. Precipitation, air temperature, and photosynthetic photon flux density (PPFD) were acquired from nearby meteorological stations (http://lter. kbs.msu.edu/data tables, accessed June 2020). Seasonal dynamics of

GPP are driven by PPFD and temperature in these temperate croplands, where GPP lowers to near-zero in the winter season — DOY 335-59 (December through February) — due to near absence of photosynthetic activity caused by snow cover, harvest as well as low PPFD and temperatures.

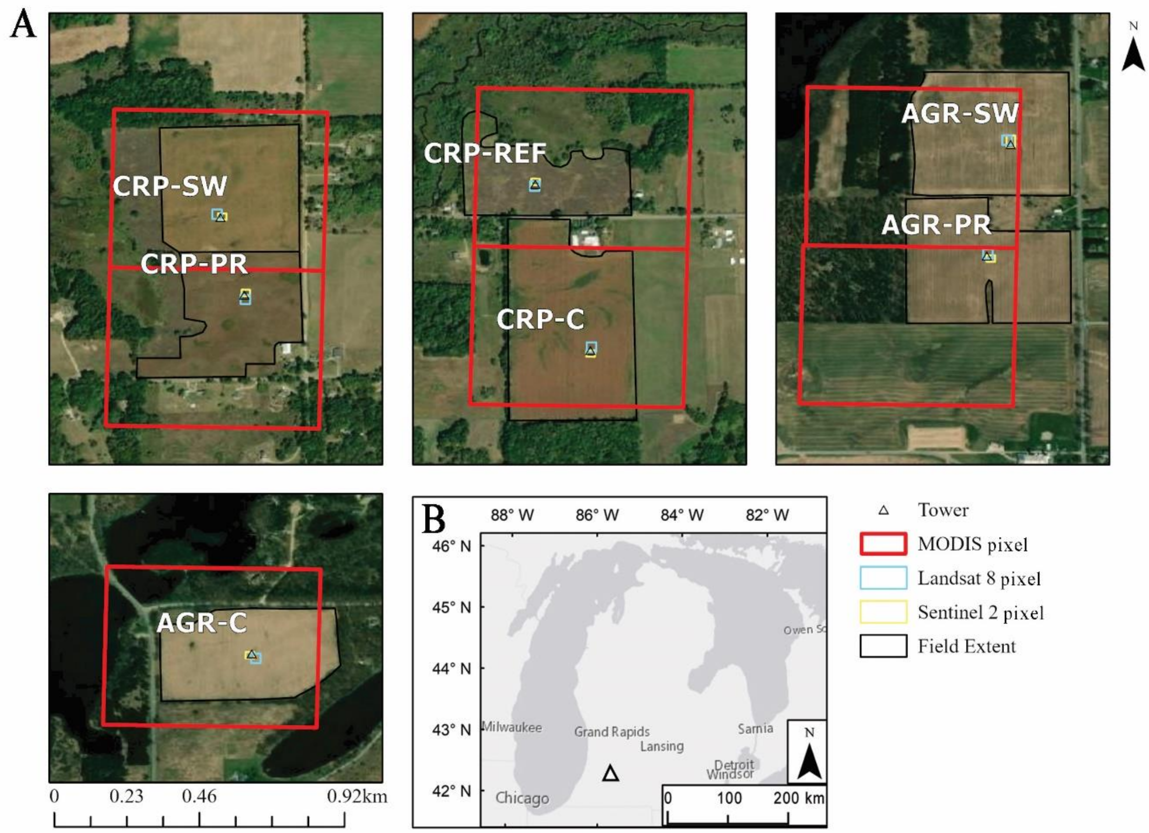

Figure 2.1. Location of eddy-covariance (EC) flux towers used in this study, where (A) are individual field extents and individual pixels for MODIS, Landsat-8, and Sentinel-2; and (B) is the location the towers at Kellogg Biological Station, Michigan, USA.

Eddy covariance

All EC systems included a LI-7500 open-path infrared gas analyzer (IRGA, LI-COR Bioscience, Lincoln, NE) for CO_2 and water (H_2O) concentration and a CSAT3 three-dimensional sonic anemometer (Campbell Scientific Inc. CSI, Logan, UT) for wind speed and direction measurements. Half-hourly meteorological measurements of incoming and outgoing radiation (CNR1, Kipp & Zonen, Delft, The Netherlands) and air temperature and relative humidity (HMP45C, CSI) were also measured at each site. All EC instruments are mounted 1.5–2.0 m above the vegetation and logged at 10Hz using a Campbell CR5000 datalogger. Half-hourly fluxes were processed in EdiRe for screening out-of-range data due to severe weather, sensors, and/or logger malfunction as well as de-spiking. For full data quality control details, please see Abraha et al. (2015).

Gapfilling and flux partitioning was completed in the standardized FLUXNET gap-filling algorithm from REddyProc (Wutzler et al., 2018). Gap-filling included a Ustar correction with thresholds estimated using the Moving Point Test (Papale et al., 2006), bootstrap uncertainty within the year, and flux partitioning by daytime (Lasslop et al., 2010). We used quality control flags ("*fqc*") of 0-3 in this study, where least reliable (i.e., *fqc*=3) estimates comprised less than 0.54% of any site-year, and values outside of three standard deviations were linearly interpolated with the package "*seismicRoll*" (Callahan et al., 2020) in RStudio 1.3.1056 (R Core Team, 2019). We present GPP uncertainty across aggregated values due to estimation of the Ustar threshold, as well as the percent NEE gap-filled prior to partitioning.

Satellite products and indices

We obtained GPP (kg C m^2) from the MOD17A2H V6 product (8-day revisit time and 500 m resolution; hereafter GPP_{MODIS}) and the Landsat 8 CONUS product (16-day revisit time and 30 m resolution; hereafter GPP_{CONUS}) (Robinson et al., 2018). Both GPP_{MODIS} and GPP_{CONUS} were retrieved from Google Earth Engine (GEE) platform (Gorelick et al., 2017) using point sampling to select the nearest pixel to the site's tower location. We considered only pixels near each tower, which brought us to consider 1 (500×500 m) MODIS pixel and

3×3 Landsat-8 (30×30 m) and Sentinel-2 (20×20 m) pixels. The models used to calculate GPP_{MODIS} and GPP_{CONUS} are based on the LUE model (Running et al., 2004). However, GPP_{MODIS} retrieves climate, land cover, *f*PAR and LAI parameters from GMAO/NASA (0.5°), MOD12Q1 (500 m), and MOD15A2H (500 m), respectively, whereas GPP_{CONUS} retrieves these parameters from Idaho Metdata (4 km), National Land Cover Database (NLCD; 30 m), and MOD09Q1 (250 m), respectively. To derive daily estimates, composite images GPP_{MODIS} and GPP_{CONUS} were divided by 8 and 16, respectively, and multiplied by 1000 to convert from kg C to g C, with final GPP units being expressed as g C m^{-2} d^{-1}.

For VPM, we used surface reflectance from MODIS, Landsat-8, and Sentinel-2 (acquisition details below) to calculate vegetation indices (VIs). The VIs include (1) the enhanced vegetation index 2 (EVI2) (Jiang et al., 2008) to account for moisture sensitivity; (2) the land surface water index (LSWI) (Xiao et al., 2004b), which is based on the shortwave-infrared (SWIR) and represents vegetation water content and soil moisture. In place of EVI2, we also test VIs including (3) the green Chlorophyll Index (CIg) and red-edge (4) Chlorophyll Index (CIr) (Gitelson et al., 2003, 2006); the (5) normal deviation index of the red edge 1 (NDRE1) (Sims & Gamon, 2002) and (6) normal deviation index of the red edge 2 (NDRE2) (Barnes et al., 2000); as well as the (7) medium- resolution imaging spectrometer, MERIS, terrestrial chlorophyll index (MTCI) (Dash & Curran, 2004). Surface reflectance and land surface temperature layers were quality checked and linearly interpolated for a representative time series. The MODIS MOD09A1 v006 product provides surface reflectance at 500 m resolution every 8 days and it was used to calculate VIs using red (620–670 nm), near-infrared (NIR; 841–875 nm) and SWIR (1628–1652 nm) bands. MODIS Terra has an overpass at 10:30 AM local time. Data was acquired using the USGS

AppEEARS online tool (https://lpdaac. usgs.gov/tools/appeears/, accessed January 2021) and screened for cloud cover and artefacts using QA/QC bits and 500m state flags, as instructed by the MODIS User Guide Tables 10–13, to select the best quality data (Vermote et al., 2015). Gaps due to inadequate quality were linearly interpolated. USGS Landsat 8 surface reflectance (Tier 1) provided 30 m resolution imagery every 16 days to calculate VIs EVI2 (Eq. 2.4) and LSWI (Eq. 2.6) using red (636-673 nm), NIR (851-879 nm), and SWIR (1566-1651 nm). As for $GPP_{LS8\text{-}VPM}$, we acquired Landsat 8 data using GEE, and we used the pixel quality band "QA_PIXEL" to identify cloud and cloud shadow pixels. The Sentinel-2 is a constellation of two polar-orbiting satellites in the same sun-synchronous orbit. Surface reflectance over the study area provides a high revisit time of 10 days at the equator for a single satellite and 5 days with two satellites under cloud-free conditions, which results in 2-3 days at mid-latitudes. Overpass for Sentinel-2 is 10:30 AM local time and is a compromise for illumination and least potential cloud cover, like the overpass time of Landsat and MODIS. Sentinel-2A spatial resolution is offered at 10, 20, and 60 m with a total of 12 multispectral bands; of which, three are red edge bands. Bands used (and their center wavelength) for EVI2 and LSWI include NIR (B8, 842 nm; 20 m spatial resolution), red (B4, 665 nm; 10 m spatial resolution), and SWIR (B11, 1610 nm; 20 m spatial resolution), respectively. For red-edge indices (Eqs. 2.5-2.9), we also included the following: B3 (green, 560 nm), B5 (red- edge, 705 nm), B6 (red-edge, 740 nm), and B7 (red-edge, 783 nm). The red band was resampled to 20 m resolution to match that of NIR and SWIR. Images were obtained from the Copernicus Open Access Hub (https://scihub.copernicus.eu/dhus/#/home, accessed February 2021) of the European Space Agency. We downloaded images as level 2A (i.e., surface reflectance) over the study area. Where level 2A was not available, we downloaded level 1C top-of-atmosphere (TOA) images that were then atmospherically corrected to obtain surface reflectance by using the default settings of the Sen2Cor (v. 2.5.5) algorithm (Müller-Wilm et al., 2018). We performed the cloud mask in RStudio by using the cloud mask probability band "MSK_CLDPRB," to identify cloud pixels, and the scene classification map band "SCL," to identify water pixels. We then used a NIR threshold to identify potential cloud shadow pixels (for more info, see https://developers.google.com/earth-engine/tutorials/community/sentinel-2-s2cloudless). We employed ArcMap (v. 10.6) to rescale the surface reflectance to 0–1.

Lastly, to understand how heterogeneous systems can benefit from fine-resolution imagery, we estimate the composition (30 m) of land cover type within each of the remote sensing pixels employed to estimate GPP, described above, within ArcGIS Pro (v. 2.9). We acquired land cover from the USGS National Land Cover Database 2019 via GEE (Dewitz & Survey, 2021). Land cover estimates included cropland, water, wetland, grassland, wetlands, developed and forest; where grassland includes pasture, hay, grassland, shrub/scrub, wetlands include woody wetlands and emergent herbaceous wetlands, developed includes open space, and low, middle, and high intensity developed areas, and forest includes evergreen, deciduous and mixed forests.

Vegetation photosynthesis model (VPM)

The VPM model is built similarly to the GPP_{MODIS} equation (Xiao et al., 2004a; Xiao et al., 2004b), however the difference lies in the creation of LUE (ε_g, Eq. 2.2) from remote sensing and meteorological in-puts rather than the use of a look up table, where:

$$VPM = \varepsilon_g \times (fPAR) \times (PAR), \qquad (2.1)$$

$\varepsilon_g = \varepsilon_{max} \times Tscalar \times Wscalar \times Pscalar$ (2.2)

Here, *VPM* represents Sentinel-2, Landsat-8 and MODIS VPMs, hereafter $GPP_{VPM\text{-}S2}$, $GPP_{VPM\text{-}LS8}$, and $GPP_{VPM\text{-}MODIS}$, respectively; *fPAR* is the fraction of photosynthetically active radiation absorbed by chlorophyll, *PAR* is photosynthetically active radiation (μmol m^{-2} s^{-1}) acquired from nearby a weather station (http://lter.kbs.msu.edu/datatables, accessed June 2020), ε_g is the LUE — the rate of CO_2 uptake (μmol CO_2 PAR^{-1}). The value of ε_{max} is maximum LUE estimated from a nonlinear hyperbolic Michaelis–Menten model (Wang et al., 2010), and *Tscalar*, *Wscalar* and *Pscalar* are the scaling regulators for the effects of air temperature, water, and leaf phenology, respectively, on the vegetation.

Common in LUE models, including PEMs, is the application of *f*PAR as a function of the normalized difference vegetation index (NDVI) (Tucker, 1979). It is well acknowledged that NDVI is constrained by sensitivity to soil moisture and saturates at high leaf densities (Huete et al., 2002). To address this, VPM applies EVI as a function of *f*PAR for an enhanced characterization of vegetation at the global scale (Huete et al., 2006; Jiang et al., 2008; Xiao et al., 2004a). To calculate *fPAR*, EVI can function as a linear function and the coefficient *a* is set to 1.0 (Xiao et al., 2005; Xiao et al., 2004b). In this study, we apply EVI2 to avoid high signal to noise ratios from atmospheric interference (e.g., aerosol or residual clouds) common in blue band wavelengths (Jiang et al., 2008).

$fPAR = a \times (EVI2)$ (2.3)

$EVI2 = 2.5\,\frac{NIR-RED}{NIR+2.4RED+1}$ (2.4)

To evaluate the potential for red-edge bands available from Sentinel-2 to advance the VPM's applications, we chose to replace EVI2 with one of five red-edge VIs, CIg, CIr, NDRE1, NDRE2 and MTCI, calculated as:

$$\text{CIg} = \frac{B7}{B3} - 1 \tag{2.5}$$

$$\text{CIr} = \frac{B7}{B5} - 1 \tag{2.6}$$

$$\text{NDRE1} = \frac{B6-B5}{B6+B5} \tag{2.7}$$

$$\text{NDRE2} = \frac{B8-B5}{B8+B5} \tag{2.8}$$

$$\text{MTCI} = \frac{B6-B5}{B5-B4} \tag{2.9}$$

where the center of each Sentinel-2 band is as follows: B3 (560 nm), B4 (665 nm), B5 (705 nm), B6 (740 nm), B7 (783 nm), B8 (842 nm).

The down regulation scalars *Wscalar, Tscalar, Pscalar* demonstrate the effects of water, temperature, and leaf phenology respectively on the vegetation's LUE. *Wscalar* is estimated as:

$$\mathrm{W}scalar = \frac{1+LSWI}{1+(LSWI)max} \tag{2.10}$$

$$\text{LSWI} = \frac{NIR-SWIR}{NIR+SWIR} \tag{2.11}$$

where (LSWI)max is the maximum LSWI during the growing season. Tscalar measures the sensitivity of photosynthesis to temperature, calculated at each time step using the equation developed for the Terrestrial Ecosystem Model (Raich et al., 1991):

$$\mathrm{T}scalar = \frac{(T-Tmin)(T-Tmax)}{[(T-Tmin)(T-Tmax)]-(T-Topt)^2} \tag{2.12}$$

where Tmin, Tmax, and Topt are the photosynthesis minimum, maximum, and optimal temperatures (°C), respectively (Raich et al., 1991) (Table A2). If the air temperature falls below Tmin, Tscalar is set to zero. Pscalar accounts for the effects of leaf phenology on photosynthesis at the canopy level. Calculation of Pscalar is dependent on the life expectancy of the leaves. Pscalar has two phases when a canopy is dominated by leaves with a life expectancy of one year (i.e., growing season) without replacement. From bud burst to full leaf expansion, Pscalar is calculated as:

$$P\mathit{scalar} = \frac{1+LSWI}{2} \tag{2.13}$$

whereas following expansion, the Pscalar is set to 1 with no alteration for senescence. Grassland systems such as prairie and switchgrass are set to 1 throughout the study period (Wang et al., 2010; Xiao et al., 2004a).

Statistical analysis and uncertainty

To understand how tower GPP estimates relate to either NDVI or EVI2, we performed sensitivity tests of both indices to GPP_{Tower} acquired from MODIS, Landsat-8 and Sentinel-2 for each site-year using a procedure outlined in Gitelson (2004):

$$S = [d(EVI2)/d(NDVI) \bullet [\Delta(EVI2)/\Delta(NDVI)]^{-1} \tag{2.14}$$

where *d(EVI2)* and *d(NDVI)* are the first derivatives of the indices with respect to GPP_{Tower} and *Δ(EVI2)* and *Δ(NDVI)* are the differences between the maximum and minimum index, respectively. Function *S* tracks the sensitivity of EVI2 and NDVI to changes in GPP_{Tower}. Values of S <1 can be interpreted where NDVI is more sensitive than EVI2 to GPP_{Tower}, and values S >1 as indicate that EVI2 was more sensitive than NDVI to GPP_{Tower}. When $S = 1$, NDVI and EVI2 are assumed to be equally sensitive. We acknowledge that *S* does not account for estimate errors of d(EVI2)/d(NDVI), which may bias sensitivity evaluations.

We evaluated seasonal dynamics of PPFD, air temperature, precipitation, as well as EVI2 and NDVI from MODIS, Landsat-8, and Sentinel-2 in a time series alongside GPP_{Tower} for each site-year. A comparison of GPP sums during the study period (March–November) and growing season (June, July, August) evaluates differences between GPP_{MODIS}, GPP_{VPM-}

$_{MODIS}$, GPP $_{VPM-LS8,}$ GPP$_{VPM-S2}$, GPP$_{CONUS}$, and GPP$_{Tower}$. Days without estimates from the VPM model or other products (i.e., days in-between acquisitions) were linearly interpolated within the R package "*zoo*" to generate cumulative GPP estimates (Zeileis & Grothendieck, 2005).

Three metrics were used to evaluate the performance of GPP satellite estimates in comparison with GPP$_{Tower}$, including the coefficient of determination (adjusted R^2, hereafter R^2), root mean square error (RMSE), and Spearman's Rho (ρ), which is a non-parametric test that estimates the model's ability to increase or decrease in a similar trend to observed values. Estimates closer to one indicate a positive relationship and those closer to -1 indicate a negative relationship. In the linear models, we only included original acquisition days (i.e., days corresponding to satellite acquisitions) that paired tower estimates. To assess model implications on GPP estimates, and by proxy the resolution implications, we tested for significant difference in GPP models among sites with the Kruskal-Wallis test and Dunn post-hoc test in the R packages "*stats*" and "*dunn.test*" (Dinno, 2017; Dunn, 1964; Kruskal & Wallis, 1952; R Core Team, 2019). The Kruskal-Wallis test extends from the Wilcoxon Rank test that is used for two samples (Vargha & Delaney, 1998), and determines if there is a significant difference (*p*-value <0.05) in the median GPP estimate between models. It replaces a one-way analysis of variance (ANOVA) when data is not normally distributed. The result of the Kruskal-Wallis is *H*, which is interpreted as chi-square; and z is result of the Dunn's Test for multiple comparisons.

Since our study area has strong seasonal changes of temperate zones, our data and predictions violate the statistical assumptions that they are independent and identically distributed. We address this concern of temporal autocorrelation in a second regression analysis by removing interannual and seasonal variation from each time series. We estimated zero-centered daily GPP anomalies and evaluated how these anomalies vary by GPP model and site-year. To generate average GPP seasonality (GPPS) on a daily time step (t) for each site (x) we averaged the daily GPP estimates from the different approaches for each year then smoothed the result with a Gaussian blur of 15 days to remove noise using the R package "smoother" (Hamilton, 2015). To remove interannual differences, we calculated $GPP_{x,yr}$ as the site-year annual mean of all GPP models. As such, GPP anomalies (GPPA) were calculated as:

$$GPPA_{x,t} = GPP_{x,t} - GPPS_{x,t} - GPP_{x,yr} \quad (2.15)$$

Therefore, when an anomaly estimate is near-zero it has a small difference from the average, zero-centered seasonal pattern. Once we calculated daily GPPA (Eq. 2.15), we only included estimates that coincide with model acquisition dates to avoid inflation in our analysis. In the linear regression of anomalies, models agreeing well with GPP_{Tower} will express similar values (i.e., differences from the mean) with GPP_{Tower}. In the linear regression of anomalies, models agreeing well with GPP_{Tower} will express similar values (i.e., differences from the mean) with GPP_{Tower}.

Results

Seasonal changes of climate, vegetation indices and tower GPP

Seasonal changes in air temperature, precipitation and PPFD at the LTER/KBS (i.e., study area) revealed that 2018 was on average warmer and drier than 2019 during the study period (March-November) (Fig. A1). For the study area in 2018, there was an average air temperature of 10.59 ˚C and a cumulative 796 mm of precipitation, whereas 2019 had an average air temperature of 9.25 ˚C and cumulative 896 mm of precipitation. We found

GPP_{Tower} increased sharply in May of both years at in all site-years (Fig. 2.2) due to the temperature increase, where the study area's monthly average air temperature from April to May increased from 4.49 ˚C to 18.18 ˚C in 2018, and 8.47 ˚C to 13.97 ˚C in 2019. We also found the study area in 2019 had notably higher cumulative monthly and average daily precipitation in spring months reaching 114(2.8), 92(2.97), and 173(5.77) mm in April, May, and June, whereas 2018 had 63(2.1), 220(7.10), and 80(2.67) mm, respectively. GPP_{Tower} uncertainty due to Ustar filtering for all site-years was < 3% (0.81–2.97%), with <28% (16.16–27.51%) of NEE identified for gapfilling (Table A4).

We found that MODIS 500 m pixels do not well represent each study site and include large aggregations of neighboring land covers (Table A3). One MODIS pixel including a tower may overlap two fields or nearby forest and marshland (Fig. 1.2). Conversely, the resolution of Sentinel-2 and Landsat 8 (20 m and 30 m, respectively) results in homogeneous pixels at each of the seven sites. Therefore, reflectance and VIs from Landsat 8 and Sentinel 2 are more likely to represent the land cover of interest and minimize influence from neighboring vegetation. Monthly variability in GPP_{Tower} during the growing season coincided well with the variations in precipitation, temperature, PPFD and EVI2/red-edge VIs. The GPP_{Tower} during the growing season peaked in late July (DOY 185–217), which closely coincides with peak PPFD and temperature in the study area (Fig. A1). Peak dates of daily GPP at AGR-C and CRP-C from 2018 were delayed by approximately 20 days in 2019; whereas AGR-PR experienced a 15-day delay, and remaining sites peaked within 11 days (Fig. 2.2).

The interannual seasonal dynamics of EVI2 differ in amplitude across sites and between satellites (Fig. 2.2). Maximum EVI2 for Sentinel-2 across sites ranged 0.65–0.86, whereas Landsat-8 and MODIS ranged 0.55–0.80 and 0.59–0.68, respectively. Sentinel-2 best captured the onset, offset, and volatility of the growing season. MODIS and, to a lesser extent, Landsat-8 EVI2 trends often exhibited lower estimates near the growing season peak. Notably, MODIS EVI2 increased before GPP_{Tower} in the onset of the growing season and lags in the offset, particularly in AGR-C, CRP-C, AGR-PR, and CRP-REF. Interannual seasonal dynamics of red-edge VIs capture peak growing season GPP well, particularly in corn systems, and reach higher peaks than EVI2 in CRP-PR and CRP-REF sites (Fig. 2.3). Red-edge VIs also demonstrate a similar trend as GPP during spring and fall in all sites.

MODIS EVI2 is more sensitive to variations in GPP_{Tower}, whereas for Landsat-8 and Sentinel-2, EVI2 and NDVI have similar sensitivity (i.e., 0.00 ± 0.10) (Table 2.1). MODIS EVI2 is more sensitive to GPP_{Tower} in all site years except CRP-SW in 2018. We note that historical cropland sites AGR-C, AGR-PR, and AGR-SW as well as CRP-REF and CRP-C have higher sensitivities to MODIS EVI2. For Landsat-8, AGR-C, AGR-PR, CRP-PR, and CRP-REF exhibit sensitivities to both NDVI and EVI2 in different years, with CRP-C, AGR-SW and CRP-SW demonstrating higher sensitivities to NDVI in both years. Similarly, Sentinel-2 saw sensitivities change between years, but exhibited slightly higher sensitivity to NDVI in AGR-C, AGR-PR and CRP-SW. Overall, we found Landsat-8 sensitivities remained within ±0.10 of 1.00 (i.e., equal sensitivity) for 9:14 (i.e., 9 out of 14) site-years, respectively, whereas Sentinel-2 exhibited sensitivities ±0.10 of 1.00 within 12:14 site-years.

Table 2.1. The relative sensitivity of EVI2 to NDVI. Values of S < 1 indicate that NDVI is more sensitive than EVI2, sensitivities are equal when S = 1, and values of S > 1 indicate EVI2 having a greater sensitivity than NDVI.

Site	MODIS		Landsat-8		Sentinel-2	
	2018	*2019*	*2018*	*2019*	*2018*	*2019*
AGR-C	1.31	1.33	1.08	0.99	0.90	0.96
AGR-PR	1.32	1.26	0.94	1.00	0.77	0.94
AGR-SW	1.30	1.22	0.94	0.92	0.99	1.01
CRP-C	1.11	1.13	0.77	0.99	0.78	1.00
CRP-PR	1.07	1.18	1.04	0.86	1.04	0.93
CRP-REF	1.20	1.21	1.22	0.81	1.01	0.91
CRP-SW	0.77	1.08	0.97	0.57	0.95	0.94

Differences between sensitivities of EVI2 and red-edge VIs to GPP_{Tower} vary (Table 2). In most cases, NDRE1 is near similar in sensitivity to EVI2 in all sites except CRP-C, where NDRE1 is more sensitive. Between NDRE2 and EVI2, most sites had near-equal sensitivities, except for AGR-SW 2018 where EVI2 has higher sensitivity. Both Clg and Clr show a lower sensitivity than EVI2 in all site-years except in CRP-C. Lastly, sensitivities of MTCI and EVI2 were near equal in all site years except AGR-SW 2018, where EVI2 has higher sensitivity. Overall, NDRE1 and NDRE2 have 8:14, Clg and Clr have 2:14, and MTCI 5:14 site years with higher sensitivity than EVI2 to GPP_{Tower}.

Table 2.2. The relative sensitivity of EVI2 to Sentinel-2 red-edge bands NDRE1, NDRE2, Clg, Clr, and MTCI. Values of S < 1 indicate that the red-edge index is more sensitive than EVI2, sensitivities are equal when S = 1, and values of S > 1 indicate EVI2 having a greater sensitivity than the respective red-edge index.

Site	NDRE1		NDRE2		Clg		Clr		MTCI	
	2018	*2019*	*2018*	*2019*	*2018*	*2019*	*2018*	*2019*	*2018*	*2019*
AGR-C	0.88	0.92	0.87	0.93	1.19	1.13	1.14	1.15	0.98	1.05
AGR-PR	1.08	1.06	1.08	1.09	1.43	1.27	1.34	1.25	1.05	1.06
AGR-SW	1.32	0.95	1.40	1.02	1.61	1.14	1.59	1.12	1.26	1.00
CRP-C	0.73	0.74	0.74	0.75	0.94	0.89	0.97	0.89	0.90	0.86
CRP-PR	0.96	0.93	0.93	0.93	1.26	1.08	1.16	1.08	1.05	0.99
CRP-REF	1.00	1.00	1.12	1.02	1.34	1.20	1.14	1.09	0.93	1.12
CRP-SW	0.96	0.91	0.96	0.94	1.12	1.13	1.26	1.18	1.13	1.04

In both years, $GPP_{VPM\text{-}S2}$ explains more variability and is statistically significant in the linear regression analysis with GPP_{Tower} during the study period (Table A5). $GPP_{VPM\text{-}S2}$ demonstrates visibly higher peaks in the growing season than other models, but occasionally overestimates in 2018 (AGR-C, AGR-PR, CRP-C, CRP-PR, CRP-REF) and in 2019 (CRP- C, CRP-REF). MODIS products underestimate these amplitudes (Figs. 2.4, 2.5). MODIS products underestimate corn and switchgrass systems where $GPP_{VPM\text{-}S2}$ captured GPP dynamics. In addition, VPMs coincide with GPP_{Tower} peaks and variations more than GPP_{MODIS} and GPP_{CONUS}, particularly in corn systems. Average daily GPP_{Tower} is higher in 2018 compared to 2019; where in 2018, the most productive sites (CRP-SW, AGR-C, and AGR-PR) reached 5.66–6.27 g C m^{-2} d^{-1} compared to the most productive sites in 2019 (CRP-PR, CRP-C, and CRP-SW) with a range of 5.73–5.78 g C m^{-2} d^{-1}. Corn systems have the highest daily productivity in both years but experienced the greatest shift in peak dates between 2018 and 2019. In both years, the highest daily sum recorded were in sites CRP-C, AGR-C, and CRP-SW while the lowest daily sum was observed in CRP-REF.

When exchanging EVI2 for a red-edge VI in the Sentinel-2 VPM, there is a significant improvement across site-years. Particularly, NDRE1 and NDRE2 improve the Sentinel-2 VPM in eight out of 14 site-years compared to other red-edge VIs. In 2018, NDRE2 improves AGR-C, CRP-C, and CRP-SW by improving explanation of variation by 8%, 11% and 4%, respectively; whereas in 2019, it improves AGR-C, AGR- PR, AGR-SW, CRP-C, and CRP-SW by 7%, 4%, 3%, 16% and 4%, respectively (Table A5). NDRE1 also improves AGR-C in both years and CRP-C in 2018 by the same explanation of variance as NDRE2. While $GPP_{VPM\text{-}LS8}$ is better than $GPP_{VPM\text{-}S2}$ in both CRP-C site-years, but with NDRE2 the VPM improves by 11% and 16% in 2018 and 2019, respectively. Red-edge VIs NDRE1, Clr and Clg do not improve the Sentinel-2 VPM beyond that of NDRE2. While MTCI does improve the Sentinel-2 VPM in CRP-REF and explain 4% more variation and is the leading GPP model for both site-years, it still overestimates during the peak growing like $GPP_{VPM\text{-}S2}$ and $VPM_{S2\text{-}Clg}$ (Fig. 2.5).

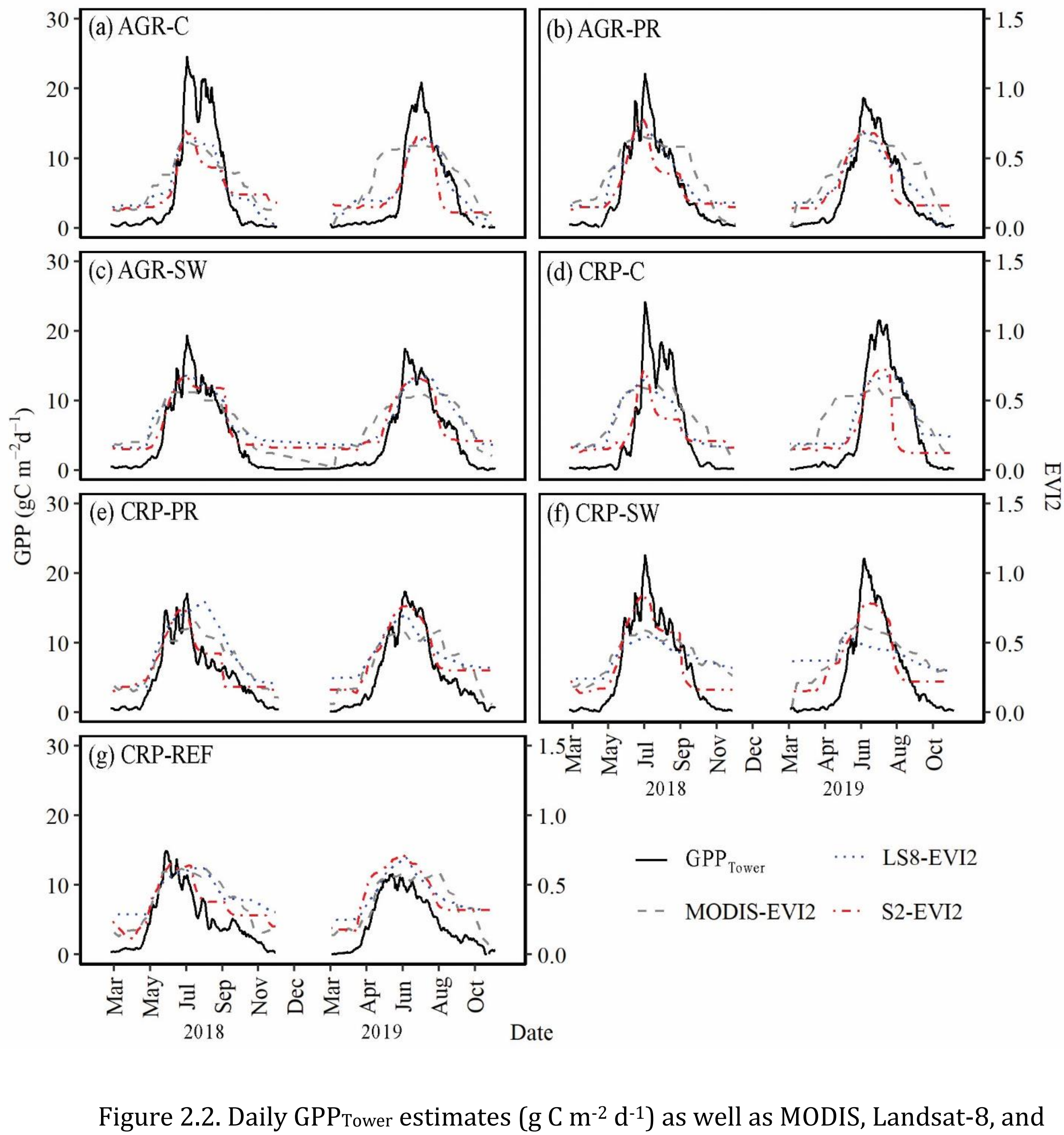

Figure 2.2. Daily GPP_{Tower} estimates (g C m^{-2} d^{-1}) as well as MODIS, Landsat-8, and Sentinel-2 EVI2 at (a) AGR-C, (b) AGR-PR, (c) AGR-SW, (d) CRP-C, (e) CRP-PR, (f),CRP-SW, and (g) CRP-REF sites 2018–2019.

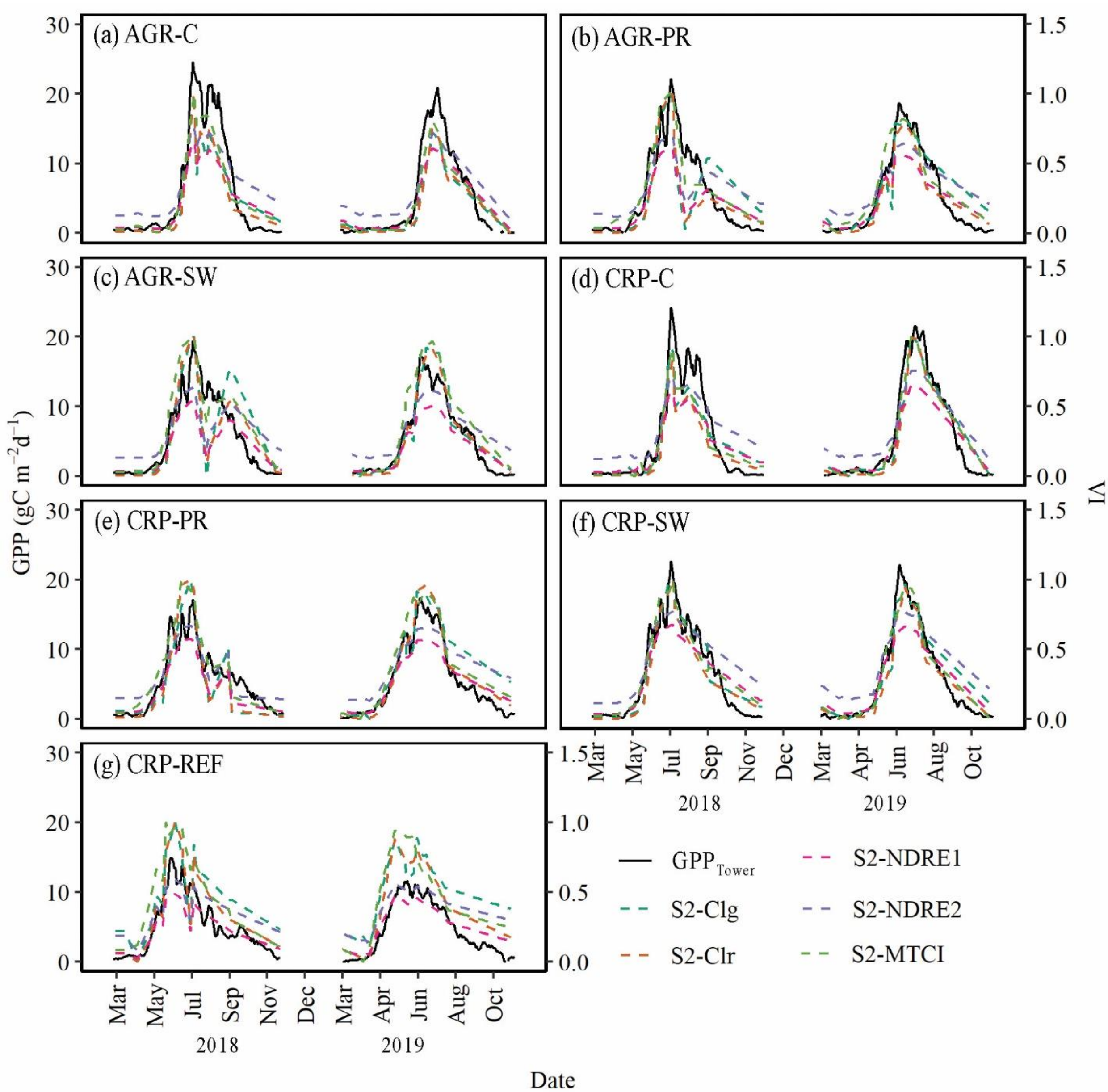

Figure 2.3. Daily GPP_{Tower} estimates (g C m^{-2} d^{-1}) as well as Sentinel-2 red edge vegetation indices Clg, Clr, NDRE1, NDRE2, and MTCI at (a) AGR-C, (b) AGR-PR, (c) AGR-SW, (d) CRP-C, (e) CRP-PR, (f),CRP-SW, and (g) CRP-REF sites 2018–2019.

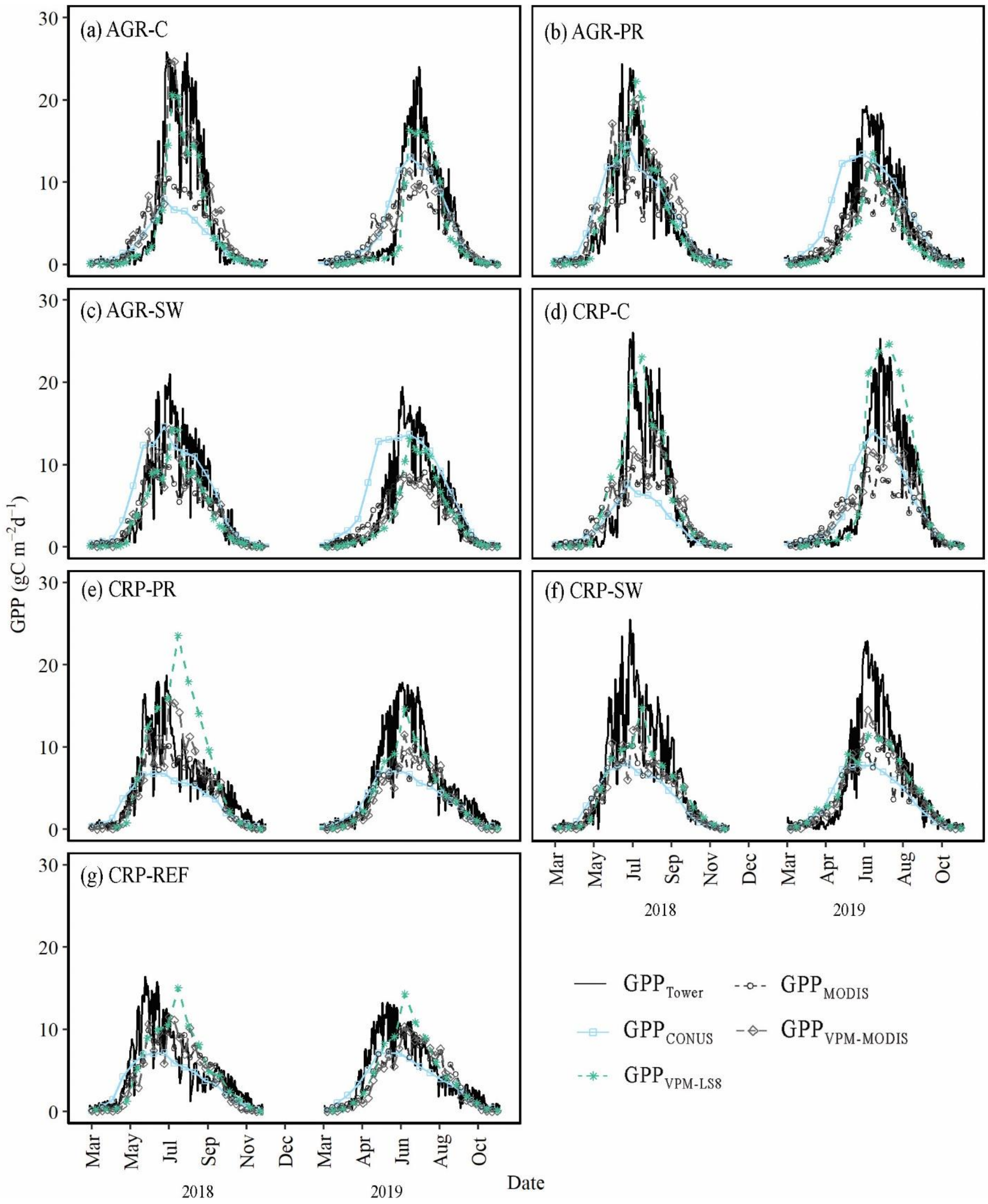

Figure 2.4. Temporal changes in GPP$_{Tower}$, conventional and VPMs including CONUS and MODIS resolutions 2018–2019 for the seven study sites: (a) AGR-C, (b) AGR-PR, (c) AGR-SW, (d) CRP-C, (e) CRP-PR, (f), CRP-SW, and (g) CRP-REF.

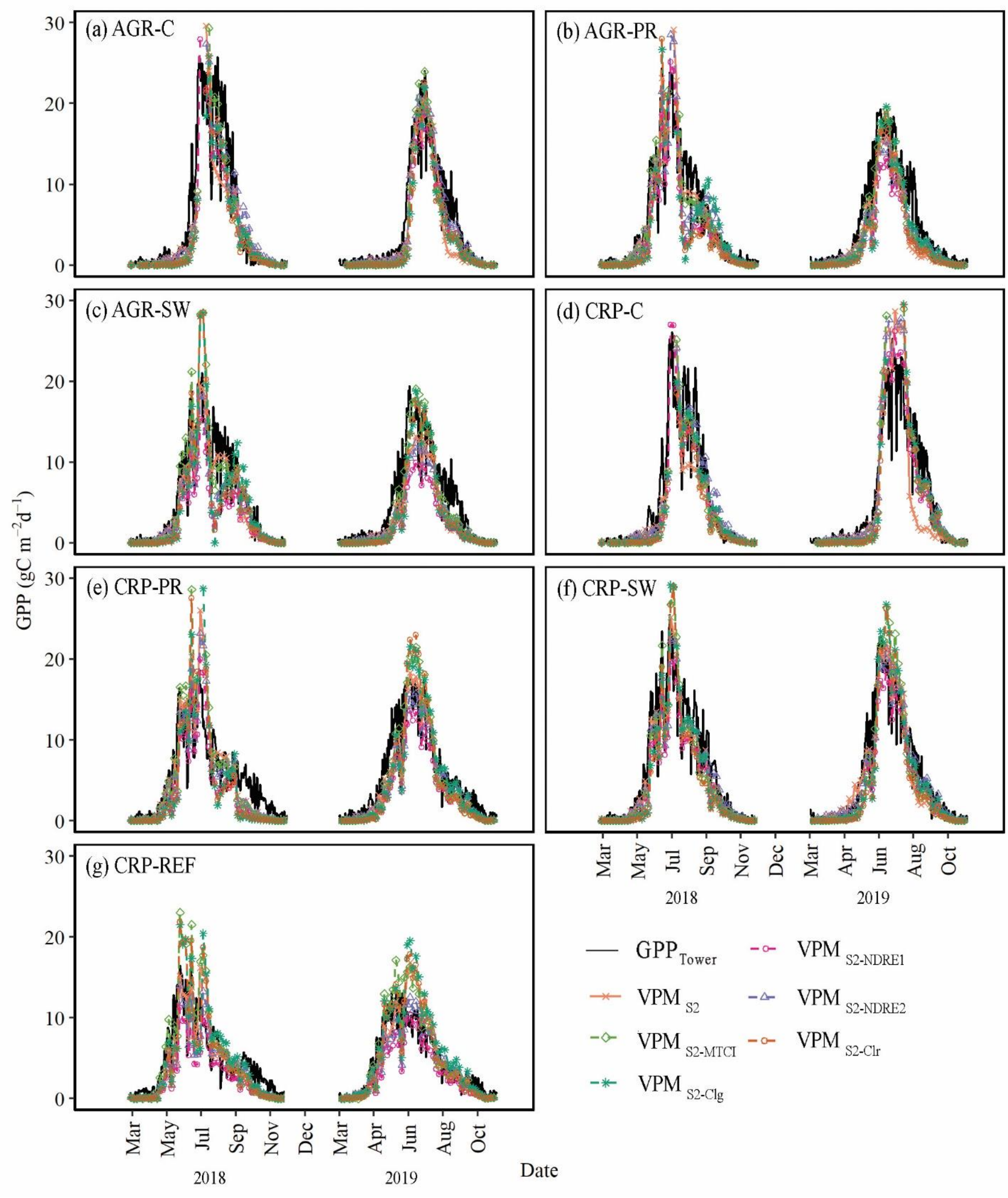

Figure 2.5. Temporal changes in GPP$_{Tower}$ and Sentinel-2 VPM RS models 2018–2019 for the seven study sites: (a) AGR-C, (b) AGR-PR, (c) AGR-SW, (d) CRP-C, (e) CRP-PR, (f) CRP-SW, and (g) CRP-REF.

During the study period, $GPP_{VPM\text{-}S2}$ estimated 5:14 site-year sums at ±10% that of GPP_{Tower} sums, whereas $GPP_{VPM\text{-}LS8}$ had 3:14, $GPP_{VPM\text{-}MODIS}$ 2:14, GPP_{MODIS} had 0:14, and GPP_{CONUS} 3:14 (Table 3). When using red-edge VIs, $VPM_{S2\text{-}NDRE1}$ models estimated 1:14, $VPM_{S2\text{-}NDRE2}$ 5:14, $VPM_{S2\text{-}MTCI}$ 6:14, $VPM_{S2\text{-}Clg}$ 4:14, and $VPM_{S2\text{-}Clr}$ had 2:14 site-year sums at ±10% that of GPP_{Tower}. Overall, Sentinel-2 VPMs were closer to the study-period sums of GPP_{Tower} than other models. Cumulative satellite GPP estimates by site-year had difference of ~9–800 g C m^{-2} from GPP_{Tower}, with an average difference of 229.69 g C m^{-2}. Models that had a site within ±10% of GPP_{Tower} in both 2018 and 2019 included $GPP_{VPM\text{-}LS8}$, $VPM_{S2\text{-}NDRE2}$, $VPM_{S2\text{-}Clr}$ for sites CRP-REF, CRP-C, and CRP-REF, respectively. Model $VPM_{S2\text{-}MTCI}$ remained within ±10% of GPP_{Tower} more often than other models including by site-year and cumulative annual GPP during the study period. GPP_{MODIS} and $VPM_{S2\text{-}NDRE1}$ underestimated all site-years, but other models overestimated occasionally, including $GPP_{VPM\text{-}LS8}$ (5:14), $GPP_{VPM\text{-}MODIS}$ (2:14), GPP_{CONUS} (4:14), $VPM_{S2\text{-}NDRE2}$ (1:14), $VPM_{S2\text{-}MTCI}$ (5:14), $VPM_{S2\text{-}Clg}$ (2:14), and $VPM_{S2\text{-}Clr}$ (2:14).

Cumulative GPP for the peak growing season (June, July, and August) indicate that $VPM_{S2\text{-}NDRE2}$ and $VPM_{S2\text{-}MTCI}$ best matched GPP_{Tower}, with 8:14 site-years within ±10% tower sums (Table 4). Non-red-edge model $GPP_{VPM\text{-}S2}$ closely followed with 7:14 site-years. When estimated by $GPP_{VPM\text{-}LS8}$ and $GPP_{VPM\text{-}S2}$ in 2018 and by $GPP_{VPM\text{-}S2}$ in 2019, cumulative GPP of all sites in the study area was within ±10% of that estimated by GPP_{Tower}. When considering red-edge models, however, $VPM_{S2\text{-}NDRE2}$, $VPM_{S2\text{-}Clg}$, and $VPM_{S2\text{-}Clr}$ are all estimated both 2018 and 2019 cumulative GPP within ±10% tower sums. However, $VPM_{S2\text{-}NDRE1}$, $VPM_{S2\text{-}NDRE2}$, $VPM_{S2\text{-}MTCI}$, $VPM_{S2\text{-}Clg}$, and $VPM_{S2\text{-}Clr}$ overestimated 1:14, 3:14, 9:14, 6:14, and 5:14 site-years, respectively. Compared to other models, $VPM_{S2\text{-}NDRE2}$ reliably estimated peak growing season cumulative GPP at individual and collective fields.

Table 2.3. March–November cumulative GPP (g C m^{-2}) as estimated from GPP_{Tower}, conventional products GPP_{MODIS} and GPP_{CONUS}, and VPM models $GPP_{VPM-MODIS}$, $GPP_{VPM-LS8}$, GPP_{VPM-S2}, $VPM_{S2-NDRE1}$, $VPM_{S2-NDRE2}$, $VPM_{S2-MTCI}$, VPM_{S2-Clg}, VPM_{S2-Clr}. Values in bold indicate ±10% of total GPP_{Tower}.

Year	SITE	GPP_{Tower}	GPP_{MODIS}	GPP_{CONUS}		GPP_{VPM-}				VPM_{S2-}		
					MODIS	*LS8*	*S2*	*NDRE1*	*NDRE2*	*MTCI*	*Clg*	*Clr*
2018	AGR-C	1598.83	1092.38	797.32	**1649.99**	1254.12	1340.96	1226.33	**1577.21**	**1597.10**	1369.89	1335.42
	AGR-PR	1554.91	1165.29	**1649.75**	1802.58	**1612.87**	**1529.12**	1124.71	**1476.40**	1786.66	**1503.21**	1345.71
	AGR-SW	1501.52	1108.52	1729.91	1241.52	1161.16	1276.53	822.97	1097.84	**1522.17**	1305.52	1218.87
	CRP-C	1417.42	1122.50	776.11	1206.72	1701.10	1184.19	1146.05	**1484.45**	**1346.03**	**1340.52**	1129.04
	CRP-PR	1469.99	1147.00	967.75	**1349.28**	1979.34	**1439.21**	1001.07	1289.68	**1592.61**	1270.01	1300.73
	CRP-REF	1327.21	1173.51	977.53	1088.91	**1341.41**	1122.34	741.01	1008.62	**1425.93**	**1343.52**	**1216.46**
	CRP-SW	1725.24	1171.74	1009.05	1152.18	1326.74	1464.69	1243.94	1519.22	1495.99	1443.48	1293.13
	Total	*10595.12*	*7980.93*	*7907.42*	*9491.18*	***10376.75***	*9357.03*	*7306.07*	*9453.42*	***10766.50***	***9576.15***	*8839.37*
2019	AGR-C	1340.88	1084.37	**1331.38**	1120.08	1075.59	1043.42	993.81	**1242.04**	1111.09	944.38	948.55
	AGR-PR	1465.36	1128.72	1717.36	1032.44	853.29	1013.46	794.34	1002.62	1109.12	1079.95	907.22
	AGR-SW	1366.86	1091.51	1838.63	795.20	1019.06	899.23	635.01	847.33	1141.78	968.39	942.40
	CRP-C	1596.14	1082.76	**1437.37**	1305.52	2031.73	**1456.51**	**1446.59**	1777.44	1888.23	1844.54	1773.22
	CRP-PR	1574.03	1077.00	975.83	1004.45	1233.13	1314.00	965.03	1225.00	1401.90	1407.05	1324.88
	CRP-REF	1265.02	1118.37	986.77	1010.13	**1227.60**	**1328.91**	846.67	1109.47	1420.46	1521.20	**1357.44**
	CRP-SW	1567.16	1128.18	1025.81	1257.41	1341.75	**1453.05**	1195.85	**1488.37**	**1443.98**	**1436.62**	1260.02
	Total	*10175.45*	*7710.90*	***9313.14***	*7525.22*	*8782.16*	*8508.59*	*6877.31*	*8692.26*	***9516.56***	***9202.13***	*8513.73*

Table 2.4. June–August cumulative GPP (g C m^{-2}) as estimated from GPP_{Tower}, conventional products GPP_{MODIS} and GPP_{CONUS}, and VPM models $GPP_{VPM\text{-}MODIS}$, $GPP_{VPM\text{-}LS8}$, $GPP_{VPM\text{-}S2}$, $VPM_{S2\text{-}NDRE1}$, $VPM_{S2\text{-}NDRE2}$, $VPM_{S2\text{-}MTCI}$, $VPM_{S2\text{-}Clg}$, $VPM_{S2\text{-}Clr}$. Values in bold indicate ±10% of total GPP_{Tower}.

Year	SITE	GPP_{Tower}	GPP_{MODIS}	GPP_{CONUS}	$GPP_{VPM\text{-}}$			$VPM_{S2\text{-}}$				
					MODIS	*LS8*	*S2*	*NDRE1*	*NDRE2*	*MTCI*	*Clg*	*Clr*
2018	AGR-C	1391.29	738.58	554.12	**1275.75**	1087.65	1131.24	1065.48	**1311.99**	**1460.64**	1225.44	1237.59
	AGR-PR	1184.43	724.16	1039.64	**1272.96**	**1278.57**	**1261.86**	902.85	**1121.71**	1505.76	**1192.06**	**1173.15**
	AGR-SW	1128.22	709.44	**1099.14**	908.67	892.78	**1022.95**	629.49	802.30	**1221.38**	993.42	983.67
	CRP-C	1209.67	722.41	539.37	880.98	1392.21	1005.68	998.37	**1232.87**	**1231.34**	**1185.96**	1042.77
	CRP-PR	904.32	732.37	540.12	**985.65**	1513.78	1117.23	807.45	1010.78	1293.86	1115.91	1144.93
	CRP-REF	729.02	**763.76**	534.06	**776.52**	952.55	**785.15**	520.92	**685.25**	986.70	928.80	876.51
	CRP-SW	1277.66	726.96	622.25	799.60	915.50	**1211.05**	1008.55	**1191.43**	**1259.59**	**1280.42**	1146.39
	Total	*7824.61*	*5117.68*	*4928.71*	*6900.13*	***8033.04***	***7535.16***	*5933.11*	***7356.32***	*8959.27*	***7922.01***	***7605.01***
2019	AGR-C	1054.59	721.68	**975.09**	816.75	904.75	**959.19**	844.38	**1034.79**	**976.78**	827.65	826.75
	AGR-PR	1166.85	711.91	**1067.32**	765.72	694.01	883.87	689.71	830.63	980.70	937.14	825.34
	AGR-SW	1043.18	710.13	1148.15	575.12	788.09	771.31	549.22	694.11	**1008.74**	874.31	851.93
	CRP-C	1198.79	677.43	1052.35	887.20	1542.26	1344.60	**1218.03**	1466.30	1630.16	1567.92	1519.85
	CRP-PR	1092.92	699.95	561.12	724.21	883.75	**1047.35**	780.58	943.20	**1170.22**	**1143.78**	**1148.72**
	CRP-REF	770.39	**722.25**	545.17	**723.68**	878.22	964.54	605.65	**767.94**	991.55	1054.68	985.61
	CRP-SW	1263.43	735.01	637.43	911.20	889.86	**1226.98**	1024.97	**1214.15**	**1293.07**	**1245.41**	**1138.83**
	Total	*7590.15*	*4978.37*	*5986.63*	*5403.88*	*6580.95*	***7197.84***	*5712.54*	***6951.12***	***8051.22***	***7650.90***	***7297.05***

Model validation

In all site years, the finer resolution $GPP_{VPM\text{-}S2}$ and $GPP_{VPM\text{-}LS8}$ out-performed GPP_{MODIS}, GPP_{CONUS} and $GPP_{VPM\text{-}MODIS}$ (Figs. 2.6, 2.7, Table A5) and agreed the best with GPP_{Tower}. Each model had a significant (p<0.05) and strong positive trend with GPP_{Tower} in 2018 and 2019. The largest variation found in model estimates were in corn systems for both years and prairie systems in 2018. $GPP_{VPM\text{-}MODIS}$, GPP_{MODIS} and GPP_{CONUS} models underestimated; and $GPP_{VPM\text{-}S2}$ and $GPP_{VPM\text{-}LS8}$ models aligned best with the 1:1 slope, except for overestimation for CRP-C 2019 and CRP-PR 2018. In CRP-REF, all models were in close agreement with GPP_{Tower}. In both years, GPP_{MODIS} and GPP_{CONUS} had the highest RMSE in corn and switchgrass systems, as well as AGR-PR. In all sites, VPM models had lower RMSE than conventional products GPP_{MODIS} and GPP_{CONUS} except for CRP-REF (both years) and CRP-PR (2018) (Fig. 2.8). Compared to $GPP_{VPM\text{-}S2}$, RMSE at corn sites was lower for $GPP_{VPM\text{-}LS8}$ for both years and lower for $GPP_{VPM\text{-}MODIS}$ in 3:4 site-years.

When considering enhancements from red-edge VIs in VPM, the NDRE1 and NDRE2 VIs increase explanation of variability in eight out of fourteen site-years. While RMSE values of red-edge VPMs were often higher in 2018 than that of the EVI2-based $GPP_{VPM\text{-}S2}$, they were near equal in 2019 (Table A5, Figs. 2.8, 2.9). Sites that benefitted in both years from red-edge VPMs included AGR-C, CRP-C, and CRP-SW; whereas AGR-PR and AGR-SW only saw benefits in 2019. While both NDRE1 and NDRE2 improve AGR-C in both years and CRP-C in 2018 by the same explanation of variance, NDRE1 has a lower RMSE in all three site-years and a closer 1:1 slope in two of three site years.

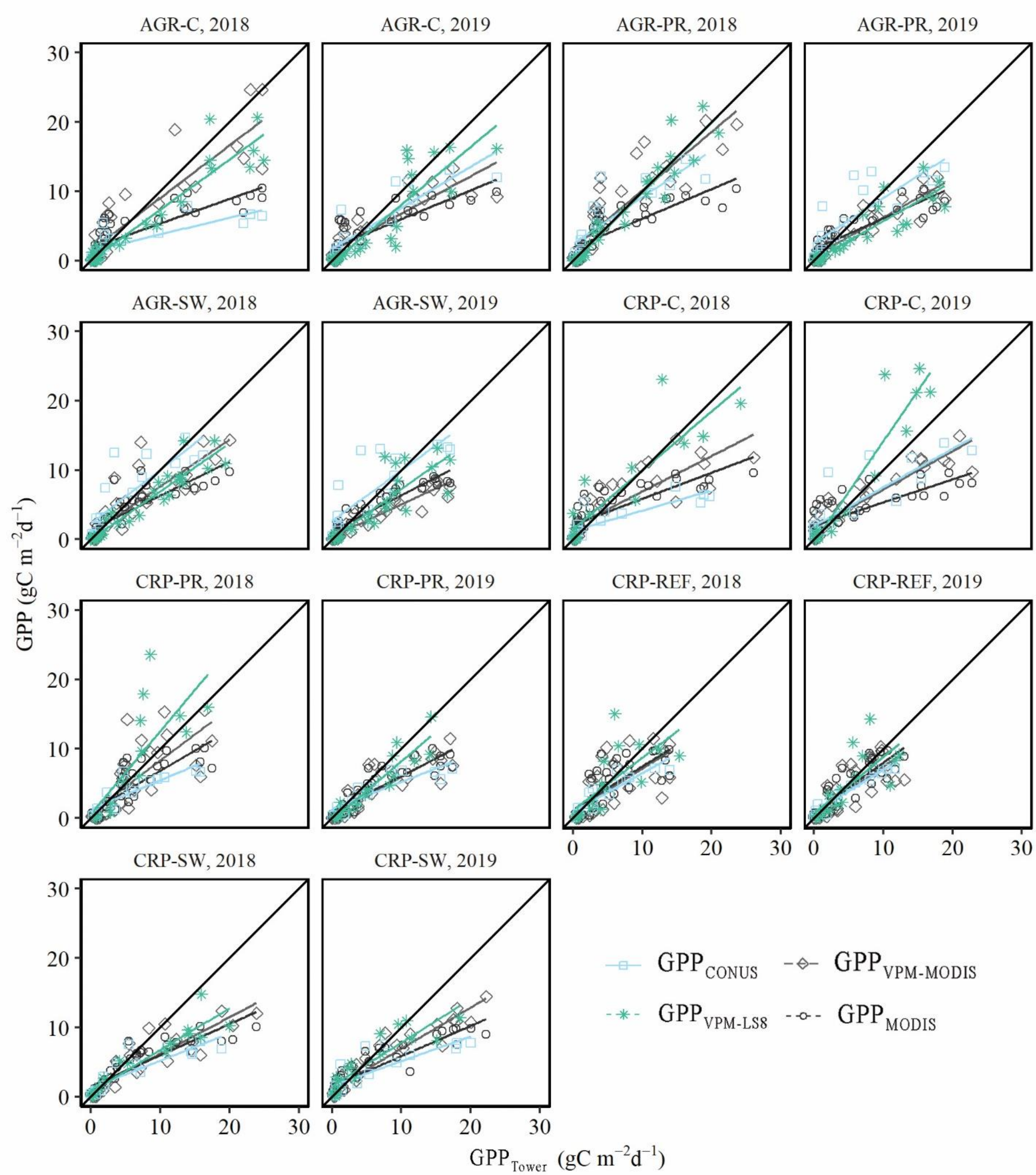

Figure 2.6. Comparison of daily GPP$_{Tower}$ with daily $_{LS8}$, GPP$_{VPM-MODIS}$, GPP$_{MODIS}$, and GPP$_{CONUS}$ by site-year. Solid black line depicts a 1:1 relationship.

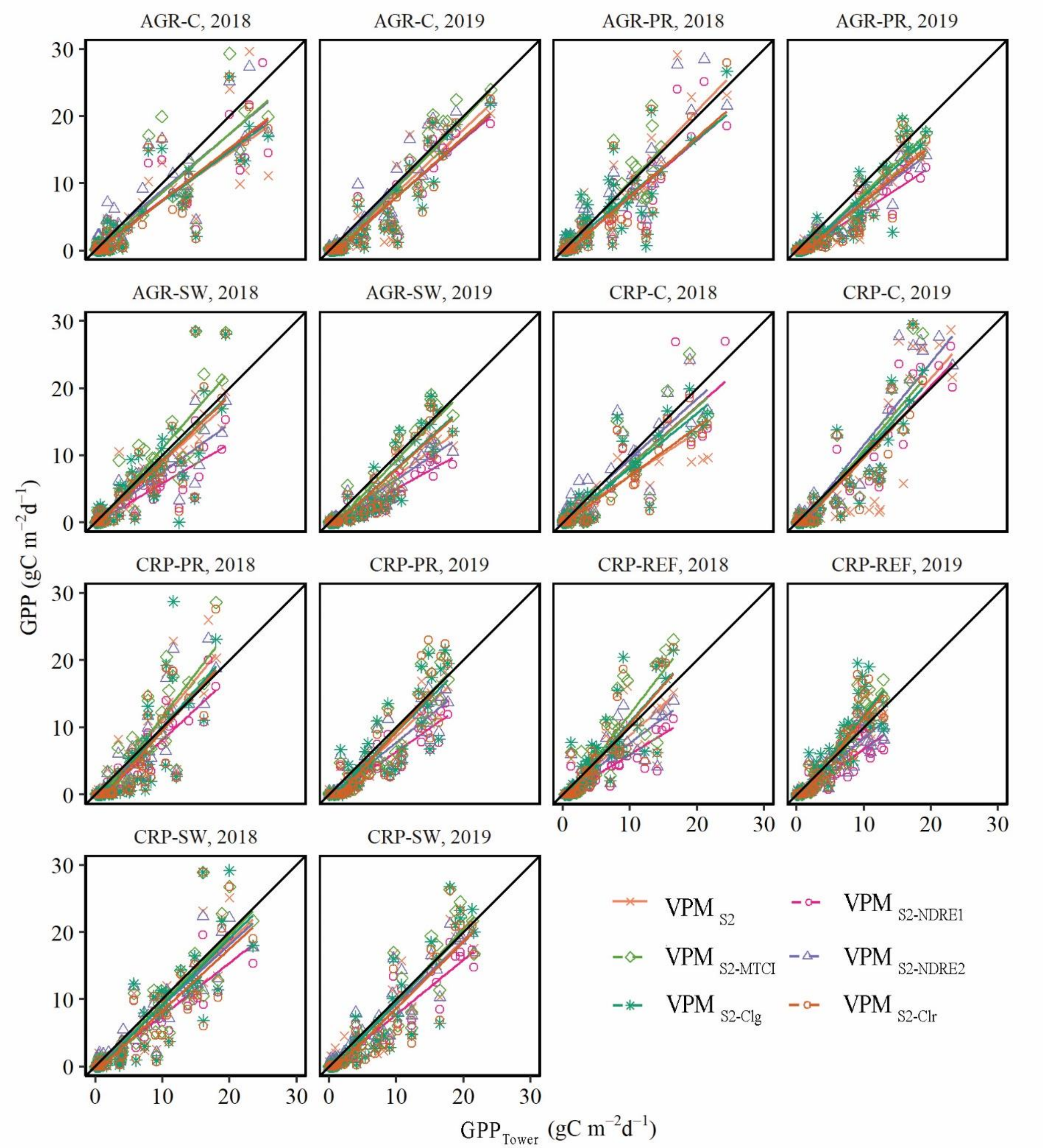

Figure 2.7. Comparison of daily GPP$_{Tower}$ with daily VPM$_{S2\text{-}MTCI}$, VPM$_{S2\text{-}Clg}$, VPM$_{S2\text{-}Clr}$, VPM$_{S2\text{-}NDRE1}$, and VPM$_{S2\text{-}NDRE2}$ by site-year. Solid black line depicts a 1:1 relationship.

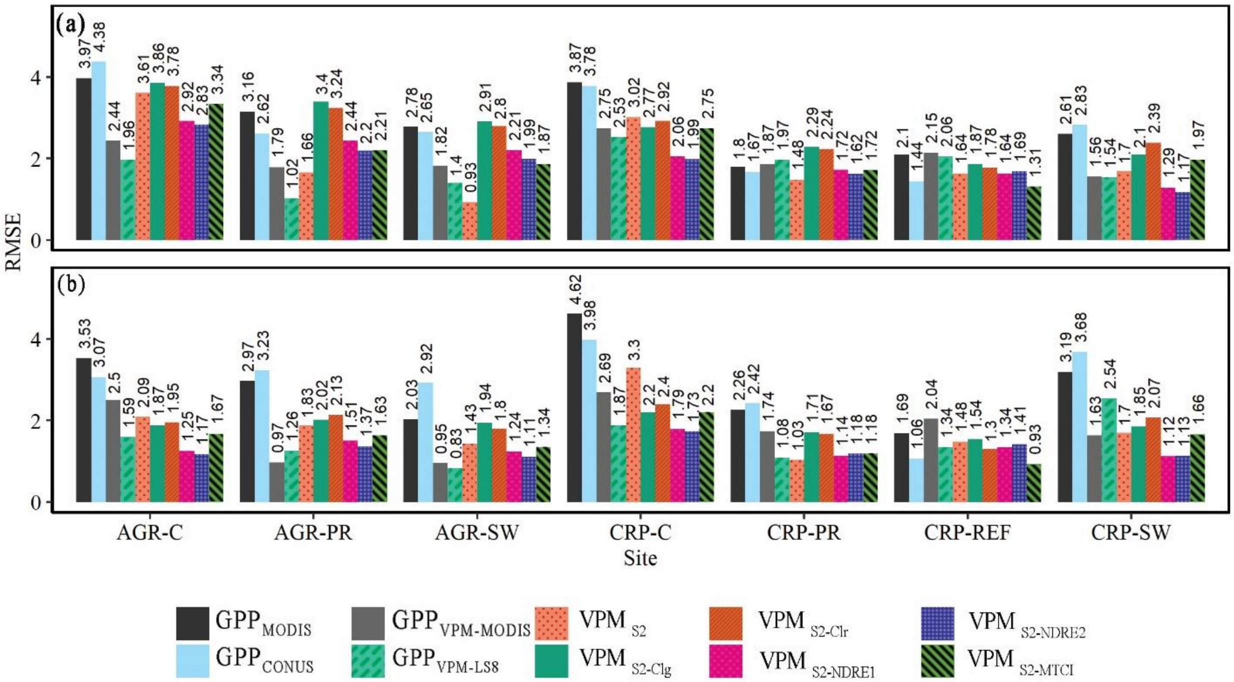

Figure 2.8. Comparison model RMSE (g C m-2 d-1) of daily GPPTower with daily remote sensing GPP models across the seven land cover types in (a) 2018 and (b) 2019.

GPP estimates are significantly different between models at all sites, except CRP-PR, according to the Kruskal-Wallis rank sum test ($p < 0.05$) (Fig. 2.9). A pair-wise post-hoc Dunn test demonstrated that in site AGR-C, significant differences were found between pairs GPP_{MODIS}:$VPM_{S2\text{-}Clr}$ and GPP_{MODIS}:$VPM_{S2\text{-}Clg}$ (z= 3.92, p=0.004; z= 3.66, p=0.01, respectively); while CRP-C had differences between GPP_{MODIS}:$VPM_{S2\text{-}Clr}$ (z= 3.62, p=0.01). In sites CRP-PR, CRP-REF, CRP-SW, AGR-PR and AGR-SW, there were no significant ($p < 0.05$) differences between model pairs.

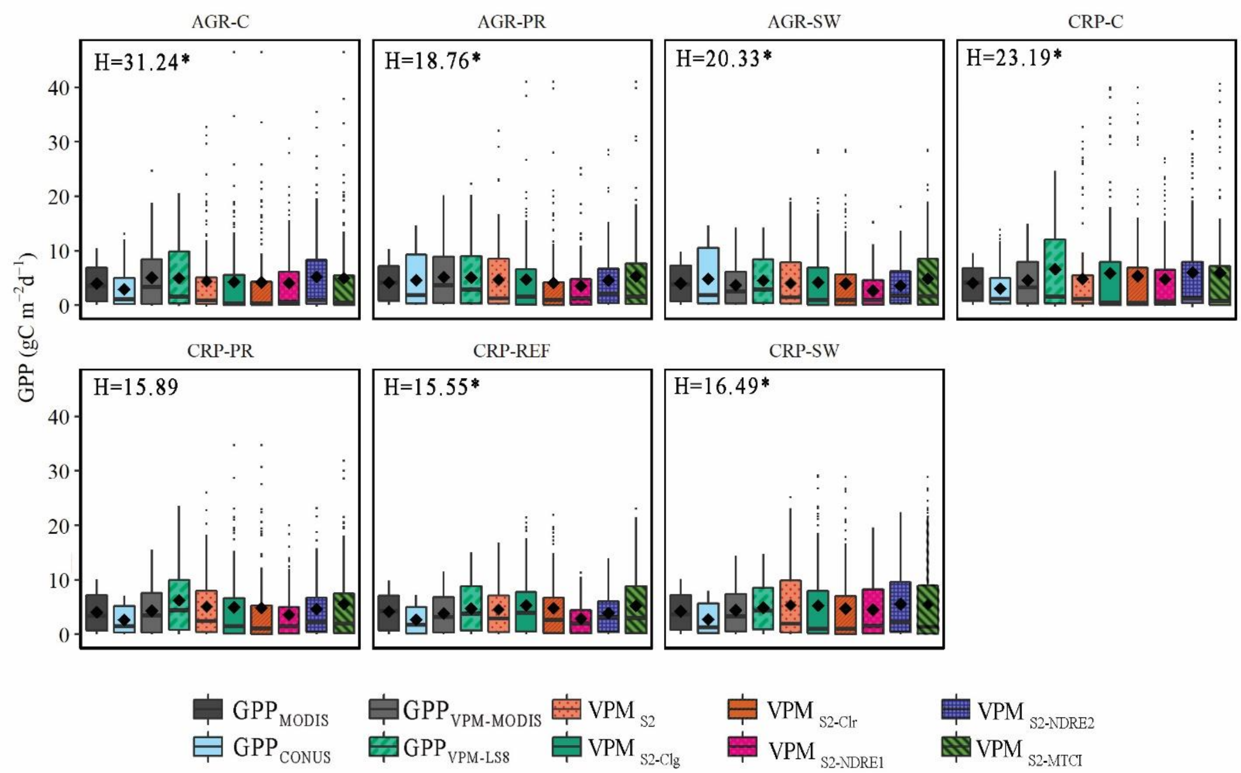

Figure 2.9. Box-plot comparisons of GPP models by land cover type during 2018–2019. Inside the boxplot, a black diamond indicates the mean, error bars mean standard error, and a black horizontal line depicts the median; outside the boxplot, whiskers indicate the maximum and minimum values and points indicate outliers. Results of the Kruskal-Wallis include *H* and is interpreted as chi-square. A significant *p*-value <0.05 is indicated with an *.

GPP anomaly estimates

We evaluated anomalies generated from each GPP model from seasonal means and found large anomalies existed in the peak growing seasons (June-August) (Fig. 2.10, 2.11). GPP_{Tower} anomalies in regression analysis demonstrated that $GPP_{VPM\text{-}S2}$ exhibited the highest positive trend out of conventional models, with a significant relationship (p<0.05) in switchgrass and prairie systems but was second to $GPP_{VPM\text{-}LS8}$ at the corn systems. CRP-REF anomalies did not match well with any model, evidenced by insignificant, positive trends (Fig. A2, A3, Table A6). In red-edge VPMs, we found that most anomalies occurred during peak growing season due to models $VPM_{S2\text{-}MTCI}$, $VPM_{S2\text{-}CIr}$, and $VPM_{S2\text{-}CIg}$, which overestimated GPP in 2018 site-years and in CRP-C 2019. Generally, $VPM_{S2\text{-}NDRE1}$ and $VPM_{S2\text{-}NDRE2}$ did not overestimate, except for CRP-C 2019, and had more underestimating outliers.

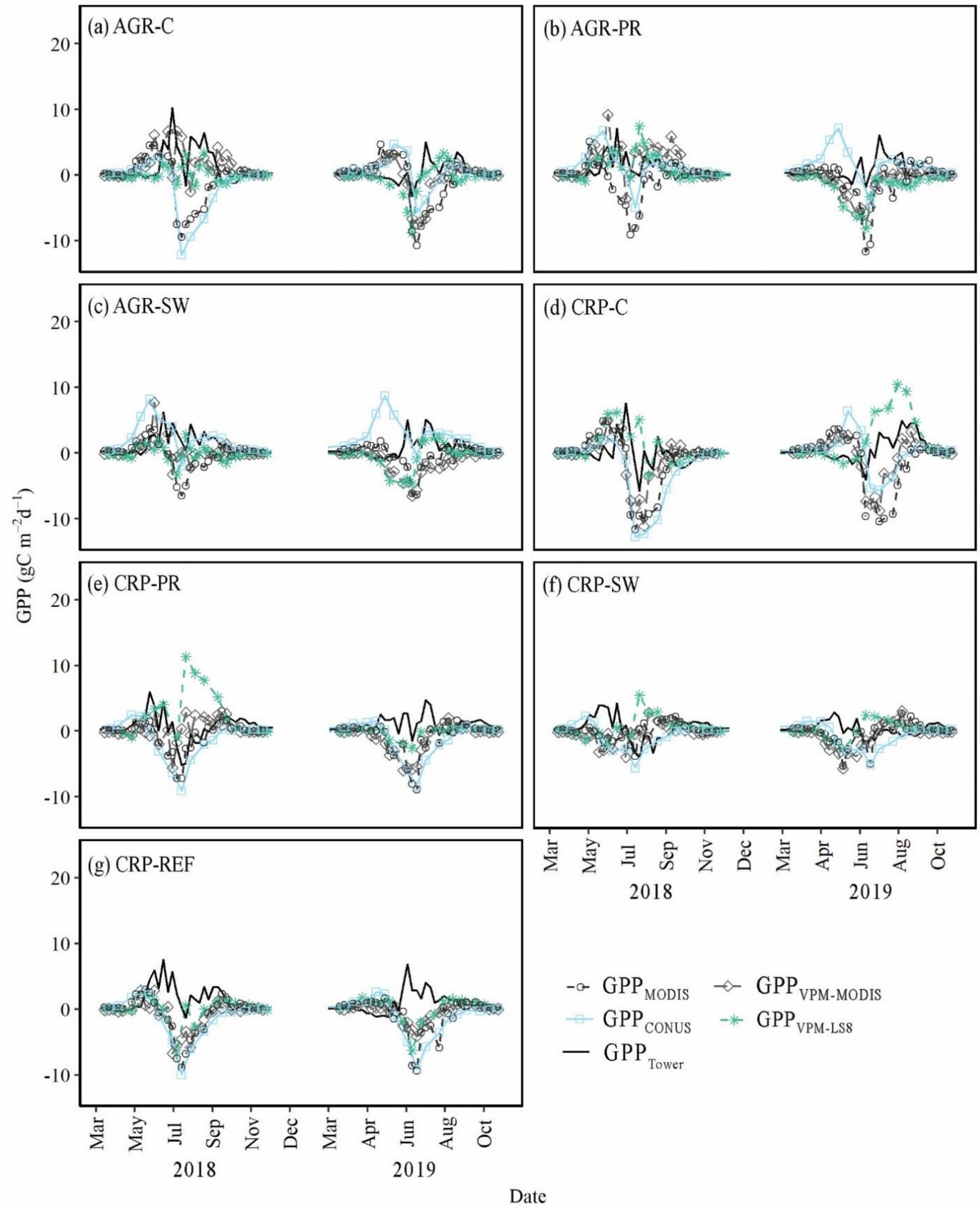

Figure 2.10. Anomalies of GPP (g C m^{-2} d^{-1}) from GPP_{MODIS}, GPP_{CONUS}, $GPP_{VPM\text{-}MODIS}$ and $GPP_{VPM\text{-}LS8}$ over time for the seven study sites: (a) AGR-C, (b) AGR-PR, (c) AGR-SW, (d) CRP-C, (e) CRP-PR, (f) CRP-REF, and (g) CRP-SW.

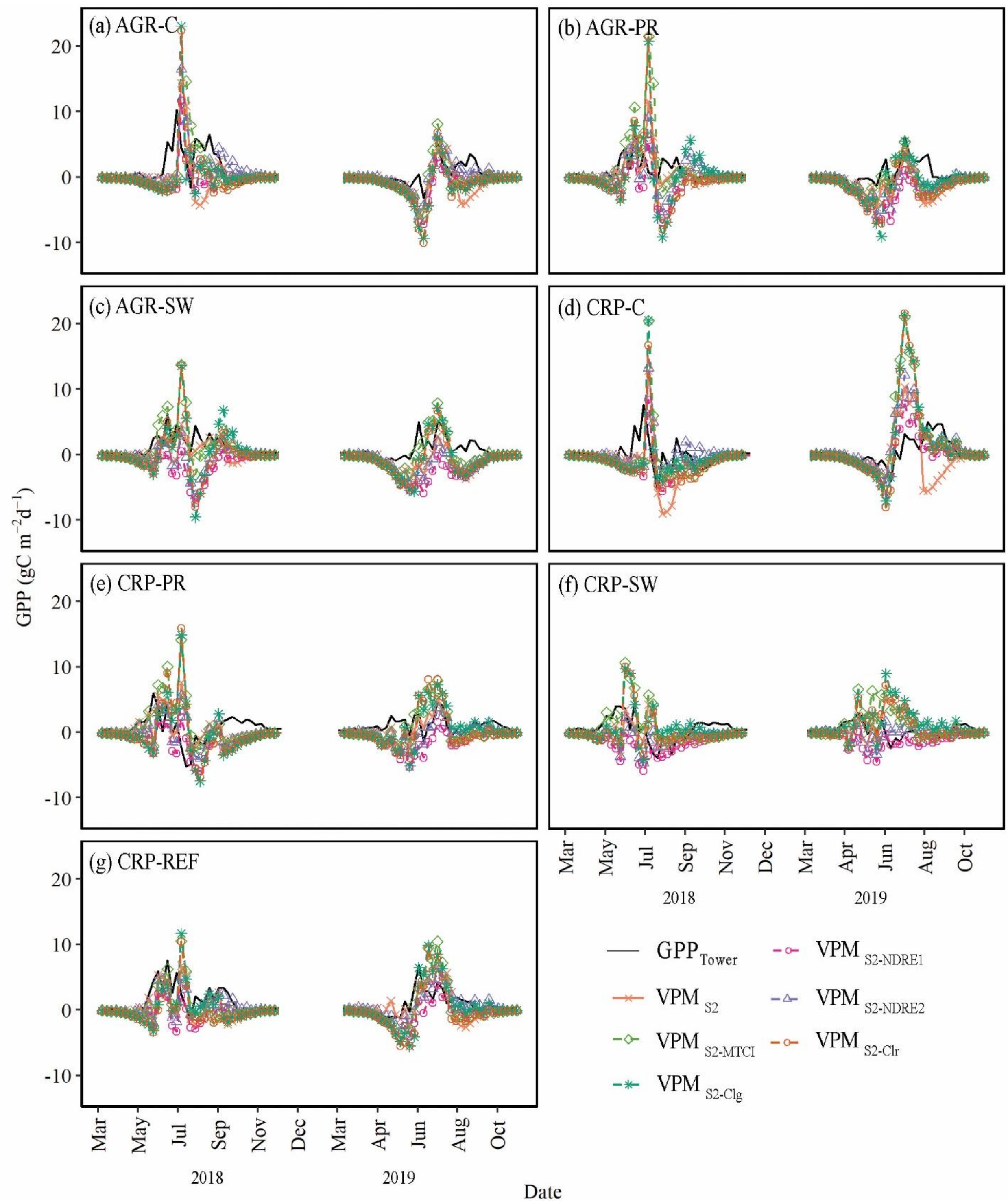

Figure 2.11. Anomalies of GPP (g C m^{-2} d^{-1}) from GPP$_{VPM\text{-}S2}$, VPM$_{S2\text{-}Clg}$, VPM$_{S2\text{-}Clr}$, VPM$_{S2\text{-}NDRE1}$, VPM$_{S2\text{-}NDRE2}$, VPM$_{S2\text{-}MTCI}$ over time for the seven study sites: (a) AGR-C, (b) AGR-PR, (c) AGR-SW, (d) CRP-C, (e) CRP-PR, (f) CRP-REF, and (g) CRP-SW.

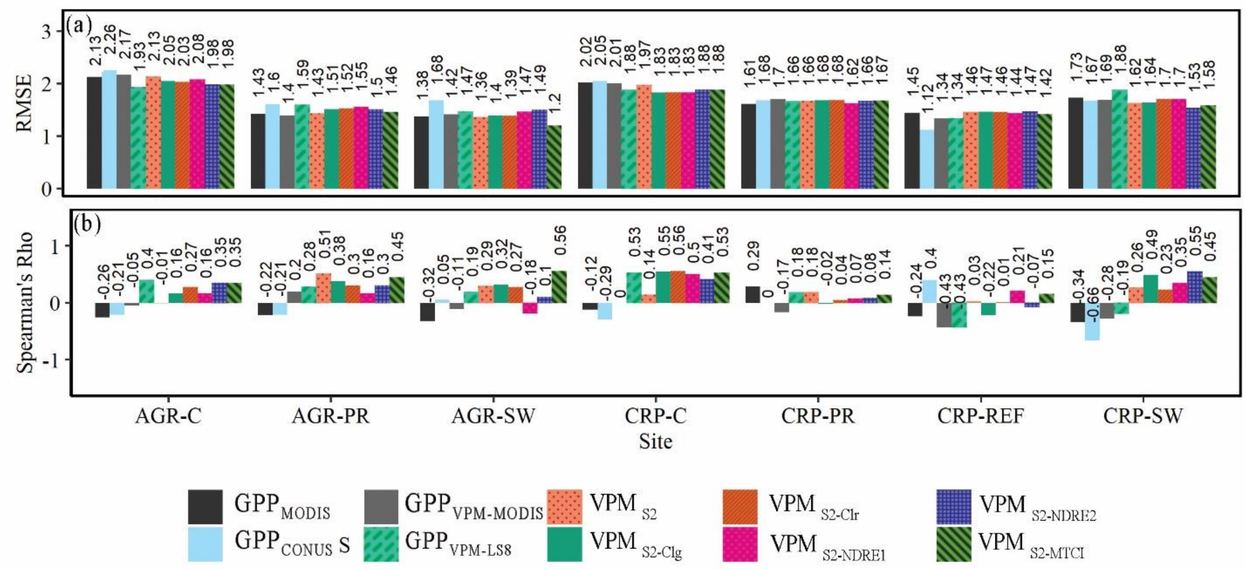

Figure 2.12. Comparison of anomaly model RMSE (g C m-2 d-1) and Spearman's Rho (ρ) coefficients of daily GPPTower with daily GPP from all remote sensing models across the seven land cover types 2018–2019.

Anomalies exhibited both positive and negative trends compared to GPP_{Tower}, with fine-resolution VPMs outperforming conventional models. Red-edge VPMs had strong, positive trend at the exception of sites AGR-SW ($VPM_{S2\text{-}NDRE1}$) and CRP-REF ($VPM_{S2\text{-}Clg}$, $VPM_{S2\text{-}NDRE2}$). $GPP_{VPM\text{-}LS8}$ exhibited the strongest, positive trend and the lowest RMSE in corn sites between conventional models and $GPP_{VPM\text{-}S2}$, whereas $GPP_{VPM\text{-}S2}$ exhibited this for remaining sites, except CRP-REF (Fig. 2.12). In red-edge models, the lowest RMSE was $VPM_{S2\text{-}MTCI}$ in AGR-C, AGR-PR, and AGR-SW; and variable in remaining sites. Sites, AGR-C, CRP-C and CRP-SW tend to have higher RMSEs. Conventional GPP_{CONUS} and GPP_{MODIS} had negative trends, except for GPP_{MODIS} in CRP-PR (ρ=0.30) and $GPP_{VPM\text{-}S2}$ in AGR-SW (ρ=0.02) and CRP-REF (ρ=0.40). Similarly, $GPP_{VPM\text{-}MODIS}$ had a negative or zero trend in all sites except for AGR-PR (ρ=0.20).

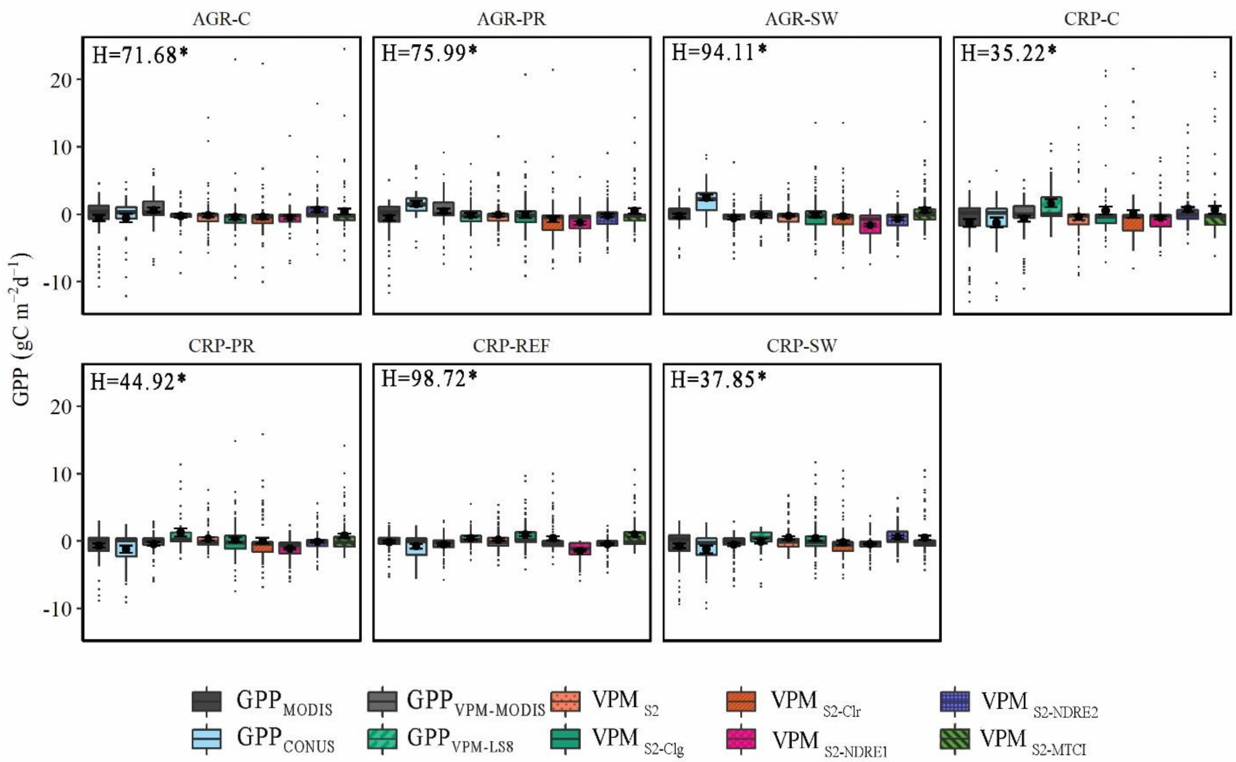

Figure 2.13. Box-plot comparisons of GPP (g C m^{-2} d^{-1}) anomalies by model at seven land cover type during 2018–2019. Inside the boxplot, a black circle indicates the mean, error bars are mean standard error, and a black horizontal line depicts the median; outside the boxplot, whiskers indicate the maximum and minimum values and points indicate outliers. Results of the Kruskal-Wallis include *H*, which is interpreted as chi-square, and significance *p*-value <0.05 is indicated with an asterisk (*).

Significant differences exist between anomaly GPP models at each site, according to the Kruskal-Wallis rank test (Fig. 2.13). The site with the greatest variance from the mean was CRP-C. From the pairwise comparison Dunn test (Table 2.5), we also observed that a significant difference in anomaly medians between GPP_{Tower} and $GPP_{VPM\text{-}S2}$ exist in five sites, including AGR-C, AGR-PR, AGR-SW, CRP-PR, and CRP-SW. Significant differences also existed between GPP_{Tower} and $GPP_{VPM\text{-}LS8}$ at AGR-PR and AGR-SW, as well as between $GPP_{VPM\text{-}LS8}$ and $GPP_{VPM\text{-}S2}$ in CRP-C. The fewest differences between red-edge VPMs and GPP_{Tower} were with $VPM_{S2\text{-}NDRE2}$ (AGR-PR, AGR-SW, CRP-PR, CRP-REF) and $VPM_{S2\text{-}MTCI}$ (AGR-C, AGR-SW, CRP-PR, CRP-REF); and the highest was with VPMS2-Clr, which was significantly different in seven sites. $VPM_{S2\text{-}NDRE2}$ and $VPM_{S2\text{-}MTCI}$ also had the fewest differences between other models.

Table 2.5. Dunn test pairwise comparison of significant differences (*p*<0.05) between models at each site 2018–2019 for GPP anomalies.

	GPP CONUS	GPP MODIS	GPP VPM-MODIS	GPP VPM-LS8	GPP VPM-S2	VPM S2-Clg	VPM S2-Clr	VPM S2-NDRE1	VPM S2-NDRE2	VPM S2-MTCI	GPP Tower
GPP CONUS	-	-	-	-	-	-	-	-	-	-	-
GPP MODIS	□□	-	-	-	-	-	-	-	-	-	-
GPP VPM-MODIS	□□		-	-	-	-	-	-	-	-	-
GPP VPM-LS8	⁕□			-	-	-	-	-	-	-	-
GPP VPM-S2	⁕□		▲▲	Δ	-	-	-	-	-	-	-
VPM S2-Clg	⁕□	▲	▲♦			-	-	-	-	-	-
VPM S2-Clr	▲⁕□	▲⁕	▲⁕	Δ■○			-	-	-	-	-
VPM S2-NDRE1	⁕□♦	▲⁕□ ■♦	▲⁕□ ■♦	□ Δ■♦	□■♦	□■♦	♦	-	-	-	-
VPM S2-NDRE2	⁕□					▲♦	▲○	▲■♦ ○	-	-	-
VPM S2-MTCI	⁕□		▲					□■♦		-	-
GPP Tower	■○■ ○	■♦○ ■♦○	□■○□ ■○	⁕□	▲⁕□ ■○▲⁕ □■○	▲⁕□ ■○	▲⁕□ Δ■♦○	▲⁕□ ■♦○	⁕□■♦	▲□■ ○	-

Sites: □: AGR-SW, ○: CRP-SW, ♦: CRP-REF, ■: CRP-PR, ⁕: AGR-PR, ▲: AGR-C, Δ: CRP-C

Discussion

While VPM developed using MODIS products still provides a valuable product that is widely available spatially and temporally, complex, and heterogeneous land cover types such as managed agricultural-prairie landscapes benefit from the use of finer spatial resolution imagery (Chen et al., 2019). Fine spatial resolution reflectance indices from Sentinel-2 and Landsat-8 increased the accuracy of VPM models in our study. Particularly, when red-edge

VIs replaces EVI2 in Sentinel 2 VPMs, we found improvements in model validation, cumulative GPP estimates, and fewer differences between GPP_{Tower} medians than that of GPP_{VPM-S2}.

Sensitivity of VIs EVI2 and NDVI to GPP_{Tower} differed between MODIS (500 m) and the finer resolutions of Landsat-8 (30 m) or Sentinel-2 (20 m). When selecting between the two in agricultural-prairie systems, it is prudent to use EVI2. For finer resolution VPMs, NDVI may be suitable upon further study. MODIS had high sensitivity to EVI2 in 13:14 site years than NDVI, of which only 2:14 site-years had sensitivity ±0.10 of 1.00 (i.e., near equal sensitivity). We find this supports similar research on MODIS LUE-based GPP models, where the ability to capture GPP variations is closely tied to the accuracy of *f*PAR and that 8-day MODIS data do not consistently capture fall and spring's rapid changes in phenology, likely introducing error to annual GPP estimates (Verma et al., 2014). Conversely, near-equal sensitivity was apparent in Landsat-8 and Sentinel-2, with 9:14 and 12:14 site-years with sensitivities ±0.10 of 1, respectively. Given EVI2 and NDVI use the same two bands (i.e., NIR, Red), the differences between satellite products could arise from differences in radiometric resolution (i.e., bandwidth), spatial resolution and sampling frequency. In fact, the wavelength ranges of MODIS, Landsat-8, and Sentinel-2 Red bands (nm) are 620–670, 636-673, 650-680, respectively; while the NIR bands are 841–875, 851-879, and 855-875, respectively. These slight differences in bandwidth, along with differences in sampling dates and spatial resolution from Landsat-8 and Sentinel-2, may have resulted in substantial differences in GPP estimates. We found that NDRE1 and NDRE2 were slightly more sensitive than EVI2 to GPP_{Tower}, with 8:14 site years, that MTCI was near-equal sensitive, and that EVI2 was more sensitive to GPP_{Tower} than Clr and Clg. Both sensitivities of pairs (1) NDRE1 and NDRE2; and (2) Clr and Clg were similar, respectively, as the equations are similar and the difference within each pair is minimal (Eqs. 2.4-2.7).

GPP estimates in our study area, and many other Midwestern cropland regions, are notably underestimated by MODIS products, due to mixed pixels (Wang et al., 2015; Zhang et al., 2016). We found that land cover (NLCD, 30 m) within a single MODIS 500 m pixel overlapped cropland, developed areas, forests, grasslands and wetlands (Table A3). Our results demonstrated that $GPP_{VPM\text{-}MODIS}$ underestimated, particularly in the peak growing season, at all sites, more than other GPP models. The least to underestimate cumulative GPP includes $VPM_{S2\text{-}MTCI}$ during the study period (9:14) and peak growing season (5:14), and $VPM_{S2\text{-}Clg}$ in the peak growing season (8:14). When comparing conventional and non-red-edge VPMs, finer resolution VPM models are closer to daily and cumulative GPP_{Tower}, with $GPP_{VPM\text{-}LS8}$ capturing the variation in corn systems best and $GPP_{VPM\text{-}S2}$ best capturing grassland systems. Additionally, heavy rainfall in the spring of 2019 (wet year) may have affected GPP production in some sites. Peak growing season (June-August) was best reflected in $GPP_{VPM\text{-}S2}$ compared to other conventional GPP products and $GPP_{VPM\text{-}LS8}$. While over- and underestimation can interfere with scaled-up estimates (Jelinski & Wu, 1996) we found finer resolution (30 m and 20 m) GPP products demonstrated the capacity to improve GPP estimates across various corn and grassland systems.

Our anomaly analysis of covariance further enhanced our ability to evaluate interannual variation and identify significant differences between model estimates. In a similar study, covariance between interannual anomalies in MODIS products did not significantly correlate with GPP_{Tower} in croplands; however, few MODIS products except VPM and MOD17A did explain substantial variance in grasslands because they include finer meteorological inputs and account for rapid development and senescence (Verma et al., 2014). Our results reflect this, as GPP_{MODIS} and $GPP_{VPM\text{-}MODIS}$ did not significantly correlate with GPP_{Tower} anomalies. We found significant differences in medians between $GPP_{VPM\text{-}S2}$, $GPP_{VPM\text{-}LS8}$ and GPP_{Tower} anomalies existed, indicating that one model simply over- or underestimated more often than its counterpart. While significant differences between medians in high-resolution and red-edge VPMs and GPP_{Tower} exist, we do not believe this undermines their demonstrated accuracy in regression analysis and in seasonal summations. Particularly, anomalies of GPP_{Tower} also have significant differences from GPP_{MODIS} and $GPP_{VPM\text{-}MODIS}$ medians at three sites, and significant differences with $GPP_{VPM\text{-}LS8}$ and GPP_{CONUS} at two sites, whereas it has significant differences with $VPM_{S2\text{-}NDRE2}$ and $VPM_{S2\text{-}MTCI}$ at four sites. Understanding that MODIS products underestimate GPP (Tables 2.3, 2.4) and aggregate nearby land covers, we recommend Landsat-8 and Sentinel-2 GPP products. More so, Sentinel-2 VPMs demonstrate greater ability than Landsat-8 products to remain within ±0.10% of both cumulative study period and peak growing season GPP_{Tower}; with red-edge $VPM_{S2\text{-}NDRE2}$ and $VPM_{S2\text{-}MTCI}$ equal to or outperforming $GPP_{VPM\text{-}S2}$, respectively.

From both regression analyses in this study, $GPP_{VPM\text{-}LS8}$ still agreed strongest with corn systems compared to $GPP_{VPM\text{-}S2}$, which performed better in grassland systems with its largest anomalies during the peak growing season. However, when incorporating NDRE2 into the Sentinel-2 VPM, it could outperform $GPP_{VPM\text{-}LS8}$ in CRP-C site-years; demonstrating a potential to use red-edge VI with high-resolution imagery in both corn and grassland covers. The only site years where $GPP_{VPM\text{-}S2}$ still outperforms all other models, including red-edge VI VPMs, was in AGR-SW 2018 and in CRP-PR 2018 and 2019, where there are narrow differences (Table A5). We conclude that red-edge VIs, particularly NDRE2, may significantly improve the VPM's ability to estimate variations in GPP when used as an alternative to EVI2.

While our study area benefitted from finer resolution models, this may not stand true in all landscapes and elsewhere. In Nordic eddy covariance flux measurement sites, modelled GPP with linear regression and EVI2 and various environmental inputs detected a minimal difference with a consistent estimate across MODIS (500 m and 250 m) and Sentinel-2 (10 m) resolutions (Cai et al., 2021). An additional consideration for future studies is GPP production from cover crops, which is a customary practice that may influence variability in annual estimates. The choice of GPP product depends on the intended application. Here, we advocate for fine-resolution imagery and the consideration of red-edge in GPP models to capture details at a local-scale that reflects land management and activities in heterogeneous cropland land. However, Landsat provides data since 1972 and offers great historical detail far beyond what Sentinel 2 can offer and may be more suitable for investigations of long-term change. Additionally, further consideration may be placed on temporal resolution, which imparts its own effect on aggregation of disturbance or land management useful for scaling investigations. Differences between Landsat and MODIS data lies in the acquisition and data retrieval, where Landsat is instantaneous and at higher risk of acquiring poor *f*PAR or LAI due to atmospheric effects and cloud cover and MODIS is a composite taking the best image from an 8-day span (Robinson et al., 2018). Future investigations on resolution and GPP estimates may consider utilizing the newly release MOD17A3HGF v061product, which may provide different results due to its updated protocol that cleans poor-quality inputs from 8-day LAI/ *f*PAR based on pixel quality control labels. Additionally, the MODIS GPP product FluxSat v2.0 offers daily estimates of

GPP using FLUXNET eddy covariance tower site data and coincident satellite data (Joiner & Yoshida, 2021).

While EC methods provide direct and suitable estimates of CO_2 fluxes at the local scale useful to both calibration and validation of remote sensing GPP models, we acknowledge they are also subject to error and uncertainty that are important to validation of remote sensing models and interannual analysis (Wang et al., 2015). Recent studies show that the flux tower footprint, used in validation and site-specific measurements, often extends beyond the target ecosystem, depending on time and atmospheric conditions (e.g., wind speed and direction) (Chu et al., 2021; Giannico et al., 2018). Consequently, in highly heterogeneous landscapes, multiple EC towers may be required to capture spatial representativeness necessary for validating global scale model grids (Wang et al., 2015). Our results support this, as GPP_{MODIS} and $GPP_{VPM\text{-}MODIS}$ underestimated cumulative GPP as well as daily estimates during the study period and growing season (June, July, August).

Evaluation and monitoring of GPP with Landsat-8 and Sentinel-2 reveals how terrestrial C responds to land management, climate mitigation policies, and disturbance in heterogeneous cropland systems. It also supports cost-effective land management programs and increases the understanding of anthropogenic disturbances to ecosystem functions. Both Landsat-8 and Sentinel-2 are available freely online and easily accessible via Google Earth Engine, improving their employability in policy and stakeholder programs. For example, the economic benefit of management and incentive programs that attract farmers to convert low-producing corn for ethanol to perennial grasses, such as switchgrass, produce co-benefits, such as C sequestration (Kreig et al., 2021). Future applications with red-edge imagery from Sentinel 2 will benefit from high spatial and temporal resolution data, paving a way towards near real-time monitoring of GPP.

Conclusions

Fine-resolution (30 m and 20 m) satellite imagery and red-edge VIs integrated within VPM generally agree with daily and cumulative GPP_{Tower} in field sites more so than coarse resolution imagery in VPM or conventional GPP products (e.g., GPP_{MODIS} or GPP_{CONUS}) do. A substitution of a red-edge VI for EVI2 in the Sentinel 2 VPMs demonstrated improved explanations of variation and cumulative GPP estimates, compared to EVI2-based GPP_{VPM-S2}.

In this work, vegetation indices of EVI2 and NDVI express different sensitivities by satellite origin, where MODIS-derived EVI2 had higher sensitivity than NDVI to GPP_{Tower} in all but one site; and Landsat-8 and Sentinel-2 EVI2 and NDVI had near equal sensitivity in most site-years. Compared to EVI2, red-edge VIs NDRE1 and NDRE2 were slightly more sensitive to GPP_{Tower}. Seasonal GPP amplitude and growing season peaks are best captured by Sentinel-2 VPMs, followed by $GPP_{VPM-LS8}$, whereas conventional products underestimate growing season peaks. Overall, Sentinel-2 VPMs demonstrate greater ability than Landsat-8 and MODIS products to remain within ±0.10% of both cumulative study period and peak growing season GPP_{Tower}; with red-edge $VPM_{S2-NDRE2}$ and $VPM_{S2-MTCI}$ equal to or outperforming GPP_{VPM-S2}, respectively. Red-edge Sentinel 2 VPMs collectively outperformed conventional GPP models and Landsat 8 products, when considering cumulative GPP estimates, model validations and significant differences between anomaly medians. Red-edge VIs, particularly NDRE2, may significantly improve our ability to estimate variations in GPP when used as an alternative to EVI2 in GPP models.

As many croplands are composed of areas less than 500 m, MODIS derived scalars may be composed of a mix of land cover types and therefore incorrectly estimate GPP. This work demonstrated the capability of using $GPP_{VPM-LS8}$, GPP_{VPM-S2} and red-edge VPM_{S2-CIr}, VPM_{S2-CIg}, $VPM_{S2-NDRE1}$, $VPM_{S2-NDRE2}$, $VPMS_{2-MTCI}$ in highly heterogeneous cropland, including corn, switchgrass, and restored prairie systems, in both historical cropland and recently converted (i.e., 2009) CRP land. Fine resolution GPP products (30 m and 20 m), and particularly red-edge Sentinel 2 VPMs, agreed best with GPPTower and are significantly different than MODIS products in multiple cropland sites with differing land use history. While existing methods using MODIS-derived GPP models serve as an important baseline for studies with large spatial extents, future endeavors to estimate GPP in managed landscapes with greater frequency and improved accuracy are accessible and affordable at 30 m and 20 m resolutions.

CHAPTER 3. LAND COVER CHANGE AND SOCIOECOLOGICAL INFLUENCES ON TERRESTRIAL CARBON PRODUCTION IN AN AGROECOSYSTEM

Reproduced with permission from Springer Nature: Shirkey, G., John, R., Chen, J., Kolluru, V., Goljani Amirkhiz, R., Marquart-Pyatt, S. T., ... & Collins, M. (2023). Land cover change and socioecological influences on terrestrial carbon production in an agroecosystem. *Landscape Ecology*, 1-23.

Abstract

This study evaluated the contributions of land cover and land use change (LCLUC) and land management to landscape carbon production through a complex cause-effect path analysis of socioecological latent variables. Socioecological contributions to landscape carbon production are essential in landscape analysis, as their processes are both independent and interactive. I quantify the coherencies of social, economic, and environmental variables and their impact on net primary production (NPP) in an agroecosystem landscape. I ask whether LCLUC contributed to increased NPP and if land management and LCLUC play a more significant role than abiotic stressors on NPP. I applied a socio-environmental system framework to evaluate anthropogenic and environmental processes in the Kalamazoo River Watershed in southwest Michigan, USA from 1987 to 2017. Structural composition and functional contribution to NPP were evaluated by land cover type. Next, I synthesized remote sensing, gridded climate, social and biophysical data, in a principal component analysis (PCA) to inform a partial least squares structural equation model (PLS-SEM). Land cover type contributed to anthropogenic processes. Cropland contributed to Land Management, forest and water contributed to Land Cover Change, and urban to the Regional Development construct. Anthropogenic activities contributed more to NPP than abiotic processes. Attitudes of environmental stewardship strongly related to land use change likelihood. In this work, I disentangled anthropogenic and climatic changes' contributions to terrestrial carbon production and the societal ties to potential carbon sequestration. No single landscape metric is suitable for all study areas; however, this framework is useful for a landscape-scale analysis of socio-environmental processes.

Introduction

Human activities and environmental changes independently and interactively affect ecosystems. Understanding their direct and indirect influences from an ecosystem to landscape, regional, and global scale is important for a sustainable future, particularly in agroecosystems requiring sustainable food production and a minimized environmental footprint. Land management practices such as tillage, urban development, fertilizer applications and land cover change collectively alter and influence the terrestrial ecosystem carbon (C) cycle, including C production (Guzman & Gulabi, 2017). Across a landscape, landscape characteristics (e.g., spatial arrangements and composition) may further couple with additional ecological processes and introduce functional changes in ecological and socioeconomic systems, and vice versa (Lausch et al., 2015; Sciusco et al., 2020; Turner, 1989). These are due to the synchronized dynamics of the physical, ecological, and social processes and their resulting complex problems (Conzen, 2014), which are approached with socio-environmental system (SES) modeling (Chen, John, Zhang, et al., 2015; Elsawah et al., 2020). As international efforts continue to regulate C emissions from anthropogenic sources, renewed efforts have risen to understand the potential terrestrial stock to offset emissions through ecosystem production known as nature-based solutions (Hemes et al., 2021; Novick et al., 2022; Robertson et al., 2022; Wiesner et al., 2022). To employ such efforts sustainably, it is imperative to consider the interactions between anthropogenic activities and abiotic factors related to terrestrial C production.

Incorporation of land cover and land use change (LCLUC) analysis can supplement our observation of ecological patterns (e.g., patches, fragmentation, edge effects) granted by advances in spatial analysis and satellite imagery (Bondeau et al., 2007; Cohen & Goward, 2004; Potapov et al., 2022). Including LCLUC analysis is necessary to understand how land cover affects atmospheric CO_2 uptake and emission, terrestrial primary productivity, the hydrologic cycle, and the energy balance at the surface-atmosphere interface. Yet, while climatic variables such as precipitation, drought and temperature have been well-documented for their influences on the C cycle, less is known about how this production varies by land cover type in human-nature systems over time (Chen et al., 2004; Euskirchen et al., 2016; Spies et al., 2018). As population growth and income alone cannot explain changing landscapes, socioeconomic opportunities and institutional factors should be considered (Lambin et al., 2001). Understanding the relative C contributions of each land cover type and their relationship with socioeconomic variables may elucidate how societal change (i.e., cropland intensification, urban to rural migration) affects spatiotemporal landscape C production (Chen et al., 2022; Kramer et al., 2017; Liu et al., 2013; Zimmerer et al., 2018).

Landscape ecology serves as an important theoretical framework for understanding the functional and structural contributions of land cover types that incorporate the consequences of a spatiotemporal, hierarchical ecosystem and land management processes (Levin, 1992; Turner, 2010). Regional and socioecological systems require long-term observations so that ecosystem dynamics (i.e., seasonality, resilience, and succession) and societal changes (e.g., urbanization, land tenure) are observable. Geographical research in the past three decades has attempted to model the process of LCLUC, project future distributions, and continue to aid in the inclusion of socially sensitive and integrated approaches to advance policy and conservation strategies (National Research Council, 2010). Here I propose that LCLUC is not restricted to conventional land cover mapping alone, but that land ownership, the density of management practice, and land use across a landscape may also improve our SES modeling and understanding. Conventionally, land cover mapping has strongly relied on remote sensing data for inventorying the extent of land cover type and associated characteristics. However, the lack of social behaviors and land management information (i.e., societal forcing) requires integrating data from various spatiotemporal resolutions and sampling strategies that may introduce uncertainties from aggregation (Jelinski & Wu, 1996; D. Yang et al., 2017). For example, US national social data is often available every 5 or 10 years, such as the American Community Survey, National Agricultural Statistic Service, or the Occupational Employment Statistics (Ruggles et al., 2022; USDA National Agricultural Statistics Service, 2022; Utterback et al., 2012). At finer spatial scales, data are omitted due to privacy concerns or where instances are less frequent. Conversely, ecological, and remote sensing derived land cover data can be obtained at a high spatiotemporal frequency, which offers 5-day, 8-day and 16-day revisit at 10-20 m, 250-500 m, and 30 m spatial resolution from Sentinel-2, MODIS, and Landsat, respectively. Meanwhile, integrating social and ecological data within a spatiotemporal analysis is absolutely needed for a holistic understanding of ecosystem processes—a lasting challenge within landscape ecology (Kugler et al., 2019; Wu, 2006).

To evaluate the interactions and contributions between environmental change and human action and address abstract concepts such as "climate change", "ecosystem structure and/or composition", "resistance and resilience", and "ecosystem service", landscape ecologists may consider the advantages of structural equation modeling (SEM) (Fan et al., 2016; Kolluru et al., 2022b). The indirect and direct relationships between environmental change and human activity exist in subsystems that make a cohesive whole. Research topics on how human activities may shape ecosystem services or the environment across scales include telecoupling (Liu et al., 2019) and coupled-human nature systems (Kramer et al., 2017). Theoretical frameworks incorporating ecosystem functions (e.g., carbon productivity) with measures of social and economic performance (e.g., population density, gross domestic productivity, and livestock density) seek to identify the tipping point of sustainability in an SES. For example, numerous studies investigate the interactions of environmental change and human action in the Asian drylands to identify sustainability challenges and modifications from political and climatic stressors (Chen et al., 2020; Chen et al., 2015; Shao et al., 2017; Kolluru et al., 2022a). To assess and evaluate multivariate causal relationships, ecologists have utilized SEM as early as 2000 with reviews offered by Fan et al. (2016), Grace et al. (2010) and Eisenhauer et al. (2015). Theoretical frameworks of SES research can be tested for causality with confirmatory factor analysis, such as that by Kolluru et al. (2022b), while users at the beginning stage or with fewer data can apply a partial-least squares (PLS) SEM to generate necessary evidence for a causal relationship and variable selection (Fan et al., 2019; Park et al., 2017). In this way, users can continue collecting long-term data while updating their hypotheses (Monecke & Leisch, 2012).

In this study, the contributions of societal and ecosystem processes to NPP (g C m^{-2} yr^{-1}) are evaluated to explore their complex relationships at the decision-making level of an agroecosystem. To quantify these interrelationships, the Kalamazoo River Watershed in southwest Michigan, USA, was selected as a testbed. I ask whether: (1) LCLUC has contributed to increased NPP; (2) regional development and land management are significantly responsible for LCLUC; and (3) whether land management and LCLUC play a more significant role than abiotic stressors on NPP. The study's hypotheses are that: (H1) land cover change has a direct and significant effect on landscape NPP; (H2) regional development can directly influence land management, which in turn shapes the LCLUC and NPP of the landscape, and (H3) anthropogenic activities have a collectively higher and more influential direct impact on LCLUC than abiotic drivers. The theoretical construct investigates the interrelationships and combined influences of social and physical variables on NPP. The watershed's structural composition and relative contribution to NPP was evaluated by land cover type from 1987 to 2017; and investigate their linear relationship. A partial least squares structural equation model (PLS-SEM) was employed to identify the relationships between social, economic, and ecological variables and their impact on NPP in a cropland-forest dominated landscape (Fan et al., 2016). Human activities are contextualized with stakeholder surveys. Contributions of this work aim to disentangle the relative contributions of anthropogenic and environmental factors in terrestrial carbon production for a deeper understanding of the societal ties to potential carbon sequestration efforts.

Methods

Study area

The Kalamazoo River Watershed (HUC8; 5,261 km^2), is approximately one hundred miles long and includes portions of ten counties: Allegan, Barry, Eaton, Van Buren, Kalamazoo, Calhoun, Jackson, Hillsdale, Kent, and Ottawa (Fig. 3.1). In this study, counties with 1% or less overlapping area with the Kalamazoo Watershed were excluded, including Kent, Ottawa, and Van Buren. The largest urban centers include Kalamazoo and Battle Creek. The

Kalamazoo River begins at a spring-fed pond in northern Hillsdale County and flows westward in a northerly arc through the cities of Albion and Battle Creek into Saugatuck before reaching Lake Michigan. The Kalamazoo Watershed is in a humid continental temperate climate with a mean annual air temperature of 9.9 °C and a cumulative average annual precipitation of 1027 mm (Michigan State Climatologist's Office, 2013). Soils are Typic Hapludalfs, well-drained sandy loams (Bhardwaj et al., 2011; Thoen, 1990). From May through September, representing the growing season, mean air temperature and total precipitation are 19.7°C and 523 mm, respectively, with the highest temperatures in July (Abraha et al., 2018).

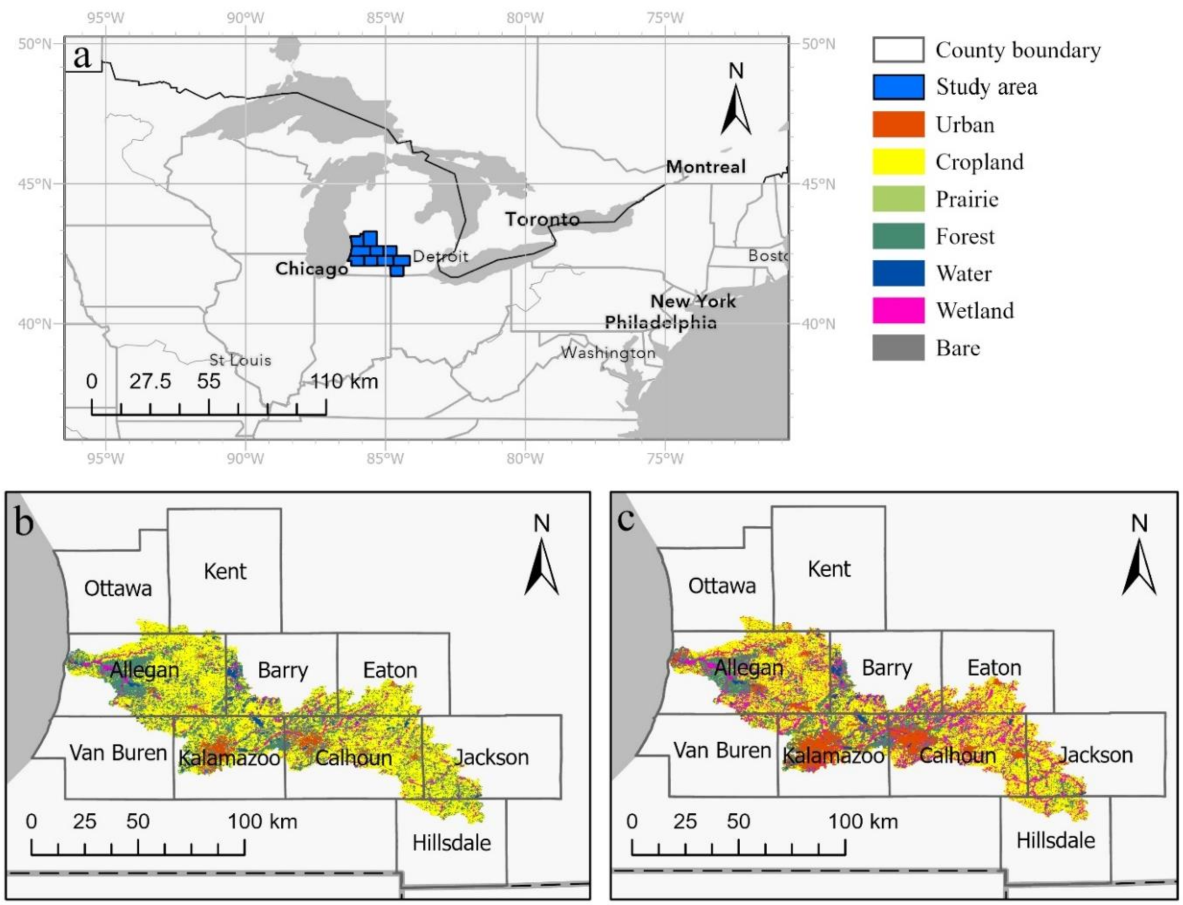

Figure 3.1. The (a) Kalamazoo River Watershed in southwest Michigan with land cover in (b) 1986 and (c) 2017 presented for visual assessment of the change.

Socioecological data

To assess spatiotemporal human-nature interrelationships using PLS-SEM, an SES dataset was composed of demographic, climate, soil, and biophysical geospatial data (Table 3.1). Multiple datasets were synthesized from remote sensing, gridded climate, and social surveys to best reflect SES activities in the study area every five years during the 30-year study period: 1987, 1992, 1997, 2002, 2007, 2012, and 2017. Therefore, each year in the study period is represented by the nearest possible data availability of the data product. As some datasets (i.e., Census, land cover classifications) are unavailable on an annual timescale, it was assumed that there was little to no change across the 2-3 years. Remote sensing data included gridded climatic datasets, land cover and surface reflectance, terrestrial carbon production, as well as soil properties. Annual climate and biophysical geospatial datasets were overlain with county boundaries to extract averages or cumulative values by county in ArcGIS Pro (v2.8.7). When variables were available for consecutive annual estimates, all years were collected to calculate anomalies over 30 years, then selected the study period years to be used in the PLS-SEM in R Statistical Software (v3.6.1) (R Core Team, 2019). Additional data management details are provided in the following sections, including data acquisition, processing, and scaling.

Land cover

Land cover classifications were acquired from two different data sources to span the extent of the study period. For 1986, 1991, and 1996, land cover data were acquired from Chen et al. (2019) at 30m resolution and are assumed unchanged from the study period years 1987, 1992, and 1997. These classifications were created using an object-oriented classification of Landsat Thematic Mapper images that were acquired on the 6th and 31st of

July each year over three Landsat scenes (21/30, 21/31, and 22/30) from Google Earth Engine (GEE) (Gorelick et al., 2017). Images were defined with per-pixel cloud and quality information (Dwyer et al., 2018) and cloudy pixels were removed. Following the Anderson et al. (1976) Tier 1 classification scheme, land covers were classified as urban, wetland, forest, cropland, bare, grassland and water bodies. The classification was conducted using segmentation in eCognition software (version 9.2). Additional information on classification methods and rules can be found in Chen et al. (2019). Accuracy assessment was conducted for each year by stratified random sampling of 700 Landsat pixels, with 100 samples per class (i.e., 700 reference pixels). The pixel land cover was identified by examining high-resolution imagery in Google Earth and historical aerial photographs produced by Michigan State University RS-GIS. Standard confusion matrices were derived as cross-tabulations of the classified versus the reference class and were used to derive user's and producer's accuracies (Foody, 2002). The overall classification accuracy was 68%, 71%, and 70% for 1986, 1991 and 1997, respectively. User and producer's accuracy of individual classes ranged from 37-92% and 42-96% for 1986; 46-97% and 56-100% for 1991; and 48-95% and 50-96% for 1996, respectively (Tables A7-9). Additional land cover datasets for the years 2001, 2006, 2011, and 2016 were acquired from the National Land Cover Database (NLCD, 30 m) (Dewitz & Survey, 2021; Homer et al., 2020; Jin et al., 2019; Wickham et al., 2021; Yang et al., 2018). It was assumed these years represented the study area land cover in 2002, 2007, 2012, and 2017, respectively. NLCD land cover was reclassified to match land covers from Chen et al., 2019 (Table A10), and the percentage land cover of each county of the watershed was tabulated to estimate each type's respective contribution to the landscape for use in the PLS-SEM. To examine landscape composition change from

1987 to 2017, functional contributions to NPP and structural composition of the study area were evaluated by land cover type. Functional contribution is calculated as the cumulative NPP (kg C km^{-2} yr^{-1}) of each land cover in the landscape. Structural contribution was estimated as the percentage of each land cover class in the study area. Their interactions are evaluated along a 1:1 trend line. This approach and associated algorithms can be found in (Wen, Chen, & Wang, 2020).

Table 3.1. Data source, spatial extent (resolution), year, and variable name used in the partial least squares structural equation model (PLS-SEM).

Variable (unit for PLS-SEM)	Extent	Year	Source
POPD (population km^{-2}), INC (income per capita km^{-2}), UHD (housing unit km^{-2}), RHD (rural housing unit km^{-2})	County	1980, 1990, 2000, 2010	Decadal Census, IPUMS (Ruggles et al., 2022)
FOR (% forest), WET (% wetland), BAR (% bare),	30 m	1986, 1991, 1996	Chen et al. (2019)
CRO (% cropland), URB (% urban), WAT (% water), GRA (% grassland)	30 m	2001, 2006, 2011, 2016	National Land Cover Database (Dewitz & Survey, 2021; Homer et al., 2020; Jin et al., 2019; Wickham et al., 2021; L. Yang et al., 2018)
IRR (% irrigation), NT (% no-till), CST (% conservation till km^{-2}), CVT (% conventional till km^{-2}), FD (count of farms km^{-2}), FINC (net farm income km^{-2}) FOW (% farmland owned km^{-2}), FRF (% farmland rented from km^{-2}), FRT (% farmland rented km^{-2}), FLD (% farmland area per km^{-2}), FINO (income per farm operation km^{-2})	County	1987, 1992, 1997, 2002, 2007, 2012, 2017	National Agricultural Statistic Service (NASS) (USDA National Agricultural Statistics Service, 2022)
NPP (net primary production kg C km^{-2})	30 m		Landsat CONUS (Robinson et al., 2018)
FP (farm phosphorus kg km^{-2}), FN (farm nitrogen kg km^{-2}), NFP (non-farm phosphorus kg km^{-2}), NFN (non-farm nitrogen kg km^{-2})	County		United States Geological Service (USGS) (Falcone, 2021)
PDI (Self-Calibrated Palmer Drought Severity Index)	4km		ScPDSI (Van der Schrier et al., 2013)
VPD (max vapor pressure deficit squared)	4 km		PRISM (Daly et al., 2008, 2015)
PTY (total annual precipitation mm), TPM (maximum air temperature standard deviation ˚C)	1 km		Daymet (Thornton et al., 1997)
GSL (annual growing season length, days)	4 km		This study
SPEI (standardized precipitation evapotranspiration index)			GRIDMET (Abatzoglou, 2013)
OMS (organic matter 0-5 cm km^{-2}), SAS (sand 0-5 cm km^{-2}), SIS (silt 0-5 cm km^{-2}), PHS (average PH 0-5 cm km^{-2}), CLS (average clay 0-5 cm km^{-2}), OMD (organic matter 5-15 cm km^{-2}), SAD (sand 5-15 cm km^{-2}), SID (silt 5-15 mm km^{-2}), PHD (average PH 5-15 mm km^{-2}), CLD (average clay 5-15 mm km^{-2})	30 m		POLARIS (Chaney et al., 2016)
CRP (% Conservation Reserve Program, county area enrolled)	County		USDA (FSA USDA, 2018)

NPP data

The 30-m Landsat CONUS Annual NPP product (Robinson et al., 2018) was selected for this study, as it provides annual cumulative values of NPP (kg C m^{-2} yr^{-1}) for each year in the study period. Estimates of urban and water body NPP are unavailable as the product was built from estimates including maximum light use efficiency (LUE) of vegetation that does not apply to non-vegetated areas. Due to data limitations, I acknowledge that NPP activity in these non-vegetated land cover types was overlooked in this study and that aggregations of adjacent land covers may contribute to variations in NPP (Shirkey et al., 2022).

Climate and physical geography data

Abiotic stress was examined in the SEM by calculating standardized anomalies of climate and physical geography variables collected during the thirty-year period. Cumulative annual precipitation (PTY) and standard deviations of average maximum air temperature (TPM) were extracted from Daymet (1 km) via GEE (Thornton et al., 1997). Annual average estimates of maximum vapor pressure deficit (VPD) squared were extracted from the monthly Oregon State PRISM gridded climate dataset AN81m (4km) in the GEE platform (Daly et al., 2008, 2015). Growing season length (GSL) is the average number of days between the date of the last hard (i.e., killing) frost in spring to the date of the hard frost in fall. In this analysis, a daily average of 0 ˚C was considered as a hard frost; and the average maximum air temperature was acquired from Daymet (1 km) annual data.

To emphasize the importance of water availability (e.g., soil moisture, relative humidity) on NPP, the annual mean Self-Calibrated Palmer Drought Severity Index (scPDSI, hereafter PDI) by the Climatic Research Unit (CRU), University of East Anglia was acquired (https://crudata.uea.ac.uk/cru/data/drought/) (Van der Schrier et al., 2013; Wells et al., 2004). The PDI is an improvement of the Palmer Drought Severity Index (PDSI) as it accounts for all the constants contained in PDSI and 'self-adjusts' constants (e.g., climate and duration factors) dynamically based on the characteristics present geographically. It is a standardized index that includes wet and dry scales, with values ranging from -5 (extreme dry) to 5 (extreme wet). Annual average estimates of the climatic water balance provided by the Standardized Precipitation Evapotranspiration Index (SPEI), which is derived from the daily Gridded Surface Meteorological (GRIDMET) dataset, were also included (Abatzoglou, 2013). The indices range from -2 (extreme drought) to +2 (extremely wet). Unlike the standardized precipitation index, SPEI includes precipitation and evapotranspiration, thus capturing the impacts of increased water demand.

Integration of soil properties was provided by POLARIS (30 m), a complete map of soil series probabilities produced with high-resolution environmental data and machine learning that remaps the Soil Survey Geography (SSURGO) database. Specifically, the percent soil organic matter was acquired at depths 0-5mm (OMS) and 5-15mm (OMD), percent sand at depths 0-5mm (SAS) and 5-15mm (SAD), percent silt at depths 0-5 mm (SIS) and 5-15 mm (SID), percent clay at depths 0-5 mm (CLS) and 5-15 mm (CLD), and average PH at depths 0-5 mm (PHS) and 5-15 mm (PHD). Data for the study region was extracted using the R Statistical Software package XPolaris (Moro Rosso et al., 2021b, 2021a). No change in soil characteristics from 1980-2017 was assumed in this study, as temporal resolution is not available in this data. Therefore, the same static soil data was used for all analyses.

Land management and demographic data

Socio-economic activities included residential population estimates, income, agricultural industry, land management and land use. County-level land use, land management, and economic information was acquired from the National Agricultural Statistics Service (NASS) via Quickstats (https://quickstats.nass.usda.gov/) on the Census of Agriculture website (USDA National Agricultural Statistics Service, 2022). The census runs once every five years and mails surveys to all farms and ranches with $1,000 or more in farm sales. Specifically, county-level variables were acquired for irrigated land (IRR), farm count (FD), net farm income (FINC), tillage practices including no-till (NT), conservation till (CST), and conventional till (CVT), farmland owned (FOW, km^{-2}), farmland rented from another owner (FRF, km^{-2}), farmland rented to another individual (FRT, km^{-2}), farmland area per km^{-2} (FLD) and income per farm operation (FINO, km^{-2}). Variables are expressed in percent area (% km^{-2}) per county-year sample (Table 3.1).

Additionally, 10-year Decennial Census records were sampled from 1980-2020, as provided in the IPUMS database, to estimate the population density (POPD) for each county, income per capita (INC), number of urban housing units (UHD) and rural housing units (RHD) (Ruggles et al., 2022). As the records are only available every ten years, values were linearly gap filled according to their closest associated year and assumed no change (i.e., 1990 = 1987, 1992; 2000 = 1997, 2002; and 2010 = 2007, 2012, 2017). Additional land management variables include Conservation Reserve Program (CRP) statistics from the United States Department of Agriculture Farm Service Agency (FSA USDA, 2018). Data included an annual record of enrollment by county since 1986. Applications of fertilizer were acquired from county-level applications (kg yr^{-1}) of farmland phosphorus and nitrogen (FP and FN, respectively) and non-farmland phosphorus and nitrogen (NFP and NFN, respectively) from the USGS (Falcone, 2021). The database was built from state-level-use estimates in tons of nutrient mass and apportioned to counties based on purchase records or acres fertilized per county for all years leading up to 2012. Beginning in 2017, nutrients were estimated with random forest decision-tree models. Data coincides with the NASS census years, and most fertilizer—defined as commercially purchased nitrogen and phosphorus—is for agricultural purposes. Land management and demographic data per county were divided by the county's respective area to estimate annual density, and standardized anomalies were estimated per county per year in R Statistical Software.

Principal component analysis (PCA)

A principal component analysis (PCA) was applied to determine if relationships exist between the socioecological variables as unique principal components. The PCA analysis was conducted in R Statistical Software with package *factoextra* (Kassambara & Mundt, 2020) with values zero-centered. The Bartlett Test of Sphericity was analyzed to determine if the SES dataset can be summarized within a few factors. The eigenvalues, which correspond to the amount of variation explained by each dimension, we further estimated. The Kaiser-Guttman rule was applied, which states that components with eigenvalues >1 should be considered, as they must have variance at least as large as a single standardized original variable (Kaiser, 1960). Each indicator with a >0.5 or <-0.5 weighted contribution (i.e., loadings) was considered and assigned to a PLS-SEM latent construct, which is a phenomenon that cannot be measured directly but rather contextualized by indicator variables. The results of the PCA were employed to revise the PLS-SEM theoretical path model (i.e., revised theoretical model).

Partial least square structural equation model

A PLS-SEM was utilized to construct the relationships between social, economic, and ecological variables in the SES dataset concerning annual landscape production of NPP (i.e., the dependent variable) (Fig. 3.2). Compared to classic regression-based approaches that assume simple model structure along with observable and perfectly measured variables (Haenlein & Kaplan, 2004), SEM is a second-generation technique that allows for the simultaneous modeling of relationships among dependent and independent constructs (Gefen et al., 2000). In SEM, one can distinguish between exogenous and endogenous latent variables, which are variables not explained by the proposed model (i.e., acting as independent variables) and those explained by the relationships in the model, respectively (Diamantopoulos, 1994). For this study, a PLS-SEM was selected as it is suitable as an exploratory technique because it has fewer assumptions than the covariance-based SEM (CB-SEM) and operates on smaller sample sizes (Bollen, 1989; Rigdon, 2012; Rigdon et al., 2020). In PLS-SEM, small sample sizes and the problem of model and parameter consistency are not obstacles to estimate the models as the variance-based PLS model will include weights that cease to influence the parameters of the path model after enough indicators are reached (McDonald, 1996; Fan et al., 2016).

The theoretical model proposes that NPP is: (1) directly affected by constructs Abiotic Stress, Land Management and Land Cover Change; (2) indirectly affected by constructs Regional Development and Soil Composition; and (3) directly affected by the interaction between Land Management and Land Cover Change. Latent constructs are designed as reflective, where indicators are measurable variables of the phenomenon and arrows connecting variables and constructs have a regression relationship. The difference between the formative and reflective construct is their conceptual relationship with indicators, where formative constructs are caused by their latent variables (i.e., formed by) and reflective constructs cause their latent variables. While the NPP construct is composed of a single indicator (NPP kg C km^{-2} yr^{-1}), all other constructs are informed by multiple latent constructs from the SES dataset. Model construction and data standardization were conducted in the SEMinR package (Hair et al., 2021) using R Statistical Software (v4.2.1).

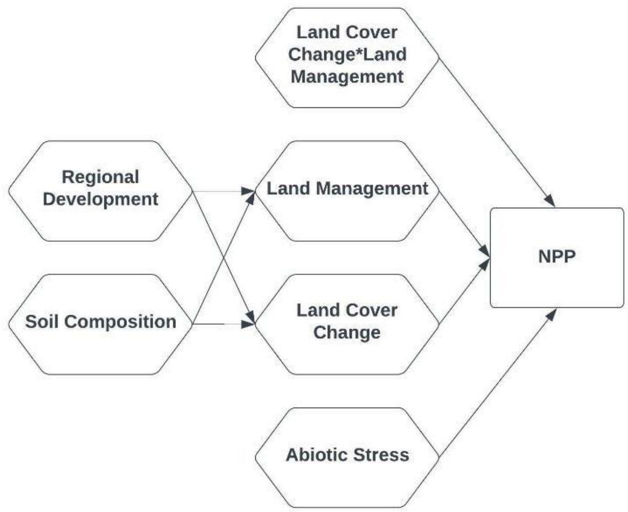

Figure 3.2. Theoretical framework of the PLS-SEM predicting net primary productivity (NPP). Both endogenous (i.e., Land Management, Land Cover Change) and exogenous constructs (Regional Development, Soil Composition, Abiotic Stress), as well as an interaction between Land Cover Change and Land Management, are proposed to explain variations in net primary productivity (NPP).

The model evaluation included assessing the measurement and the nonparametric PLS-SEM's structural model (Fan et al., 2016). First, the measurement models were assessed to understand the relationships between a single construct and its indicators, known as indicator reliability. The indicator reliability was estimated by examining how much of each indicator's variance was explained by its construct. This is estimated by the square of the indicator loading, where values >0.708 are recommended since they indicate >50% explanation of the indicator's variance (Hair et al., 2021). Second, the reliability and validity were determined as to whether the construct indicators were associated with one another, known as internal consistency reliability. Three separate measures were considered. One primary measure was Jöreskog's (1971) composite reliability rho_c. Values between 0.60 and 0.70 are considered acceptable in exploratory research, 0.70-0.90 are satisfactory to good, 0.90-0.94 can be problematic, and those >0.95 indicate redundant indicators and reduces construct validity (Diamantopoulos et al., 2012). Values >0.95 can also trigger undesirable patterns (e.g., straight-lining) and trigger inflated correlations among indicator error terms. Cronbach's alpha (hereafter alpha) provided another measure that assumes the same threshold as rho_c. This estimate was used for a conservative lower-bounding, assuming all indicator loadings are the same in the population (i.e., tau-equivalence), and any violations would generate a lower value than rho_c. For a balance between liberal rho_c and conservative alpha estimates, I also employed Dijkstra's (2010, 2014, 2015) reliability coefficient rho_a which usually lies between the two and is therefore considered an acceptable compromise (Hair et al., 2021).

The third step in evaluating reflective measurement models was convergent validity, which is the extent to which the construct converges to explain the variation of its indicators. Convergent validity was estimated using the average variance extracted (AVE), which is the grand mean value of the squared loadings of the indicators associated with the construct. Thus, AVE is equivalent to the communality of a construct, with acceptable ranges >0.50 (i.e., explaining more than 50% of the indicator's variance in that construct). The reflective measured constructs' discriminant validity was also assessed and compared with other construct measures in the same model using the heterotrait-monotrait (HTMT) ratio of correlations. While collinearity issues can be indicated by a variance inflation factor (VIF), where above 5 indicates probable collinearity issues (Becker et al., 2015; Mason &

Perreault, 1991), these are used for formative and not reflective constructs that expect high correlations (Hair et al., 2021). The HTMT is defined as the mean value of the indicator correlations across constructs relative to the geometric mean of the average correlations for the indicators measuring the same construct. Discriminant validity problems exist when values are high. Henseler et al. (2015) suggest that conceptually similar constructs remain below 0.90 and distinct constructs aim for <0.80 HTMT values.

Next, the structural model was evaluated, which includes the relationship between constructs and their predictive power. To explore the significance and relevance of the model relationships between constructs, a bootstrap with ten thousand subsamples was applied to estimate standard errors that were used to compute *t*-stats of path coefficients and confidence intervals (Streukens & Leroi-Werelds, 2016). The percentile method is preferred to generate confidence intervals, where path coefficients are significant at the 5% level if the value zero does not fall within the 95% confidence interval (Aguirre-Urreta & Rönkkö, 2018). The structural model collinearity of predictor constructs was inspected to discern each endogenous construct with VIF scores. Path coefficients were reported between -1 and +1, with values closer to -1 indicating strong negative relationships and those closer to +1 indicating strong positive relationships. Path coefficients indicate changes in endogenous construct values associated with a predictor construct's change in standard deviation, holding all other predictor constructs constant. For example, a path coefficient of 0.5 indicates that an endogenous construct will increase by 0.5 standard deviation units given the predictor construct's one-unit change in standard deviation. Lastly, total path relationships were evaluated, considering the combined direct and indirect effects linking one construct to another in the model, to comprehensively review the structural relationships (Nitzl et al., 2016).

Landowner surveys of land use land cover change decision-making

Historical land ownership was evaluated through mailed surveys with Michigan Centennial Farmers to better interpret and contextualize in the theoretical framework and PLS-SEM results. This population comprises Michigan farms with >10 working farmland acres that have remained in the same family for 100 years or more. This population is a notable subsample of the study area as it has historically witnessed the change in land management in croplands and farmlands, which is the scope of this study. This population represents the study scope, as the NASS data is also sampled from this population. Each participant was contacted through the post to request self-administered completion of a survey regarding their farm, family history and management practices. A four-letter mailing campaign included: (1) a letter of notification sent two weeks before distributing the survey; (2) a packet with an official survey invitation and paper survey with a requested return date; (3) a reminder and thank you letter two weeks following the survey; (4) and a final reminder and thank you letter sent four weeks after distributing the survey. The English unit of "acre" (1 acre = 0.4047 ha) was used because of its familiarity with the farmers in the USA. After adjusting for undeliverable surveys, the survey response rate was 23% (n=103). Participant demographics were dominantly white, non-Hispanic males with an average age of 74 years old; 50% own 70-139 total acres, 15% own 200-259 acres and 11% own 1-49 acres.

To estimate the associations between land cover change, land management and landowners' attitudes and behaviors, a Fisher's exact test of independence was applied between responses to survey questions provided on Likert scales (values 0-5, where 0= I do not know; 1= Completely Disagree; 5= Completely Agree). Spearman's correlation analysis was also applied, denoted by rho (ρ), to measure the nonparametric monotonic relationships of the rank values, and exclude values of zero. Spearman's ρ ranges from -1 to +1, where the sign indicates a negative or positive monotonic relationship, respectively. Positive relationships signify that as one variable increases, the other also tends to increase; whereas a negative relationship signifies that as one variable increases, the other tends to decrease. A near-zero coefficient indicates no relationship between variables. To explore whether the belief that an individual's land management influences the carbon cycle is related to environmental altruism, the potential to significantly change their land cover type, or climate change concerns, the ρ relationships were evaluated between landowner self-reported agreements with the following questions from the survey:

(A) Agreement that their land management strategy affects the carbon cycle.

(B) Agreement that environmental stewardship and belief influence their land management.

(C) Agreement that they are likely to change some uses of land in the next 5-10 years (e.g., from non-forest to forest).

(D) Agreement that climate change influences their current land management decisions.

(E) Agreement that they consider environmental impact when managing the land's productivity.

Results

Landscape composition

The largest contributors to functional NPP and structural composition in the Kalamazoo

River Watershed 1987-2017 were found to be cropland, followed by forest and urban areas (Fig. 3.3). Bare, water and prairie land covers totaled to <10% structural contribution and functional NPP in all years. Cropland structural contribution ranged from 59.35% in 1987 to 53.29% in 1997, whereas forest structural contribution ranged from 32.18% in 1987 to 25.34% in 2017. Functional NPP of croplands ranged from 58.75% in 1987 to 54.56% in 1997; and forest functional NPP ranged from 32.97% in 1987 to 25.30 % in 2012. The relationship between structural contribution and functional NPP is linear and falls along a 1:1 line, suggesting that the structural and functional contributions of each type to landscape NPP are the same. Cumulative area and NPP by land cover type and year are available in Table A11.

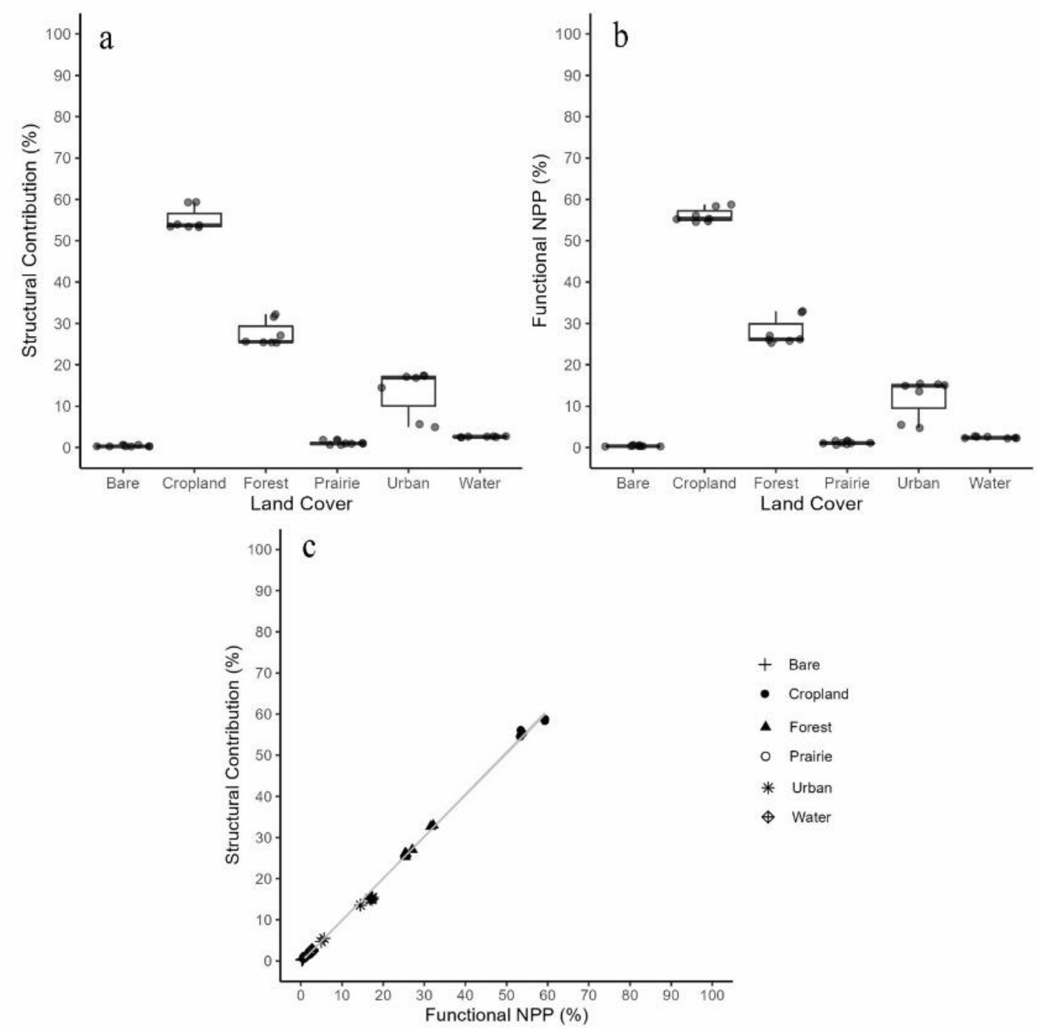

Figure 3.3. The (a) structural composition (%) and (b) functional contributions to NPP (%) in the landscape by land cover type, as well as their (c) linear relationship.

Socioecological PCA

The socioecological dataset was found acceptable based on PCA analysis, as the results of the Bartlett Test of Sphericity reported χ^2 of 12833.34 and a p-value < 0.001, indicating that the data is significantly different from an identity matrix and suitable for data reduction (Table 3.2). The PCA resulted in ten components suitable for further consideration, as they were acceptable by the Kaiser-Guttman rule with an eigenvalue greater than 1 (Fig. 3.4, Table A12). The cumulative variance of the ten dimensions totals 91.04%, ranging from 32.09% in the first dimension to 2.30% in the tenth dimension. The first three dimensions explained only 55.47% of the variation, suggesting diverse influences from multiple forcings.

Table 3.2. Results of the PCA eigenvalues, percent variance and cumulative percent variance for the first ten components (i.e., dimensions). For all component eigenvalues, see Table A12.

Dimension	Eigenvalue	Variance (%)	Cumulative Variance (%)
1	14.12	32.09	32.09
2	5.91	13.43	45.52
3	4.38	9.95	55.47
4	3.79	8.61	64.08
5	3.12	7.09	71.18
6	2.86	6.50	77.68
7	2.09	4.74	82.42
8	1.47	3.33	85.76
9	1.31	2.99	88.74
10	1.01	2.30	91.04

Each PCA dimension of 1-8 included demographic, land management and/or abiotic data with high loading contributions >0.5 or < -0.5 (Fig. 3.4) were used to assess constructs within a revised PLS-SEM for an intermediate step (Table A12). Loadings >0.5 in dimension one included no till (NT), conservation reserve program (CRP), farmland owned (FOW), farm density (FD), farmland field density (FLD), cropland (CRO), sand 0-5 cm (SAS), and sand 5-15 cm (SAD). These were attributed to the Land Management construct. Loadings < -0.5 in dimension one included a mix of soil variables and land cover. Therefore, silt 5-15 cm (SID), silt 0-5 cm (SIS), average PH 5-15 cm (PHD), clay 5-15 cm (CLD), average PH 0-5 cm (PHS), clay 0-5 cm (CLS), and organic matter 5-15 cm (OMD) were attributed to Soil Composition and forest (FOR), rural housing density (RHD), and water (WAT) to Land Cover Change. Loadings >0.5 in dimension two include irrigation (IRR), population density (POPD), income per farm operation (FINO), non-farm nitrogen (NFN), urban housing density (UHD), and urban land cover (URB) and consequently were attributed to the Regional Development construct. No unique clusters were detected in dimension 3, where organic matter 5-15 cm (OMD) and organic matter 0-5 cm (OMS) was >0.5 and net farm income (FINC) was < -0.5. Dimension four loadings < -0.5 include vapor pressure deficit (VPD) and wetland (WET), whereas dimension six loadings >0.5 include average maximum air temperature (TPM) alone. Lastly, dimension five loadings <-0.5 included conventional-till (CVT), while loadings >0.5 included NT. Dimensions 7-10 explain <5% of the variance and were not considered in the revised PLS-SEM constructs.

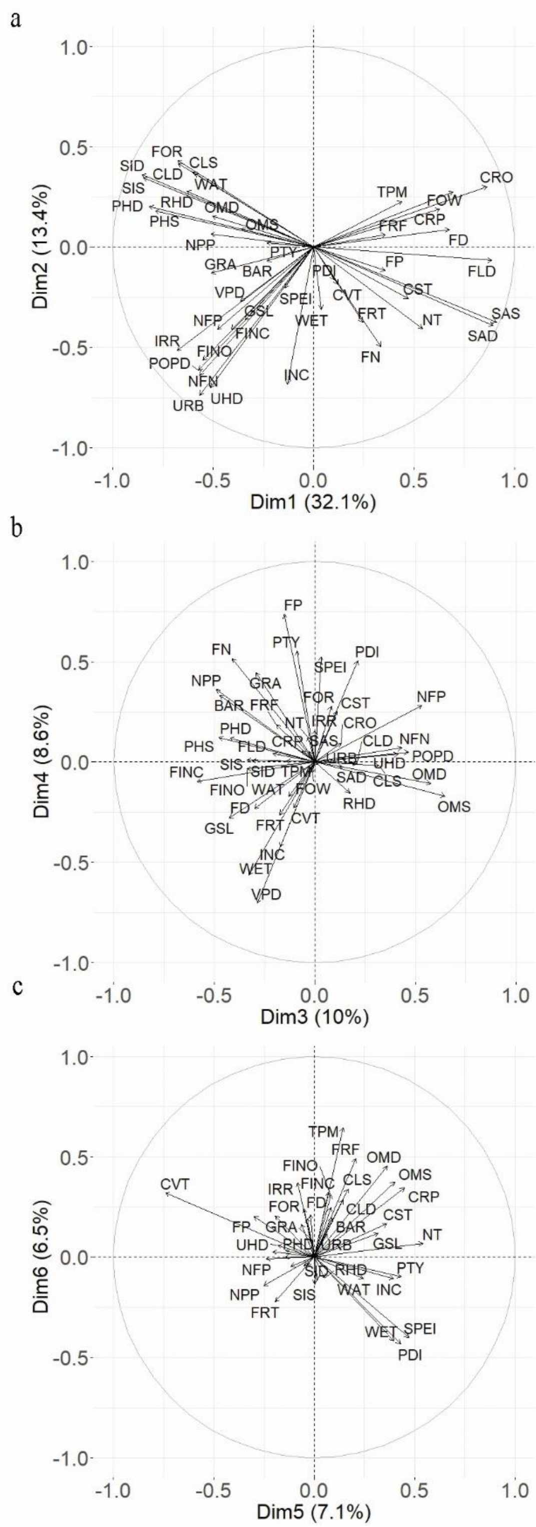

Figure 3.4. PCA loading plots, including dimensions (a) 1 and 2; (b) 3 and 4; (c) 5 and 6. Indicators are weighted by their contribution to a dimension ranging from -1 to 1.

PLS-SEM

Following revision of the theoretical framework, intermediate improvements were made to a revised PLS-SEM, given the PCA's indicator loadings (Appendix B), before finalizing the constructs and variables in PLS-SEM 2.0 (Fig. 3.5). After removing low indicator loadings (<0.708) and those that confounded discriminant validity between constructs, a noticeable improvement was found in the measurement models' internal consistency reliability (Table 3.3). Indicators removed include RHD from Land Cover; URD from Regional Development; NT, SAS, and SAD from Land Management; WET from Water Stress, as well as NFP and FN from Soil and Plant Nutrients. The strong HTMT scores between Land Management, Land Cover Change and Soil Composition can be understood as the result of their indicators expressing strong contributions and high loadings in PCA dimension one (Fig. 3.4). Therefore, the soil indicators (e.g., CLS, OMD, PHS, CLD) were replaced with soil contributors SAS and NT, which express >0.5 loadings in PCA dimension one. As a result, all internal consistency reliability metrics, indicator loadings, and HTMT estimates of discriminant variability are within the acceptable ranges (Tables A13-14). Values of HTMT are again well below 0.85, except for Soil Composition and Land Cover Change, which are 0.919 and conceptually similar and accepted for this study.

The structural model expressed acceptable levels of collinearity between predictor and endogenous constructs, with the largest VIF score of 2.23 between Land Management and NPP, which is well below the concerning level (>5). Endogenous constructs—Land Management and Land Cover Change—both had a VIF of 1.10 with Regional Development and Soil Composition. Construct NPP had <2.23 VIF scores with Land Cover Change (1.37), Water Stress (1.89), Land Cover Change * Land Management (1.52), Soil and Plant

Nutrients (1.85), Heat Stress (1.50), and Tillage (1.52).

Table 3.3. The internal consistency reliability metrics Cronbach's alpha, composite reliability rho_c, and reliability coefficient rho_a were used to determine how indicators perform within individual constructs in the PLS-SEM 2.0, where values between 0.60 and 0.70 are considered acceptable in exploratory research, 0.70-0.90 range from satisfactory to good, and those >0.95 indicate redundant indicators and reduced construct validity. Convergent validity was estimated using the average variance extracted (AVE).

	alpha	rho_c	AVE	rho_a
Regional Development	0.93	0.95	0.79	0.94
Soil Composition	0.74	0.88	0.78	0.87
Land Management	0.90	0.93	0.72	0.91
Land Cover Change	0.80	0.91	0.83	0.85
Abiotic Stress	1.00	1.00	1.00	1.00
Land Cover Change*Land Management	1.00	1.00	1.00	1.00
Soil and Plant Nutrients	1.00	1.00	1.00	1.00
Heat Stress	1.00	1.00	1.00	1.00
Tillage	1.00	1.00	1.00	1.00
NPP	1.00	1.00	1.00	1.00

It was discovered that the model explained Land Management well (R^2=0.715) and had a strong explanation for Land Cover Change (R^2=0.569), considering the leftover indicators—FOR and WAT (Table 3.4). Significant path relationships were strong for the effect of Soil Composition on Land Cover Change (-0.764***, *t*-stat -13.764), Soil Composition on Land Management (0.530***, *t*-stat 8.937), followed by Land Management and NPP (-0.562***, *t*-stat -3.853), Soil and Plant Nutrients and NPP (0.336*, *t*-stat 1.887), and lastly from Regional Development to Land Management (-0.521***, *t*-stat -9.888) (Fig. 3.5, Table 3.4). This indicates that when Soil Composition increases a standard deviation unit, Land Management will increase by 0.530 [when that value is positive]; whereas Land Cover Change will decrease by -0.764 [when that value is negative]. Similarly, if Regional Development increases/decreases by one standard deviation, Land Management will increase/decrease by -0.521 standard deviation units. Water stress, Tillage and Heat Stress do not have significant relationships with NPP. In moderation analysis, Land Management does have a significant effect on Land Cover Change, and their combined effect on NPP was 0.31* (*t*-stat 1.948). Significant indirect effects were found from Regional Development to NPP, with an estimate of 0.293 (*t*-stat = 3.781) through Land Management; as well as from Soil Composition to NPP, with an estimate of -0.298 (*t*-stat = -3.40) through Land Management.

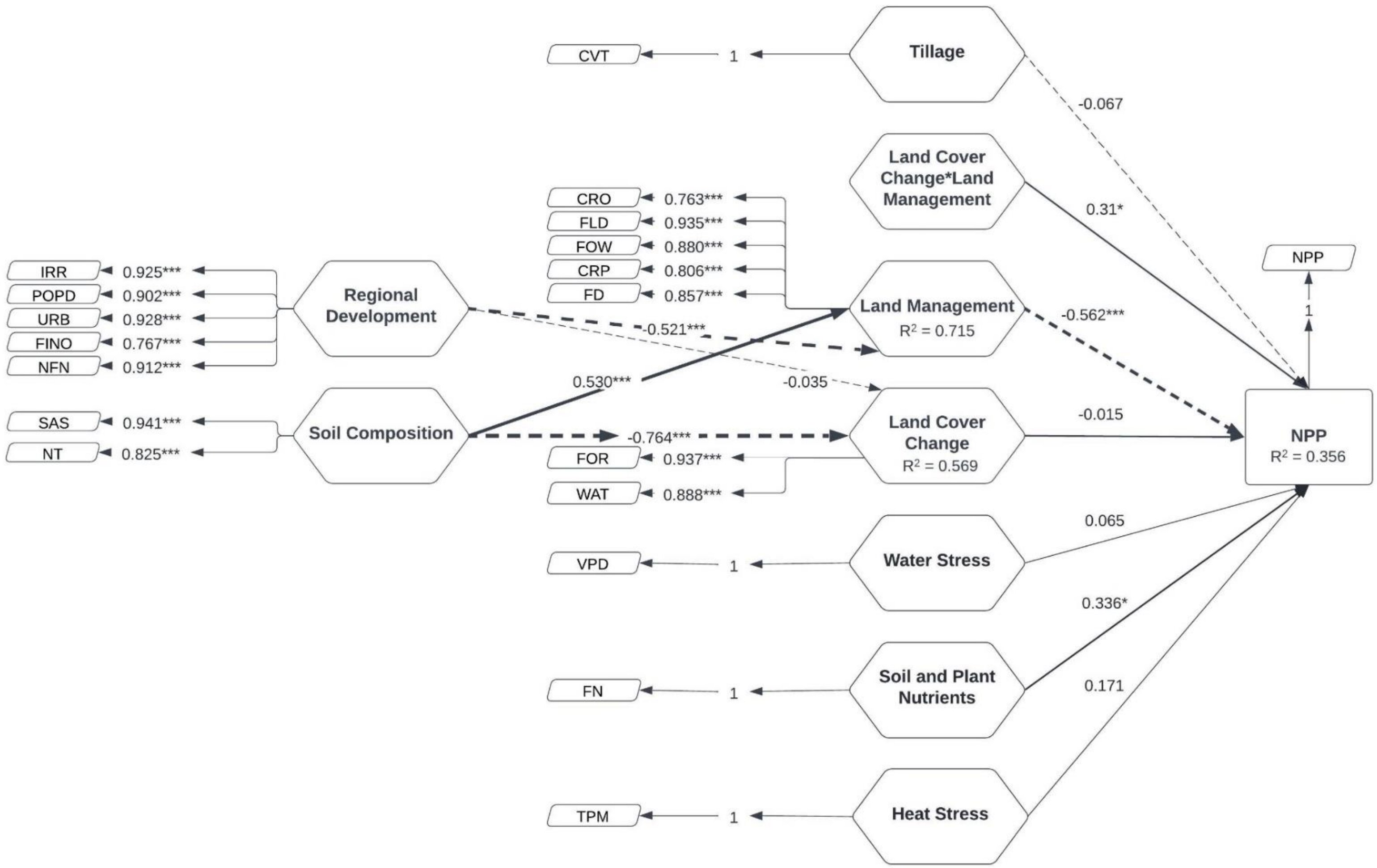

Figure 3.5. Indicator loadings, path coefficients, and coefficient of determination (R^2) values from the PLS-SEM 2.0 within the structural model. Dashed and solid paths indicate negative and positive relationships, respectively, and line size indicates magnitude. Significance is indicated with * according to *t*-stat values, where *, ** and *** indicate *p*-value<0.05, <0.01, and <0.001, respectively (Table 3.4).

Table 3.4. Coefficients of determination, bootstrapped total paths and indirect effects from exogenous constructs to NPP through Land Management in PLS-SEM 2.0, where SD is standard deviation, CI is confidence interval and LCC*LM indicates Land Cover Change * Land Management.

		R^2	Adj. R^2	Orig. est.	Boot est.	Boot SD	*t*-stat	5% CI	95% CI
Path from	***Path to***								
Regional Development	LM			-0.521	-0.522	0.053	-9.888	-0.611	-0.437
	LCC			-0.035	-0.038	0.090	-0.392	-0.174	0.115
Soil Composition	LM			0.530	0.535	0.059	8.937	0.436	0.630
	LCC			-0.764	-0.767	0.056	-13.764	-0.850	-0.669
LM	NPP			-0.562	-0.570	0.146	-3.853	-0.797	-0.325
LCC	NPP			-0.015	-0.023	0.139	-0.111	-0.244	0.204
LCC*LM	NPP			0.310	0.071	0.167	0.391	-0.204	0.344
Water Stress	NPP			0.065	0.342	0.159	1.948	0.081	0.599
Soil and Plant Nutrients	NPP			0.336	0.373	0.178	1.887	0.085	0.670
Heat Stress	NPP			0.171	0.196	0.170	1.005	-0.069	0.490
Tillage	NPP			-0.067	-0.066	0.163	-0.411	-0.337	0.199
Indirect effects									
Regional Development: Land Management: NPP				0.293	0.300	0.077	3.781	0.166	0.418
Soil Composition: Land Management: NPP				-0.298	-0.305	0.088	-3.400	-0.449	-0.165
Coefficients of determination									
Land Management		0.715	0.703						
Land Cover Change		0.569	0.551						
NPP		0.356	0.246						

Landowner surveys

Results reveal correlations between some but not all attitudinal measures (Table 3.5). Of all the measures, (B)—the agreement that environmental stewardship and belief influence their management—and (D) — an agreement that climate change influences their current land management decisions—had the most significant, positive relationships with other attitudinal measures. This suggests that landowners contextualize land management motivation from an environmental stewardship and environmental impact perspective or from a climate mitigation perspective. A strong positive correlation was found between questions (B) and (E), that environmental impact is considered when managing the land's productivity (ρ = 0.60***), as well as a positive correlation between (B) and (C) (ρ = 0.31*), and (B) and (D) (ρ = 0.26*). Also, a positive correlation was found between (A), the agreement that their land management affects the carbon cycle, and (D), the agreement that climate change influences their current land management decisions (ρ = 0.64***). The likelihood of changing land uses in the next 5-10 years (C) had a significant positive relationship with (B) alone (ρ = 0.31*), indicating that attitudes of environmental stewardship have a stronger relationship to land use change than attitudes of climate change or contributions to the carbon cycle (i.e., D or A, respectively).

Table 3.5. Spearman's rho (ρ) coefficients from survey questions A-E, where (A) Agreement that their land management strategy affects the carbon cycle; (B) Agreement that environmental stewardship and belief influences their land management; (C) Agreement that they are likely to change some uses of land in the next 5-10 years (e.g., from non-forest to forest); (D) Agreement that climate change influences their current land management decisions; (E) Agreement that they consider environmental impact when managing the land's productivity.

	A	B	C	D	E
A	-	-	-	-	-
B	0.17	-	-	-	-
C	0.02	0.31*	-	-	-
D	0.64***	0.26*	-0.08	-	-
E	0.29	0.60***	-0.13	0.44*	-

p-values are indicated as * (<0.05), ** (<0.01), and *** (<0.001).

Discussion

By integrating both societal and ecological geospatial data, an SES modeling framework was constructed for applications in future landscape studies to evaluate the patterns and processes of human-environmental interactions. These findings support the hypotheses that human activities— including regional development and land management—have a collectively higher impact on net primary productivity (NPP) and LCLUC than abiotic drivers. The use of PLS-SEM and stakeholder surveys are recommended to inform and revise theoretical SES frameworks, which can be particularly advanced by landscape ecology.

Land cover change effects on landscape net primary production

Anthropogenic and conventional measures of LCLUC were found to contribute to variations in NPP 1987-2017 for the Kalamazoo Watershed, MI USA through structural and functional contributions, as well as indicators (%) within PLS-SEM latent constructs. Structural and functional contributions to NPP (kg $km^{-2}yr^{-1}$) were highly correlated, indicating that contributions to cumulative NPP increased as cumulative area increased. Similarly, the ratio of cumulative NPP to the cumulative area remained consistent between land cover classes – possibly because of stable landscape structure during the study period (Fig. 3.1) (Sciusco et al., 2022). Cropland composed most of the structural and functional contributions to NPP in the study area, followed by forest land cover; however, they decreased during the study period while urban land cover slightly increased. This points to the urbanization of the agroecosystem. The consequences of which, can decrease NPP due to the removal of cropland, forests, and prairies, decreasing not just food/fiber available but also carbon stock in the soil. With urbanization, an increase in managed turf has been estimated to annually offset 40-210 gCm^{-2} (e.g., sport fields, golf courses) (Schneider et al., 2012). This, in turn, increases water demand, with turf termed the largest irrigated "crop" in the U.S. (Milesi et al., 2003).

Therefore, this agrees with past research that LCLUC significantly influences carbon, water, and energy budgets. However, this study had a low rate of LCLUC and a low self-reported likelihood to change land cover by key stakeholders. Therefore, in areas with low LCLUC, the persistent composition has more influence on NPP than the rate of change. This persistence in LCLUC depends on the intensity of urbanization and the landowner's likelihood to change land management practices. These findings also indicate that SES models may benefit from including multiple measures of LCLUC to explore how conventional land cover change indicators interact with socioeconomic measures of land management and land use, particularly across LCLUC rates of intensity. This study also demonstrates that LCLUC can manifest within multiple SES processes (i.e., PLS-SEM constructs), each with unique relationships to NPP. I pose that land cover indicators may behave differently in PLS-SEMs in rapidly urbanizing or landscapes with notable land cover change, given the relative persistence in LCLUC in the study area.

Regional development influences on land management

During the study period, urban land's structural composition and functional contribution to NPP increased. This aligns with records of shifting land ownership in farmlands to rental farming, resulting in a loss in smaller farms (40-200 acres) (Rudy et al., 2008). Land ownership and tenure can have implications for the adoption of conservation practices and sources of information in land management (Varble, Secchi, & Druschke, 2016). Therefore, Land Management's negative relationship with Regional Development and NPP may respond to this urbanization, ownership transition, and cropland intensification, such as the loss of small-farm owners and an area within farmsteads and increase in industrial farming since the 1970's. However, Regional Development also made a significant, moderate contribution to NPP through Land Management (0.293, *t*-stat 3.781). One explanation is that agricultural intensity increased, which similarly increased fertilizer/soil applications, income, yield, and irrigation per acre while decreasing the operations of smaller farmlands due to operation costs. This aligns with observed landscape transitions in the study area by Castoriadis et al. (2008), which recorded these land ownership and management changes in response to emerging economic transitions. Moreover, shifts in ownership are known to influence land management, such as tillage practices, enrollment in conservation programs, and sources of information (Lind-Riehl et al., 205; Varble et al., 2016). This supports the hypothesis that regional development can directly influence land management, which in turn shapes the LCLUC and NPP of the landscape. In another study, increases in regional development, such as gross domestic product and population density, also had significant positive contributions to NPP (Kolluru et al., 2022a, 2022b). Similarly, a neighboring landscape in southeast Michigan found that exurban/rural areas witnessed increased or maturing forest land at the expense of farmlands during this time period (Zhao et al., 2007). This may further explain variations in NPP not captured in this model, which best captured agricultural land management and tenure.

Influences of anthropogenic activities on land cover land use change

Agroecosystems account for a significant amount of carbon stock potential in regional budgets that depend on land management such as cover crops, fertilization, production intensity and water use (Guzman & Golabi, 2017). In the study, anthropogenic activities in Regional Development and Soil and Plant Nutrients had stronger relationships with NPP than abiotic processes Land Cover Change, Heat Stress or Water Stress alone. When Land Management interacted with Land Cover Change, there was a strong, positive relationship with NPP comparable to Soil and Plant Nutrients. This was slightly expected, as the highest structural and functional contributions to NPP in the study area are croplands, which are known to have high contributions to NPP throughout the Midwest due to large corn-soy rotations (Hicke & Lobell, 2004). Spatial representation of LCLUC may explain how these indicators performed statistically, as they may be capable of capturing some but not all processes at scale (Amirkhiz et al., 2023). Also, the area has not undergone significant land cover change, but rather socioeconomic changes in land management. For example, the study area is known to have undergone substantial changes in land use, farmland management and shifts in land ownership and tenure (Rudy et al., 2008). Therefore, land use and management (i.e., anthropogenic activities) may have stronger influences on NPP than land cover change alone, which can remain steady while land use/management continues to change.

Surveys with Centennial Farmers contextualized land management decision-making and changes over time, which elaborated on land use intensity indicators. Landowner self-reported environmental stewardship was found to have the strongest relationship with the likelihood of changing land use or land cover. Also, landowners contextualized land management motivation slightly more from an environmental stewardship and environmental impact perspective than a climate mitigation perspective. Family traditions, community relationships, and locally defined social norms play key roles in shaping LCLUC options available to individual landowners (Lind-Riehl et al., 2015). While this study was limited to a single landowner survey, future research may routinely survey populations in tandem with other socioecological data to further explore decision making and social influence in land management. Self-reported environmental stewardship as an indicator in land management may serve as a stronger indicator in SES models than climate change or carbon cycle concerns.

Structural equation model potential in socioecological research for spatiotemporal analysis

A challenge to landscape ecologists is to meld the ecology-centered spatial view with the society-centered holistic view to understand how spatial-temporal heterogeneity affects the resilience of the ecosystems of the Earth on which all organisms depend (Kugler et al., 2019; Wu, 2006). The application of PCA and PLS-SEM on an SES framework offers insight into the interrelationships of environmental change and human activities related to LCLUC (Castoriadis, 2008; Zhao et al., 2007; Kolluru et al., 2022a). Increasing efforts to sample spatiotemporal high-resolution data has resulted in ethical advancements in social science to address concerns of privacy, data preservation and data sharing for reproducibility (Kugler et al., 2019). While volunteered geographic information, such as opt-in tracking services or surveys, is a popular method to sample land management data (Goodchild, 2007; Yang et al., 2017), this study demonstrates how an SES model can adopt historical census records into a geospatial approach. County-scale census data use is encouraged, as it offers long-term records that adhere to standardized sampling and privacy protocols. Country land use allocation and use is a reporting requirement to the Food and Agriculture Organization (FAO) statistics and the global forest resources' assessment, as well as those reporting to the Kyoto protocol and the UN Collaborative Program on Reducing Emissions from Deforestation and Forest Degradation—UN-REDD (Arévalo et al., 2020; IPCC 2019, 2019; Olofsson et al., 2014). Conversely, ecological remote sensing and climatic data are often available at higher spatiotemporal precision than social data. Therefore, these were aggregated to county-level estimates to compare with socioeconomic data within the PLS-SEM SES model. Moreover, finer-scale ecological data (30 m) can be used for land cover functional contribution and structural composition to NPP. In this approach, matching spatiotemporal socioecological interactions at one scale (i.e., county-scale) and further investigating the geospatial variation in land cover change and carbon productivity is possible. Future research may also consider metrics such as edge-effects, fragmentation, and patchiness of land cover types to further evaluate landscape composition in SES models.

Applications of SEM in ecology often perform confirmatory/exploratory factor analysis on abstract concepts, such as “climate change,” “ecosystem structure and/or composition,” “resilience,” and more with the applications of latent variables (Fan et al., 2016; Giannico et al., 2021; Kolluru et al., 2022a; Yang et al., 2021). However, such models may be challenged by limited observations at the landscape scale, as they require normally distributed data and large sample sizes. The use of PLS-SEM has been under-utilized in SES and ecological modeling despite its performance in small sample sizes and exploratory research and greater statistical power (Hair et al., 2011). Successful examples of PLS-SEM in SES research have investigated highly urbanizing environments driven by rapid socioeconomic change (Fan et al., 2019; Park et al., 2017). A second obstacle to SES modeling is the extensive number of metrics that exist for landscape analysis, with no single way to determine the unique dimensions of a landscape structure (Cushman et al., 2008). This was addressed by first applying a PCA to inform the PLS-SEM theoretical constructs. Similar applications of PCA followed by PLS-SEM were used in psychological resilience theories (Munoz et al., 2017). Therefore, a PCA analysis has potential to inform an exploratory PLS-SEM in complex SES modeling unique to each landscape, given a theoretical foundation.

Limitations and future research

In this study, interannual variability is not clearly depicted in land cover types, which impeded the understanding of annual vegetation patterns. For example, a single species (i.e., cheatgrass) was responsible for dramatic changes in landscape vegetation patterns that were hypothesized to be caused by LCLUC (Bradley & Mustard, 2005). This is also because spectral differences exist between vegetation types and respond differently to weather events and seasonality (Compton et al., 1985). Future research may consider variables related to phenology if interannual variability and seasonality are essential representations of the ecosystem. Second, using a PCA for selecting land cover metrics can ignore the connections with organisms or process responses (Cushman et al., 2008). Future research may consider how these connections are incorporated, be it in the SES dataset analyzed or in the interpretation of the result. More so, the same PLS-SEM would not fit another sample drawn from the same population (Sharma et al., 2019). Therefore, pathways, loadings, and constructs are anticipated to strengthen, weaken, or emerge given a larger sample of the same population. This process is necessary to better understand where representation matters in SES systems. In fact, users are encouraged to apply a PLS-SEM in small samples while collecting additional data to formalize their theoretical framework before beginning a covariance-based SEM to estimate causality (Hair et al., 2011, 2021).

Landscape ecology and geography are well-suited for high-priority research directions focusing on the sustainability and profound changes made to Earth's surface. Relating the metrics used to determine landscape patterns and change to ecological processes is an ongoing research area (Gergel & Turner, 2017). Future work can address the effects of environmental change on people, complex interactions, values associated with or attributed to environmental services, changes under management, as well as sustainability in an urbanizing world (Harden, 2012; Zimmerer, 2010).

Conclusions

This study evaluated how LCLUC and land management jointly contributed to changes in NPP through a complex cause-effect analysis of socioecological latent variables. While many of these activities can be understood through direct modeling of variations of NPP, a path analysis such as PLS-SEM allowed a cross-comparison between interrelationships with NPP simultaneously, which is important for understanding an agroecosystem's landscape level processes. It was found that LCLUC manifested as contributors to various PLS-SEM constructs, estimated by the PCA analysis, indicating that respective land cover types are tied to anthropogenic processes. Cropland (CRO) contributed to the Land Management construct, forest (FOR) and water (WAT) to the Land Cover Change construct, and urban land cover (URB) to the Regional Development construct. Of abiotic (i.e., Water Stress, Heat Stress) and anthropogenic (Rural Development, Land Management, Land Cover Change) constructs, the latter contributed more explanation to NPP in the study period. The findings in this study build a new understanding of human-nature connections and illuminate how ecosystem processes may respond to economic activity and land management choices that are difficult to capture due to their spatiotemporal resolution (i.e., decadal sampling, political spatial extent). Deploying nature-based solution strategies in this region would need to consider historical and current land use, as well as decision-making and priorities for landowners.

This framework is suitable for application to other research areas, with the understanding that no single set of model metrics can be expected to estimate or predict NPP. Rather, variations in the indicators extracted from the PCA for the PLS-SEM indicate the relevant socioecological contributors to this landscape. Practically, landscape ecologists are encouraged to continue connecting the ecology-centered spatial view with the society-centered holistic view to improve understanding of how spatial-temporal heterogeneity affects the resilience of the ecosystems. Landscape heterogeneity and change may be used to understand the processes and flows of materials and energy, abiotic and biotic processes, and help us understand flows and changes of carbon. In turn, this may be used to inform climate change projections and anticipate socioenvironmental consequences. Future applications with PLS-SEM may include questions and applications of pattern detection to describe how a landscape has changed through time, estimate future predictions regarding the landscape change, or evaluate alternative land management strategies in terms of the C productivity and landscape patterns that may result.

CHAPTER 4. CARBON OFFSET POTENTIAL OF MIDWEST AGROECOSYSTEMS: A SPATIALIZED LIFE-CYCLE ASSESSMENT FRAMEWORK

Abstract

The intensification of agricultural practices in agroecosystems in the US since the 1950s has led to increased environmental impacts and greenhouse gas emissions. To address these concerns, global policies such as the United Nations Sustainable Development Goals (SDGs) are calling for Nature-based Climate Solutions that balance climate change mitigation with resource protection, sustainable energy transitions, and food security. Policymakers must therefore evaluate agroecosystems from both an anthropogenic and ecological perspective, leading to initiatives such as Natural Working Lands by the US Climate Alliance. However, climate mitigation may also have adverse effects, underscoring the importance of considering land management alongside indirect resource use and consumption and biophysical feedbacks. This chapter proposes linking geospatial land cover land use change (LCLUC) approaches with life cycle assessment (LCA) by land cover type. While environmental and climate data are available at higher spatiotemporal resolutions, reliable records of land management are limited to coarse resolution surveys conducted every 5 years and aggregated to state or county-level extents. To overcome this limitation, this work evaluates the intensity rates and ecological processes of cropland management within a 1 km extent and compares emissions scenarios from select inputs to predictions of land cover and carbon stock, testing a carbon offset approach. The results indicate that upstream processes have similar or larger emissions than onsite resource consumption. With land cover change prediction, it is found that carbon stocks may slightly decline by 2050, the year by which the SDGs aim for carbon neutrality. This study demonstrates the capacity to spatialize LCA with a functional unit of square area land managed and discusses aggregating socioecological processes for policymakers.

Introduction

Global efforts to utilize nature-based climate solutions (NbCS) are rising, with many efforts focused on both reducing anthropogenic greenhouse gas (GHG) emissions and harnessing the potential of terrestrial carbon capture and storage. The Kyoto Protocol, United Nations Sustainable Development Goals, The Paris Agreement, and Conference of the Parties efforts' have resulted in state-level policy and goal setting, particularly in the United States. In 2021, the United States re-joined the Paris Agreement and pledged to reduce nationwide greenhouse gas (GHG) emissions 50-52% from 2005 levels by 2030 and to reach net-zero emissions by 2050 (IEA, 2020). However, even if substantial reductions in anthropogenic GHG emissions are achieved, efforts to sequester these emissions will be necessary to reach safe levels of atmospheric carbon and mitigate climate change (Kane, 2015; Portner et al., 2022). NbCS offers strategies to manage landscapes for the purpose of increasing carbon stock and/or reducing GHG emissions (Novick et al., 2022). New and existing programs are accelerating progress in the USA to reach these goals, including an integrated US GHG Monitoring & Information System, which coordinates the use of atmospheric-based and activity-based approaches (NASA, 2023). Climate mitigation is essential to offset GHG emissions and sequester past emissions, particularly in intensively managed agroecosystems that have witnessed a rise in intensely regulated and specialized systems (e.g., large farms continue growing, small operations are decreasing, crop diversity is declining) (Spangler et al., 2020). Unique cultural practices, resources, and economic strategies contribute to stakeholder decision-making in land and resource management. Therefore, policymakers require a monitoring framework that can capture the variation in land use and land management across scales. At the landscape or local scale, they must identify where climate mitigation resources are best allocated; whereas at the national scale, policymakers should have access to normalized and comparable estimates to avoid conflicting methodologies.

Applications of NbCS may vary by government body due to policy maker's prioritization of natural resources and climate mitigation goals. The US Climate Alliance (USCA) is a bipartisan coalition of 24 governors collaborating to achieve Paris Agreement temperature increases below 1.5deg C. Many alliances include Natural Working Lands (NWL) in their GHG mitigation goals and climate policies but remain challenged as to how NWLs can integrate with existing net-zero and other economy-wide targets (USCA, 2022). Approximately 714 million MT of C per year, equal to ~12% of annual US GHG emissions, are sequestered by NWL (EPA, 2019) such as forests, woodlands, grasslands, shrublands, croplands, rangelands, wetlands, and urban green spaces. With few years remaining to reach 2030 and 2050 carbon neutral goals, a key challenge to NbCS is determining where to prioritize their implementation. Numerous studies have evaluated the relationships between ecological processes in managed and unmanaged agroecosystems, providing essential understanding on the ecological feedback and health within long-term studies. These studies can provide baselines estimates for carbon stock and flux. However, the lack of spatial land management data has limited our understanding of where and how intense land management practices occur. This challenge is exasperated due to scaling and the assumptions during aggregation. As ecosystem processes and carbon production can be monitored and scaled in process-based models using functional relationships, significant advances in their spatiotemporal resolution and data availability have far outpaced that of land management estimates. Conversely, methodology to estimate land management cannot acquire instantaneous or interannual samples over large extents. Methodology includes surveys with stakeholders or extrapolation from sales records monthly, annually or every 5- or 10-years. Scaling and gap filling data is not as simple as functional relationships as land management decisions significantly vary due to unobserved socioeconomic variables.

Process-based tools such as life cycle assessments (LCA) can evaluate anthropogenic GHG emissions, resource consumption and waste as well as indicate the geographic location of processes. LCA is a modeling technique used to quantify the environmental impacts of a product or service over its entire life cycle, and it typically involves four main stages: goal and scope definition, inventory analysis, impact assessment, and interpretation. The processes evaluated in an LCA range from upstream processes (e.g., resource extraction, manufacturing, transportation), use stage (e.g., consumption, combustion), and downstream processes (e.g., recycling, waste, distribution). Yet, spatial approaches to LCA are still under development in literature and can indicate several ways in which spatial information is incorporated into the LCA analysis (Hiloidhari et al., 2017; Nguyen et al., 2022; Wu et al., 2022). Geographic approaches have estimated the land use (i.e., occupied or transformed) and the source of materials-water-energy within processes (i.e., regionalized LCA or territorial LCA) (Frischknecht et al., 2019; Loiseau & Margni, 2018). Combined, these approaches can be powerful for global economic production cycles, evaluating international trade and resource consumption for a specific product. However, this approach is less useful for policy and decision makers evaluating landscape and regional land management and land use activities, who need to compare local emissions with ecosystem processes to monitor carbon offset, ecosystem health and resource management. In the model, processes may only represent a single land management choice available to a stakeholder, for example whether to irrigate or not. In another spatialized LCA, multiple farms' field logs were evaluated within an impact assessment and mapped, using Moran's I to estimate the strength of geographic relationships (Wu et al., 2022). However, these approaches still consider the production cycle of one decision maker as opposed to a population, which is needed in land management policy. Therefore, LCA must consider the square area of production as the functional unit and estimate the average land management practice within the life cycle inventory. In this way, multiple decision makers are represented, for example the rate of intensity can be used to represent various tillage methods rather than a single tillage method alone.

Land cover land use change (LCLUC) is one approach to link biophysical feedbacks and anthropogenic emissions geographically, spatializing LCA processes modeling average land management within a square area. By identifying land cover and utilizing existing land change models such as Terrset and InVEST, it is possible to note where land cover and potential land use will change over time. Additional knowledge from literature, stakeholders and policymakers can then collocate ecosystems with management. Carbon stock models coupled with LCLUC establish projections of land cover change and consequential C stock gained/lost (e.g., REDD+, Natural Working Lands, and others) (Kanowski et al., 2011; USCA, 2022). While these programs are limited to generalized C stock coefficients, this can be addressed with detailed landcover mapping that includes multiple land cover types at fine-scale resolutions. Regional and landscape-scale estimates may utilize the primary data and localized biophysical feedback made available from long-term ecological observation networks (e.g., FLUXNET, Long-term Agricultural Research, Long-term Ecological Research, iLEAPS). For anthropogenic emissions, land cover type can inform which land management practices will likely occur, such as cropland area and irrigation. Rich records of land management are available from federal and state level programs linked to land cover may offer baseline knowledge of where concentrations of anthropogenic GHG are sourced. In the US, the National Agricultural Statistics Service (NASS) has recorded farmland management (including forests, grasslands, and croplands) since 1863 at state and county-level and offers cropland data layers by crop type from 1997 to present. The USDA Economic Service (ERS), established in 1961, similarly provides geospatial data on the rural economy, farm program distribution and indicators for food access. Linking both land cover types with known ecosystem models and land management records may pave the way for a socioecological analysis of NbCS potential.

In this study, I evaluate a framework where the GWP impact of a socioecological system can evaluate both ecosystem and anthropogenic processes in a contiguous spatial representation. Land management and respective GWP emissions can be evaluated with LCA and projected spatially at the landscape scale when linked to land cover type. To accomplish this, I replace conventional LCA functional units, such as a commodity produced or cost, with a spatial functional unit: cropland managed km^2. To demonstrate the framework within a carbon offset scenario, present and future carbon stock and storage scenarios are evaluated against select cropland management emissions recorded by the USDA NASS census. This study does not account for all cropland management processes, as that is outside the scope of this study. Rather, the goal of the study is to demonstrate a framework suitable for future LCA research where processes and impact assessments may be linked to land cover type, which can be readily evaluated geospatially and include land management records.

This study area encompasses the Kalamazoo Watershed of southwest Michigan, USA, which is home to rich primary ecological data from the Great Lakes Bioenergy Research Center and Long-term Ecological Research station at the Kellogg Biological Station, as well as agricultural intensification and secondary forests. In this study, I ask (1) can GHG emissions and global warming potential (GWP) from historical cropland management records be geospatially represented in LCA; (2) can spatial variation in GWP estimates be detected in useful ways to inform NbCS strategies; and (3) how do these results inform state policy and climate goals to reach carbon neutrality by 2050? I hypothesize that GWP spatial variability will be driven by cropland management intensity, sourced from social data, and that rates of land cover change will influence carbon stock predictions. To achieve this, cropland management processes and GHG emissions from an LCA and carbon stock estimates are linked to NLCD cropland land cover to estimate the net difference between current and predicted land cover. As such, estimates of carbon stock and potential offset can evaluate collocated environmental impacts in present and future scenarios. This approach can serve as a framework for policy and decision makers to generate baselines for comparison with NbCS efforts to reach carbon neutrality goals and visualize them spatially to identify high-priority areas.

Methods

This framework includes three overall stages, the first is a land cover change model (LCM), the second is C stock estimation using the Ecosystem Services Modeler (ESM), and the third is a life-cycle analysis (LCA) to estimate the anthropogenic GWP of cropland management. The outcome is a spatialized LCA where GWP is mapped across cropland in the study area and carbon stock is estimated as potential offset (Fig. 4.1). Geospatial analysis for data preparation was conducted in ArcGIS Pro (3.0.0), while the LCM and ESM were conducted in TerrSet software (19.0.7) (Eastman, 2020). The LCM includes land cover change detection, transition sub-model selection, variable selection, transition potential modelling, change demand modelling, model validation and land cover change prediction. The ESM was used to estimate C stock per land cover type, particularly in the predicted land cover, following the IPCC Tier 1 approach. The LCA estimates the GWP of select cropland management activities (inputs and processes) during the Use Stage to evaluate the capacity of the approach. The cropland management processes selected for this study represent variation in management between counties and are therefore best suited for evaluating the model, whereas other processes that may have significant contributions to GWP were assumed to be equal across the study area. All estimates were mapped to the extent of the study area to evaluate carbon offset from 2017 to 2050, when the State of Michigan aims to reach carbon neutrality.

This framework is evaluated in a watershed-scale agroecosystem within a participating USCA state leveraging a NWL action plan to reach carbon neutral goals. In the State of Michigan, USA, Governor Whitmer founded the Council on Climate Solutions in 2020 to serve as an advisory body in the Department of Environment, Great Lakes, and Energy (EGLE) (Executive Order 2020-182, 2020). The Council includes five advisory workgroups to help the state reach carbon neutrality by 2050, one of which is Natural Working Lands and Forest Products. The state is home to 20.3 million acres of forestland, with projections of forestland to decrease to 19.2-18.7 by 2060 due to population increase, climate change, and invasive species (Michigan Forests, 2014). The state also is home to

~10 million acres of farmland and ~47,600 farms that produce more than 300 commodities commercially. The food and agriculture industry contributes $104.7 billion annually to the state's economy, with field crops contributing $5.12 billion, and accounts for ~17% of the state's employment (MDARD, n.d.). As cropland has given way to reforestation in the region, changes in carbon stock over time and the cropland management GWP are evaluated in this framework.

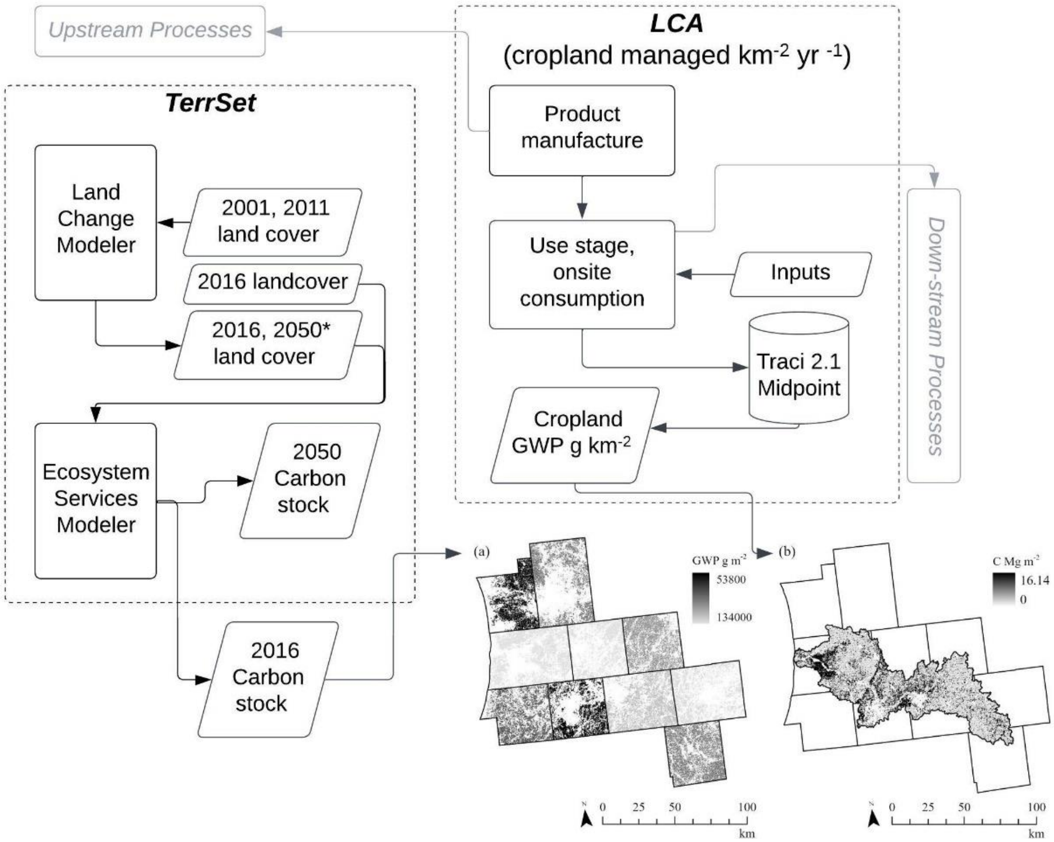

Figure 4.1. The conceptual framework to link ecosystem processes with historical land management records, using cropland management km-2 yr-1 as an example. TerrSet Software processes include the (1) Land Change Modeler, which *predicts future land cover (i.e., 2050) based on 2001 and 2011 land cover data; and (2) the Ecosystem Services Modeler, which provides carbon stock estimates for years 2050 and 2016. The life cycle assessment (LCA) models cropland management km-2 yr-1 including processes and flows from product manufacture and use. Upstream and down-stream processes in grey indicate LCA stages outside the scope of this study. A midpoint impact assessment with Traci 2.0 attributes global warming potential (GWP). Land cover type geospatially links GWP and carbon stock estimates for a geospatial analysis.

Study area

The Kalamazoo River Watershed (HUC8; 5,261 km2), is approximately one hundred miles wide and includes portions of ten counties: Allegan, Barry, Eaton, Van Buren, Kalamazoo, Calhoun, Jackson, Hillsdale, Kent, and Ottawa (Fig. 4.2). The watershed has undergone little land cover change, however its land management and land use (e.g., regional development and cropland management) has considerable influence on terrestrial carbon production (Shirkey et al., 2023). The largest urban centers include Kalamazoo and Battle Creek. The Kalamazoo River begins as a spring-fed pond in northern Hillsdale County and flows westward in a northerly arc through the cities of Albion and Battle Creek into Saugatuck before reaching Lake Michigan. The Kalamazoo Watershed is in a humid continental temperate climate with a mean annual air temperature of 9.9 °C and a cumulative average annual precipitation of 1027 mm (Michigan State Climatologist's Office, 2013). Soils are Typic Hapludalfs, well-drained sandy loams (Bhardwaj et al., 2011; Thoen, 1990). From May through September, representing the growing season, mean air temperature and total precipitation are 19.7°C and 523 mm, respectively, with the highest temperatures in July (Abraha et al., 2018).

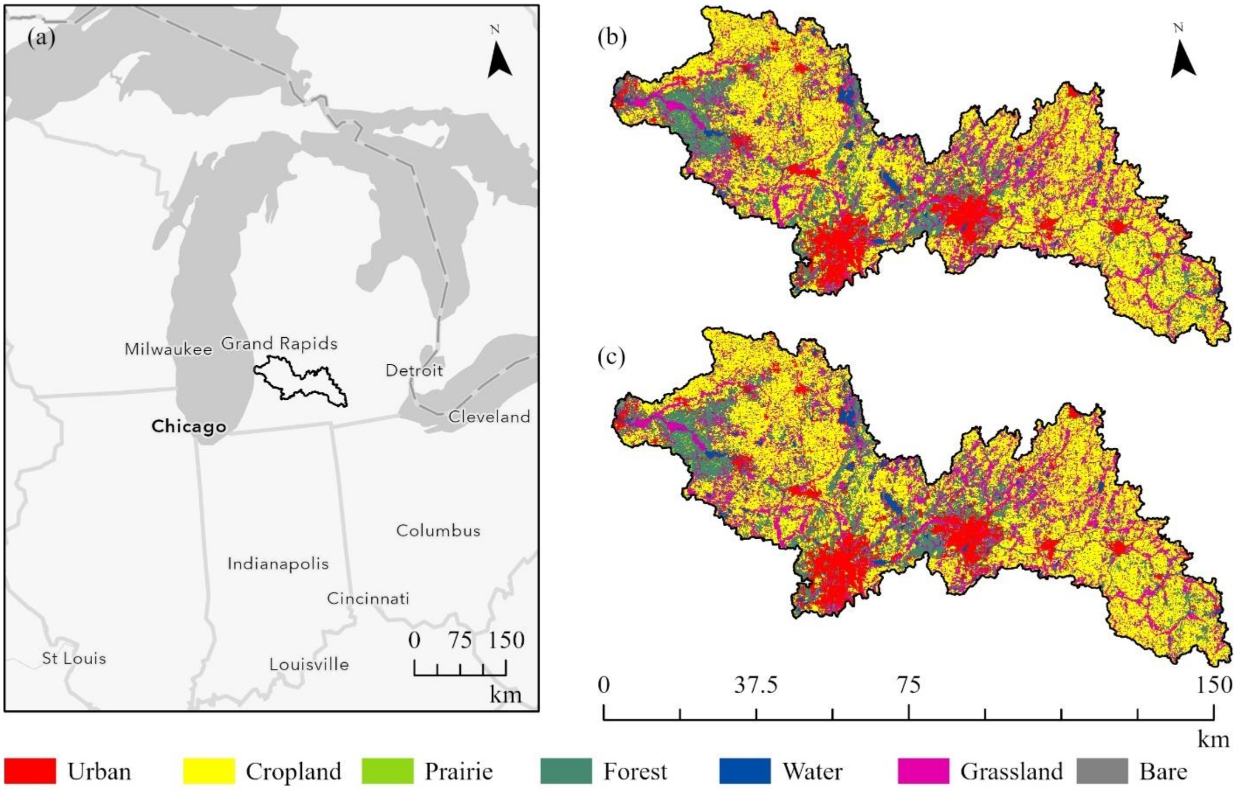

Figure 4.2. The (a) Kalamazoo River Watershed (HUC8; 5,261 km^2) in southwest Michigan, USA; with (b) reclassified NLCD land cover (Table A10) in 2001 (c) and 2011 presented for visual assessment of land cover change and composition of dominant land covers Cropland and Forest.

Land cover change model

Land cover change detection was conducted with TerrSet version 19.0.7 LCM using NLCD land cover data from 2001 and 2011 for modeling training, and 2016 for model validation. Net loss/gain of all land cover types were evaluated for visual spatial trends of change, with a particular focus on modeling drivers of land cover transitions from cropland and forest to urban areas. Urbanization and reforestation sub-models were conducted as a multi-layer perception (MLP) neural network model, which allows modeling of multiple transitions at once. The MLP model examines potential transitions for each land-cover according to driver variables (see section 2.3.1) provided and applies a backward stepwise constant forcing procedure to indicate which variables best predict change (Atkinson & Tatnall, 1997; Eastman, 2020). The MLP neural network consists of 'input,' 'hidden,' and 'output' layers that are used to define complex, non-linear relationships between LCLUC and driving variables. The minimal number of randomly selected pixels from each land cover class was set to 5525 (i.e., the minimum cells that transitioned from 2001 to 2011); where 50% of pixels trained and 50% tested model prediction across ten thousand iterations. The criteria for acceptable model outcome was set at 80% (Eastman, 2006). The outcome are accurate estimates of transition potential (Eastman, 2020; Sangermano et al., 2010), which represent the "behavioral propensity of the actors determining land-use change" defined by inferred logic from transition rules (Roodposhti et al., 2019). In the following sections, more details about the MLP model drivers and land change prediction methodology is provided.

Land cover change data

Land cover datasets for 2001, 2013, and 2016 were acquired from the National Land Cover

Database (NLCD, 30 m) (Homer et al., 2015) and were reclassified to Level 1 LCMAP land cover classifications, including Urban, Cropland, Prairie, Forest, Water, Wetland and Bare (Table A10). US Decennial Census 2010 population density from census tract level were acquired from IPUMS database to estimate the population density (POPD) (Ruggles et al., 2022). Slope and Elevation from the Shuttle Radar Topography Mission (SRTM) 1 Arc-Second Global were acquired from USGS Earth explorer (https://doi.org/10.5066/F7PR7TFT). Streams and rivers were acquired from Michigan's GIS Open Data Portal and the Stream Rivers Assessment Units – 2020, which is a subset of Michigan's hydrological features in the 2020 Integrated Report on water resources generated by the Michigan Department of Environment, Great Lakes, and Energy. Primary and secondary roads were acquired from the US Census Bureau Department of Commerce TIGER/Line shapefile for Michigan 2015. Primary roads are divided, limited-access highways within the interstate highway system or under State management. Secondary roads are main arteries, usually within the US, State, and/or County Highway system, and may or may not be divided with one or more lands of traffic in each direction. Data processing for the land cover change model variables was conducted in ArcGIS Pro. Distance from roads, rivers, and urban areas were calculated by Euclidean distance. Population density was estimated from total population at 2010 census tract level, resampled to 30m resolution. All variables for the land change model in Terrset were clipped to the extent of the Kalamazoo HUC 8 watershed.

Table 4.1. Land cover change model variables and their spatial resolution, description, and source.

Dataset	Source	Spatial Resolution	Description
National Land Cover Dataset (NLCD)	Homer *et al.,* 2015	30 m	Land cover classification for 2001, 2013, and 2022
US Decennial Census	Ruggles *et al.,* 2022	30 m	Population density by 2010 census track
USGS Shuttle Radar Topography Mission	USGS (n.d.)	30 m	DEM for elevation and slope
TIGER/Line Shapefile, 2015, Michigan Primary and Secondary Roads	U.S. Census Bureau, 2015	-	Michigan Primary and Secondary Roads
Streams Rivers Assessment Units – 2020	MI EGLE, 2020	-	Michigan rivers and streams

Drivers for LCLUC

Transition sub-models require variables of land cover change, hereafter called land change drivers, which consist of physical and human geography variations across the study area (Fig. A3). Drivers of urbanization such as distance to urban areas, population density, and distance to roads were included (Leta et al., 2021). Distance to water bodies (i.e., rivers, lakes, streams) were also included, as development of residential areas congregate around in this region. In addition, slope and elevation are commonly used as driver variables; however, given the topography of the study area, these variables have low variation and therein less contribution to model explanatory power. Lastly, the LCM offers variable transformation using event likelihood, an empirical probability of change, between earlier and later land cover maps. This was included as an evidence-based likelihood, as drivers of past changes are assumed to be sustained and expected to influence future changes. Distance from roads, distance from water, distance from urban area, population density, and evidence likelihood were set as dynamic (i.e., as opposed to static) as they are anticipated to change over time. To evaluate model performance and avoid model inflation, variables were eliminated by evaluating backwards stepwise constant forcing of variable combinations. As such, variables are removed if they have trivial effect on model performance when held constant. It is acknowledged that Cramer's V is also a valid method to determine variable qualification, even though it does not represent the scientific prerequisites and multifaceted nature of relationships (Hasan et al., 2020). The power of model performance reporting available from the MLP neural network was chosen as it offers superior accuracy (Clark Labs, 2021).

Future land cover prediction

Michigan's long-term strategic goal is to obtain carbon-neutrality by 2050 and implement the Working Lands climate mitigation program. To simulate current LCLUC development in the study area and what it might mean for policy makers and stakeholders, the model projected land cover in 2050 using the same setting of predictive driver variables used to simulate the 2016 land cover map. The prediction assumes that land cover change is driven by the same variable characteristics in the future. Transition potentials determined by the MLP neural network model were applied within a Markov Chain (MC) to simulate land cover in 2016 given past changes in TerrSet 2020 v19.0.7 software (Eastman, 2020; Mungai et al., 2022).

The MC process determines the state of a system by knowing its previous state and the probability of transitioning from one state to the next. This is not simply a linear extrapolation from past transition potential to future years, but rather a matrix where transition potentials change over time as various transitions reach an equilibrium state (Borana & Yadav, 2017; Clark Labs, 2021; Mishra & Rai, 2016; Gibson et. al, 2018). The outcomes are a soft and hard prediction. In the soft prediction, a map of vulnerability was generated in which each pixel is assigned a value 0 to 1 for risk of transition from low to high, respectively. In the hard prediction, a simulated map of the predicted year was evaluated, where each pixel is assigned a land cover category. After the 2016 simulation is created, a validation process compared the simulated land cover with the actual NLCD 2016 land cover map by applied using kappa index statistics.

In this study, the years 2001 and 2016 are used to predict land cover in 2050. For model validation between the NLCD 2016 land cover and the modeled 2016 land cover, a Kappa index was applied. Specifically, Kno, Klocation, KlocationStrata, and Kstandard estimate the agreement beyond percent correct, but also the quantity and locational agreement between two images (Pontius, 2002). For all Kappa statistics, 0% indicates agreement is equal to that of chance and 100% indicates perfect agreement. Overall agreement is indicated by Kno. Klocation indicates agreement in terms of the location of each category, whereas KlocationStrata indicates agreement for stratum-level location. Lastly, Kstandard indicates the traditional Kappa Index of Agreement. The validation was conducted from predictions for the 2016 land cover referenced with the NLCD 2016 land cover map. Validation confirmed that the model prediction of land cover in 2016 agreed well with the NLCD 2016 reference land cover. Results between the simulated prediction and the reference image estimated by Kappa indices—Kno, Klocation, KlocationStrata, and Kstandard—are presented in Table A15. All values are well above the desirable threshold minimum for Kappa indices and indicate that the prediction agrees well overall with the reference land cover. More so, the agreeability also accounts for the location of land covers.

Carbon stock potential

Present and future carbon storage potential of the study area was estimated with the

Terrset Ecosystem Services Modeler (Clark Labs, 2021). I estimate current and future carbon stored in the landscape with consideration of four carbon pools: above ground, below ground, soil, and dead organic matter. Carbon pool information is acquired from local resources, where available, or from regional estimates if unavailable (Table 4.2). Urban, Water and Bare land covers were assumed to have no C stock; and Wetland values are acquired from national estimates for the United States. Cropland, Prairie, and Forest estimates were collected from Morris et al., 2007, which evaluated afforestation in agricultural lands near the study area at the Fred Russ Forest Experiment Station (421000N latitude and 851580W longitude) located in Cass County in southwest Michigan that includes a 44-acre hardwood study area with four treatments: a control plot, shelterwood, clear cut and group cut harvest. Cropland biomass followed IPCC Tier 1 guidelines, which assumes that all NPP (i.e., above-ground biomass) is removed from cropland, as it is harvested. Regionally representative carbon pool estimates (Table 4.2) were applied to land cover classes from NLCD 2016 and the predicted 2050 land cover to estimate their cumulative difference.

Table 4.2. Carbon pool estimates (Mg C ha^{-1}) used to represent land cover classes within the Kalamazoo River Watershed and their sources, including aboveground biomass (AGB) and belowground biomass (BGB).

Land cover	AGB	BGB	Soil C	Dead organic matter	Source
Urban	0.00	0.00	0.00	0.00	Sharp et al., 2020
Cropland	0.00	1.10	51.77	1.41	Morris *et al.*, 2007
Prairie	145.00	4.00	25.00	1.00	Morris *et al.*, 2007
Forest	93.22	14.16	70.21	1.80	Morris *et al.*, 2007
Water	0.00	0.00	0.00	0.00	Sharp et al., 2020
Wetland	10.00	5.00	20.00	0.00	Sharp et al., 2020
Bare	0.00	0.00	0.00	0.00	Sharp et al., 2020

LCA goal, scope, and functional unit

Select cropland management activities were evaluated within a life cycle assessment (LCA) to GWP emissions (i.e., $CO_{2\text{-eq}}$) with a function unit of cropland managed $km^{-2}yr^{-1}$. The scope of the LCA is to estimate emissions between manufacturing and use stage processes (Fig. 4.3) with the goal of evaluating the variation between estimates per county within the Kalamazoo Watershed. Processes were evaluated in openLCA software (1.11.0) with a midpoint analysis in Traci 2.1 to estimate GWP. Processes and cropland management evaluated are sampled from the National Agricultural Statistic Service (NASS) and estimated as rates of intensity per km^2 of cropland. As NASS surveys provide average county-level management estimates and historical records of sampling accuracies, it was assumed that these values well represent land management practices in the study area.

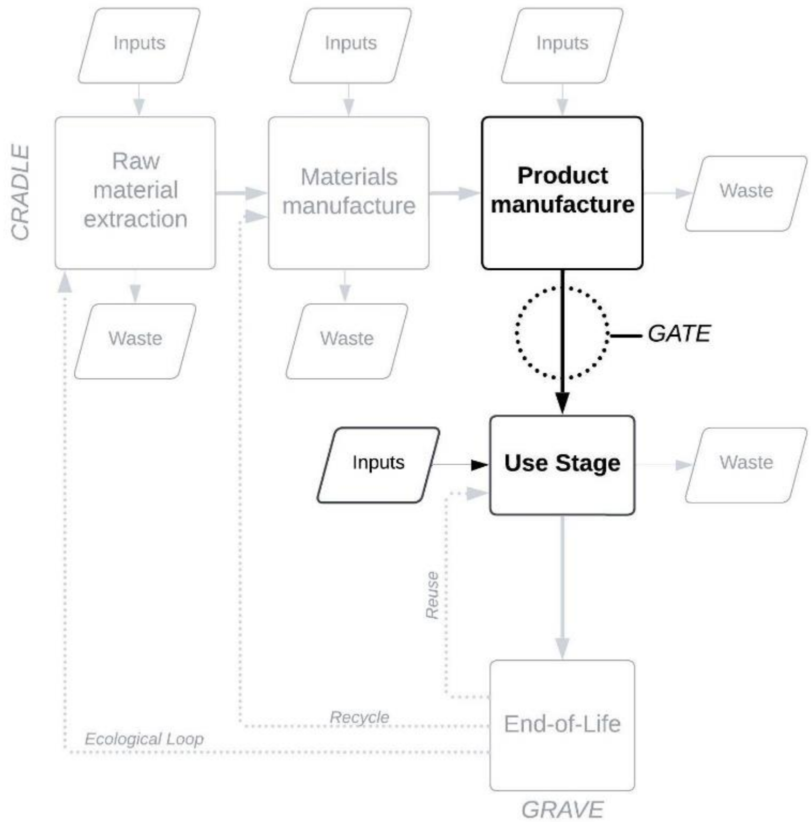

Figure 4.3. The multiple stages within a life cycle assessment from cradle, gate to grave. In this study, only items in black were evaluated, whereas items in grey are options for future research. The functional unit is cropland managed per km^2 yr^{-2}.

Life cycle inventory

Agricultural land management contributions to regional global warming potential varies by individual stakeholder. To account for this, NASS Census records and regional literature were evaluated by county-cropland area to determine rates of intensity per cropland managed km^{-2} yr^{-2} (Tables A16-21). As such, management intensity is estimated as total input per total cropland km2 for each respective county. Resources and inputs per process were sourced from regional literature to represent local practice (Table 4.3). It was assumed that all production and processes were for maize, which is the major crop in the area, and that all cropland is planted and harvested.

Upstream processes include the production of diesel, nitrogen and phosphorus and generation of electricity. Emissions for diesel, phosphorus and nitrogen production were acquired from US DOE (2019). The electricity used to pump water for irrigation was acquired from West and Marland (2002a) and emissions reflect the fuel mix that generated the electricity for the study area postal code 49060, as estimated by McGill et al., 2018. Use-stage onsite consumption included the combustion of diesel and consumption of nitrogen and phosphate. Diesel consumption rates were estimated from field logs for planting and fertilizing processes (Abraha, et. al 2019), as well as the average consumption rates across various machinery used to cultivate soil (USDA NRCS, n.d.), and harvest (West and Marland, 2002). Emissions from fertilizers were acquired from Abraha et al., 2019 within the study site, as well as Blonk Consultants, 2012.

Table 4.3. Land management processes considered for cropland management and their respective inputs, value, and global warming potential ($CO_{2\text{-eq}}$) coefficient for land cover 2016.

Process	Input	Value	Unit	$CO_{2\text{-eq}}$	Reference
Upstream processes					
Diesel production	Diesel at refinery/US	*	l km^{-2}	0.468 kg	US DOE, 2019
Nitrogen production	Inorganic nitrogen fertilizer, as N to generic market for organic nitrogen fertilizer, as N	**	kg km^{-2}	5.99 kg	US DOE, 2019
Phosphorus production	Inorganic phosphorus, as P205 to generic market for organic phosphorus, as P205	**	kg km^{-2}	2.80 kg	US DOE, 2019
Electricity generation	Electricity	13.30	GJ ha^{-1} m^{-1}	14.40-34.70 g m^{-2}yr^{-1}	McGill et al., 2018; West and Marland (2002)
Use stage onsite consumption					
Reduced till	Diesel	2842.50	l km^{-2}		USDA NRCS, n.d.
Conventional till	Diesel	5685.00	l km^{-2}		USDA NRCS, n.d.
Conservation till	Diesel	4737.50	l km^{-2}	2689.28 g	USDA NRCS, n.d.
Planting	Diesel	586	l km^{-2}		Abraha et al., 2019
Fertilizing	Diesel	430	l km^{-2}		Abraha et al., 2019
	Nitrogen	6052.46–10091.58*	kg km^{-2}	6.04 kg	Abraha et al., 2019; Blonk Consultants, 2012
	Phosphate	895.44–1720.34**	kg km^{-2}	0.22 kg	
Irrigation	--	--	--	--	--
Harvest	Diesel	1114.00	l km^{-1}	2689.29 g	West and Marland (2002)

* Varies, refer to use stage onsite consumption values
** Varies by county, see Table A16-21

Scaling LCA GWP to cropland extent

The output of the LCA provides estimates of GWP g m^{-2} that are unique to each county, which is incorporated into the NLCD 2016 land cover map in place of Cropland in ArcGIS

Pro (v3.1). As the NLCD raster is 30 m resolution, values of GWP g m^{-2} are multiplied by the square area of the cell (i.e., 900m^2) so that each 1 m^2 pixel in the cell will equal the GWP g m^{-2} generated from the LCA. After extracting and replacing the Cropland land cover with the GWP rates, the map was clipped to the Kalamazoo Watershed extent and cumulative GWP per county was estimated. In this way, an estimate the GWP g m^{-2} of cropland managed within a portion of a county is generated rather than the county's cumulative emissions.

It was assumed that land management records from the NASS 2017 is practiced in the same cropland extent as the NLCD 2016, due to low LCLUC in the area (Shirkey et al., 2023). However, this method is still limited to the aggregation of management practices to county extents, which can be limited in areas with large county extents. Additionally, this study assumes that NASS land management activities occur within the NLCD cropland extent; however, this may not always be the case as they are independently estimated with differing methodology. Further limitations involved with scaling and LCA to county level is the loss of accurate and divergent inputs to the product system. As cropland management varies across the landscape, it is possible that the averages simplify the socioecological system. Variations in management may include crop type, rate of fertilizers/pesticides, variations in machinery and fuel consumption, or farm operations specific to field or crop type. For example, diesel consumption during fertilizer applications varies by source, with estimates of 430 l km^{-2} (Abraha et al., 2019), 982 l km^{-2} (Bowers, 1992), 94.75 l km^{-2} (Downs & Hansen. 1998), and 284.17 l km^{-2} (Parsons, 1980). As such, future applications are encouraged to approach this framework as a general account of cropland management and to investigate site-specific inputs for their own production systems where appropriate;

and utilize averages and other estimates where necessary.

Results

LCLUC in the Kalamazoo Watershed

Little land cover change was found between 2001 and 2011 in the study area, with the largest net change in Urban and Cropland land cover (Table 4.4, Fig. 4.4). Net gain by land cover category includes 21.14 km^2 Urban, 11.04 km^2 Water, and km^2 1.13 of Prairie, whereas net loss included -16.44 km^2 Cropland, -6.43 km^2 Forest, -9.80 km^2 Wetland, and -0.65 km^2 Bare. Increased urbanization occurred in the surrounding areas of Kalamazoo, Michigan due primarily to Cropland and Forest loss, with 14.39 km^2 and 4.97 km^2, respectively; and there was no recorded loss in Urban land cover. Cropland gained 10.92 km^2 and lost 27.36 km^2 and was replaced by Urban areas (14.39 km^2) surrounding Kalamazoo and stretching towards Battle Creek, Michigan.

Areas with greatest loss and gain were in the southwest (Battle Creek, MI) and western (Allegan, MI) watershed, with most land covers persisting. Trends of Cropland loss stretched between Kalamazoo to Battle Creek, but also northwest towards Kent County. Forest gained 7.79 km^2 and lost 14.23 km^2, replacing 2.20 km^2 of Cropland surrounding Kalamazoo and west towards Allegan County. Notably, transitions of Cropland and Forestland to other land covers aside from Urban were in the northern and eastern rural areas outside of Kalamazoo and Battle Creek. Overall, land cover classes remained within 1% of their contribution to the study area across all years 2001, 2011, and 2016, indicating a stable composition.

Table 4.4. Land cover (km²) and percent composition from 2001, 2011 and 2016 in the Kalamazoo Watershed, and their respective net change by category (2001-2011).

Land Cover Type	2001		2011		Change (2001-2011)	2016	
	km²	%	km²	%	km²	km²	%
Urban	741.53	14.09	762.67	14.49	21.14	766.98	14.58
Cropland	2376.13	45.15	2359.69	44.83	-16.44	2352.42	44.71
Prairie	39.94	0.76	41.07	0.78	1.13	47.44	0.90
Forest	1127.62	21.43	1121.18	21.30	-6.43	1116.44	21.22
Water	107.48	2.04	118.53	2.25	11.04	110.91	2.11
Wetland	858.14	16.30	848.34	16.12	-9.80	856.42	16.28
Bare	12.24	0.23	11.59	0.22	-0.65	11.07	0.21

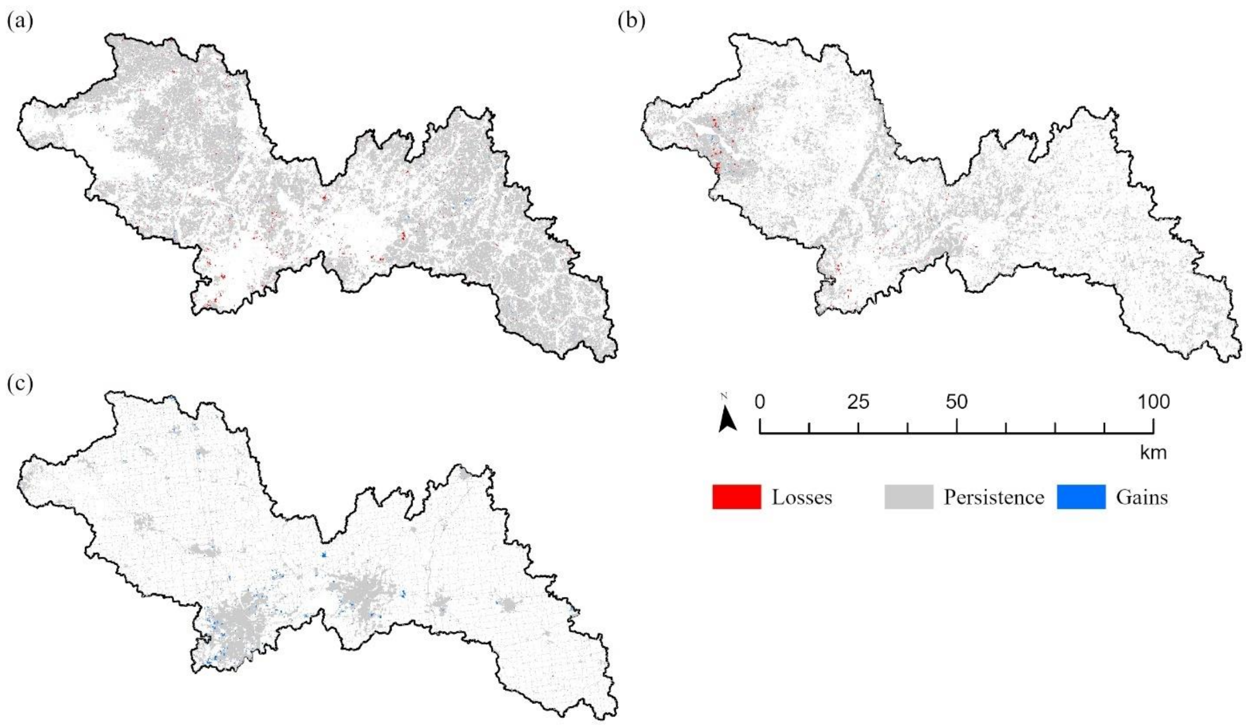

Figure 4.4. The Kalamazoo Watershed evaluated loss, gain, and persistence of land covers (a) Cropland, (b) Forest, and (c) Urban land covers between years 2001 to 2011. Minor change is observed, where red areas indicate loss, grey indicates persistence, and blue indicates gain between years.

Land cover model

Land change sub-models Urbanization, Reforestation and Other were modeled for land covers greater than 4.5 km^2, which included Forest and Cropland to Urban (i.e., Urbanization), Cropland to Forest (i.e., Reforestation), as well as transitions Cropland to Wetland, Forest to Prairie, and Wetland to Cropland and Water (i.e., Other) (Table 4.5). Transitions were named based on observed processes in the study area (Brown, 2000; Shirkey et al., 2023).

Table 4.5. Sub-model results of Urbanization, Reforestation and Other from the MLP model.

Sub-model	Class skill measure (ratio)	Accuracy (%)	Skill measure	RMS Training	RMS Testing
Reforestation		100.00	1.0000	0.4976	0.4976
Transition: Cropland to Forest	1.0000				
Persistence: Cropland	1.0000				
Urbanization		91.13	0.8817	0.3474	0.3473
Transition: Forest to Urban	1.0000				
Transition: Cropland to Urban	1.0000				
Persistence: Cropland	0.5315				
Persistence: Forest	1.0000				
Other		39.60	0.2953	0.3104	0.3110
Transition: Cropland to Wetland	0.6085				
Transition: Forest to Prairie	0.4493				
Transition: Wetland to Cropland	0.4812				
Transition: Wetland to Water	-0.1334				
Persistence: Cropland	-0.0521				
Persistence: Forest	0.5480				
Persistence: Wetland	0.1598				

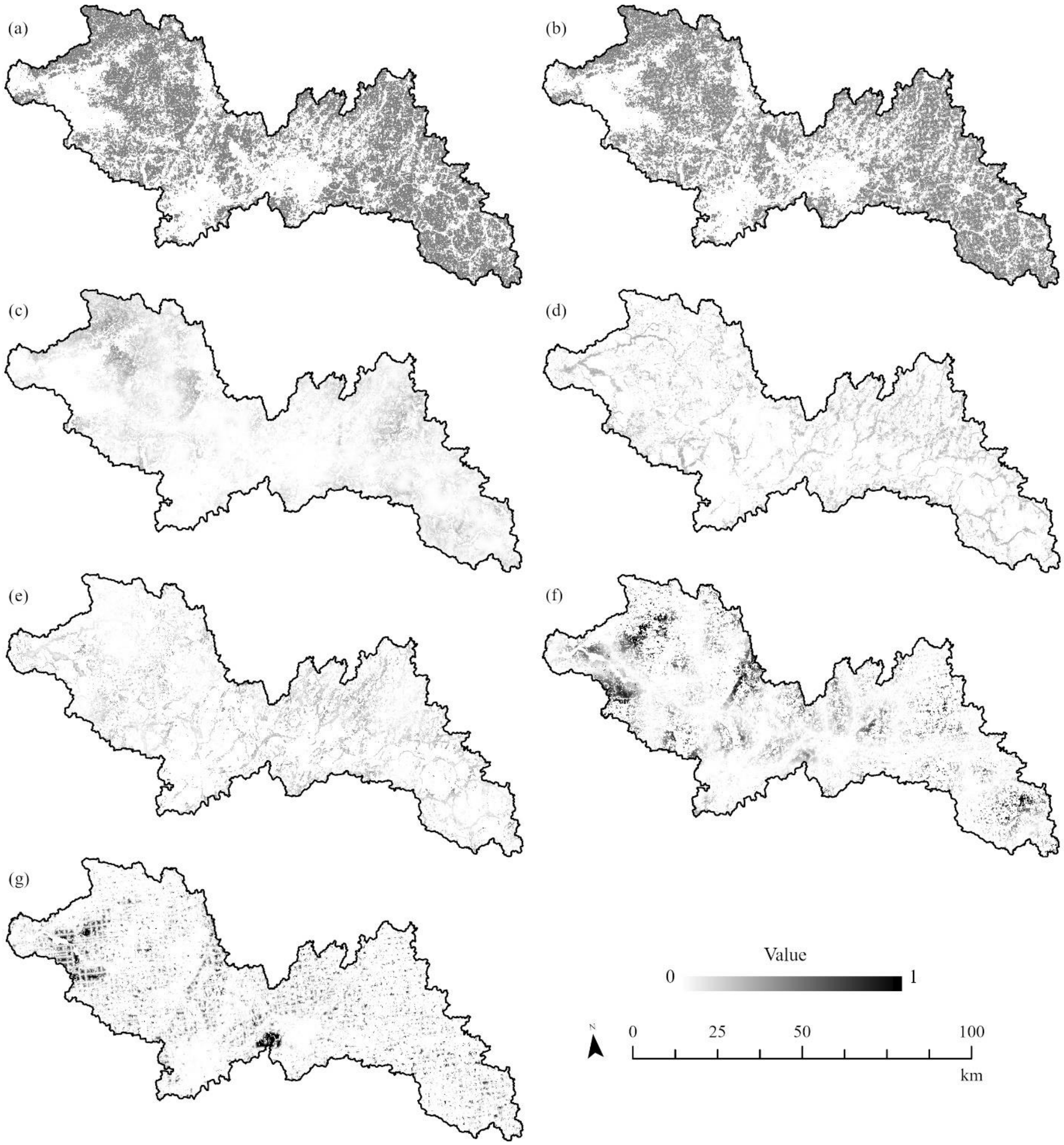

Figure 4.5. Transition potential maps for the study area used by the Land Change Modeler to estimate 2050 land cover. Transition values range from low to high likelihood, 0-1. Here, (a) is cropland to forest, (b) cropland to urban, (c) cropland to wetland, (d) wetland to water, (e) wetland to cropland, (f) forest to prairie, and (g) is forest to urban.

Transition likelihood indicates a high probability of all land covers persisting (>0.9), except for Prairie and Bare, from 2016 to 2050 (Fig. 4.4, Table 4.6). The MLP-Markov chain modeling matrix estimated that Urban land cover (0.9999) is highly unlikely to change. Therefore, areas of urbanization will continue to grow at this pace with minimal loss to other land covers. Cropland, Forest, Water and Wetland all have high persistence as well (>0.9) and indicate that some areas may experience transition, but that it is also highly unlikely. Remaining land covers Prairie and Bare have 0.5955 and 0.6494 transition likelihoods, respectively, indicating that there is moderate likelihood for transition. Prairie has a higher likelihood to transition to Forest (0.1968) or Cropland (0.1237) in 2050 than any other land class. Additionally, Bare landcover may transition to Water (0.1932) or Urban (0.0739) land covers.

Table 4.6. The Markov probability of land cover in the Kalamazoo Watershed from 2011 (rows) to 2050 (columns). Values in bold indicate persistence.

	Urban	Cropland	Prairie	Forest	Water	Wetland	Bare
Urban	**0.9999**	0.0001	0.0000	0.0000	0.0000	0.0000	0.0000
Cropland	0.0234	**0.9560**	0.0011	0.0078	0.0021	0.0091	0.0005
Prairie	0.0485	0.1237	**0.5955**	0.1968	0.0173	0.0152	0.0030
Forest	0.0173	0.0098	0.0143	**0.9532**	0.0039	0.0013	0.0002
Water	0.0042	0.0051	0.0064	0.0086	**0.9222**	0.0492	0.0044
Wetland	0.0040	0.0284	0.0004	0.0008	0.0429	**0.9233**	0.0001
Bare	0.0739	0.0221	0.0020	0.0344	0.1932	0.0249	**0.6494**

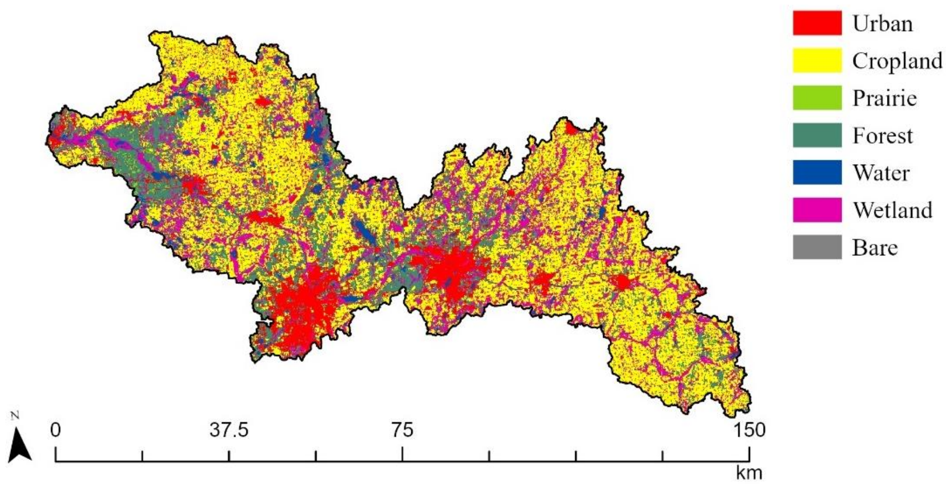

Figure 4.6. The Kalamazoo Watershed predicted land cover in 2050 following the Land Cover Model, which evaluated transition potentials (Fig. 4.4) between land cover and transition sub-model variables (Fig. A3).

Projected land cover in 2050 indicates that Urban land will gain another 21.14 km^2 and is anticipated to increase from 14.58% to 15.91% of the total area by 2050 (Fig. 4.5, Table 4.7). Water and Prairie will also gain 11.04 km^2 and 1.13 km^2, respectively. Land cover net loss is anticipated for Cropland (16.44 km^2), Wetland (9.80 km^2), Forest (6.43 km^2), and Bare (0.65 km^2). Urban land cover gains are at the cost of Cropland loss (14.39 km^2) and Forest loss (4.97 km^2), with remaining losses in Prairie, Wetland, Bare and Water land covers less than 1 km^2 each. Forestland gains were also due to losses of Cropland (2.20 km^2). The only gains for Cropland were due to losses of Prairie and Wetland, estimated at 0.75 km^2 each.

Table 4.7. Area statistics for the predicted land use land cover change in 2050 in the Kalamazoo Watershed, compared to the area statistics of the National Land Cover Database in 2016.

Land cover	2016		2050	
	km^2	%	km^2	%
Urban	766.98	14.58	837.29	15.91
Cropland	2352.42	44.71	2288.69	43.49
Prairie	47.44	0.90	57.11	1.09
Forest	1116.44	21.22	1104.16	20.98
Water	110.91	2.11	154.92	2.94
Wetland	856.42	16.28	809.33	15.38
Bare	11.07	0.21	11.59	0.22

Carbon stock offset of anthropogenic emissions from cropland management

Between 2016 and 2050 land covers, an estimated 1.30% of total C stock potential is anticipated to decrease. Loss of Forests and Wetlands and increases in Urban, Water and Bare contribute to the decrease in carbon stock potential. The development of Urban areas surrounding roads and with a 0.0234 likelihood replacing Cropland and 0.0173 likelihood of replacing Forest (Table 4.6) is predicted to occur in surrounding regions of Battle Creek, MI (southwest). Forest and Wetland loss is most likely to occur in the western watershed and forestland, where in the central watershed forest and cropland may convert to urban areas. These predicted changes in land cover inform where carbon stock will increase (positive value) or decrease (negative value), according to the land cover's respective carbon pools used in the model (Table 4.2, Fig. 4.8).

Anthropogenic emissions from cropland management demonstrated a noticeable variation by county, where Kalamazoo held the highest overall GWP, followed by Ottawa, Van Buren, Kent, Hillsdale, Eaton, Calhoun, Jackson, Barry, and Allegan (Fig. 4.6, Table 4.9). In all counties, the onsite consumption of diesel, nitrogen and phosphorus during the fertilization process generated the most GWP. Emissions from fertilization can vary significantly from 21-62 Mg $CO_{2\text{-eq}}$ km^{-2} cropland managed in the watershed, which stretches ~150 km. All cropland was assumed to be fertilized equally; therefore, management variation is homogeneous across the county but varied between counties. A smaller variation was found between counties in emissions from planting or harvesting (e.g., diesel consumption during these processes), which suggests that some management activities will have higher variations than others across the same landscape. Notably, upstream processes (e.g., diesel, electricity, and fertilizer production) increased the cumulative GWP emission rates in counties with higher consumption of fertilizers, such as Nitrogen. Kalamazoo County, the highest consumer of fertilizers, has an emission of 59 Mg $CO_{2\text{-eq}}$ km^{-2} associated with Nitrogen production whereas Allegan County reported 20 Mg $CO_{2\text{-eq}}$ km^{-2}. Contributions to the Kalamazoo Watershed GWP are determined by the county's cropland area within the watershed. As such, county rates of cropland GWP emissions are multiplied by their respective cropland area within the watershed (Fig. 4.6).

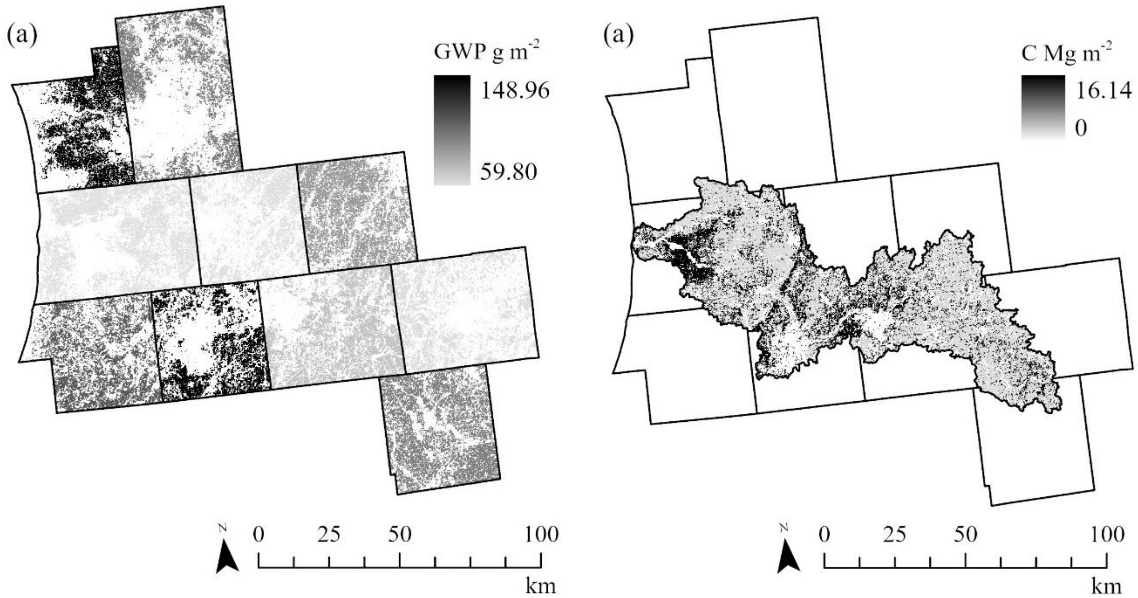

Figure 4.7. Variability in anthropogenic and ecological carbon production across the study area in 2016, where (a) is global warming potential (GWP g m^{-2}) of cropland activities occurring in the NLCD land cover 'Cropland' across counties; and (b) is terrestrial carbon stock and (C Mg m^{-2}) estimated by the Earth System Model within the Kalamazoo Watershed. Cumulative watershed GWP from cropland management is estimated by multiplying the county GWP rates by its respective cropland area.

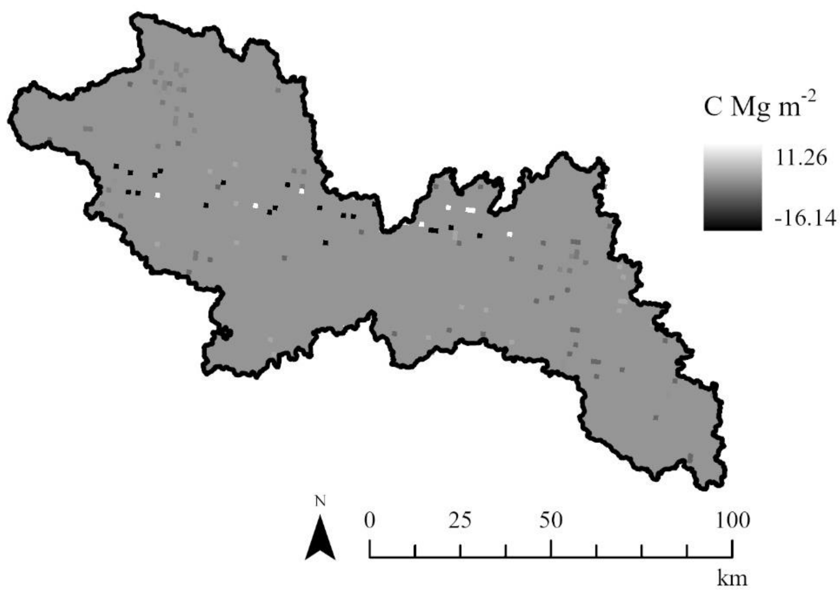

Figure 4.8. Net gain and loss in carbon stock due to predicted land cover change across the Kalamazoo Watershed between 2016 and 2050 rescaled to 1 km extents.

Table 4.8. The rate of global warming potential (GWP) Mg $CO_{2\text{-eq}}$ km^{-2} of each county's cropland management in 2017.

	Allegan	Barry	Calhoun	Eaton	Hillsdale	Jackson	Kalamazoo	Kent	Ottawa	Van Buren
Upstream production										
Nitrogen	20	36	39	44	46	37	59	49	60	52
Phosphorus	1	3	3	3	4	3	4	4	5	4
Diesel	2	2	2	2	3	2	2	2	2	2
Electricity	3	1	2	0	1	1	9	3	4	5
Total upstream	27	42	46	50	53	43	75	57	72	63
Onsite consumption										
Planting	1	1	1	1	1	1	1	1	1	1
Fertilizing*	21	38	41	46	48	39	61	51	62	54
Irrigation**	--	--	--	--	--	--	--	--	--	--
No-till	1	2	3	3	2	2	1	1	2	1
Conv. Till	3	2	1	3	3	2	4	2	3	2
Cons. Till	4	3	3	3	4	4	4	4	4	3
Harvest	2	2	2	3	3	2	2	2	3	2
Total onsite	33	49	52	59	61	50	74	61	75	62
GWP Mg km^{-2}	60	92	98	109	115	93	149	118	146	125
Cropland (km2)	921.51	518.67	846.34	783.73	858.83	605.11	533.41	626.85	620.32	691.04

**Fertilizing includes emissions from diesel, nitrogen, and phosphorus consumption*

***No onsite consumption for Irrigation, as electricity used is generated in an upstream process*

Table 4.9. The cropland extent, GWP Mg CO_2-eq emission, carbon stock Mg C and carbon stock Mg C lost to offset of cropland emissions for 2016 by county. Total cropland emissions are the product of cropland area (km^2) and GWP rates (kg CO_2-eq km^{-2}) in Table 4.8. Carbon stock was multiplied by 3.67 (IPCC, 2006) to obtain Mg CO_2. Carbon stock decrease is the percent C stock allocated to offset cropland GWP, where total indicates the average county loss.

County	Cropland km^2	Cropland GWP Mg CO_2-eq	C Stock Mg C	C Stock Decrease %
Allegan	921.51	55111	7898211	0.19%
Barry	518.67	47547	1966399	0.66%
Calhoun	846.34	83267	175278	12.94%
Eaton	783.73	85308	12238627	0.19%
Hillsdale	858.83	98578	632314	4.25%
Jackson	605.11	56117	2690434	0.57%
Kalamazoo	533.41	79456	321702	6.73%
Kent	626.85	73905	3653294	0.55%
Ottawa	620.32	90846	5661256	0.44%
Van Buren	691.04	86371	1278997	1.84%
Total	*7005.81*	*756507*	*36516512*	*3.00%*

Discussion

This study applied historical census records of cropland management to estimate the global warming potential (GWP) of the Kalamazoo Watershed in comparison to carbon stock estimates in 2050. The study found that the carbon stock and storage of the watershed offsets the cropland anthropogenic emissions caused by planting, fertilizing, tillage, irrigation, and harvesting, despite a slight decrease in carbon stock by 2050 due to cropland loss and urban area gains. The GWP emissions varied by county, with higher irrigation and fertilizing rates contributing to increased fuel consumption and GWP emissions. Emissions linked to cropland management were driven by up-stream processes, including the production of nitrogen and phosphorus. Cross-disciplinary methods were found capable of estimating spatial variations in carbon offset at the landscape scale with freely available land management data. Overall, the study highlights the importance of cross-disciplinary methods and LCA in estimating the spatial variations of carbon offset at the landscape scale. It also emphasizes the need to consider more than just carbon offset potential in climate mitigation strategies and to consider the impacts of land use change and management intensifications on biodiversity and biogeophysical changes.

Geospatial representation of land management and ecosystem processes

By linking land management intensity and ecosystem processes by land cover type, I demonstrated that anthropogenic emissions and offset potential can be geospatially overlain to evaluate spatial variability. The strength of this approach is the ability to estimate partial emissions across previously aggregated estimates of land management. A portion of the land area's emissions was estimated within a county rather than being restricted to the county extent---which is the spatial scale of most anthropogenic activities.

This overcame limits to privacy, sampling costs, and relied on existing resources with credible sampling methodologies. In this demonstration, the spatial variability of cropland management GWP was driven by management intensity, which agrees with the hypothesis. Given the rate of management, a LCA provided a temporal analysis of emissions along the production cycle of inputs used in the management activity. Notably, up-stream processes during the production of fertilizers, particularly nitrogen, significantly increased the rate of GWP emissions per county. Whereas diesel consumption for planting, harvest, and fertilizing were high, the production of materials used on-site hold considerable influence and may be considered in climate mitigation efforts beyond on-site NbCS. By considering up- and down-stream processes, a sustainable solution can be identified without risk of indirect emissions or environmental impact.

Spatial LCA has the potential to provide more accurate and detailed assessments of environmental impacts compared to traditional LCA approaches that do not consider spatial variations in environmental data (Wu, S.R., 2022). However, While the creation of spatial databases and geospatial tools has eased the implementation of spatial LCA in practical settings, obstacles remain with respect to data accessibility and quality, and there is a need for data standardization and harmonization (Hiloidhari et al., 2017). Additional data is needed to understand the rate of resources purchased as opposed to consumed to limit uncertainty, as present studies estimate inputs from sales records and assume that all inputs are consumed. However, LCA is a strong tool to explore assumptions and provides avenues for sensitivity analysis to determine if some inputs would have significant effects on the estimated outcome. This can be an asset to assessing the outcome of climate mitigation approaches and scaling the emissions across a study area.

While this study focused on GWP, other emissions from soil carbon, nitrous oxide, methane, and management activities were not considered as it was outside the scope of this study. Applications for climate mitigation efforts towards carbon neutrality should consider more than carbon offset potential, including the biodiversity and biogeophysical implications from land use change and land management intensifications. Past research using LCA approaches in land management determined the carbon debt of field-scale conservation reserve program grasslands convert to biofuel crops (Abraha et. al, 2019); the ecosystem water-use efficiency of crops in consideration of land use history (Abraha et al., 2016); the water and energy footprints of bioenergy crops (Bhardwaj et al., 2011); and has considered biofuel land use change-induced surface albedo in LCA (Cai et al., 2016; Goosse 2015). In the same agroecosystem as this study, the $CO_{2\text{-eq}}$ mitigation of cropland-dominated landscapes were 52% stronger than those of forest-dominated landscapes (Sciusco et al., 2020).

Limitations associated with linking socioecological processes by land cover type

While this study was able to detect spatial variation in cropland emissions and carbon stock across a county, additional considerations should be taken when linking socioecological processes to a single landcover. Future work may consider how to estimate GWP from soil and crop specific tillage and irrigation practices in landscape GWP estimates when the location is unknown. While this study relied on average rates of practice, it was limited to overall assumptions and cannot account for ecosystem responses unique to how each practice might have been combined. For example, the irrigation values assumed that all land was no-till; however, emissions may be higher at croplands with greater than average irrigation intensities and conventional tillage than those with no-till (Gelfald et al., 2013, West and Marland, 2002b). These combinations uniquely drive the GHG emissions from croplands and can impact C stock. This framework can be used to increase or decrease particularly land management rates for planning various mitigation scenarios, such as an increase in no-till and cover cropping practices that can store and sequester higher rates of C, respectively.

Lastly, integrating multiple datasets comes with the risk that values do not correspond between sources. This study estimated the cropland area using the NLCD dataset and found the extent does not match the cropland harvested or farmland reported by the NASS census due to differing methodologies. Nonetheless, the integration of social and geospatial data is still recommended for the sake of benchmarking land management activities and contextualizing stakeholder decision-making. Further research is needed to improve the spatial resolution and accuracy of data used in spatial LCA, as well as to develop more advanced methods for analyzing and visualizing spatial data.

Land cover change was minimal in the study area, due to the rate of change detected by the land change model from 2001-2011. This rate informed the prediction of 2050 land cover, which assumed the same rate of change. While this study area noted declines in cropland and forests, other studies at larger extents note that Michigan is undergoing reforestation by secondary forests (Brown et. al., 2000). The study area extent may influence the rate of change and therein the transition potentials and sub-processes that inform land cover predictions (Pontius, 2002). Other study areas may not have persistent land cover and point readers to resources on land change/use planning, areas of protection, and more within the Land Change Model of Terrset (Clark Labs, 2021). Additional land cover classifications may be required to determine if rates of change significantly vary or are likely to change. Expert knowledge and understanding of policy goals can be incorporated into the ecosystem services modeler and land change modeler for land change prediction (Clark Labs, 2021; Eastman, 2020).

LCLUC is the second most important source of GHG emissions, following fossil fuels, due to the release of carbon from long-term storage; however, it also affects the climate through biogeophysical and biogeochemical changes (IPCC cite, Mattila et al., 2011). Land cover change in this study was reclassified to Tier 1 NLCD, aggregating many cover types into one. However, this may overlook some of the known biogeophysical feedbacks and carbon debt caused by land cover change (e.g., from conservation reserve prairie to cropland) and therefore LCLUC must be carefully considered to achieve sustainability goals (Abraha et al., 2019).

Key take-aways for policy-makers and climate mitigation efforts

Natural working lands and forest production can play key roles in climate mitigation and net zero goals (Cooper & Whitcomb, 2021). Energy, material, and water use/consumption in cropland production should be evaluated to identify opportunities to reduce GHG emissions (Bowers, 1992; Downs & Hansen, 1998). Agricultural intensity has proven to have a direct relationship with terrestrial carbon processes, particularly in this study area, where increases in management and decreases in farm size and tenure has influenced terrestrial carbon production since the 1980s (Shirkey, et al., 2023). Future land cover change scenarios, such as the prediction of land cover in 2050 when Michigan aims for carbon neutrality, can inform land management decisions (Gibson et al., 2018; Hasan et al., 2020). This model provides a unique approach for a baseline estimate of anthropogenic emissions in a spatial context that can be geospatially located within natural working lands such as forestland and cropland.

Understanding where both anthropogenic and ecological processes are occurring is essential, as negotiating land use and land management must take careful consideration of social, economic, and environmental impacts (Gillon, 2010). Additionally, NWL are a cost-effective and enduring NbCS. However, C stock is not guaranteed long-term due to land use change, wildfire, insect infestation, and natural disasters or extreme weather events. Therefore, the NWL sector should set near- and long-term goals/targets to reduce GHG emissions on NWL and maximize their C stock potential (USCA, 2022). Overall, climate mitigation is most effective when stakeholders participate and issues of land governance, such as tenure and resource rights, are considered in the program (Kanowki et al., 2011).

Management inputs such as fertilizers and irrigation continue to steadily increase in these croplands (Tables S3-8). Assuming rates of land cover change remain steady, it can be expected that terrestrial carbon stock will continue to offset many cropland management practices until 2050. However, increasing rates of management intensity and other GHG emissions not considered in this demonstration are essential for robust policy recommendations. Particularly, upstream processes linked to fertilizer use, such as nitrogen and phosphorus in this study, have significant environmental impacts in their production process (Blonk Consultants, 2012). Understanding where the highest concentration of fertilizer use lies in a landscape will aid in a decision- and policy-makers efforts for climate mitigation and NbCS. By using LCA, it is possible to understand emissions, land occupation/use, water footprint, toxicity, and more related to square area of land managed.

Spatial representation of land management is only possible with continuous surveys of stakeholders. By using the NASS dataset, this study demonstrated how readily available land management information is available at county level. However, large county extents may not benefit from this scale and therefore additional surveys may be necessary to identify where within a county agricultural intensification may occur. For example, fertilizer applications were assumed to be equally applied across all croplands within a county; when, this would vary by crop or soil type requirements and farmer goals (Cammarano et. al, 2021). Therefore, additional consideration is advised to employ supplemental stakeholder engagement beyond the baseline set in this framework.

Conclusion

This study developed a novel framework to spatialize LCA with applied historical census records of cropland management for a spatial estimate of GWP, linking ecological processes and anthropogenic activities within cropland extents. The framework was demonstrated in a carbon offset scenario, where the State of Michigan aims to reach carbon neutrality by 2050 and may use terrestrial carbon stock to offset emissions associated within Natural Working Lands. The Kalamazoo Watershed carbon stock was found to offset cropland anthropogenic emissions from selected cropland management processes, including planting, fertilizing, tillage, irrigation and harvesting well into the future. Cropland GWP emissions varied between counties, due to upstream processes related to the production of diesel, electricity, and fertilizers. Upstream processes increased the rate of GWP emissions when combined with on-site consumption of fertilizers, as the production process for nitrogen and phosphorus resulted in increased emissions. A low likelihood of land cover change in the area was detected, as found in earlier studies (Shirkey et. al, 2023). Small cropland loss and urban area gains by the year 2050 caused a slight decrease in carbon stock and storage by 2050. Assuming rates of land cover change and GWP emissions remain steady, it can be expected that terrestrial carbon will continue to offset cropland management until 2050 as demonstrated in this framework.

Land use implies the anthropogenic and ecosystem benefits from a land cover type, whereas land cover change is driven by society's need for additional ecosystem services. Land use and land management are well known to be difficult to monitor due to privacy concerns and feasibility to survey regularly; therefore, this study advocates for benchmarking using available census records from NASS, as employed in this framework. Historical records of land management dating well beyond a century at the county-level can provide evidence of regional land use intensification that can be readily paired with emissions and impact assessments. Land management may continue to intensify as seen in NASS records and future work can utilize LCA methodology to evaluate upstream and downstream processes linked to material, water, and energy consumption.

Coupling LCLUC with LCA methodology advances interdisciplinary science (i.e., environmental engineering and geography) and benefits applications for climate mitigation with land management. Furthermore, LCLUC can be used beyond estimations of carbon stocks as done in this study. Land cover impacts landscape and regional biogeophysical fluxes. Therefore, future research may incorporate additional ecosystem processes into this framework such as evapotranspiration and albedo, as well as carbon production. This framework has the potential to evaluate implications to biodiversity, toxicity, water footprint and more. Decision makers may investigate their own landscape or region to consider additional cropland management activities that align with their climate mitigation goals. To manage and reduce GWP emissions and maintain environmental health, it is important to collocate anthropogenic emissions and ecosystem processes or resources at the decision-making level. This study advocates that LCA and ecosystem processes may be linked by land cover type in effort to establish baselines for NbCS and to estimate spatial variations at the landscape scale. Future work may expand on this framework to consider additional environmental impacts and ecological processes within managed lands.

CHAPTER 5. CONCLUSIONS

Key lessons and conclusions

Both biophysical and socioeconomic factors play important roles in determining the carbon fluxes and dynamics at the landscape scale. Additionally, C sequestration strength is dependent on land management such as cover crops, fertilization, production intensity and water use. In this dissertation, I found that spatial resolution, coupled with advancing spectral resolution, can improve estimates of carbon production in managed croplands (Shirkey et. al 2022). Moreover, this work was essential to explore the impacts that landscape composition and changes within agroecosystems may contribute to under or overestimations of carbon budgets.

The composition of landscape structure is tied to historical agricultural intensification, with cropland management and tenure driven by agricultural intensity. This is significant as land ownership and tenure can drive the adoption of conservation practices and sources of information in land management (Varble, Secchi, & Druschke, 2016). However, forestland and water were not affected by this intensification, as seen in my SEM from Chapter 3 (Shirkey et. al 2023). In fact, surveyed stakeholders indicated reluctance to change land management practices and emphasized the importance of their forest stands over croplands, which have become a secondary income. This slightly contrasted with overall projections of land cover change (Chapter 4), which found slight decreases in forestland and cropland, giving rise to more urban and water bodies. Spatial representation of LCLUC may explain how these indicators performed statistically, as they may be capable of capturing some but not all processes at scale (Amirkhiz et al., 2023). However, stakeholder engagement was essential to contextualize the decision-making in land use management. In sum, socioeconomic factors drove cropland land management and tenure, which in turn has contributed to landscape composition.

Management practices such as tillage, fertilization and crop cover type have significant impacts on carbon dynamics (Guzman & Golabi, 2017) and significant work by decision and policy-makers are driving interest in Nature-based Climate Solutions (NbCS) and Natural Working Lands (NWL) (Cooper & Whitcomb, 2021). This research provides valuable knowledge on long-term anthropogenic impacts on C production at the landscape scale, including how terrestrial C production estimates are influenced by land management, how human-nature interactions drive C production, and a unique framework to link historical land management records with innovative earth observations. In Chapter 2, variations in cumulative GPP varied by crop cover type and land use history. In Chapters 3, I found that cropland management had significantly stronger relationships with landscape carbon production than abiotic processes alone (e.g., heat and water stress). This is largely because socioecological contributions to landscape carbon production are essential in landscape analysis, as their processes are both independent and interactive. Chapter 4 discussed that upstream production and on-site consumptions of diesel and fertilizers, as well as respective GHG emissions, can spatially vary within a landscape and negate benefits from various land cover stocks. While these inputs have increased terrestrial C productivity, their emissions have negatively contributed to GHG emissions. As such, the integration of biophysical and socioeconomic data is essential for understanding the complex interactions between human activities and ecosystem processes that determine carbon dynamics at the landscape scale. When evaluating policy-related climate mitigation measures, it is essential to consider both socioeconomic and biophysical processes for accurate models of landscape-scale C production and GWP (Gelfand et al., 2013).

Major contributions

This dissertation developed a novel framework for integrating socioeconomic processes into ecosystem modeling to evaluate the impacts of land management on carbon stocks and fluxes at the landscape scale. By investigating landscape composition and their spatiotemporal variability, as well as the contributions between physical and social aspect to terrestrial carbon production, a more accurate understanding of how human management and disturbance influences the role of terrestrial ecosystems within the global carbon budget. In Chapter 2, I demonstrated the use of high spatiotemporal red-edge remote sensing data to estimate carbon fluxes across different land use types, which can help to improve the understanding of the impacts of land use change on carbon dynamics. Human-nature interactions drive C production, and historical land management records can be linked with innovative earth observations to provide a unique framework for understanding long-term changes in carbon stocks and fluxes. In Chapter 3, I identified key drivers of carbon production in agroecosystems including land management practices and human-nature interactions, which were greater than climate drivers alone. I advanced the capacity of PLS-SEM for socioecological research, demonstrating how to simultaneously evaluate socioeconomic measures, landscape structure and composition, as well as records of ecosystem processes. Lastly, this dissertation developed a novel framework for integrating socioeconomic processes with ecosystem modeling to evaluate the impacts of land management on carbon stocks and fluxes at the landscape scale using life cycle assessment (LCA) framework. While LCA has been extensively used in farmland management (Abraha et al., 2019; Gelfand et al., 2013), spatialization of LCA is still under development and lacks spatiotemporal context and input (Wu et al., 2022). Landscape ecologists, geographers and environmental engineers may particularly benefit from the outcome of this dissertation efforts to model socioecological systems and advance NbCS must consider the biophysical and socioeconomic consequences of climate mitigation strategies (Novick et al., 2022). The interdisciplinary approach used in this dissertation provides valuable knowledge on long-term anthropogenic impacts on C production at the landscape scale. In sum, it highlights the importance of considering both biophysical and socioeconomic factors when modeling carbon dynamics at the landscape scale. This approach can be used to inform land management decisions and develop strategies for climate mitigation.

Uncertainty and limitations

Uncertainty in EVI and other red-edge indices is impacted by the heterogeneous distributions across the space in agroecosystems and the atmospheric and environmental conditions of the time of measurement. Interpretation of the VI may be used to indicate vegetation health, 'greeness,' and overall C production, but it does not provide information on specific plant traits or functions, such as biomass or nutrient content. Therefore, it is important to interpret these VIs carefully in consideration of other information on the agroecosystem monitored.

Remaining uncertainties are in the assumptions regarding land use management, which are aggregated to administrative unit (e.g., county) and annual or decennial measurements. This imposes difficulties in monitoring climate mitigation efforts and reporting results, as various land covers and ecosystems exist within the county-boundary. While this dissertation aimed to resolve the spatiotemporal disconnect of land management data by allotting land management to land cover type, key assumptions were made that still impose uncertainty. First, the land management practice is assumed to occur uniformly across the land cover type, within the county-extent. Second, land management is not attributed to a particular vegetation or crop. In the case of Chapter 4, cropland management included assumptions built on acres irrigated, planted, and harvested, where processes of management may include multiple harvests (e.g., winter wheat) or single harvest (e.g., corn). Moreover, cover crops can increase C stocks and potentially improve soil quality but were not estimated in this dissertation. This increases the spatiotemporal variation in land management and consequently the impact on C production and anthropogenic emissions.

To address these land management uncertainties, additional data are needed to link management practices with land cover type, and across the administrative units. This may include collaborations with existing organizations to routinely evaluate how populations are managing their land, such as how the American Community Survey conducts sub-samples between the 10-year US Census. This will capture variations and patterns without the cost of extensive surveys. In this dissertation, surveys with Centennial Farmers provided essential context to NASS Census data on cropland management, including a stakeholders' willingness to change, where they receive information, and their perceived contributions to climate change (see Supplementary Materials). These responses can inform policymakers where to allocate climate mitigation resources and efforts. Targeted efforts may employ the CropScape product from the USDA NASS and Agricultural Research Service, which provides geospatial data on crop cover from 1997 to present. Additionally, surveys and census materials may allocate land management to specific crops, so that a finer resolution of land cover and land management may be acquired. This is essential, as cropland may be composed of numerous crop types, each with their own demands for nutrients, soil cultivation, irrigation, and harvest rates. Furthermore, there is still within-crop uncertainty, such as the variation of C production between two identical crop fields with different land use histories, and consequently different soil composition and nutrient availability (Chapter 2). Until these methods are in place, assumptions will need to be made to contextualize the general inputs, processes, and outputs on managed landscapes. Assumptions and mitigation potential can meanwhile be explored within a spatialized LCA, to understand how increases and decreases in land management may influence anthropogenic emissions.

Lastly, land cover change estimates and projections are driven by observations of change. In this dissertation, I acknowledge that projections of land cover and C stock assume a business a usual trend in land use and land cover. Land cover change models have the capacity to acknowledge areas that are resistant to change, such as protected or preserved areas, but may not be suitable for long-term projections in areas where land cover is likely to change significantly. Short term projections and routine evaluation are therefore necessary, as C stocks can significantly change due to land management and land cover type. While this work used NLCD data to demonstrate how national-level data may be utilized in a standardized approach, land cover classifications from the past may also be implemented to evaluate long term changes prior to the 2000s. Classification methods should report detailed accuracy assessments that look beyond the percent agreement, as conventionally done, and estimate the quantity and locational agreement between two images (Pontius, 2002). As such, classification models and predictions could address concerns generated from misclassified pixels and identify within which land covers these issues may arise.

Recommendations for Future Research

To further advance our understanding of sustainable land management, future research should examine the impacts of land use across a range of scales beyond the HUC8 watershed level considered in this dissertation. It is important to investigate how the scale of the study area may affect the relationship between socioecological processes, particularly in agroecosystems where environmental impact is directly tied to the provision of ecosystem services. This dissertation focused primarily on evaluating croplands and did not account for above ground biomass harvested and consumed outside of the landscape. Future research should expand on the spatial life cycle assessment framework presented here to evaluate cropland upstream and downstream emission scenarios in the context of the total landscape carbon budget. This could be useful not only in achieving carbon offset and net neutrality goals but also in aligning with the objectives of the US Climate Action and Natural Working Lands (NWL) working groups. In addition to carbon emissions, other impact assessments available within LCA such as water footprint, toxicity, and land use/occupation could also be considered (Sciusco et al, 2022). As such, it is possible to investigate the potential benefits and drawbacks of various agroecosystem management practices, such as regenerative agriculture, agroforestry, and organic farming. Moreover, incorporating long-term records of biophysical feedback from strong ecological observation networks such as FLUXNET and iLEAPS could enhance the life cycle inventory for both social and ecological contributions (Novick et al., 2022). Overall, future research should build on this framework to evaluate new strategies for Nature-based Climate Solutions (NbCS) within agroecosystems and achieve the United Nations Sustainable

Development Goals (SDGs) (Pachauri et al., 2014; United Nations, 2015).

REFERENCES

1. Abatzoglou, J. T. (2013). Development of gridded surface meteorological data for ecological applications and modelling. *International Journal of Climatology*, *33*(1), 121–131. https://doi.org/https://doi.org/10.1002/joc.3413

2. Abraha, M., Chen, J., Chu, H., Zenone, T., John, R., Su, Y. J., Hamilton, S. K. & Robertson, G. P. (2015). Evapotranspiration of annual and perennial biofuel crops in a variable climate. *Global Change Biology Bioenergy*, *7*(6), 1344–1356. https://doi.org/10.1111/gcbb.12239

3. Abraha, M., Gelfand, I., Hamilton, S. K., Shao, C., Su, Y. J., Robertson, G. P. & Chen, J. (2016). Ecosystem water-use efficiency of annual corn and perennial grasslands: contributions from land-use history and species composition. *Ecosystems*, *19*(6), 1001–1012. https://doi.org/10.1007/s10021-016-9981-2

4. Abraha, M., Gelfand, I., Hamilton, S. K., Chen, J. & Robertson, G. P. (2018). Legacy effects of land use on soil nitrous oxide emissions in annual crop and perennial grassland ecosystems. *Ecological Applications*, *28*(5), 1362–1369. https://doi.org/10.1002/eap.1745

5. Abraha, M., Hamilton, S. K., Chen, J. & Robertson, G. P. (2018). Ecosystem carbon exchange on conversion of Conservation Reserve Program grasslands to annual and perennial cropping systems. *Agricultural and Forest Meteorology*, *253–254*(February), 151–160. https://doi.org/10.1016/j.agrformet.2018.02.016

6. Abraha, M., Gelfand, I., Hamilton, S. K., Chen, J. & Robertson, G. P. (2019). Carbon debt of field-scale conservation reserve program grasslands converted to annual and perennial bioenergy crops. *Environmental Research Letters*, *14*(2). https://doi.org/10.1088/1748-9326/aafc10

7. Aguirre-Urreta, M. I., & Rönkkö, M. (2018). Statistical inference with PLSc using bootstrap confidence intervals. *MIS Quarterly*, *42*(3), 1001–1020.

8. Allred, B. W., Smith, W. K., Twidwell, D., Haggerty, J. H., Running, S. W., Naugle, D. E., & Fuhlendorf, S. D. (2015). Ecosystem services lost to oil and gas in North America. *Science, 348*(6233), 401-402.

9. Amirkhiz, R. G., John, R., & Swanson, D. L. (2023). A Bayesian approach for multiscale modeling of the influence of seasonal and annual habitat variation on relative abundance of ring-necked pheasant roosters. *Ecological Informatics*, *75*, 102003.

10. Anav, A., Friedlingstein, P., Beer, C., Ciais, P., Harper, A., Jones, C., Murray-Tortarolo, G., Papale, D., Parazoo, N. C., Peylin, P., Piao, S., Sitch, S., Viovy, N., Wiltshire, A. & Zhao, M. (2015). Spatiotemporal patterns of terrestrial gross primary production: A review. *Reviews of Geophysics*, *53*(3), 785–818. https://doi.org/10.1002/2015RG000483

11. Arévalo, P., Bullock, E. L., Woodcock, C. E., & Olofsson, P. (2020). A suite of tools for continuous land change monitoring in Google Earth Engine. *Frontiers in Climate*, *2*, 576740. https://doi.org/10.3389/fclim.2020.576740

12. Atkinson, P. M., & Tatnall, A. R. L. (1997). Introduction neural networks in remote sensing. *International Journal of Remote Sensing, 18*(4), 699–709. https://doi.org/10.1080/014311697218700

13. Aubinet, M., Vesala, T. & Papale, D. (Eds.). (2012). *Eddy covariance: a practical guide to measurement and data analysis* (1st ed.). Springer Dordrecht. https://doi.org/10.1007/978-94-007-2351-1

14. Baldocchi, D., Reichstein, M., Papale, D., Koteen, L., Vargas, R., Agarwal, D. & Cook, R. (2012). The role of trace gas flux networks in the biogeosciences. *Eos*, *93*(23), 217–218. https://doi.org/10.1029/2012EO230001

15. Barnes, E. M., Clarke, T. R., Richards, S. E., Colaizzi, P. D., Haberland, J., Kostrzewski, M., Waller, P., Choi, C., Riley, E., Thompson, T. & Lascano, R. J. (2000). Coincident detection of crop water stress, nitrogen status and canopy density using ground based multispectral data. *In Proceedings of the Fifth International Conference on Precision Agriculture*, (Vol. 1619, 6).

16. Becker, J., Ringle, C. M., Sarstedt, M., & Völckner, F. (2015). How collinearity affects mixture regression results. *Marketing Letters*, *26*, 643–659. https://doi.org/10.1007/s11002-014-9299-9

17. Beer, C., Reichstein, M., Tomelleri, E., Ciais, P., Jung, M., Carvalhais, N., Rödenbeck, C., Arain, M. A., Baldocchi, D., Bonan, G. B., Bondeau, A., Cescatti, A., Lasslop, G., Lindroth, A., Lomas, M., Luyssaert, S., Margolis, H., Oleson, K. W., Roupsard, O., … Papale, D. (2010). Terrestrial gross carbon dioxide uptake: Global distribution and covariation with climate. *Science*, *329*(5993), 834–838. https://doi.org/10.1126/science.1184984

18. Bhardwaj, A. K., Zenone, T., Jasrotia, P., Robertson, G. P., Chen, J., & Hamilton, S. K. (2011). Water and energy footprints of bioenergy crop production on marginal lands. *Global Change Biology Bioenergy*, *3*(3), 208–222. https://doi.org/10.1111/j.1757-1707.2010.01074.x

19. Blonk Consultants (2012) http://www.blonkconsultants.nl/wp-content/uploads/2016/06/fertilizer_production-D03.pdf

20. Bollen, K. A. (1989). *Structural equations with latent variables*. John Wiley & Sons. https://doi.org/10.1002/9781118619179

21. Bondeau, A., Smith, P. C., Zaehle, S., Schaphoff, S., Lucht, W., Cramer, W., Gerten, D., Lotze-campen, H., Müller, C., Reichstein, M. & Smith, B. (2007). Modelling the role of agriculture for the 20th century global terrestrial carbon balance. *Global Change Biology*, *13*(3), 679–706. https://doi.org/10.1111/j.1365-2486.2006.01305.x

22. Borana, S.L.; Yadav, S.K. (2017) Modelling and prediction of land use changes in Jodhpur City using multi-layer perceptron Markov techniques. *International Journal of Research in Engineering, IT and Social Sciences, 7*(11), 14–21

23. Bowers, W. (1992). Agricultural field equipment. *Energy in farm production, 6*, 117-129.

24. Bradley, B. A., & Mustard, J. F. (2005). Identifying land cover variability distinct from land cover change: Cheatgrass in the Great Basin. *Remote Sensing of Environment*, *94*(2), 204–213. https://doi.org/10.1016/j.rse.2004.08.016

25. Brown, D. G., Pijanowski, B. C., & Duh, J. D. (2000). Modeling the relationships between land use and land cover on private lands in the Upper Midwest, USA. Journal of Environmental Management, 59(4), 247-263.

26. Cai, H., Wang, J., Feng, Y., Wang, M., Qin, Z., & Dunn, J. B. (2016). Consideration of land use change-induced surface albedo effects in life-cycle analysis of biofuels. *Energy & Environmental Science*, *9*(9), 2855-2867.

27. Cai, Z., Junttila, S., Holst, J., Jin, H., Ardö, J., Ibrom, A., Peichl, M., Mölder, M., Jönsson, P., Rinne, J., Karamihalaki, M. & Eklundh, L. (2021). Modelling daily gross primary productivity with sentinel-2 data in the nordic region–comparison with data from modis. *Remote Sensing*, *13*(3), 1–18. https://doi.org/10.3390/rs13030469

28. Callahan, J., Casey, R., Templeton, M. & Sharer, G. (2020). *seismicRoll: Fast Rolling Functions for Seismology using "Rcpp."* R package version 1.1.4. https://cran.r-project.org/package=seismicRoll

29. Castoriadis, C. (2008). The Political Ecology of southwest Michigan agriculture. In C. L. Redman & D. R. Foster (Eds.), *Agrarian landscapes in transition* (p. 298). Oxford University Press, Inc.

30. Chaney, N. W., Wood, E. F., McBratney, A. B., Hempel, J. W., Nauman, T. W., Brungard, C. W., & Odgers, N. P. (2016). POLARIS: A 30-meter probabilistic soil series map of the contiguous United States. *Geoderma*, *274*, 54–67. https://doi.org/10.1016/j.geoderma.2016.03.025

31. Chen, B., Coops, N. C., Fu, D., Margolis, H. A., Amiro, B. D., Barr, A. G., Black, T. A., Arain, M. A., Bourque, C. P. A., Flanagan, L. B. & Lafleur, P. . (2011). Assessing eddy-covariance flux tower location bias across the Fluxnet-Canada Research Network based on remote sensing and footprint modelling. *Agricultural and Forest Meteorology*, *151*(1), 87–100.

32. Chen, J., Brosofske, K. D., Noormets, A., Crow, T. R., Bresee, M. K., Le Moine, J. M., Euskirchen, E. S., Mather, S. V., & Zheng, D. (2004). A working framework for quantifying carbon sequestration in disturbed land mosaics. *Environmental Management*, *33*(1), S210–S221. https://doi.org/10.1007/s00267-003-9131-4

33. Chen, J., John, R., Shao, C., Fan, Y., Zhang, Y., Amarjargal, A., Brown, D. G., Qi, J., Han, J., Lafortezza, R., & Dong, G. (2015). Policy shifts influence the functional changes of the CNH systems on the Mongolian plateau. *Environmental Research Letters*, *10*(8). https://doi.org/10.1088/1748-9326/10/8/085003

34. Chen, J., John, R., Zhang, Y., Shao, C., Brown, D. G., Batkhishig, O., Amarjargal, A., Ouyang, Z., Dong, G., Wang, D., & Qi, J. (2015). Divergences of two coupled human and natural systems on the Mongolian Plateau. *BioScience*, *65*(6), 559–570. https://doi.org/10.1093/biosci/biv050

35. Chen, M., Griffis, T. J., Baker, J. M., Wood, J. D., Meyers, T. & Suyker, A. (2018). Comparing crop growth and carbon budgets simulated across AmeriFlux agricultural sites using the Community Land Model (CLM). *Agricultural and Forest Meteorology*, *256–257*, 315–333. https://doi.org/10.1016/J.AGRFORMET.2018.03.012

36. Chen, J., Sciusco, P., Ouyang, Z., Zhang, R., Henebry, G. M., John, R. & Roy, D. P. (2019). Linear downscaling from MODIS to landsat: connecting landscape composition with ecosystem functions. *Landscape Ecology*, *34*(12), 2917–2934. https://doi.org/10.1007/s10980-019-00928-2

37. Chen, J., Ouyang, Z., John, R., Henebry, G. M., Groisman, P. Y., Karnieli, A., Pueppke, S., Kussainova, M., Amartuvshin, A., Tulobaev, A., Yespolov, T.I., Crank, C., Kadhim, A., Qi, J., & Gutman, G. (2020). Social-Ecological Systems Across the Asian Drylands Belt (ADB). In: Gutman, G., Chen, J., Henebry, G., Kappas, M. (eds) Landscape Dynamics of Drylands across Greater Central Asia: People, Societies and Ecosystems. Landscape Series, vol 17. Springer, Cham. https://doi.org/10.1007/978-3-030-30742-4_10

38. Chen, J., John, R., Yuan, J., Mack, E. A., Groisman, P., Allington, G., Wu, J., Fan, P., Beurs, K. M. De, Karnieli, A., Gutman, G., Kappas, M., Dong, G., Zhao, F., Ouyang, Z., Pearson, A. L., Sat, B., Graham, N. A., Shao, C., … Qi, J. (2022). Sustainability challenges for the social- environmental systems across the Asian Drylands Belt. *Environmental Research Letters*, *17*(2), 023001.

39. Chu, H., Baldocchi, D. D., John, R., Wolf, S. & Reichstein, M. (2017). Fluxes all of the time? A primer on the temporal representativeness of FLUXNET. *Journal of Geophysical Research: Biogeosciences*, *122*(2), 289–307. https://doi.org/10.1002/2016JG003576

40. Chu, H., Luo, X., Ouyang, Z., Chan, W. S., Dengel, S., Biraud, S. C., Torn, M. S., Metzger, S., Kumar, J., Arain, M. A., Arkebauer, T. J., Baldocchi, D., Bernacchi, C., Billesbach, D., Black, T. A., Blanken, P. D., Bohrer, G., Bracho, R., Brown, S., … Zona, D. (2021). Representativeness of eddy-covariance flux footprints for areas surrounding AmeriFlux sites. *Agricultural and Forest Meteorology*, *301–302*, 108350. https://doi.org/https://doi.org/10.1016/j.agrformet.2021.108350

41. Clark Labs. (2021). *TerrSet Manual*. Worcester, MA: Clark University

42. Clevers, J. G. & Gitelson, A. A. (2013). Remote estimation of crop and grass chlorophyll and nitrogen content using red-edge bands on Sentinel-2 and-3. *International Journal of Applied Earth Observation and Geoinformation*, *23*, 344–351.

43. Cohen, W. B., & Goward, S. N. (2004). Landsat's role in ecological applications of remote sensing. *BioScience*, *54*(6), 535–545.

44. Compton, T. J., Goff, T. E., & Townshend, J. R. G. (1985). African land-cover classification using satellite data. *Science*, *227*(4685), 369–375.

45. Conzen, M. P. (Ed.). (2014). *The making of the American landscape* (2nd ed.). Routledge.

46. Cooper, L. T., & Whitcomb, S. (2021). *Michigan council on climate solutions: Natural working lands and forest products workgroup recommendations*. Retrieved from: https://www.michigan.gov/egle/about/groups/council-on-climate-solutions/workgroup-recommendations

47. Cox, P. M., Pearson, D., Booth, B. B., Friedlingstein, P., Huntingford, C., Jones, C. D., & Luke, C. M. (2013). Sensitivity of tropical carbon to climate change constrained by carbon dioxide variability. *Nature, 494*(7437), 341-344.

48. Cushman, S. A., McGarigal, K., & Neel, M. C. (2008). Parsimony in landscape metrics: strength, universality, and consistency. *Ecological Indicators*, *8*(5), 691–703. https://doi.org/10.1016/j.ecolind.2007.12.002

49. Daly, C., Halbleib, M., Smith, J. I., Gibson, W. P., Doggett, M. K., Taylor, G. H., & Pasteris, P. P. (2008). Physiographically sensitive mapping of climatological temperature and precipitation across the conterminous United States. *International Journal of Climatology*, *28*(15), 2031–2064. https://doi.org/10.1002/joc

50. Daly, C., Smith, J. I., & Olson, K. V. (2015). Mapping atmospheric moisture climatologies across the conterminous United States. *PLoS ONE*, *10*(10), e0141140. https://doi.org/10.1371/journal.pone.0141140

51. Damm, A., Guanter, L., Paul-Limoges, E., van der Tol, C., Hueni, A., Buchmann, N., Eugster, W., Ammann, C. & Schaepman, M. E. (2015). Far-red sun-induced chlorophyll fluorescence shows ecosystem-specific relationships to gross primary production: An assessment based on observational and modeling approaches. *Remote Sensing of Environment*, *166*, 91–105. https://doi.org/10.1016/j.rse.2015.06.004

52. Dash, J. & Curran, P. J. (2004). The MERIS terrestrial chlorophyll index. *International Journal of Remote Sensing*, *25–23*, 5403–5413. https://doi.org/10.1080/0143116042000274015

53. Dewitz, J., & Survey, U. S. G. (2021). *National Land Cover Database (NLCD) 2019 Products (ver. 2.0, June 2021): U.S. Geological Survey data release*. https://doi.org/10.5066/P9KZCM54

54. Diamantopoulos, A. (1994). Modelling with LISREL: a guide for the uninitiated. *Journal of Marketing Management*, *10*(1–3), 105–136.

55. Diamantopoulos, A., Sarstedt, M., Fuchs, C., Wilczynski, P., & Kaiser, S. (2012). Guidelines for choosing between multi-item and single-item scales for construct measurement: A predictive validity perspective. *Journal of the Academy of Marketing Science*, *40*(3), 434–449.

56. Dijkstra, T. K. (2010). Latent variables and indices: Herman Wold's basic design and partial least squares. In V. Esposito Vinzi, W. W. Chin, J. Henseler, & H. Wang (Eds.), *Handbook of partial least squares: Concepts, methods, and applications Springer Handbooks of Computational Statistics Series* (Vol. II, pp. 23–46). Berlin: Springer.

57. Dijkstra, T. K. (2014). PLS' Janus face–response to professor Rigdon's 'rethinking

partial least squares modeling: In praise of simple methods. *Long Range Planning*, *47*(3), 146–153.

58. Dijkstra, T. K., & Henseler, J. (2015). Consistent partial least squares path modeling. *MIS Quarterly*, *39*(2), 297–316.

59. Dinno, A. (2017). *dunn.test: Dunn's Test of Multiple Comparisons Using Rank Sums*. R Package Version 1.3.5. https://cran.r-project.org/package=dunn.test

60. Downs, H. W., & Hansen, R. W. (1998). *Estimating farm fuel requirements*. Farm and Ranch Series: Equipment Fact Sheet 5.006. Colorado State University Extension.

61. Dunn, O. J. (1964). Multiple Comparisons Using Rank Sums. *Technometrics*, *6*(3), 241–252. https://doi.org/10.1080/00401706.1964.10490181

62. Dwyer, J., Roy, D., Sauer, B., Jenkerson, C., Zhang, H., & Lymburner, L. (2018). Analysis ready data enabling analysis of the Landsat archive. *Remote Sensing*, *10*(9), 1363.

63. Eastman, J. R. (2006). *IDRISI Andes Tutorial*.

64. Eastman, J. R. (2020). *TerrSet 2020 Geospatial Monitoring and Modeling System.* Clark Labs.

65. Eisenhauer, N., Bowker, M., Grace, J., & Powell, J. (2015) From patterns to causal understanding: structural equation modeling (SEM) in soil ecology. *Pedobiologia, 58*(2):65–72.

66. Elsawah, S., Filatova, T., Jakeman, A. J., Kettner, A. J., Zellner, M. L., Athanasiadis, I. N., Hamilton, S. H., Axtell, R. L., Brown, D. G., Gilligan, J. M., Janssen, M. A., Robinson, D. T., Rozenberg, J., Ullah, I. I. T., & Lade, S. J. (2020). Eight grand challenges in socio-environmental systems modeling. *Socio-Environmental Systems Modelling*, *2*, 16226. https://doi.org/10.18174/sesmo.2020a16226

67. Euskirchen, E. S., Chen, J., Li, H., Gustafson, E. J., & Crow, T. R. (2002). Modeling landscape net ecosystem productivity (LandNEP) under alternative management regimes. *Ecological modelling*, *154*(1-2), 75-91.

68. Euskirchen, E. S., Bennett, A. P., Breen, A. L., Genet, H., Lindgren, M. A., Kurkowski, T. A., McGuire, A. D., & Rupp, T. S. (2016). Consequences of changes in vegetation and snow cover for climate feedbacks in Alaska and northwest Canada. *Environmental Research Letters*, *11*(10). https://doi.org/10.1088/1748-9326/11/10/105003

69. Executive Order 2020-182. (2020, September 23). Establishing the Council on Climate Solutions. https://www.michigan.gov/whitmer/0,9309,7-387-90499_90640_90703-541837--,00.html

70. Falcone, J. A. (2021). Estimates of county-level nitrogen and phosphorus from fertilizer and manure from 1950 through 2017 in the conterminous United States. In *U.S. Geological Survey Open-File Report 2020–1153*. https://doi.org/10.3133/ofr20201153

71. Fan, P., Ouyang, Z., Duong, D., Thuy, T., Nguyen, H., Park, H., & Chen, J. (2019). Urbanization, economic development, environmental and social changes in transitional economies: Vietnam after Doimoi. *Landscape and Urban Planning*, *187*, 145–155. https://doi.org/10.1016/j.landurbplan.2018.10.014

72. Fan, Y., Chen, J., Shirkey, G., John, R., Wu, S. R., Park, H., & Shao, C. (2016). Applications of structural equation modeling (SEM) in ecological studies: an updated review. *Ecological Processes*, *5*(1). https://doi.org/10.1186/s13717-016-0063-3

73. Fernández-Martínez, M., Sardans, J., Chevallier, F., Ciais, P., Obersteiner, M., Vicca, S., Canadell, J.G., Bastos, A., Friedlingstein, P., Sitch, S., Piao, S.L., Janssens, I.A., Peñuelas, J. (2019). Global trends in carbon sinks and their relationships with CO2 and temperature. *Nature Climate Change, 9*(1), 73-79.

74. Field, C. B., Randerson, J. T. & Malmström, C. M. (1995). Global net primary production: Combining ecology and remote sensing. *Remote Sensing of Environment*, *51*(1), 74–88. https://doi.org/10.1016/0034-4257(94)00066-V

75. Foley, J. A., DeFries, R., Asner, G. P., Barford, C., Bonan, G., Carpenter, S. R., Chapin, F. S., Coe, M. T., Daily, G. C., Gibbs, H. K., Helkowski, J. H., Holloway, T., Howard, E. A., Kucharik, C. J., Monfreda, C., Patz, J. A., Prentice, I. C., Ramankutty, N. & Snyder, P. K. (2005). Global consequences of land use. *Science*, *309*(5734), 570–574.

76. Foody, G. M. (2002). Status of land cover classification accuracy assessment. *Remote Sensing of Environment*, *80*, 185–201.

77. Frischknecht, R., Stucki, M., & Lehmann, M. (2019). Regionalized life cycle assessment: a review of methods and applications. *The International Journal of Life Cycle Assessment, 24*(3), 379-388.

78. FSA USDA. (2018). *CRP enrollment and rental payments by county, 1986-2019*.

79. Gates, D. M., Keegan, H. J., Schleter, J. C., & Weidner, V. R. (1965). Spectral properties of plants. *Applied Optics*, *4*(1), 11–20.

80. Gefen, D., Straub, D., & Boudreau, M. (2000). Structural equation modeling and regression: guidelines for research practice. *Communications of the Association for Information Systems*, *4*(1). https://doi.org/10.17705/1CAIS.00407

81. Gelfand, I., Sahajpal, R., Zhang, X., Izaurralde, R. C., Gross, K. L., & Robertson, G. P. (2013). Sustainable bioenergy production from marginal lands in the US Midwest. *Nature*, *493*(7433), 514–517. https://doi.org/10.1038/nature11811

82. Gelybó, G., Barcza, Z., Kern, A. & Kljun, N. (2013). Effect of spatial heterogeneity on the validation of remote sensing based GPP estimations. *Agricultural and Forest Meteorology*, *174–175*, 43–53. https://doi.org/10.1016/j.agrformet.2013.02.003

83. Gergel, S. E., & Turner, M. G. (Eds.). (2017). *Learning Landscape Ecology: a practical guide to concepts and techniques* (2nd ed.). Springer. https://doi.org/10.1007/978-1-4939-6374-4_20

84. Giannico, V., Chen, J., Shao, C., Ouyang, Z., John, R. & Lafortezza, R. (2018). Contributions of landscape heterogeneity within the footprint of eddy-covariance towers to flux measurements. *Agricultural and Forest Meteorology*, *260–261*, 144–153. https://doi.org/10.1016/j.agrformet.2018.06.004

85. Giannico, V., Spano, G., Elia, M., Este, M. D., Sanesi, G., & Lafortezza, R. (2021). Green spaces, quality of life, and citizen perception in European cities. *Environmental Research*, *196*, 110922. https://doi.org/10.1016/j.envres.2021.110922

86. Gibson, L., Münch, Z., Palmer, A., & Mantel, S. (2018). Future land cover change scenarios in South African grasslands–implications of altered biophysical drivers on land management. *Heliyon, 4*(7), e00693.

87. Gillon, S. (2010). Fields of dreams: Negotiating an ethanol agenda in the Midwest United States. *Journal of Peasant Studies, 37*(4), 723–748. https://doi.org/10.1080/03066150.2010.512456

88. Gitelson, A. A. & Merzlyak, M. N. (1996). Signature analysis of leaf reflectance spectra : algorithm development for remote sensing of chlorophyll. *Journal of Plant Physiology*, *148*(3–4), 494–500. https://doi.org/10.1016/S0176-1617(96)80284-7

89. Gitelson, A. A., Verma, S. B., Keydan, G., Leavitt, B., Arkebauer, T. J., Burba, G. G., Suyker, A. E., Rundquist, D. C., Keydan, G. & Leavitt, B. (2003). *Novel technique for*

remote estimation of CO 2 flux in maize. *30*(9), 2–5. https://doi.org/10.1029/2002GL016543

90. Gitelson, A. A. (2004). Wide dynamic range vegetation index for remote quantification of biophysical characteristics of vegetation. *Journal of Plant Physiology*, *161*(2), 165–173.

91. Gitelson, A. A., Viña, A., Verma, S. B., Rundquist, D. C., Arkebauer, T. J., Keydan, G., Leavitt, B., Ciganda, V., Burba, G. G. & Suyker, A. E. (2006). Relationship between gross primary production and chlorophyll content in crops: Implications for the synoptic monitoring of vegetation productivity. *Journal of Geophysical Research Atmospheres*, *111*(8), 1–13. https://doi.org/10.1029/2005JD006017

92. Godfray, H. C. J., Beddington, J. R., Crute, I. R., Haddad, L., Lawrence, D., Muir, J. F., Pretty, J., Robinson, S., Thomas, S. M. & Toulmin, C. (2010). Food security: The challenge of feeding 9 billion people. *Science*, *327*(5967), 812–818. https://doi.org/10.1126/science.1185383

93. Goetz, S. J., Prince, S. D., Goward, S. N., Thawley, M. M. & Small, J. (1999). Satellite remote sensing of primary production: An improved production efficiency modeling approach. *Ecological Modelling*, *122*(3), 239–255. https://doi.org/10.1016/S0304-3800(99)00140-4

94. Goetz, S. J., Prince, S. D., Small, J. & Gleason, A. C. R. (2000). Interannual variability of global terrestrial primary production: Results of a model driven with satellite observations. *Journal of Geophysical Research: Atmospheres*, *105*(D15), 20077–20091. https://doi.org/10.1029/2000JD900274

95. Goodchild, M. F. (2007). Citizens as sensors: the world of volunteered geography. *GeoJournal*, *69*(4), 211–221. https://doi.org/10.1007/s10708-007-9111-y

96. Goosse, H. (2015). *Climate system dynamics and modeling*. Cambridge University Press.

97. Gorelick, N., Hancher, M., Dixon, M., Ilyushchenko, S., Thau, D. & Moore, R. (2017). Google Earth Engine: Planetary-scale geospatial analysis for everyone. *Remote Sensing of Environment*, *202*, 18–27. https://doi.org/10.1016/j.rse.2017.06.031

98. Grace, J. B., Anderson, M., Olff, H., & Sheiner, S. M. (2010). On the specification of structural equation models for ecological systems. *Ecological Monographs*, *80*(1), 67–87. https://doi.org/10.2307/27806874

99. Guzman, J., & Golabi, M. H. (2017). Agroecosystem net primary productivity and carbon footprint. In M. M. Al-Kaisi & B. Lowery (Eds.), *Soil health and intensification of agroecosytems* (pp. 215–230). Elsevier Inc. https://doi.org/10.1016/B978-0-12-805317-1.00010-5

100. Haberl, H., Erb, K. H., Krausmann, F., Gaube, V., Bondeau, A., Plutzar, C., Gingrich, S., Lucht, W. & Fischer-Kowalski, M. (2007). Quantifying and mapping the human appropriation of net primary production in earth's terrestrial ecosystems. *Proceedings of the National Academy of Sciences of the United States of America*, *104*(31), 12942–12947. https://doi.org/10.1073/pnas.0704243104

101. Haenlein, M., & Kaplan, A. M. (2004). A beginner's guide to partial least squares analysis. *Understanding Statistics*, *3*(4), 283–297. https://doi.org/10.1207/s15328031us0304_4

102. Hair, J. F., Ringle, C. M., & Sarstedt, M. (2011). PLS-SEM: indeed, a silver bullet. *Journal of Marketing Theory and Practice*, *19*(2), 139–151. https://doi.org/10.2753/MTP1069-6679190202

103. Hair, J. F., Hult, G. T. M., Ringle, C. M., Sarstedt, M., Danks, N. P., & Ray, S. (2021). *Partial least squares structural equation modeling (PLS-SEM) using R: a workbook*. Springer Nature. https://doi.org/10.1007/978-3-030-80519-7

104. Harden, C. P. (2012). Framing and reframing questions of human-environment interactions. *Annals of the Association of American Geographers*, *102*(4), 737–747. https://doi.org/10.1080/00045608.2012.678035

105. Hasan, S., Shi, W., Zhu, X., Abbas, S., & Khan, H. U. A. (2020). Future simulation of land use changes in rapidly urbanizing South China based on land change modeler and remote sensing data. *Sustainability, 12*(11), 4350. https://doi.org/10.3390/su12114350

106. Hemes, K. S., Runkle, B. R. K., Novick, K. A., Baldocchi, D. D. & Field, C. B. (2021). An ecosystem-scale flux measurement strategy to assess natural climate solutions. *Environmental Science and Technology*, *55*(6), 3494–3504. https://doi.org/10.1021/acs.est.0c06421

107. Henseler, J., Ringle, C. M., & Sarstedt, M. (2015). A new criterion for assessing discriminant validity in variance-based structural equation modeling. *Journal of the Academy of Marketing Science*, *43*(1), 115–135.

108. Hibbard, K. A., Hoffman, F. M., Huntzinger, D. & West, T. O. (2017). Changes in Land

Cover and Terrestrial Biogeochemistry. In and T. K. M. Wuebbles, D.J., D.W. Fahey, K.A. Hibbard, D.J. Dokken, B.C. Stewart (Ed.), *Climate science special report: fourth national climate assessment, volume I* (pp. 277–302). U.S. Global Change Research Program. https://doi.org/10.7930/J0416V6X.U.S.

109. Hicke, J. A., & Lobell, D. B. (2004). Spatiotemporal patterns of cropland area and net primary production in the central United States estimated from USDA agricultural information. *Geophysical Research Letters*, *31*(20). https://doi.org/10.1029/2004GL020927

110. Hiloidhari, M., Baruah, D. C., & Gogoi, P. (2017). Spatial life cycle assessment: A review and perspectives for future research directions. Journal of Cleaner Production, 142(Part 4), 1595-1609.

111. Homer, C., Dewitz, J., Yang, L., Jin, S., Danielson, P., Xian, G., ... & Megown, K. (2015). Completion of the 2011 National Land Cover Database for the conterminous United States–representing a decade of land cover change information. *Photogrammetric Engineering & Remote Sensing*, *81*(5), 345-354.

112. Homer, C., Dewitz, J., Jin, S., Xian, G., Costello, C., Danielson, P., Gass, L., Funk, M., Wickham, J., Stehman, S., Auch, R., & Riitters, K. (2020). Conterminous United States land cover change patterns 2001–2016 from the 2016 National Land Cover Database. *ISPRS Journal of Photogrammetry and Remote Sensing*, *162*, 184–199. https://doi.org/https://doi.org/10.1016/j.isprsjprs.2020.02.019

113. Horler, D. N. H., Dockray, M. & Barber, J. (1983). The red edge of plant leaf reflectance. *International Journal of Remote Sensing*, *4*(2), 273–288.

114. Houghton, R. A., House, J. I., Pongratz, J., Werf, G. R. Van Der, Defries, R. S., Hansen, M. C. & Qu, C. Le. (2012). *Carbon emissions from land use and land-cover change*. *4*, 5125–5142. https://doi.org/10.5194/bg-9-5125-2012

115. Huete, A. R., Didan, K., Miura, T., Rodriguez, E. P., Gao, X. & Ferreira, L. G. (2002). Overview of the radiometric and biophysical performance of the MODIS vegetation indices. *Remote Sensing of Environment*, *83*(1–2), 195–213. https://doi.org/10.1016/S0034-4257(02)00096-2

116. Huete, A. R., Didan, K., Shimabukuro, Y. E., Ratana, P., Saleska, S. R., Hutyra, L. R., Yang, W., Nemani, R. R. & Myneni, R. (2006). Amazon rainforests green-up with sunlight in dry season. *Geophysical Research Letters*, *33*(6), 2–5. https://doi.org/10.1029/2005GL025583

117. International Energy Agency. (2020). *Energy technology perspectives 2020*. Retrieved from https://www.iea.org/reports/energy-technology-perspectives-2020

118. IPCC 2019. (2019). *2019 Refinement to the 2006 IPCC guidelines for national greenhouse gas inventories* (E. Calvo Buendia, K. Tanabe, A. Kranjc, J. Baasansuren, M. Fukuda, & S. Ngarize, S., Osako, A., Pyrozhenko, Y., Shermanau, P. and Federici, Eds.; Vol. 2). IPCC. https://doi.org/10.21513/0207-2564-2019-2-05-13

119. Jelinski, D. E., & Wu, J. (1996). The modifiable areal unit problem and implications for landscape ecology. *Landscape Ecology*, *11*(3), 129–140.

120. Jiang, Z., Huete, A. R., Didan, K. & Miura, T. (2008). Development of a two-band enhanced vegetation index without a blue band. *Remote Sensing of Environment*, *112*(10), 3833–3845. https://doi.org/10.1016/j.rse.2008.06.006

121. Jin, S., Homer, C., Yang, L., Danielson, P., Dewitz, J., Li, C., Zhu, Z., Xian, G., & Howard, D. (2019). Overall methodology design for the United States National Land Cover Database 2016 products. *Remote Sensing, 11*(24). https://doi.org/10.3390/rs11242971

122. John, R., Chen, J., Noormets, A., Xiao, X., Xu, J., Lu, N. & Chen, S. (2013). Modelling gross primary production in semi-arid Inner Mongolia using MODIS imagery and eddy covariance data. *International Journal of Remote Sensing*, *34*(8), 2829–2857. https://doi.org/10.1080/01431161.2012.746483

123. Joiner, J. & Yoshida, Y. (2020). Satellite-based reflectances capture large fraction of variability in global gross primary production (GPP) at weekly time scales. *Agricultural and Forest Meteorology*, *291*, 108092. https://doi.org/10.1016/j.agrformet.2020.108092

124. Joiner, J. & Yoshida, Y. (2021). *Global MODIS and FLUXNET-derived daily gross primary production, V2*. ORNL DAAC. https://doi.org/doi.org/10.3334/ORNLDAAC/1835

125. Jöreskog, K. G. (1971). Simultaneous factor analysis in several populations. *Psychometrika, 36*(4), 409-426.

126. Jung, M., Reichstein, M. & Bondeau, A. (2009). Towards global empirical upscaling of FLUXNET eddy covariance observations: Validation of a model tree ensemble approach using a biosphere model. *Biogeosciences*, *6*(10), 2001–2013. https://doi.org/10.5194/bg-6-2001-2009

127. Kaiser, H. F. (1960). The application of electronic computers to factor analysis. *Educational and Psychological Measurement*, *20*(1), 141–151.

128. Kane, D (2015). *Carbon sequestration potential on agricultural lands: a review of current science and available practices*. National Sustainable Agriculture Coalition, 1-35.

129. Kanowski, P. J., Mcdermott, C. L., & Cashore, B. W. (2011). Implementing REDD +: lessons from analysis of forest governance. *Environmental Science and Policy, 14*(2), 111–117. https://doi.org/10.1016/j.envsci.2010.11.007

130. Kassambara, A., & Mundt, F. (2020). *factoextra: extract and visualize the results of multivariate data analyses. R package version 1.0.7.*

131. Kolluru, V., John, R., Chen, J., Xiao, J., Amirkhiz, R. G., Giannico, V., & Kussainova, M. (2022b). Optimal ranges of social-environmental drivers and their impacts on vegetation dynamics in Kazakhstan. *Science of the Total Environment*, *847*. https://doi.org/10.1016/j.scitotenv.2022.157562

132. Kolluru, V., John, R., Chen, J., Jarchow, M., & Amirkhiz, R. G. (2022a). Untangling the impacts of socioeconomic and climatic changes on vegetation greenness and productivity in Kazakhstan. *Environmental Research Letters*, *17*, 095007. 10.1088/1748-9326/ac8c59

133. Kramer, D. B., Hartter, J., Boag, A. E., Jain, M., Stevens, K., Nicholas, K. A., McConnell, W. J., Liu, J. (2017). Top 40 questions in coupled human and natural systems (CHANS) research. *Ecology and Society*, *22*(2), 44. https://doi.org/10.5751/ES-09429-220244

134. Kreig, J. A. F., Parish, E. & Jager, H. I. (2021). Growing grasses in unprofitable areas of US Midwest croplands could increase species richness. *Biological Conservation*, *261*, 109289. https://doi.org/10.1016/j.biocon.2021.109289

135. Kruskal, W. H. & Wallis, W. A. (1952). Use of ranks in one-criterion variance analysis. *Journal of the American Statistical Association*, *47*(260), 583–621. https://doi.org/10.1080/01621459.1952.10483441

136. Kugler, T. A., Grace, K., Wrathall, D. J., Sherbinin, A. De, Riper, D. Van, Aubrecht, C., Comer, D., Adamo, S. B., Cervone, G., Engstrom, R., Hultquist, C., Gaughan, A. E., Linard, C., Moran, E., Stevens, F., Tatem, A. J., Tellman, B., & Van Den Hoek, J. (2019). People and pixels 20 years later: the current data landscape and research trends blending population and environmental data. *Population and the Environment*, *41*,

209–234. https://doi.org/doi.org/10.1007/s11111-019-00326-5

137. Kumar, L. & Mutanga, O. (2017). Remote sensing of above-ground biomass. *Remote Sensing*, *9*(9), 1–8. https://doi.org/10.3390/rs9090935

138. Lambin, E. F., Turner, B. L., Geist, H., Agbola, S. B., Angelsen, A., Bruce, J. W., Coomes, O., Dirzo, R., Fisher, G., Folke, C., George, P. S., Homewood, K., Imbernon, J., Leemans, R., Li, X., Moran, E. F., Mortimore, M., Ramakrishnan, P. S., Richards, J. F., … Xu, J. (2001). The causes of land-use and land-cover change: moving beyond the myths. *Global Environmental Change*, *11*(4), 261–269.

139. Lasslop, G., Reichstein, M., Papale, D., Richardson, A., Arneth, A., Barr, A., Stoy, P. & Wohlfahrt, G. (2010). Separation of net ecosystem exchange into assimilation and respiration using a light response curve approach: Critical issues and global evaluation. *Global Change Biology*, *16*(1), 187–208. https://doi.org/10.1111/j.1365-2486.2009.02041.x

140. Lausch, A., Blaschke, T., Haase, D., Herzog, F., Syrbe, R. U., Tischendorf, L., & Walz, U. (2015). Understanding and quantifying landscape structure – a review on relevant process characteristics, data models and landscape metrics. *Ecological Modelling*, *295*, 31–41. https://doi.org/10.1016/j.ecolmodel.2014.08.018

141. Law, B. E., Falge, E., Gu, L., Baldocchi, D. D., & Bakwin, P. (2001). Gap filling strategies for defensible annual sums of net ecosystem exchange. *Agricultural and Forest Meteorology, 107*(1), 43-69.

142. Le Quéré, C., Andrew, R. M., Friedlingstein, P., Sitch, S., Hauck, J., Pongratz, J., ... & Zheng, B. (2018). Global carbon budget 2018. *Earth System Science Data*, *10*(4), 2141-2194.

143. Lei, C., Abraha, M., Chen, J. & Su, Y. (2021). Long-term variability of root production in bioenergy crops from ingrowth core measurements. *Plant Ecology*, *14*(5), 757–770. https://doi.org/10.1093/jpe/rtab018

144. Leta, M. K., Demissie, T. A., & Tränckner, J. (2021). Modeling and prediction of land use land cover change dynamics based on land change modeler (LCM) in Nashe watershed, upper Blue Nile basin, Ethiopia. *Sustainability, 13*(7). https://doi.org/10.3390/su13073740

145. Levin, S. A. (1992). The problem of pattern and scale in ecology. *Ecology*, *73*(6), 1943–1967. https://doi.org/10.2307/1941447

146. Li, F., Wang, X., Zhao, J., Zhang, X. & Zhao, Q. (2013). A method for estimating the gross primary production of alpine meadows using MODIS and climate data in China. *International Journal of Remote Sensing*, *34*(23), 8280–8300. https://doi.org/10.1080/01431161.2013.834394

147. Li, J. & Roy, D. P. (2017). A global analysis of Sentinel-2a, Sentinel-2b and Landsat-8 data revisit intervals and implications for terrestrial monitoring. *Remote Sensing*, *9*(9). https://doi.org/10.3390/rs9090902

148. Li, Z., Yu, G., Xiao, X., Li, Y., Zhao, X., Ren, C., Zhang, L. & Fu, Y. (2007). Modeling gross primary production of alpine ecosystems in the Tibetan Plateau using MODIS images and climate data. *Remote Sensing of Environment*, *107*(3), 510–519. https://doi.org/10.1016/j.rse.2006.10.003

149. Lin, S., Li, J., Liu, Q., Li, L., Zhao, J. & Yu, W. (2019). Evaluating the effectiveness of using vegetation indices based on red-edge reflectance from Sentinel-2 to estimate gross primary productivity. *Remote Sensing*, *11*(11). https://doi.org/10.3390/rs11111303

150. Lind-Riehl, J., Jeltema, S., Morrison, M., Shirkey, G., Mayer, A. L., Rouleau, M., & Winkler, R. (2015). Family legacies and community networks shape private forest management in the western Upper Peninsula of Michigan (USA). *Land Use Policy*, *45*, 95–102. https://doi.org/10.1016/j.landusepol.2015.01.005

151. Liu, J., Herzberger, A., Kapsar, K., Carlson, A. K., & Connor, T. (2019). What Is Telecoupling? In *Telecoupling* (pp. 19–48). Springer International Publishing. https://doi.org/10.1007/978-3-030-11105-2_2

152. Liu, J., Hull, V., Batistella, M., deFries, R., Dietz, T., Fu, F., Hertel, T. W., Cesar Izaurralde, R., Lambin, E. F., Li, S., Martinelli, L. A., McConnell, W. J., Moran, E. F., Naylor, R., Ouyang, Z., Polenske, K. R., Reenberg, A., Rocha, G. de M., Simmons, C. S., … Zhu, C. (2013). Framing sustainability in a telecoupled world. *Ecology and Society*, *18*(2). https://doi.org/10.5751/ES-05873-180226

153. Loiseau, E., Peña-Lévano, L., & Margni, M. (2018). Territorial life cycle assessment: A literature review and future research agenda. *The International Journal of Life Cycle Assessment, 23*(1), 1-17.

154. Mason, C. H., & Perreault, W. D. Jr. (1991). Collinearity, power, and interpretation of multiple regression analysis. *Journal of Marketing Research*, *28*(3), 268–280.

155. Mattila, T., Helin, T., Antikainen, R., Soimakallio, S., Pingoud, K., & Wessman, H.

(2011). Land use in life cycle assessment. In *The Finnish Environment* (Vol. 24). Syke, Helsinki. ISBN 978-952-11-3926-0

156. McGill, B. M., Hamilton, S. K., Millar, N., & Robertson, G. P. (2018). The greenhouse gas cost of agricultural intensification with groundwater irrigation in a Midwest US row cropping system. *Global Change Biology, 24*(12), 5948-5960.

157. Michigan Department of Agriculture and Rural Development (MDARD). (n.d.). *Michigan agriculture resources*. Retrieved from https://www.michigan.gov/mdard/about/mi-agriculture/michigan-agriculture-resources

158. Michigan Department of Environment, Great Lakes, and Energy. (2020). Stream Rivers Assessment Units 2020 [Data file]. ArcGIS Open Data. https://gis-michigan.opendata.arcgis.com/datasets/egle::stream-rivers-assessment-units-2020

159. Michigan State Climatologist's Office. (2013). *Gull Lake (3504)*. http://climate.geo.msu.edu/climate_mi/stations/3504/. Accessed November 22, 2021.

160. Milesi, C., Elvidge, C. D., Nemani, R. R., & Running, S. W. (2003). Assessing the impact of urban land development on net primary productivity in the southeastern United States, *86*, 401–410. https://doi.org/10.1016/S0034-4257(03)00081-6

161. Mishra, V. N., & Rai, P. K. (2016). A remote sensing aided multi-layer perceptron-Markov chain analysis for land use and land cover change prediction in Patna district (Bihar), India. *Arabian Journal of Geosciences, 9*, 1-18.

162. Monecke, A., & Leisch, F. (2012). semPLS: structural equation modeling using partial least squares. *Journal of Statistical Software*, *48*(3), 1–32.

163. Monteith, J. L. (1972). Solar radiation and productivity in tropical ecosystems. *Journal of Applied Ecology*, *9*(3), 747–766.

164. Monteith, J. L. (1977). Climate and the efficiency of crop production in Britain. *Philosophical Transactions of the Royal Society of London Series B: Biological Sciences*, *281*(980), 277–294.

165. Morales, P., Sykes, M. T., Prentice, I. C., Smith, P., Smith, B., Bugmann, H., Zierl, B., Friedlingstein, P., Viovy, N., Sabaté, S., Sánchez, A., Pla, E., Gracia, C. A., Sitch, S., Arneth, A. & Ogee, J. (2005). Comparing and evaluating process-based ecosystem model predictions of carbon and water fluxes in major European forest biomes.

Global Change Biology, *11*(12), 2211–2233. https://doi.org/10.1111/j.1365-2486.2005.01036.x

166. Moro Rosso, L. H., de Borja Reis, A. F., Correndo, A. A., & Ciampitti, I. A. (2021b). XPolaris: an R-package to retrieve United States soil data at 30-meter resolution. *BMC Research Notes*, *14*(1), 1–3. https://doi.org/10.1186/s13104-021-05729-y

167. Moro Rosso, L. H., de Borja Reis, A. F., Correndo, A. A., & Ciampitti, I. A. (2021a). *Retrieving POLARIS data using R-software* (V2 ed.). Harvard Dataverse. https://doi.org/doi:10.7910/DVN/DCZ0N3

168. Morris, S. J., Bohm, S., Haile-Mariam, S., & Paul, E. A. (2007). Evaluation of carbon accrual in afforested agricultural soils. *Global Change Biology*, *13*(6), 1145–1156. https://doi.org/10.1111/j.1365-2486.2007.01359.x

169. Müller-Wilm, U., Devignot, O. & Pessiot, L. (2018). *S2 MPC: Sen2Cor configuration and user manual*. http://step.esa.int/thirdparties/sen2cor/2.9.0/docs/S2-PDGS-MPC-L2A-SUM-V2.9.0.pdf

170. Mungai, L. M., Messina, J. P., Zulu, L. C., Qi, J., & Snapp, S. (2022). Modeling Spatiotemporal Patterns of Land Use/Land Cover Change in Central Malawi Using a Neural Network Model. *Remote Sensing, 14*(14), 3477.

171. Myneni, R. B. & Ross, J. (2012). *Photon-Vegetation interactions: applications in optical remote sensing and plant ecology*. Springer Science & Business Media.

172. National Aeronautics and Space Administration (NASA). (2023). *GHGMIS Draft Strategy for Public Comment*. Retrieved from https://www.federalregister.gov/d/2023-04328

173. Nguyen, T. H., Field, J. L., Kwon, H., Hawkins, T. R., Paustian, K., & Wang, M. Q. (2022). A multi-product landscape life-cycle assessment approach for evaluating local climate mitigation potential. *Journal of Cleaner Production*, 354. https://doi.org/10.1016/j.jclepro.2022.131691</div>

174. Nitzl, C., Roldan, J. L., & Cepeda, G. (2016). Mediation analysis in partial least squares path modeling: Helping researchers discuss more sophisticated models. *Industrial Management & Data Systems*, *116*(9), 1849–1864. https://doi.org/10.1108/IMDS-07-2015-0302

175. Novick, K. A., Metzger, S., Anderegg, W. R. L., Barnes, M., Cala, D. S., Guan, K., Hemes, K. S., Hollinger, D. Y., Kumar, J., Litvak, M., Lombardozzi, D., Normile, C. P., Oikawa, P.,

Runkle, B. R. K., Torn, M., & Wiesner, S. (2022). Informing nature-based climate solutions for the United States with the best-available science. *Global Change Biology*, *28*(12), 3778–3794. https://doi.org/10.1111/gcb.16156

176. Olofsson, P., Foody, G. M., Herold, M., Stehman, S. V., Woodcock, C. E., & Wulder, M. A. (2014). Good practices for estimating area and assessing accuracy of land change. *Remote Sensing of Environment*, *148*, 42–57. https://doi.org/10.1016/j.rse.2014.02.015

177. Pachauri, R. K., Allen, M. R., Barros, V. R., Broome, J., Cramer, W., Christ, R., Church, J.A., Clarke, L., Dahe, Q., Dasgupta, P. and Dubash, N.K. (2014). *Climate change 2014: synthesis report. Contribution of Working Groups I, II and III to the fifth assessment report of the Intergovernmental Panel on Climate Change* (p. 151). Ipcc.g/10.5194/bg-9-5125-2012

178. Papale, D., Reichstein, M., Aubinet, M., Canfora, E., Bernhofer, C., Kutsch, W., Longdoz, B., Rambal, S., Valentini, R., Vesala, T. & Yakir, D. (2006). Towards a standardized processing of net ecosystem exchange measured with eddy covariance technique: Algorithms and uncertainty estimation. *Biogeosciences*, *3*(4), 571–583. https://doi.org/10.5194/bg-3-571-2006

179. Park, H., Fan, P., John, R., & Chen, J. (2017). Urbanization on the Mongolian Plateau after economic reform: Changes and causes. *Applied Geography*, *86*, 118–127. https://doi.org/10.1016/j.apgeog.2017.06.026

180. Parsons, S. D. (1980). Estimating fuel requirements for field operations. Ext. Pub. AE-110. Coop. Ext., Purdue University, West Lafayette. *Available online at http://www.agcom.purdue.edu/AgCom/Pubs/AE/AE-110. html*

181. Piao, S., Ciais, P., Friedlingstein, P., De Noblet-Ducoudré, N., Cadule, P., Viovy, N. & Wang, T. (2009). Spatiotemporal patterns of terrestrial carbon cycle during the 20th century. *Global Biogeochemical Cycles*, *23*(4), 1–16. https://doi.org/10.1029/2008GB003339

182. Pontius, R. G. Jr. 2002. Statistical methods to partition effects of quantity and location during comparison of categorical maps at multiple resolutions. *Photogrammetric Engineering & Remote Sensing 68*(10) p. 1041-1049.

183. Potapov, P., Turubanova, S., Hansen, M. C., Tyukavina, A., Zalles, V., Khan, A., Song, X.-P., Pickens, A., Shen, Q., & Cortez, J. (2022). Global maps of cropland extent and change show accelerated cropland expansion in the twenty-first century. *Nature Food*, *3*(1), 19–28. https://doi.org/10.1038/s43016-021-00429-z

184. Portner, H.O., Roberts, D.C., & Constable, A. (2022). *IPCC, 2022: Summary for Policymakers, Climate Change 2022: Impacts, Adaptation and Vulnerability*. Contribution of Working Group II to the Sixth Assessment Report of the Intergovernmental Panel on Climate Change, Cambridge University Press, Cambridge, UK, 3-33.

185. Potapov, P., Turubanova, S., Hansen, M. C., Tyukavina, A., Zalles, V., Khan, A., Song, X.-P., Pickens, A., Shen, Q., & Cortez, J. (2022). Global maps of cropland extent and change show accelerated cropland expansion in the twenty-first century. *Nature Food*, *3*(1), 19–28. https://doi.org/10.1038/s43016-021-00429-z

186. R Core Team. (2019). *R: A language and environment for statistical computing.* R Foundation for Statistical Computing.

187. Raich, A. J. W., Rastetter, E. B., Melillo, J. M., Kicklighter, D. W., Steudler, P. A., Peterson, J., Grace, A. L., Iii, B. M. & Vörösmarty, C. J. (1991). Potential net primary productivity in South America: application of a global model. *Ecological Applications*, *1*(4), 399–429.

188. Ramankutty, N., Evan, A. T., Monfreda, C. & Foley, J. A. (2008). Farming the planet: 1. Geographic distribution of global agricultural lands in the year 2000. *Global Biogeochemical Cycles*, *22*(GB1003). https://doi.org/10.1029/2007GB002952

189. Reeves, M. C., Zhao, M. & Running, S. W. (2005). Usefulness and limits on MODIS GPP for estimating wheat yield. *International Journal of Remote Sensing*, *26*(7), 1403–1421. https://doi.org/10.1080/01431160512331326567

190. Reichstein, M., Falge, E., Baldocchi, D., Papale, D., Aubinet, M., Berbigier, P., Bernhofer, C., Buchmann, N., Gilmanov, T., Granier, A., Grünwald, T., Havránková, K., Ilvesniemi, H., Janous, D., Knohl, A., Laurila, T., Lohila, A., Loustau, D., Matteucci, G., … Valentini, R. (2005). On the separation of net ecosystem exchange into assimilation and ecosystem respiration: Review and improved algorithm. *Global Change Biology*, *11*(9), 1424–1439. https://doi.org/10.1111/j.1365-2486.2005.001002.x

191. Rigdon, E. E. (2012). Rethinking partial least squares path modeling: in praise of simple methods. *Long Range Planning*, *45*(5–6), 341–358. https://doi.org/10.1016/j.lrp.2012.09.010

192. Rigdon, E. E., Sarstedt, M., & Ringle, C. (2020). On comparing results from CB-SEM and PLS-SEM: five perspectives and five recommendations. *Journal of Research and Management*, *39*(3), 4–16.

193. Robinson, N. P., Allred, B. W., Smith, W. K., Jones, M. O., Moreno, A., Erickson, T. A., Naugle, D. E., & Running, S. W. (2018). Terrestrial primary production for the conterminous United States derived from Landsat 30 m and MODIS 250 m. *Remote Sensing in Ecology and Conservation*, *4*(3), 264–280. https://doi.org/10.1002/rse2.74

194. Roodposhti, M. S., Aryal, J., & Bryan, B. A. (2019). A novel algorithm for calculating transition potential in cellular automata models of land-use/cover change. *Environmental Modelling and Software, 112*, 70–81. https://doi.org/10.1016/j.envsoft.2018.10.006

195. Rudy, A. P., Harris, C. K., Thomas, B. J., Worosz, M. R., Kaplan, S. S. K., & O'Donnell, E. (2008). The Political Ecology of southwest Michigan agriculture. In C. L. Redman & D. R. Foster (Eds.), *Agrarian landscapes in transition* (p. 298). Oxford, New York: Oxford University Press, Inc.

196. Ruggles, S., Flood, S., Goeken, R., Schouweiler, M., & Sobek, M. (2022). *IPUMS USA: Version 12.0 [dataset]*. IPUMS.

197. Ruimy, A., Kergoat, L. & Bondeau, A. (1999). Comparing global models of terrestrial net primary productivity (NPP): Analysis of differences in light absorption and light-use efficiency. *Global Change Biology*, *5*(S1), 56–64. https://doi.org/10.1046/j.1365-2486.1999.00007.x

198. Running, S. W., Nemani, R. R., Heinsch, F. A., Zhao, M., Reeves, M. & Hashimoto, H. (2004). A continuous satellite-derived measure of global terrestrial primary production. *BioScience*, *54*(6), 547–560. https://doi.org/10.1641/0006-3568(2004)054[0547:ACSMOG]2.0.CO;2

199. Running, S. W. & Zhao, M. (2015). *Daily GPP and annual NPP (MOD17A2/A3) products NASA Earth Observing System MODIS land algorithm. MOD17 user's guide*. The Numerical Terradynamic Simulation Group. http://www.ntsg.umt.edu/sites/ntsg.umt.edu/files/modis/MOD17UsersGuide2015_v3.pdf

200. Sangermano, F., Eastman, J. R., & Zhu, H. (2010). Similarity weighted instance-based learning for the generation of transition potentials in land use change modeling. *Transactions in GIS, 14*(5), 569–580. https://doi.org/10.1111/j.1467-9671.2010.01226.x

201. Schneider, A., Logan, K. E., & Kucharik, C. J. (2012). Impacts of urbanization on ecosystem goods and services in the U.S. Corn Belt. *Ecosystems*, *15*, 519–541. https://doi.org/10.1007/s10021-012-9519-1

202. Sciusco, P., Chen, J., Abraha, M., Lei, C., Robertson, G. P., Zhang, R., Lafortezza, R., Shirkey, G., Ouyang, Z., Zhang, R., & John, R. (2020). Spatiotemporal variations of albedo due to land use: contributions to global warming impacts in managed agricultural landscapes. *Landscape Ecology, 35(6), 1385–1402.*

203. Sciusco, P., Chen, J., Giannico, V., Abraha, M., Lei, C., Shirkey, G., Yuan, J., & Robertson, G. P. (2022). Albedo-Induced global warming impact at multiple temporal scales within an Upper Midwest USA Watershed. *Land*, *11*(2). https://doi.org/10.3390/land11020283

204. Shao, C., Chen, J., Chu, H., Lafortezza, R., Dong, G., Abraha, M., Batkhishig, O., John, R., Ouyang, Z., Zhang, Y., & Qi, J. (2017). Grassland productivity and carbon sequestration in Mongolian grasslands: The underlying mechanisms and nomadic implications. *Environmental Research*, *159*. https://doi.org/10.1016/j.envres.2017.08.001

205. Shao, C., Chen, J., Ouyang, Z., Fan, D., Zhao, Y., Wang, Q., & Wu, J. (2017). Greenhouse gas budget and its driving factors in a reclaimed coastal area in eastern China. *Agricultural and Forest Meteorology*, 232, 72–83.

206. Sharma, P., Sarstedt, M., Shmueli, G., Kim, K. H., & Thiele, K. O. (2019). PLS-based model selection: The role of alternative explanations in information systems research. *Journal of the Association for Information Systems*, *20*(4), 4.

207. Sharp, R., Douglass, J., Wolny, S., Arkema, K., Bernhardt, J., Bierbower, W., Chaumont, N., Denu, D., Fisher, D., Glowinski, K., Griffin, R., Guannel, G., Guerry, A., Johnson, J., Hamel, P., Kennedy, C., Kim, C.K., Lacayo, M., Lonsdorf, E., Mandle, L., Rogers, L., Silver, J., Toft, J., Verutes, G., Vogl, A. L., Wood, S, and Wyatt, K. (2020). *InVEST 3.8.9. User's Guide*. The Natural Capital Project, Stanford University, University of Minnesota, The Nature Conservancy, and World Wildlife Fund.

208. Shirkey, G., John, R., Chen, J., Dahlin, K., Abraha, M., Sciusco, P., Lei, C., & Reed, D. E. (2022). Fine resolution remote sensing spectra improves estimates of gross primary production of croplands. *Agricultural and Forest Meteorology*, *326*, 109175. https://doi.org/10.1016/j.agrformet.2022.109175

209. Shirkey, G., John, R., Chen, J., Kolluru, V., Goljani Amirkhiz, R., Marquart-Pyatt, S.T., Cooper, L.T., & Collins, M. (2023). Land cover change and socioecological influences on terrestrial carbon production in an agroecosystem. *Landscape Ecology,* 35, 1385-1402.

210. Sims, D. A. & Gamon, J. A. (2002). Relationships between leaf pigment content and spectral reflectance across a wide range of species, leaf structures and

developmental stages. *Remote Sensing of Environment*, *81*(2–3), 337–354. https://doi.org/10.1016/S0034-4257(02)00010-X

211. Spangler, K., Burchfield, E. K., & Schumacher, B. (2020). Past and current dynamics of U.S. agricultural land use and policy. *Frontiers in Sustainable Food Systems, 4*. https://doi.org/10.3389/fsufs.2020.00098

212. Spies, T. A., Long, J. W., Stine, P., Cerveny, L., Marcot, B. G., Reeves, G., Hessburg, P. F., Lesmeister, D., Reilly, M. J., Raphael, M. G., & Davis, R. J. (2018). Integrating ecological and social science to inform land management in the area of the Northwest Forest Plan. In *Synthesis of science to inform land management within the Northwest Forest Plan Area. Gen. Tech. Rep. PNW-GTR-966* (pp. 919–1020). US Department of Agriculture, Forest Service, Pacific Northwest Research Station.

213. Streukens, S., & Leroi-Werelds, S. (2016). Bootstrapping and PLS-SEM: a step-by-step guide to get more out of your bootstrap results. *European Management Journal*, *34*(6), 618–632. https://doi.org/10.1016/j.emj.2016.06.003

214. Thoen, G. (1990). *Soil survey of Barry County, Michigan*. USDA Soil Conservation Service, Michigan State University Agricultural Experiment Station, and Michigan Technological University.

215. Thornton, P. E., Running, S. W., & White, M. A. (1997). Generating surfaces of daily meteorological variables over large regions of complex terrain. *Journal of Hydrology*, *190*, 214–251.

216. Tian, L., & Chen, J. (2022). Urban expansion inferenced by ecosystem production on the Qinghai-Tibet plateau. *Environmental Research Letters*, *17*(3), 035001. https://doi.org/10.1088/1748-9326/ac3178

217. Tilman, D., Balzer, C., Hill, J. & Befort, B. L. (2011). Global food demand and the sustainable intensification of agriculture. *Proceedings of the National Academy of Sciences of the United States of America*, *108*(50), 20260–20264. https://doi.org/10.1073/pnas.1116437108

218. Tucker, C. J. (1979). Red and photographic infrared linear combinations for monitoring vegetation. *Remote Sensing of Environment*, *8*(2), 127–150. https://doi.org/10.1016/0034-4257(79)90013-0

219. Turner, M. G. (1989). Landscape ecology: the effect of pattern on process. *Annual Review of Ecology and Systematics. Vol. 20*, 171–197. https://doi.org/10.1146/annurev.es.20.110189.001131

220. Turner, D. P., Ritts, W. D., Cohen, W. B., Gower, S. T., Zhao, M., Running, S. W., Wofsy, S. C., Urbanski, S., Dunn, A. L. & Munger, J. W. (2003). Scaling Gross Primary Production (GPP) over boreal and deciduous forest landscapes in support of MODIS GPP product validation. *Remote Sensing of Environment*, *88*(3), 256–270. https://doi.org/10.1016/j.rse.2003.06.005

221. Turner, M. G. (2010). Disturbance and landscape dynamics in a changing world. *Ecology*, *91*(10), 2833–2849.

222. U.S. Census Bureau. (2015). TIGER/Line Shapefile, 2015, state, Michigan, Primary and Secondary Roads State-based Shapefile [Data file]. Retrieved from https://catalog.data.gov/dataset/tiger-line-shapefile-2015-state-michigan-primary-and-secondary-roads-state-based-shapefile

223. U.S. Environmental Protection Agency (EPA). (2019). U.S. Greenhouse Gas Inventory Report: 1990-2017. Retrieved from https://www.epa.gov/sites/default/files/2019-04/documents/us-ghg-inventory-2019-main-text.pdf.

224. U.S. Geological Survey. (n.d.). USGS EROS Archive - Digital Elevation - Shuttle Radar Topography Mission (SRTM) 1 Arc-Second Global. [Dataset]. Retrieved from https://www.usgs.gov/centers/eros/science/usgs-eros-archive-digital-elevation-shuttle-radar-topography-mission-srtm-1

225. United Nations. (2015). *Transforming our world: the 2030 agenda for sustainable development*. https://doi.org/10.1163/15718093-12341365

226. United States Climate Alliance (USCA) (2022). *Natural and working lands and climate action: A state guide to enhance the sector's contribution to state and national climate goals*. Retrieved from http://www.usclimatealliance.org/publications-1

227. U.S. Department of Energy (DOE). (2019). US Life Cycle Inventory Database - ecoinvent [Data file]. Retrieved from https://www.lcacommons.gov/uslci

228. USDA Forest Service Resource Bulletin (2017) *Michigan Forests 2014, NRS-110.*

229. USDA National Agricultural Statistics Service. (2022). *Census of Agriculture*. http://www.nass.usda.gov/Census of Agriculture/index.asp

230. USGCRP. (2018). Impacts, risks, and adaptation in the United States, Volume II. In D. R. Reidmiller, C. W. Avery, K. E. Easterling, K. E. Kunkel, K. L. M. Lewis, T. K. Maycock & B. C. Stewart (Eds.), *Fourth National Climate Assessment: Vol. II*. U.S. Global Change Research Program. https://doi.org/10.7930/NCA4.2018

231. Ustin, S. L. & Middleton, E. M. (2021). Current and near-term advances in Earth observation for ecological applications. *Ecological Processes*, *10*(1), 1–57. https://doi.org/10.1186/s13717-020-00255-4

232. Utterback, D. F., Charles, L. E., Schnorr, T. M., Tiesman, H. M., Storey, E., & Vossenas, P. (2012). Occupational injuries, illnesses, and fatalities among workers in the services sector industries: 2003 to 2007. *Journal of Occupational and Environmental Medicine*, *54*(1), 31–41. https://doi.org/10.1097/JOM.0b013e3182398e36

233. Van der Schrier, G., Barichivich, J., Briffa, K., & Jones, P. (2013). A scPDSI-based global data set of dry and wet spells for 1901-2009. *Journal of Geophysical Research: Atmospheres*, *118*, 4025–4048. https://doi.org/10.1002/jgrd.50355

234. Varble, S., Secchi, S., & Druschke, C. G. (2016). An examination of growing trends in land tenure and conservation practice adoption: Results from a farmer survey in Iowa. *Environmental Management*, *57*(2), 318–330. https://doi.org/10.1007/s00267-015-0619-5

235. Vargha, A. & Delaney, H. D. (1998). The Kruskal-Wallis test and stochastic homogeneity. *Journal of Educational and Behavioral Statistics*, *23*(2), 170–192. https://doi.org/10.3102/10769986023002170

236. Verma, M., Friedl, M. A., Richardson, A. D., Kiely, G., Cescatti, A., Law, B. E., Wohlfahrt, G., Gielen, B., Roupsard, O., Moors, E. J., Toscano, P., Vaccari, F. P., Gianelle, D., Bohrer, G., Varlagin, A., Buchmann, N., Van Gorsel, E., Montagnani, L. & Propastin, P. (2014). Remote sensing of annual terrestrial gross primary productivity from MODIS: An assessment using the FLUXNET La Thuile data set. *Biogeosciences*, *11*(8), 2185–2200. https://doi.org/10.5194/bg-11-2185-2014

237. Vermote, E., Roger, J. C. & Ray, J. P. (2015). MODIS surface reflectance user's guide: collection 6. In *NASA EOSDIS Land Processes DAAC*. http://modis-sr.ltdri.org

238. Wagle, P., Xiao, X. & Suyker, A. E. (2015). Estimation and analysis of gross primary production of soybean under various management practices and drought conditions. *ISPRS Journal of Photogrammetry and Remote Sensing*. https://doi.org/10.1016/j.isprsjprs.2014.10.009

239. Wang, J., Zhuang, J., Wang, W., Liu, S. & Xu, Z. (2015). Assessment of uncertainties in eddy covariance flux measurement based on intensive flux matrix of HiWATER-MUSOEXE. *IEEE Geoscience and Remote Sensing Letters*, *12*(2), 259–263. https://doi.org/10.1109/LGRS.2014.2334703

240. Wang, W., Dungan, J., Hashimoto, H., Michaelis, A. R., Milesi, C., Ichii, K. & Nemani, R. R. (2011). Diagnosing and assessing uncertainties of terrestrial ecosystem models in a multimodel ensemble experiment: 1. Primary production. *Global Change Biology*, *17*(3), 1350–1366.

241. Wang, Z., Xiao, X. & Yan, X. (2010). Modeling gross primary production of maize cropland and degraded grassland in northeastern China. *Agricultural and Forest Meteorology*, *150*(9), 1160–1167. https://doi.org/10.1016/j.agrformet.2010.04.015

242. Wells, N., Goddard, S., & Hayes, M. J. (2004). A Self-Calibrating Palmer Drought Severity Index. *Journal of Climate*, *17*(12), 2335–2351. https://doi.org/10.1175/1520-0442(2004)017<2335:ASPDSI>2.0.CO;2

243. Wen, H., Chen, J., & Wang, Z. (2020). Disproportioned performances of protected areas in the Beijing-Tianjin-Hebei region. *Sustainability*, *12*(16), 1–15. https://doi.org/10.3390/RS12162581

244. West, T. O., & Marland, G. (2002a). A synthesis of carbon sequestration, carbon emissions, and net carbon flux in agriculture: comparing tillage practices in the United States. *Agriculture, Ecosystems & Environment, 91*(1-3), 217-232.

245. West, T. O., & Marland, G. (2002b). Net carbon flux from agricultural ecosystems: methodology for full carbon cycle analyses. Environmental Pollution, 116(3), 439-444.

246. Wickham, J., Stehman, S. V, Sorenson, D. G., Gass, L., & Dewitz, J. A. (2021). Thematic accuracy assessment of the NLCD 2016 land cover for the conterminous United States. *Remote Sensing of Environment, 257*, 112357. https://doi.org/https://doi.org/10.1016/j.rse.2021.112357

247. Wiesner, S., Desai, A. R., Duff, A. J., Metzger, S., & Stoy, P. C. (2022). Quantifying the natural climate solution potential of agricultural systems by combining eddy covariance and remote sensing. *JGR Biogeosciences*, *127*, e2022JG006895. https://doi.org/10.1029/2022JG006895

248. Wolanin, A., Camps-Valls, G., Gómez-Chova, L., Mateo-García, G., van der Tol, C., Zhang, Y. & Guanter, L. (2019). Estimating crop primary productivity with Sentinel-2 and Landsat 8 using machine learning methods trained with radiative transfer simulations. *Remote Sensing of Environment*, *225*, 441–457. https://doi.org/10.1016/j.rse.2019.03.002

249. Wu, C., Niu, Z., Tang, Q. & Huang, W. (2008). Estimating chlorophyll content from

hyperspectral vegetation indices: Modeling and validation. *Agricultural and Forest Meteorology*, *148*(8–9), 1230–1241.

250. Wu, Chaoyang, Chen, J. M. & Huang, N. (2011). Predicting gross primary production from the enhanced vegetation index and photosynthetically active radiation: Evaluation and calibration. *Remote Sensing of Environment*, *115*(12), 3424–3435. https://doi.org/10.1016/j.rse.2011.08.006

251. Wu, J. (2006). Landscape ecology, cross-disciplinarity, and sustainability science. *Landscape Ecology*, *21*(1), 1–4. https://doi.org/10.1007/s10980-006-7195-2

252. Wu, S. R., Liu, X., Wang, L., Chen, J., Zhou, P., & Shao, C. (2022). Integrating life cycle assessment into landscape studies: a postcard from Hulunbuir. *Landscape Ecology, 37*(5), 1347-1364.

253. Wutzler, T., Lucas-Moffat, A., Migliavacca, M., Knauer, J., Sickel, K., Šigut, L., Menzer, O. & Reichstein, M. (2018). Basic and extensible post-processing of eddy covariance flux data with REddyProc. *Biogeosciences*, *15*(16), 5015–5030. https://doi.org/10.5194/bg-15-5015-2018

254. Xiao, J., Zhuang, Q., Law, B. E., Baldocchi, D. D., Chen, J., Richardson, A. D., Melillo, J. M., Davis, K. J., Hollinger, D. Y., Wharton, S., Oren, R., Noormets, A., Fischer, M. L., Verma, S. B., Cook, D. R., Sun, G., McNulty, S., Wofsy, S. C., Bolstad, P. V., … Torn, M. S. (2011). Assessing net ecosystem carbon exchange of U.S. terrestrial ecosystems by integrating eddy covariance flux measurements and satellite observations. *Agricultural and Forest Meteorology*, *151*(1), 60–69. https://doi.org/10.1016/j.agrformet.2010.09.002

255. Xiao, X., Hollinger, D., Aber, J., Goltz, M., Davidson, E. A., Qingyuan, Z. & Berrien, M. I. (2004a). Satellite-based modeling of gross primary production in an evergreen needleleaf forest. *Remote Sensing of Environment*, *89*, 519–534. www.elsevier.codloeate/rse

256. Xiao, X., Zhang, Q., Braswell, B., Urbanski, S., Boles, S., Wofsy, S., Moore, B. & Ojima, D. (2004b). Modeling gross primary production of temperate deciduous broadleaf forest using satellite images and climate data. *Remote Sensing of Environment*, *91*(2), 256–270. https://doi.org/10.1016/j.rse.2004.03.010

257. Xiao, X., Zhang, Q., Saleska, S., Hutyra, L., De Camargo, P., Wofsy, S., Frolking, S., Boles, S., Keller, M. & Moore, B. (2005). Satellite-based modeling of gross primary production in a seasonally moist tropical evergreen forest. *Remote Sensing of Environment*, *94*(1), 105–122. https://doi.org/10.1016/j.rse.2004.08.015

258. Yang, D., Fu, C. S., Smith, A. C., & Yu, Q. (2017). Open land-use map: a regional land-use mapping strategy for incorporating OpenStreetMap with Earth observations. *Geo-Spatial Information Science*, *20*(3), 269–281. https://doi.org/10.1080/10095020.2017.1371385

259. Yang, L., Jin, S., Danielson, P., Homer, C., Gass, L., Bender, S. M., Case, A., Costello, C., Dewitz, J., Fry, J., Funk, M., Granneman, B., Liknes, G. C., Rigge, M., & Xian, G. (2018). A new generation of the United States National Land Cover Database: requirements, research priorities, design, and implementation strategies. *ISPRS Journal of Photogrammetry and Remote Sensing*, *146*, 108–123. https://doi.org/https://doi.org/10.1016/j.isprsjprs.2018.09.006

260. Yang, L., Jin, S., Danielson, P., Homer, C., Gass, L., Bender, S. M., Case, A., Costello, C., Dewitz, J., Fry, J., Funk, M., Granneman, B., Liknes, G. C., Rigge, M., & Xian, G. (2018). A new generation of the United States National Land Cover Database: requirements, research priorities, design, and implementation strategies. *ISPRS Journal of Photogrammetry and Remote Sensing, 146*, 108–123. https://doi.org/https://doi.org/10.1016/j.isprsjprs.2018.09.006

261. Yang, L., Shen, F., Zhang, L., Cai, Y., Yi, F., & Zhou, C. (2021). Quantifying influences of natural and anthropogenic factors on vegetation changes using structural equation modeling: a case study in Jiangsu Province, China. *Journal of Cleaner Production*, *280*, 124330. https://doi.org/10.1016/j.jclepro.2020.124330

262. Zabel, F., Delzeit, R., Schneider, J. M., Seppelt, R., Mauser, W. & Václavík, T. (2019). Global impacts of future cropland expansion and intensification on agricultural markets and biodiversity. *Nature Communications*, *10*(1), 1–10. https://doi.org/10.1038/s41467-019-10775-z

263. Zeileis, A. & Grothendieck, G. (2005). zoo: S3 Infrastructure for Regular and Irregular Time Series. *Journal of Statistical Software*, *14*(6), 1–27. https://doi.org/10.18637/jss.v014.i06

264. Zenone, T., Chen, J., Deal, M. W., Wilske, B., Jasrotia, P., Xu, J., Bhardwaj, A. K., Hamilton, S. K. & Philip Robertson, G. (2011). CO2 fluxes of transitional bioenergy crops: Effect of land conversion during the first year of cultivation. *Global Change Biology Bioenergy*, *3*(5), 401–412. https://doi.org/10.1111/j.1757-1707.2011.01098.x

265. Zhang, F., Chen, J. M., Chen, J., Gough, C. M., Martin, T. A. & Dragoni, D. (2012). Evaluating spatial and temporal patterns of MODIS GPP over the conterminous U.S. against flux measurements and a process model. *Remote Sensing of Environment*, *124*, 717–729. https://doi.org/10.1016/j.rse.2012.06.023

266. Zhang, Y., Xiao, X., Jin, C., Dong, J., Zhou, S., Wagle, P., Joiner, J., Guanter, L., Zhang, Y., Zhang, G., Qin, Y., Wang, J. & Moore, B. (2016). Consistency between sun-induced chlorophyll fluorescence and gross primary production of vegetation in North America. *Remote Sensing of Environment*, *183*, 154–169. https://doi.org/10.1016/j.rse.2016.05.015

267. Zhao, T., Brown, D. G., & Bergen, K. M. (2007). Increasing gross primary production (GPP) in the urbanizing landscapes of southeastern Michigan. *Photogrammetric Engineering & Remote Sensing*, *73*(10), 1159–1167.

268. Zhao, Y., Ciais, P., Peylin, P., Viovy, N., Longdoz, B., Bonnefond, J. M., Rambal, S., Klumpp, K., Olioso, A., Cellier, P., Maignan, F., Eglin, T. & Calvet, J. C. (2012). How errors on meteorological variables impact simulated ecosystem fluxes: A case study for six French sites. *Biogeosciences*, *9*(7), 2537–2564. https://doi.org/10.5194/bg-9-2537-2012

269. Zimmerer, K. S. (2010). Retrospective on nature–society geography: tracing trajectories (1911–2010) and reflecting on translations. *Annals of the Association of American Geographers*, *100*(5), 1076–1094.

270. Zimmerer, K. S., Lambin, E. F., & Vanek, S. J. (2018). Smallholder telecoupling and potential sustainability. *Ecology and Society*, *23*(1).

APPENDIX A. SUPPLEMENTARY INFORMATION

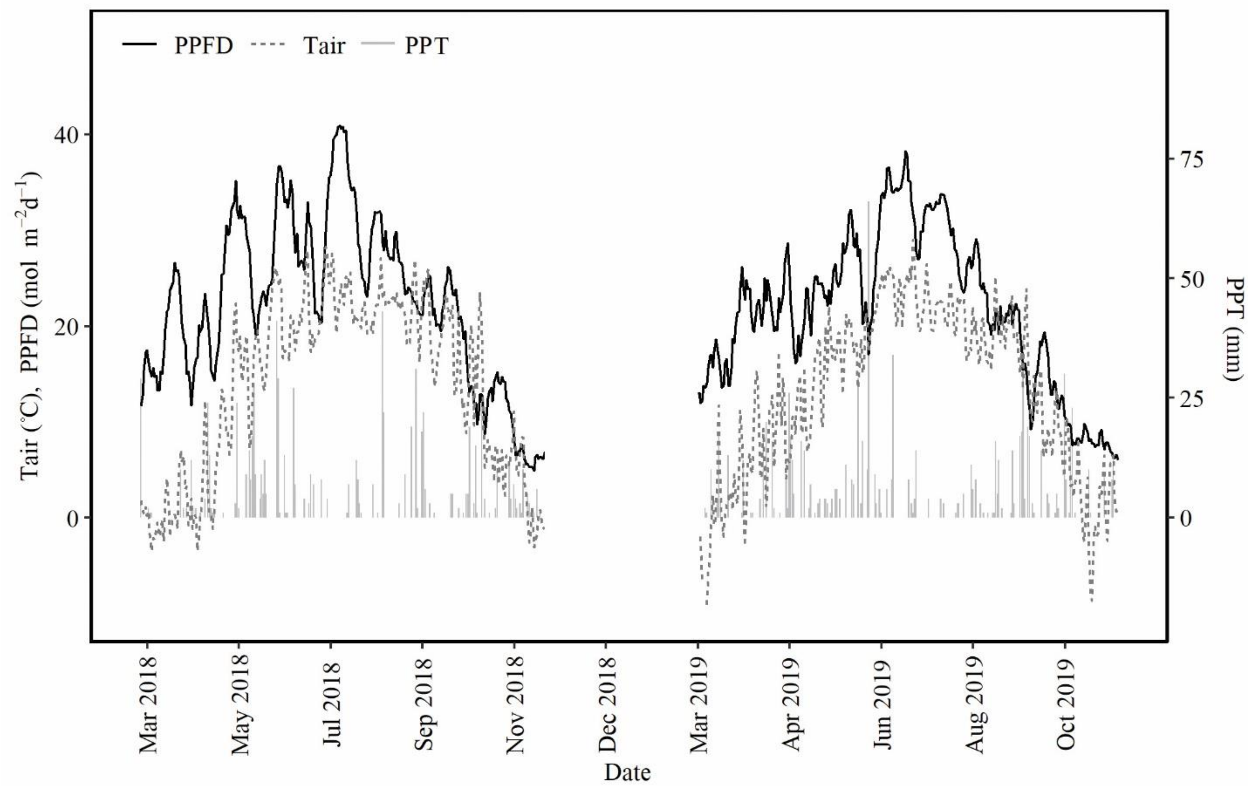

Figure A1. Changes in rainfall (PPT), air temperature (Tair), and photosynthetic photon flux density (PPFD) March–November in 2018 and 2019 for the study area.

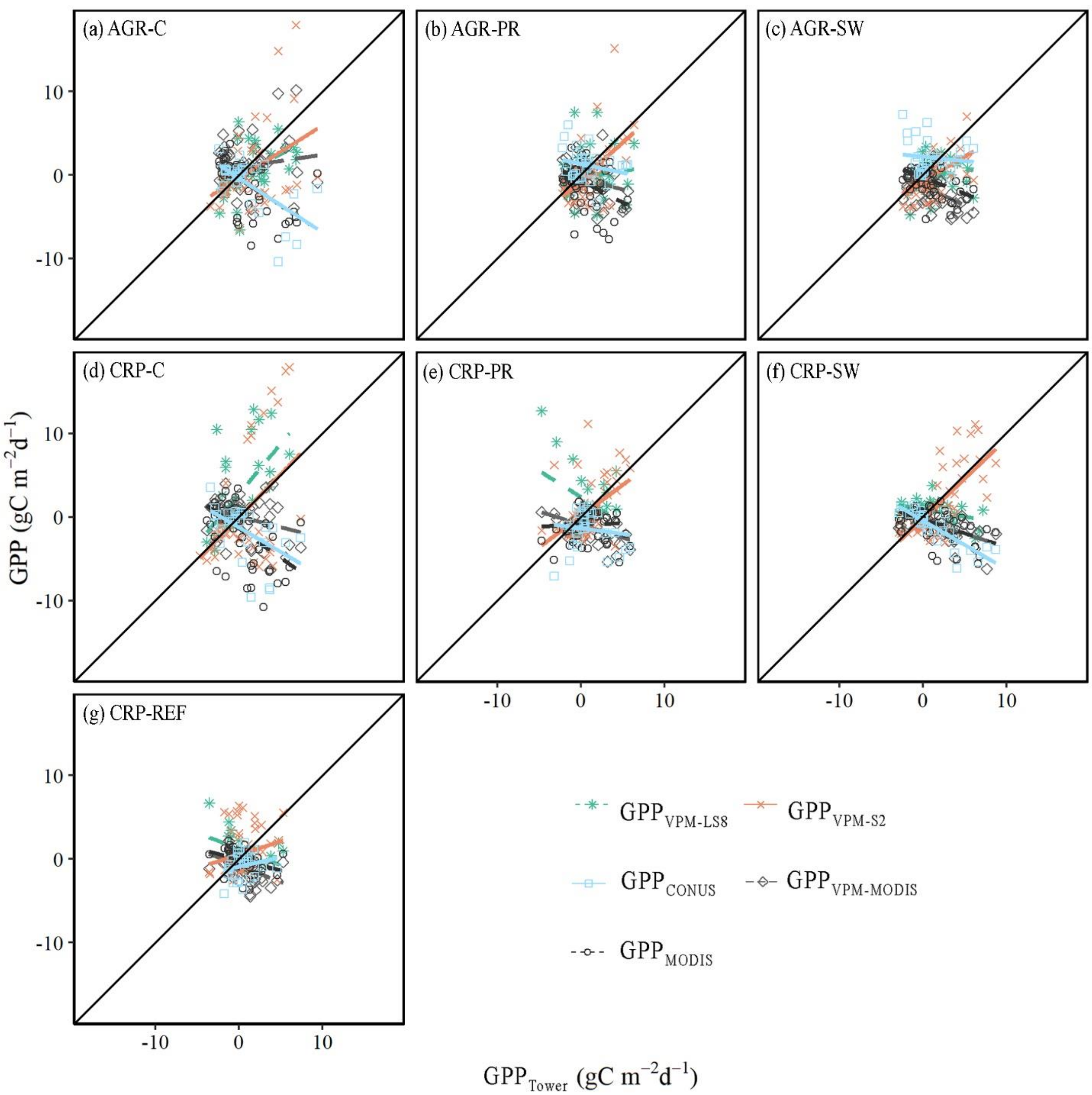

Figure A2. The linear regressions of study period anomalies for the seven study sites: (a) AGR-C, (b) AGR-PR, (c) AGR-SW, (d) CRP-C, (e) CRP-PR, (f) CRP-SW, and (g) CRP-REF.

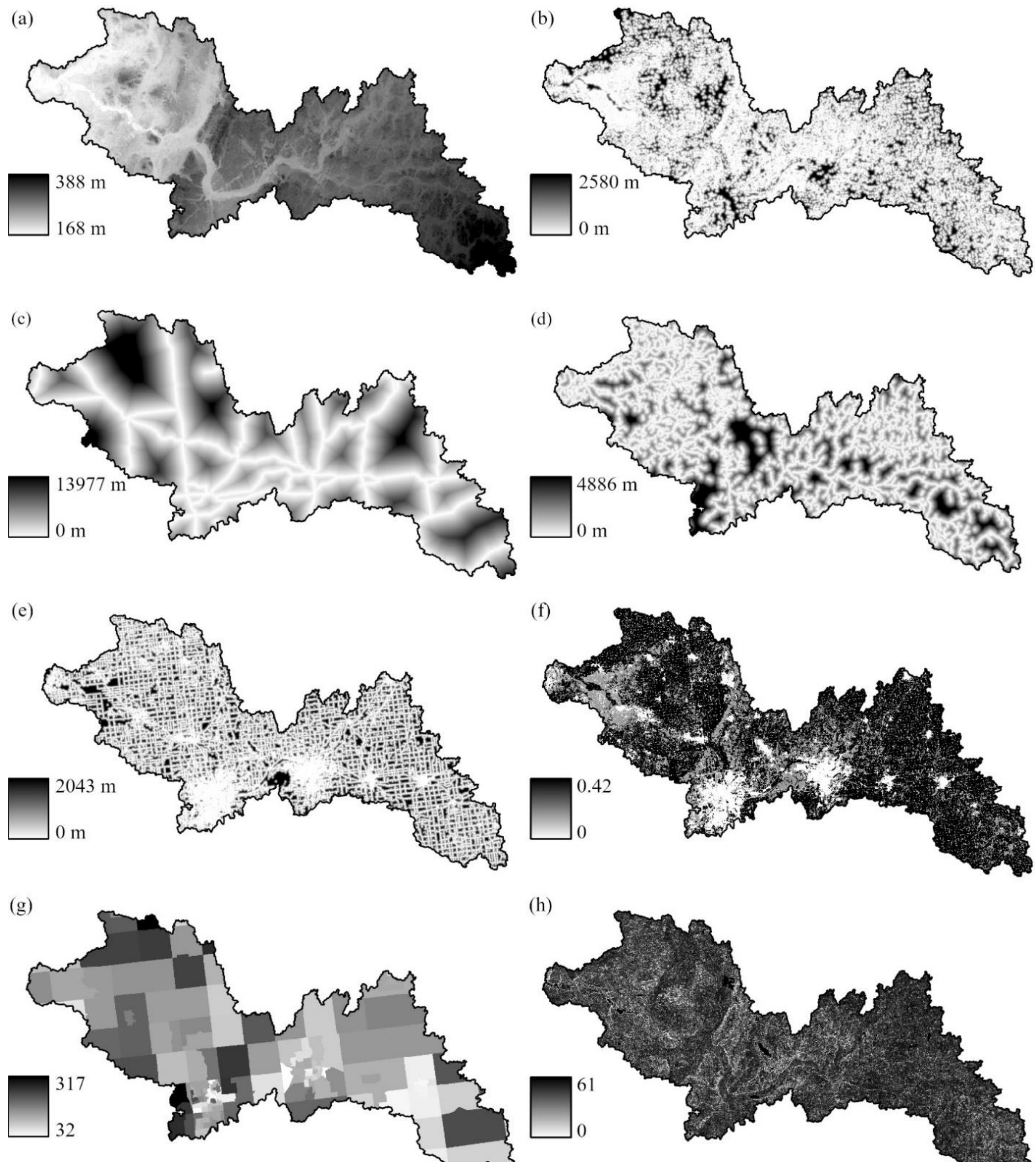

Figure A3. Transition sub-model variables considered in the Land Change Model, where (a) is elevation, (b) distance to Forest, (c) distance to roads, (d) distance to rivers and streams, (e) distance to Urban, (f) is event likelihood; (g) is population density km^2, and (h) is slope.

Table A1. Site location and flux tower characteristics in the study area. Land use includes conservation reserve program (CRP) and historically farmed land (AGR). Prairies are C3 dominant.

Site	MODIS	Location		
		Lat.	*Long.*	*Alt. (m)*
AGR-C	Corn	42.484740	-85.442162	299.17
AGR-PR	Restored prairie (C3)	42.473500	-85.447470	297.79
AGR-SW	Switchgrass	42.476670	-85.446792	292.40
CRP-C	Corn	42.437620	-85.328620	291.15
CRP-PR	Restored prairie (C3)	42.444040	-85.309752	295.80
CRP-REF	Smooth brome grass (C3)	42.442350	-85.330190	280.49
CRP-SW	Switchgrass	42.446250	-85.310436	293.42

Table A2. Site-level parameters used in VPMs include minimum air temperature (Tmin), maximum air temperature (Tmax), and optimal air temperature (Topt) developed by the Terrestrial Ecosystem Model (Raich et al., 1991); as well as LUE where KM is the Michaelis constant indicating the halfway point of PPFD to maximum LUE.

Site	Tmin	Tmax	Topt	2018			2019		
	(°C)	(°C)	(°C)	*e0*	*KM*	*LSWImax*	*e0*	*KM*	*LSWImax*
AGR-C	-1	48	23.10	0.101	999.11	0.47	0.082	1194.20	0.77
AGR-PR	0	48	23.10	0.084	1165.36	0.63	0.052	1480.28	0.69
AGR-SW	0	48	23.10	0.060	1176.00	0.39	0.045	1920.60	0.69
CRP-C	-1	48	22.45	0.100	730.69	0.68	0.110	845.69	0.78
CRP-PR	0	48	22.46	0.073	956.83	0.62	0.057	1394.82	0.65
CRP-SW	0	48	22.45	0.062	1806.12	0.64	0.066	1727.19	0.66
CRP-REF	0	48	22.45	0.056	526.25	0.61	0.057	526.25	0.69

Table A3. Composition of land cover (m^2) within MODIS (500 m) remote sensing pixels encompassing the tower, as depicted in Fig. 1.1. The land cover was acquired from the National Landcover Database 2019 (30 m) and is assumed to represent both site-years 2018 and 2019.

Site	Water	Developed	Forest	Grassland	Crop	Wetland
AGR-C	3600	17100	40500	79200	59400	50400
AGR-PR	0	5400	61200	13500	166500	0
AGR-SW	0	5400	61200	13500	166500	0
CRP-C	0	900	34200	99900	117900	0
CRP-PR	0	6300	6300	118800	72000	43200
CRP-SW	0	6300	6300	118800	72000	43200
CRP-REF	0	25200	4500	133200	9000	75600

Table A4. Gap-filled eddy covariance half-hourly NEE identified as a gap and aggregated GPP uncertainty due to Ustar estimation for each site during the study period.

Site	NEE gap-filled (%)		GPP uncertainty (%)		GPP ($g\ C\ m^{-2}$)	
	2018	2019	2018	2019	2018	2019
AGR-C	16.17	27.51	2.74	1.05	43.78	13.90
AGR-PR	16.16	18.83	2.13	0.25	33.11	3.63
AGR-SW	18.78	22.80	2.30	0.73	34.43	10.03
CRP-C	19.36	22.76	2.87	0.96	40.60	15.24
CRP-PR	20.21	23.21	1.25	0.81	18.33	12.74
CRP-SW	16.99	22.34	1.42	1.96	24.54	30.71
CRP-REF	23.43	24.42	2.15	2.97	28.42	37.43

Table A5. Estimated GPP anomalies of RS models to GPP_{Tower}, with the respective root mean square error (RMSE), adjusted R^2, and linear equation. All linear models and Spearman's Rho (ρ) are significant at *p*-values of <0.001.

Site	Model	R^2	RMSE	Rho	Linear Eq.	R^2	RMSE	Rho	Linear Eq.
				2018				*2019*	
AGR-C	GPP_{MODIS}	0.72	4.38	0.89	y=-1.75x + 1.90	0.67	3.07	0.91	y=-1.38x + 1.57
	GPP_{CONUS}	0.61	3.97	0.92	y=-1.15x + 2.27	0.76	3.53	0.93	y=-1.12x + 1.24
	$GPP_{VPM-MODIS}$	0.89	1.96	0.97	y=-0.40x + 1.03	0.83	1.59	0.97	y=-0.78x + 1.37
	$GPP_{VPM-LS8}$	0.93	2.44	0.96	y= 0.66x + 1.15	0.94	2.50	0.95	y= 0.99x + 1.02
	GPP_{VPM-S2}	0.78	3.61	0.96	y= 1.56x + 0.88	0.89	2.09	0.94	y= 1.32x + 0.93
AGR-PR	GPP_{MODIS}	0.72	2.62	0.85	y=-0.87x + 1.53	0.72	3.23	0.83	y=-1.05x + 1.55
	GPP_{CONUS}	0.73	3.16	0.92	y=-0.54x + 0.94	0.66	2.97	0.88	y=-0.81x + 0.98
	$GPP_{VPM-MODIS}$	0.91	1.02	0.98	y=-0.33x + 0.91	0.97	1.26	0.96	y=-0.39x + 1.52
	$GPP_{VPM-LS8}$	0.97	1.79	0.98	y= 0.64x + 0.88	0.95	0.97	0.94	y= 0.91x + 1.47
	GPP_{VPM-S2}	0.92	1.66	0.94	y= 1.30x + 0.78	0.90	1.83	0.96	y= 1.36x + 1.08
AGR-SW	GPP_{MODIS}	0.74	2.65	0.88	y=-0.25x + 1.42	0.84	2.92	0.85	y=-1.19x + 1.55
	GPP_{CONUS}	0.70	2.78	0.96	y=-0.23x + 0.84	0.65	2.03	0.90	y=-0.58x + 0.82
	$GPP_{VPM-MODIS}$	0.89	1.4	0.99	y= 0.35x + 1.13	0.97	0.83	0.97	y=-0.37x + 1.84
	$GPP_{VPM-LS8}$	0.93	1.82	0.98	y= 0.68x + 1.17	0.98	0.95	0.95	y= 0.61x + 1.19
	GPP_{VPM-S2}	0.97	0.93	0.98	y= 0.72x + 1.02	0.92	1.43	0.96	y= 1.04x + 1.20
CRP-C	GPP_{MODIS}	0.65	3.78	0.9	y=-1.64x + 1.66	0.55	3.98	0.86	y=-1.06x + 1.73
	GPP_{CONUS}	0.61	3.87	0.87	y=-0.87x + 2.00	0.68	4.62	0.90	y=-0.57x + 1.23
	$GPP_{VPM-MODIS}$	0.82	2.53	0.98	y=-0.88x + 1.37	0.85	1.87	0.94	y=-1.06x + 1.44
	$GPP_{VPM-LS8}$	0.84	2.75	0.95	y= 0.12x + 0.81	0.92	2.69	0.91	y= 0.50x + 0.71
	GPP_{VPM-S2}	0.80	3.02	0.95	y= 1.41x + 0.87	0.78	3.30	0.92	y= 2.23x + 0.68
CRP-PR	GPP_{MODIS}	0.84	1.67	0.89	y= 0.36x + 1.20	0.81	2.42	0.88	y=-0.17x + 1.50
	GPP_{CONUS}	0.80	1.80	0.94	y=-0.15x + 1.46	0.77	2.26	0.93	y=-1.21x + 1.93
	$GPP_{VPM-MODIS}$	0.82	1.97	0.97	y= 1.25x + 0.84	0.88	1.08	0.94	y= 0.47x + 1.44
	$GPP_{VPM-LS8}$	0.76	1.87	0.97	y= 1.93x + 0.50	0.95	1.74	0.95	y= 0.42x + 1.18
	GPP_{VPM-S2}	0.89	1.48	0.98	y= 1.82x + 0.68	0.96	1.03	0.96	y= 1.28x + 0.93
CRP-REF	GPP_{MODIS}	0.72	1.44	0.93	y= 0.66x + 0.98	0.80	1.06	0.92	y= 0.31x + 1.05
	GPP_{CONUS}	0.83	2.10	0.90	y=-0.24x + 1.35	0.92	1.69	0.88	y=-1.05x + 1.57
	$GPP_{VPM-MODIS}$	0.70	2.06	0.95	y= 1.32x + 0.89	0.70	1.34	0.94	y= 1.15x + 0.94
	$GPP_{VPM-LS8}$	0.71	2.15	0.88	y= 1.23x + 0.74	0.87	2.04	0.90	y= 0.88x + 0.83
	GPP_{VPM-S2}	0.84	1.64	0.95	y= 1.59x + 0.80	0.85	1.48	0.95	y= 1.15x + 0.71
CRP-SW	GPP_{MODIS}	0.83	2.83	0.76	y=-1.14x + 1.74	0.75	3.68	0.86	y=-1.29x + 1.69
	GPP_{CONUS}	0.74	2.61	0.90	y=-0.65x + 1.75	0.63	3.19	0.93	y=-0.91x + 1.77
	$GPP_{VPM-MODIS}$	0.94	1.54	0.92	y=-0.38x + 1.58	0.93	2.54	0.98	y=-0.97x + 1.45
	$GPP_{VPM-LS8}$	0.93	1.56	0.94	y=-0.34x + 1.37	0.83	1.63	0.97	y=-1.56x + 1.48
	GPP_{VPM-S2}	0.93	1.70	0.93	y= 1.33x + 0.93	0.93	1.70	0.96	y= 0.85x + 0.92

Table A6. Estimated GPP of RS models to GPP_{Tower}, from 2018 and 2019 combined, with the respective root mean square error (RMSE), adjusted R^2, and linear equation, as well as Spearman's Rho (ρ) and *p*-value.

Site	Model	Adj. R^2	*p*-value	RMSE	ρ	*p*-value	Linear Eq.
AGR-C	GPP_{MODIS}	0.34	***	2.13	-0.62	***	y= 0.62+ -0.63
	GPP_{CONUS}	0.42	***	2.25	-0.42	*	y= 0.74+ -0.76
	$GPP_{VPM-MODIS}$	0.01	.	2.61	-0.07	.	y= 0.85+ 0.18
	$GPP_{VPM-LS8}$	0.25	***	2.17	0.62	***	y= 1.20+ 0.62
	GPP_{VPM-S2}	0.15	***	2.36	0.14	.	y= 0.97+ 0.31
AGR-PR	GPP_{MODIS}	0.23	***	1.44	-0.39	**	y= 0.17+ -0.35
	GPP_{CONUS}	0.13	*	1.74	-0.44	**	y= 1.16+ -0.43
	$GPP_{VPM-MODIS}$	-0.01	.	1.65	0.05	.	y= 0.47+ 0.05
	$GPP_{VPM-LS8}$	0.00	.	1.72	0.15	.	y= 0.72+ 0.10
	GPP_{VPM-S2}	0.34	***	1.39	0.60	***	y= 0.65+ 0.37
AGR-SW	GPP_{MODIS}	0.19	***	1.56	-0.31	**	y= 0.40+ -0.51
	GPP_{CONUS}	-0.01	.	1.95	-0.04	.	y= 1.18+ -0.16
	$GPP_{VPM-MODIS}$	0.00	.	1.74	-0.08	.	y= 0.60+ -0.10
	$GPP_{VPM-LS8}$	-0.01	.	1.69	0.06	.	y= 0.94+ 0.08
	GPP_{VPM-S2}	0.28	***	1.46	0.46	***	y= 1.00+ 0.52
CRP-C	GPP_{MODIS}	0.34	***	2.03	-0.52	***	y= 0.06+ -0.51
	GPP_{CONUS}	0.16	**	2.45	-0.45	**	y= 0.40+ -0.41
	$GPP_{VPM-MODIS}$	0.09	**	2.39	-0.15	.	y= 0.41+ -0.43
	$GPP_{VPM-LS8}$	0.37	***	1.84	0.63	***	y= -0.26+ 0.37
	GPP_{VPM-S2}	0.21	***	2.17	0.21	.	y= 0.60+ 0.26
CRP-PR	GPP_{MODIS}	0.01	.	1.65	-0.11	.	y= 0.77+ -0.18
	GPP_{CONUS}	0.04	.	1.72	-0.15	.	y= 0.71+ -0.22
	$GPP_{VPM-MODIS}$	0.33	***	1.35	-0.44	***	y= 0.61+ -0.63
	$GPP_{VPM-LS8}$	0.09	*	1.55	0.09	.	y= 1.07+ -0.19
	GPP_{VPM-S2}	0.17	***	1.51	0.36	***	y= 0.76+ 0.29
CRP-REF	GPP_{MODIS}	0.07	*	1.50	-0.38	**	y= 0.47+ -0.44
	GPP_{CONUS}	0.04	.	1.34	0.28	.	y= 0.72+ 0.25
	$GPP_{VPM-MODIS}$	0.26	***	1.33	-0.64	***	y= 0.23+ -0.63
	$GPP_{VPM-LS8}$	0.25	**	1.55	-0.42	*	y= 0.87+ -0.66
	GPP_{VPM-S2}	0.02	.	1.57	0.17	.	y= 0.45+ 0.15
CRP-SW	GPP_{MODIS}	0.27	***	2.14	-0.50	***	y= 0.9+ -0.79
	GPP_{CONUS}	0.68	***	1.53	-0.85	***	y= 0.21+ -1.15
	$GPP_{VPM-MODIS}$	0.05	*	2.43	-0.10	.	y= 1.14+ -0.59
	$GPP_{VPM-LS8}$	0.15	**	2.20	-0.15	.	y= 1.42+ -0.90
	GPP_{VPM-S2}	0.50	***	1.73	0.58	***	y= 0.94+ 0.59

*** = < 0.001, ** = < 0.01, * = < 0.05, '.' = NS

Table A7. Number of validation samples by cover type in 1986 for the Kalamazoo River Watershed, including producer's and user's accuracy.

	Urban	Crop	Grassland	Forest	Water	Wetland	Bare	User's accuracy
Urban	85	2	8	1	0	0	4	85%
Crop	5	54	26	13	0	2	0	54%
Grassland	23	3	61	2	0	9	2	61%
Forest	3	5	18	68	1	5	0	68%
Water	2	0	1	1	80	16	0	80%
Wetland	1	2	0	2	2	92	1	92%
Bare	8	0	32	15	0	8	37	37%
Producer's accuracy	66.93%	81.82%	41.78%	66.67%	96.39%	69.70%	84.10%	**68.14%**

Table A8. Number of validation samples by cover type in 1991 for the Kalamazoo River Watershed, including producer's and user's accuracy.

	Urban	Crop	Grassland	Forest	Water	Wetland	Bare	User's accuracy
Urban	81	7	4	2	0	3	3	81%
Crop	11	55	22	6	0	3	3	55%
Grassland	21	0	71	2	0	4	2	71%
Forest	6	3	6	83	0	2	0	83%
Water	2	1	3	2	66	26	0	66%
Wetland	1	0	1	1	0	97	0	97%
Bare	24	2	9	10	0	9	46	46%
Producer's accuracy	55.48%	80.88%	61.21%	78.30%	100%	67.36%	85.19%	**71.29%**

Table A9. Number of validation samples by cover type in 1996 for the Kalamazoo River Watershed, including producer's and user's accuracy.

	Urban	Crop	Grassland	Forest	Water	Wetland	Bare	User's accuracy
Urban	67	12	14	2	0	4	1	67%
Crop	4	68	20	4	0	0	4	68%
Grassland	13	2	54	19	1	6	5	54%
Forest	5	1	6	84	1	3	0	84%
Water	2	1	2	4	77	12	2	77%
Wetland	1	2	1	1	0	95	0	95%
Bare	6	25	13	1	1	6	48	48%
Producer's accuracy	68.36%	61.26%	49.09%	73.04%	96.25%	75.40%	80%	**70.42%**

Table A10. Reclassification of the National Land Cover Database (NLCD) in land cover change analysis.

NLCD classification	Grouped classification
Evergreen Forest	Forest
Deciduous Forest	
Mixed Forest	
Shrub/Scrub	Grassland
Grassland/Herbaceous	
Barren Land	Bare
Woody Wetlands	Wetland
Emergent herbaceous wetlands	
Cultivated Crops	Cropland
Pasture / Hay	
Developed, High intensity	Urban
Developed, Medium Intensity	
Developed, Low intensity	
Developed, Open space	
Open Water	Water

Table A11. Structural contribution (%), area (km^2), functional NPP (%), and NPP (kg $km^{-2}yr^{-1}$) by land cover type for the study period.

Year	Land Cover	Structural Contribution (%)	Area (km^2)	Functional NPP (%)	NPP (kg $km^{-2}yr^{-1}$)
1987	Bare	0.26	13.05	0.21	86907
1987	Cropland	59.35	2927.82	58.75	23942748
1987	Forest	32.18	1587.44	32.97	13437190
1987	Prairie	0.67	33.15	0.78	317769
1987	Urban	4.91	242.29	4.72	1923482
1987	Water	2.62	129.48	2.57	1046933
1992	Bare	0.23	11.59	0.24	115643
1992	Cropland	59.29	2926.92	58.36	27899392
1992	Forest	31.59	1559.51	32.69	15628909
1992	Prairie	0.64	31.68	0.64	308134
1992	Urban	5.63	277.88	5.48	2618515
1992	Water	2.62	129.13	2.58	1233027
1997	Bare	0.62	28.55	0.54	234865
1997	Cropland	53.29	2462.61	54.56	23827134
1997	Forest	27.09	1251.82	27.03	11807175
1997	Prairie	1.82	84.15	1.59	695782
1997	Urban	14.47	668.86	13.55	5920048
1997	Water	2.71	125.24	2.72	1190035
2002	Bare	0.28	12.21	0.33	130410
2002	Cropland	53.94	2375.24	55.33	21839380
2002	Forest	25.60	1127.37	26.07	10289990
2002	Prairie	0.91	39.94	1.01	398364
2002	Urban	16.83	741.32	15.06	5943187
2002	Water	2.44	107.48	2.20	869936
2007	Bare	0.27	11.95	0.33	141388
2007	Cropland	53.77	2368.27	55.22	23862539
2007	Forest	25.43	1119.96	25.78	11140256
2007	Prairie	0.97	42.59	1.11	480858
2007	Urban	17.11	753.44	15.29	6608880
2007	Water	2.46	108.50	2.27	981316
2012	Bare	0.26	11.56	0.32	113922
2012	Cropland	53.45	2358.81	56.08	19887579
2012	Forest	25.40	1120.94	25.30	8974209
2012	Prairie	0.93	41.07	1.05	371135
2012	Urban	17.28	762.45	14.93	5296408
2012	Water	2.69	118.52	2.32	821109
2017	Bare	0.25	11.07	0.33	161642
2017	Cropland	53.40	2352.42	54.72	26895845
2017	Forest	25.34	1116.44	26.16	12857591
2017	Prairie	1.08	47.44	1.08	532919
2017	Urban	17.41	766.98	15.43	7585081
2017	Water	2.52	110.91	2.28	1119426

Table A12. Results of the PCA eigenvalues, percent variance and cumulative percent variance.

Dimension	Eigenvalue	Variance (%)	Cumulative Variance (%)
1	14.12	32.09	32.09
2	5.91	13.43	45.52
3	4.38	9.95	55.47
4	3.79	8.61	64.08
5	3.12	7.09	71.18
6	2.86	6.50	77.68
7	2.09	4.74	82.42
8	1.47	3.33	85.76
9	1.31	2.99	88.74
10	1.01	2.30	91.04
11	0.76	1.73	92.78
12	0.58	1.32	94.10
13	0.50	1.13	95.22
14	0.46	1.04	96.27
15	0.38	0.86	97.13
16	0.26	0.59	97.72
17	0.22	0.50	98.22
18	0.18	0.40	98.62
19	0.10	0.22	98.84
20	0.09	0.21	99.05
21	0.08	0.19	99.24
22	0.08	0.17	99.42
23	0.07	0.15	99.57
24	0.04	0.10	99.67
25	0.03	0.06	99.74
26	0.02	0.05	99.79
27	0.02	0.05	99.84
28	0.02	0.04	99.88
29	0.02	0.03	99.92
30	0.01	0.03	99.95
31	0.01	0.02	99.96
32	0.01	0.01	99.98
33	0.00	0.01	99.99
34	0.00	0.01	99.99
35	0.00	0.00	100.00
36	0.00	0.00	100.00
37	0.00	0.00	100.00
38	0.00	0.00	100.00
39	0.00	0.00	100.00
40	0.00	0.00	100.00
41	0.00	0.00	100.00
42	0.00	0.00	100.00
43	0.00	0.00	100.00
44	0.00	0.00	100.00

Table A13. Indicator loadings for the PLS-SEM 2.0 where LCC*LM indicates the interaction between Land Cover Change and Land Management.

	Regional Development	Soil Composition	LM	LCC	Water Stress	LCC*LM	Soil and Plant Nutrients	Heat Stress	Tillage	NPP
IRR	0.925	0	0	0	0	0	0	0	0	0
URB	0.928	0	0	0	0	0	0	0	0	0
FINO	0.767	0	0	0	0	0	0	0	0	0
NFN	0.912	0	0	0	0	0	0	0	0	0
POPD	0.902	0	0	0	0	0	0	0	0	0
FD	0	0	0.857	0	0	0	0	0	0	0
CRP	0	0	0.806	0	0	0	0	0	0	0
FOW	0	0	0.880	0	0	0	0	0	0	0
FLD	0	0	0.935	0	0	0	0	0	0	0
CRO	0	0	0.763	0	0	0	0	0	0	0
VPD	0	0	0	0	1.00	0	0	0	0	0
WAT	0	0	0	0.888	0	0	0	0	0	0
FOR	0	0	0	0.937	0	0	0	0	0	0
SAS	0	0.941	0	0	0	0	0	0	0	0
NT	0	0.825	0	0	0	0	0	0	0	0
FP	0	0	0	0	0	0	0.885	0	0	0
TPM	0	0	0	0	0	0	0	1.00	0	0
CVT	0	0	0	0	0	0	0	0	1.00	0
LCC*LM	0	0	0	0	0	0.809	0	0	0	0

Table A14. Discriminant validity as estimated by the heterotrait-monotrait ratio (HTMT) for the PLS-SEM 2.0.

	Regional Development	Soil Composition	LM	LCC	Abiotic Stress	LCC*LM	Soil and Plant Nutrients	Heat Stress	Tillage	NPP
Regional Development	NA	NA	NA	NA	NA	NA	NA	NA	NA	NA
Soil Composition	0.320	NA	NA	NA	NA	NA	NA	NA	NA	NA
LM	0.727	0.780	NA	NA	NA	NA	NA	NA	NA	NA
LCC	0.207	0.919	0.520	NA	NA	NA	NA	NA	NA	NA
Abiotic Stress	0.399	0.256	0.322	0.170	NA	NA	NA	NA	NA	NA
LCC*LM	0.185	0.523	0.504	0.187	0.038	NA	NA	NA	NA	NA
Soil and Plant Nutrients	0.112	0.402	0.344	0.253	0.450	0.286	NA	NA	NA	NA
Heat Stress	0.350	0.288	0.593	0.288	0.132	0.292	0.200	NA	NA	NA
Tillage	0.120	0.360	0.198	0.217	0.274	0.028	0.266	0.168	NA	NA
NPP	0.247	0.535	0.514	0.218	0.019	0.365	0.063	0.167	0.007	NA

Table A15. Validation Kappa indices of predicted 2016 land cover based on reference land cover from the National Land Cover Database 2016.

Kappa index	Value
Kno	0.9844
Klocation	0.9864
KlocationStrata	0.9864
Kstandard	0.9811

Table A16. Nitrogen (kg) fertilizer applications on cropland (km^2) per county-year and corresponding rates ($kg\ km^{-2}$).

County	Survey year	Nitrogen	Landcover year	Cropland	Rate
Allegan	2002	7210155.00	2001	924.74	7796.92
Allegan	2012	6060813.00	2011	923.61	6562.07
Allegan	2017	7085762.00	2016	921.51	7689.33
Barry	2002	3168253.00	2001	513.47	6170.23
Barry	2012	2223124.00	2011	517.96	4292.10
Barry	2017	3139220.00	2016	518.67	6052.46
Calhoun	2002	4158332.00	2001	849.52	4894.92
Calhoun	2012	4047835.00	2011	848.59	4770.06
Calhoun	2017	5573698.00	2016	846.34	6585.62
Eaton	2002	4481276.00	2001	785.43	5705.53
Eaton	2012	4137279.00	2011	784.25	5275.47
Eaton	2017	5761957.00	2016	783.73	7351.97
Hillsdale	2002	4771926.00	2001	858.20	5560.41
Hillsdale	2012	4572719.00	2011	859.44	5320.59
Hillsdale	2017	6587567.00	2016	858.83	7670.37
Jackson	2002	3236241.00	2001	607.65	5325.79
Jackson	2012	3169983.00	2011	605.28	5237.19
Jackson	2017	3754328.00	2016	605.11	6204.40
Kalamazoo	2002	4041902.00	2001	543.73	7433.63
Kalamazoo	2012	3695829.00	2011	535.65	6899.73
Kalamazoo	2017	5280494.00	2016	533.41	9899.52
Kent	2002	4709037.00	2001	631.27	7459.60
Kent	2012	2931465.00	2011	627.54	4671.35
Kent	2017	5108180.00	2016	626.85	8148.97
Ottawa	2002	4273062.00	2001	635.61	6722.75
Ottawa	2012	5043504.00	2011	624.66	8073.98
Ottawa	2017	6259970.00	2016	620.32	10091.58
Van Buren	2002	3773349.00	2001	693.06	5444.47
Van Buren	2012	3629467.00	2011	692.06	5244.43
Van Buren	2017	5951864.00	2016	691.04	8612.87

Table A17. Phosphorus (kg) fertilizer applications on cropland (km^2) per county-year and corresponding rates (kg km^{-2}).

County	Survey year	Phosphorus	Landcover year	Cropland	Rate
Allegan	2002	1119635.00	2001	924.74	1210.75
Allegan	2012	747126.00	2011	923.61	808.92
Allegan	2017	1110906.00	2016	921.51	1205.53
Barry	2002	491985.00	2001	513.47	958.15
Barry	2012	274048.00	2011	517.96	529.09
Barry	2017	519306.00	2016	518.67	1001.23
Calhoun	2002	645730.00	2001	849.52	760.11
Calhoun	2012	498983.00	2011	848.59	588.01
Calhoun	2017	825463.00	2016	846.34	975.33
Eaton	2002	695879.00	2001	785.43	885.99
Eaton	2012	510009.00	2011	784.25	650.32
Eaton	2017	894044.00	2016	783.73	1140.76
Hillsdale	2002	741013.00	2001	858.20	863.45
Hillsdale	2012	563686.00	2011	859.44	655.88
Hillsdale	2017	1124993.00	2016	858.83	1309.91
Jackson	2002	502542.00	2001	607.65	827.02
Jackson	2012	390769.00	2011	605.28	645.60
Jackson	2017	541839.00	2016	605.11	895.44
Kalamazoo	2002	627650.00	2001	543.73	1154.34
Kalamazoo	2012	455591.00	2011	535.65	850.54
Kalamazoo	2017	846618.00	2016	533.41	1587.18
Kent	2002	731247.00	2001	631.27	1158.37
Kent	2012	361366.00	2011	627.54	575.84
Kent	2017	822509.00	2016	626.85	1312.13
Ottawa	2002	663546.00	2001	635.61	1043.95
Ottawa	2012	621721.00	2011	624.66	995.29
Ottawa	2017	1067156.00	2016	620.32	1720.34
Van Buren	2002	585948.00	2001	693.06	845.45
Van Buren	2012	447410.00	2011	692.06	646.49
Van Buren	2017	1034251.00	2016	691.04	1496.65

Table A18. Irrigated farmland and cropland extent (km^2) per county-year and corresponding rates ($kg\ km^{-2}$).

County	Survey year	Irrigated	Landcover year	Cropland	Rate
Allegan	2002	62.11	2001	924.74	0.21
Allegan	2012	113.92	2011	923.61	0.36
Allegan	2017	119.85	2016	921.51	0.20
Barry	2002	10.99	2001	513.47	0.19
Barry	2012	17.31	2011	517.96	0.16
Barry	2017	23.75	2016	518.67	0.15
Calhoun	2002	42.16	2001	849.52	0.05
Calhoun	2012	43.15	2011	848.59	0.23
Calhoun	2017	62.99	2016	846.34	0.09
Eaton	2002	6.89	2001	785.43	0.22
Eaton	2012	5.90	2011	784.25	0.31
Eaton	2017	3.98	2016	783.73	0.20
Hillsdale	2002	16.55	2001	858.20	0.23
Hillsdale	2012	36.99	2011	859.44	0.10
Hillsdale	2017	40.83	2016	858.83	0.19
Jackson	2002	18.51	2001	607.65	0.31
Jackson	2012	15.82	2011	605.28	0.32
Jackson	2017	24.99	2016	605.11	0.11
Kalamazoo	2002	119.85	2001	543.73	0.26
Kalamazoo	2012	158.05	2011	535.65	0.43
Kalamazoo	2017	188.45	2016	533.41	0.29
Kent	2002	34.81	2001	631.27	0.28
Kent	2012	40.41	2011	627.54	0.25
Kent	2017	67.02	2016	626.85	0.11
Ottawa	2002	54.79	2001	635.61	0.15
Ottawa	2012	73.21	2011	624.66	0.19
Ottawa	2017	107.76	2016	620.32	0.17
Van Buren	2002	96.50	2001	693.06	0.17
Van Buren	2012	137.78	2011	692.06	0.18
Van Buren	2017	149.56	2016	691.04	0.16

Table A19. No-till farmland and cropland extent (km^2) per county-year and corresponding rates ($kg\ km^{-2}$).

County	Survey year	No-till	Landcover year	Cropland	Rate
Allegan	2002	33.61	2001	924.74	0.04
Allegan	2012	111.16	2011	923.61	0.12
Allegan	2017	134.30	2016	921.51	0.15
Barry	2002	65.06	2001	513.47	0.13
Barry	2012	121.18	2011	517.96	0.23
Barry	2017	144.80	2016	518.67	0.28
Calhoun	2002	121.90	2001	849.52	0.14
Calhoun	2012	230.08	2011	848.59	0.27
Calhoun	2017	332.41	2016	846.34	0.39
Eaton	2002	76.36	2001	785.43	0.10
Eaton	2012	262.62	2011	784.25	0.34
Eaton	2017	295.88	2016	783.73	0.38
Hillsdale	2002	102.73	2001	858.20	0.12
Hillsdale	2012	413.81	2011	859.44	0.48
Hillsdale	2017	261.47	2016	858.83	0.30
Jackson	2002	60.70	2001	607.65	0.10
Jackson	2012	166.91	2011	605.28	0.28
Jackson	2017	140.97	2016	605.11	0.23
Kalamazoo	2002	57.32	2001	543.73	0.11
Kalamazoo	2012	65.61	2011	535.65	0.12
Kalamazoo	2017	84.39	2016	533.41	0.16
Kent	2002	47.11	2001	631.27	0.08
Kent	2012	95.24	2011	627.54	0.15
Kent	2017	112.58	2016	626.85	0.18
Ottawa	2002	26.29	2001	635.61	0.04
Ottawa	2012	38.52	2011	624.66	0.06
Ottawa	2017	145.63	2016	620.32	0.24
Van Buren	2002	24.57	2001	693.06	0.04
Van Buren	2012	54.04	2011	692.06	0.08
Van Buren	2017	64.85	2016	691.04	0.09

Table A20. Conventional-till farmland and cropland extent (km^2) per county-year and corresponding rates ($kg\ km^{-2}$).

County	Survey year	Conventional till	Landcover year	Cropland	Rate
Allegan	2002	195.35	2001	924.74	0.21
Allegan	2012	332.98	2011	923.61	0.36
Allegan	2017	187.76	2016	921.51	0.20
Barry	2002	97.72	2001	513.47	0.19
Barry	2012	83.30	2011	517.96	0.16
Barry	2017	76.92	2016	518.67	0.15
Calhoun	2002	45.10	2001	849.52	0.05
Calhoun	2012	190.90	2011	848.59	0.23
Calhoun	2017	75.31	2016	846.34	0.09
Eaton	2002	169.93	2001	785.43	0.22
Eaton	2012	240.73	2011	784.25	0.31
Eaton	2017	153.08	2016	783.73	0.20
Hillsdale	2002	194.02	2001	858.20	0.23
Hillsdale	2012	83.00	2011	859.44	0.10
Hillsdale	2017	160.79	2016	858.83	0.19
Jackson	2002	188.71	2001	607.65	0.31
Jackson	2012	190.95	2011	605.28	0.32
Jackson	2017	64.70	2016	605.11	0.11
Kalamazoo	2002	142.60	2001	543.73	0.26
Kalamazoo	2012	227.49	2011	535.65	0.43
Kalamazoo	2017	156.71	2016	533.41	0.29
Kent	2002	176.54	2001	631.27	0.28
Kent	2012	155.87	2011	627.54	0.25
Kent	2017	65.65	2016	626.85	0.11
Ottawa	2002	94.37	2001	635.61	0.15
Ottawa	2012	120.65	2011	624.66	0.19
Ottawa	2017	103.48	2016	620.32	0.17
Van Buren	2002	114.80	2001	693.06	0.17
Van Buren	2012	122.22	2011	692.06	0.18
Van Buren	2017	108.54	2016	691.04	0.16

Table A21. Conservation-till farmland and cropland extent (km^2) per county-year and corresponding rates (kg km^{-2}).

County	Survey year	Conservation	Landcover year	Cropland	Rate
Allegan	2002	73.30	2001	924.74	0.08
Allegan	2012	190.89	2011	923.61	0.21
Allegan	2017	297.26	2016	921.51	0.32
Barry	2002	65.93	2001	513.47	0.13
Barry	2012	215.14	2011	517.96	0.42
Barry	2017	125.89	2016	518.67	0.24
Calhoun	2002	124.63	2001	849.52	0.15
Calhoun	2012	389.50	2011	848.59	0.46
Calhoun	2017	219.98	2016	846.34	0.26
Eaton	2002	87.85	2001	785.43	0.11
Eaton	2012	321.08	2011	784.25	0.41
Eaton	2017	193.65	2016	783.73	0.25
Hillsdale	2002	103.94	2001	858.20	0.12
Hillsdale	2012	475.57	2011	859.44	0.55
Hillsdale	2017	294.15	2016	858.83	0.34
Jackson	2002	75.05	2001	607.65	0.12
Jackson	2012	234.68	2011	605.28	0.39
Jackson	2017	200.36	2016	605.11	0.33
Kalamazoo	2002	75.91	2001	543.73	0.14
Kalamazoo	2012	141.85	2011	535.65	0.27
Kalamazoo	2017	150.65	2016	533.41	0.28
Kent	2002	66.61	2001	631.27	0.11
Kent	2012	140.35	2011	627.54	0.22
Kent	2017	184.54	2016	626.85	0.29
Ottawa	2002	48.01	2001	635.61	0.08
Ottawa	2012	108.23	2011	624.66	0.17
Ottawa	2017	180.77	2016	620.32	0.29
Van Buren	2002	43.51	2001	693.06	0.06
Van Buren	2012	94.67	2011	692.06	0.14
Van Buren	2017	146.24	2016	691.04	0.21

APPENDIX B. REVISED PLS-SEM

PLS-SEM revised theoretical framework

The PCA loadings provided initial groupings for variables within constructs and updated others (Fig. B1), providing an intermediary step before achieving the final PLS-SEM 2.0. Given the division between the variables labeled as abiotic stressors, the construct was divided into two new constructs: Heat Stress and Water Stress. Given the stronger contribution of CVT than no-till (NT) in PCA dimension five, a new construct—Tillage—was formed to include CVT. However, it was found that the revised PLS-SEM theoretical framework incorporating the PCA constructs did not satisfy all the model evaluation metrics for measurement models. Rather, it demonstrated strong indicator and construct relationships suitable for revision. The indicator reliability was greater than the recommended 0.708 for all indicators except average clay 0-5 cm (CLS) (0.673), average organic matter 5-15 cm (OMD) (0.502), no-till (NT) (0.611), rural housing density (RHD) (0.691), and wetland (WET) (0.471) (Table A7). Internal consistency reliability in the revised PLS-SEM demonstrated RhoA of ~0.95, indicating unsatisfactory similarity between indicators within the construct, whereas AVE reported well above the required 0.5 thresholds, demonstrating unique constructs (Table A8). Particularly, Water Stress and Soil and Plant Nutrients reported a RhoA (11.99 and 1.19), showing that these indicators were not suitable and were too similar. Additionally, discriminant variability was acceptable between all constructs, with HTMT values well below 0.85 for all construct pairs except for Soil Composition–Land Management (0.916), Soil Composition–Land Cover Change (1.065), and Land Management–Land Cover Change (0.896) (Table A9). This revised theoretical framework was not further evaluated as a structural model.

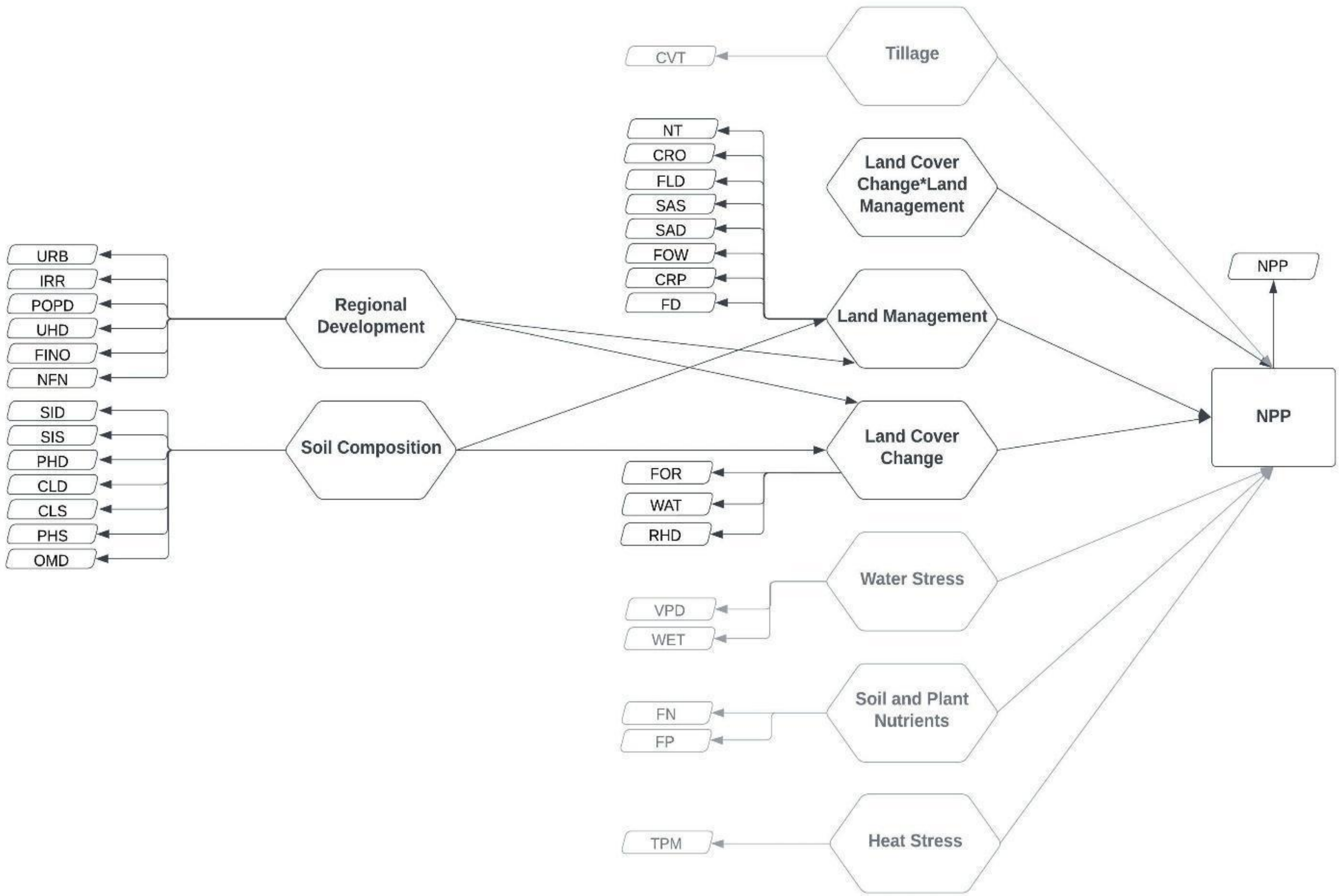

Figure B1. Revised PLS-SEM theoretical framework including new latent constructs (hexagons) and their indicators (parallelograms) from PCA dimensions. Gray constructs are new constructs, where 'Water Stress' and 'Heat Stress' replaced 'Abiotic Stress.' Construct 'Land Management * Land Cover Change' indicates the interaction between 'Land Management' and 'Land Cover Change' constructs. Variable names are available in Table 3.1.

Table B1. Indicator loadings for the revised theoretical framework where LCC*LM indicates the interaction between Land Cover Change and Land Management.

	Regional Development	Soil Composition	LM	LCC	Water Stress	LCC*LM	Soil and Plant Nutrients	Heat Stress	Tillage	NPP
IRR	0.914	0	0	0	0	0	0	0	0	0
UHD	0.941	0	0	0	0	0	0	0	0	0
FINO	0.744	0	0	0	0	0	0	0	0	0
NFN	0.924	0	0	0	0	0	0	0	0	0
POPD	0.919	0	0	0	0	0	0	0	0	0
URB	0.922	0	0	0	0	0	0	0	0	0
FD	0	0	0.764	0	0	0	0	0	0	0
CRP	0	0	0.722	0	0	0	0	0	0	0
FOW	0	0	0.764	0	0	0	0	0	0	0
FLD	0	0	0.952	0	0	0	0	0	0	0
SAS	0	0	0.903	0	0	0	0	0	0	0
SAD	0	0	0.892	0	0	0	0	0	0	0
NT	0	0	0.611	0	0	0	0	0	0	0
CRO	0	0	0.766	0	0	0	0	0	0	0
VPD	0	0	0	0	0.999	0	0	0	0	0
WET	0	0	0	0	0.471	0	0	0	0	0
RHD	0	0	0	0.691	0	0	0	0	0	0
FOR	0	0	0	0.884	0	0	0	0	0	0
WAT	0	0	0	0.842	0	0	0	0	0	0
CLD	0	0.763	0	0	0	0	0	0	0	0
CLS	0	0.673	0	0	0	0	0	0	0	0
PHD	0	0.902	0	0	0	0	0	0	0	0
OMD	0	0.502	0	0	0	0	0	0	0	0
SID	0	0.952	0	0	0	0	0	0	0	0
SIS	0	0.940	0	0	0	0	0	0	0	0
PHS	0	0.866	0	0	0	0	0	0	0	0
FN	0	0	0	0	0	0	0.973	0	0	0
FP	0	0	0	0	0	0	0.885	0	0	0
TPM	0	0	0	0	0	0	0	1.00	0	0
CVT	0	0	0	0	0	0	0	0	1.00	0
LCC*LM	0	0	0	0	0	0.725	0	0	0	0

Table B2. Internal consistency reliability for the revised PLS-SEM theoretical framework.

	Alpha	RhoC	AVE	RhoA
Regional Development	0.95	0.96	0.80	0.96
Soil Composition	0.91	0.93	0.66	0.93
Land Management	0.92	0.93	0.65	0.94
Land Cover Change	0.73	0.85	0.66	0.75
Water Stress	0.61	0.74	0.61	11.99
Land Cover Change*Land Management	1.00	1.00	1.00	1.00
Soil and Plant Nutrients	0.86	0.93	0.86	1.19
Heat Stress	1.00	1.00	1.00	1.00
Tillage	1.00	1.00	1.00	1.00
NPP	1.00	1.00	1.00	1.00

Table B3. Discriminant validity estimated by the heterotrait-monotrait ratio (HTMT) for the revised theoretical PLS-SEM, where NPP was NA (not applicable) across all composites.

	Regional Development	Soil Composition	LM	LCC	Abiotic Stress	LCC*LM	Soil and Plant Nutrients	Heat Stress	Tillage
Regional Development	NA	NA	NA	NA	NA	NA	NA	NA	NA
Soil Composition	0.354	NA	NA	NA	NA	NA	NA	NA	NA
LM	0.592	0.916	NA	NA	NA	NA	NA	NA	NA
LCC	0.237	1.065	0.896	NA	NA	NA	NA	NA	NA
Abiotic Stress	0.394	0.325	0.352	0.422	NA	NA	NA	NA	NA
LCC*LM	0.142	0.445	0.691	0.354	0.036	NA	NA	NA	NA
Soil and Plant Nutrients	0.145	0.440	0.458	0.556	0.514	0.464	NA	NA	NA
Heat Stress	0.370	0.260	0.504	0.415	0.194	0.277	0.248	NA	NA
Tillage	0.122	0.215	0.249	0.240	0.336	0.043	0.273	0.168	NA
NPP	0.216	0.584	0.563	0.225	0.015	0.480	0.110	0.167	0.007

Table B4. Indicator loadings for the revised theoretical framework where LCC*LM indicates the interaction between Land Cover Change and Land Management.

	Regional Development	Soil Composition	LM	LCC	Water Stress	LCC*LM	Soil and Plant Nutrients	Heat Stress	Tillage	NPP
IRR	0.914	0	0	0	0	0	0	0	0	0
UHD	0.941	0	0	0	0	0	0	0	0	0
FINO	0.744	0	0	0	0	0	0	0	0	0
NFN	0.924	0	0	0	0	0	0	0	0	0
POPD	0.919	0	0	0	0	0	0	0	0	0
URB	0.922	0	0	0	0	0	0	0	0	0
FD	0	0	0.764	0	0	0	0	0	0	0
CRP	0	0	0.722	0	0	0	0	0	0	0
FOW	0	0	0.764	0	0	0	0	0	0	0
FLD	0	0	0.952	0	0	0	0	0	0	0
SAS	0	0	0.903	0	0	0	0	0	0	0
SAD	0	0	0.892	0	0	0	0	0	0	0
NT	0	0	0.611	0	0	0	0	0	0	0
CRO	0	0	0.766	0	0	0	0	0	0	0
VPD	0	0	0	0	0.999	0	0	0	0	0
WET	0	0	0	0	0.471	0	0	0	0	0
RHD	0	0	0	0.691	0	0	0	0	0	0
FOR	0	0	0	0.884	0	0	0	0	0	0
WAT	0	0	0	0.842	0	0	0	0	0	0
CLD	0	0.763	0	0	0	0	0	0	0	0
CLS	0	0.673	0	0	0	0	0	0	0	0
PHD	0	0.902	0	0	0	0	0	0	0	0
OMD	0	0.502	0	0	0	0	0	0	0	0
SID	0	0.952	0	0	0	0	0	0	0	0
SIS	0	0.940	0	0	0	0	0	0	0	0
PHS	0	0.866	0	0	0	0	0	0	0	0
FN	0	0	0	0	0	0	0.973	0	0	0
FP	0	0	0	0	0	0	0.885	0	0	0
TPM	0	0	0	0	0	0	0	1.00	0	0
CVT	0	0	0	0	0	0	0	0	1.00	0
LCC*LM	0	0	0	0	0	0.725	0	0	0	0

Table B5. Discriminant validity estimated by the heterotrait-monotrait ratio (HTMT) for the revised theoretical PLS-SEM.

	Regional Development	Soil Composition	LM	LCC	Abiotic Stress	LCC*LM	Soil and Plant Nutrients	Heat Stress	Tillage	NPP
Regional Development	NA	NA	NA	NA	NA	NA	NA	NA	NA	NA
Soil Composition	0.354	NA	NA	NA	NA	NA	NA	NA	NA	NA
LM	0.592	0.916	NA	NA	NA	NA	NA	NA	NA	NA
LCC	0.237	1.065	0.896	NA	NA	NA	NA	NA	NA	NA
Abiotic Stress	0.394	0.325	0.352	0.422	NA	NA	NA	NA	NA	NA
LCC*LM	0.142	0.445	0.691	0.354	0.036	NA	NA	NA	NA	NA
Soil and Plant Nutrients	0.145	0.440	0.458	0.556	0.514	0.464	NA	NA	NA	NA
Heat Stress	0.370	0.260	0.504	0.415	0.194	0.277	0.248	NA	NA	NA
Tillage	0.122	0.215	0.249	0.240	0.336	0.043	0.273	0.168	NA	NA
NPP	0.216	0.584	0.563	0.225	0.015	0.480	0.110	0.167	0.007	NA